

# ***Disposal Concepts for a High-Temperature Repository in Shale***

## **Spent Fuel and Waste Disposition**

***Prepared for  
US Department of Energy  
Spent Fuel and Waste Science and  
Technology***

***Emily R. Stein, Charles Bryan, David C. Dobson,  
Ernest L. Hardin, Carlos Jové-Colón, Carlos M. Lopez,  
Edward N. Matteo, Sitakanta Mohanty, Martha Pendleton,  
Frank V. Perry, Jeralyn L. Prouty, David C. Sassani,  
Yifeng Wang***

***Sandia National Laboratories***

***Jonny Rutqvist, LianGe Zheng  
Lawrence Berkeley National Laboratory***

***Kirsten B. Sauer, Florie Caporuscio  
Los Alamos National Laboratory***

***Robert Howard, Abiodun Adeniyi, Kaushik Banerjee, and  
Robby Joseph  
Oak Ridge National Laboratory***

***October 2020***

**M3SF-21SN010304064**

**SAND2020-12471 R**

#### DISCLAIMER

This information was prepared as an account of work sponsored by an agency of the U.S. Government. Neither the U.S. Government nor any agency thereof, nor any of their employees, makes any warranty, expressed or implied, or assumes any legal liability or responsibility for the accuracy, completeness, or usefulness, of any information, apparatus, product, or process disclosed, or represents that its use would not infringe privately owned rights. References herein to any specific commercial product, process, or service by trade name, trade mark, manufacturer, or otherwise, does not necessarily constitute or imply its endorsement, recommendation, or favoring by the U.S. Government or any agency thereof. The views and opinions of authors expressed herein do not necessarily state or reflect those of the U.S. Government or any agency thereof.



**Sandia National Laboratories**

Sandia National Laboratories is a multi-mission laboratory managed and operated by National Technology & Engineering Solutions of Sandia, LLC., a wholly owned subsidiary of Honeywell International, Inc., for the U.S. Department of Energy's National Nuclear Security Administration under contract DE-NA0003525.

Revision 6  
10/7/2019

## APPENDIX E NFCSC DOCUMENT COVER SHEET<sup>1</sup>

Name/Title of Deliverable/Milestone/Revision No. Disposal Concepts for a High-Temperature Repository in Shale

Work Package Title and Number GDSA Repository Systems Analysis – SNL - SF-21SN01030406

Work Package WBS Number 1.08.01.03.04

Responsible Work Package Manager Tara LaForce  
(Name/Signature)

Date Submitted

Quality Rigor Level for Deliverable/Milestone <sup>2</sup>	<input type="checkbox"/> QRL-1 <input type="checkbox"/> Nuclear Data	<input type="checkbox"/> QRL-2	<input checked="" type="checkbox"/> QRL-3	<input type="checkbox"/> QRL-4 Lab QA Program <sup>3</sup>
--	---	--------------------------------	---	---

This deliverable was prepared in accordance with Sandia National Laboratories  
(Participant/National Laboratory Name)

QA program which meets the requirements of  
 DOE Order 414.1     NQA-1     Other

**This Deliverable was subjected to:**

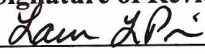
Technical Review

**Technical Review (TR)**

**Review Documentation Provided**

- Signed TR Report or,  
 Signed TR Concurrence Sheet or,  
 Signature of TR Reviewer(s) below

**Name and Signature of Reviewers**

Laura Price 

---



---

Peer Review

**Peer Review (PR)**

**Review Documentation Provided**

- Signed PR Report or,  
 Signed PR Concurrence Sheet or,  
 Signature of PR Reviewer(s) below

---



---

**NOTE 1:** Appendix E should be filled out and submitted with the deliverable. Or, if the PICS:NE system permits, completely enter all applicable information in the PICS:NE Deliverable Form. The requirement is to ensure that all applicable information is entered either in the PICS:NE system or by using the NFCSC Document Cover Sheet.

- In some cases there may be a milestone where an item is being fabricated, maintenance is being performed on a facility, or a document is being issued through a formal document control process where it specifically calls out a formal review of the document. In these cases, documentation (e.g., inspection report, maintenance request, work planning package documentation or the documented review of the issued document through the document control process) of the completion of the activity, along with the Document Cover Sheet, is sufficient to demonstrate achieving the milestone.

**NOTE 2:** If QRL 1, 2, or 3 is not assigned, then the QRL 4 box must be checked, and the work is understood to be performed using laboratory QA requirements. This includes any deliverable developed in conformance with the respective National Laboratory / Participant, DOE or NNSA-approved QA Program.

**NOTE 3:** If the lab has an NQA-1 program and the work to be conducted requires an NQA-1 program, then the QRL-1 box must be checked in the work Package and on the Appendix E cover sheet and the work must be performed in accordance with the Lab's NQA-1 program. The QRL-4 box should not be checked.

## SUMMARY

Disposal of large, heat-generating waste packages containing the equivalent of 21 pressurized water reactor (PWR) assemblies or more is among the disposal concepts under investigation for a future repository for spent nuclear fuel (SNF) in the United States. Without a long (>200 years) surface storage period, disposal of 21-PWR or larger waste packages (especially if they contain high-burnup fuel) would result in in-drift and near-field temperatures considerably higher than considered in previous generic reference cases that assume either 4-PWR or 12-PWR waste packages (Jové Colón et al. 2014; Mariner et al. 2015; 2017). Sevougian et al. (2019c) identified high-temperature process understanding as a key research and development (R&D) area for the Spent Fuel and Waste Science and Technology (SFWST) Campaign.

A two-day workshop in February 2020 brought together campaign scientists with expertise in geology, geochemistry, geomechanics, engineered barriers, waste forms, and corrosion processes to begin integrated development of a high-temperature reference case for disposal of SNF in a mined repository in a shale host rock. Building on the progress made in the workshop, the study team further explored the concepts and processes needed to form the basis for a high-temperature shale repository reference case. The results are described in this report and summarized below.

**Geologic Setting of Major Shale Deposits (Section 2)**—Two shale endmembers, ductile and brittle, are proposed for future high-temperature shale reference cases. The characteristics of ductile and brittle shales are described and placed in the context of United States sedimentary basins. Whether a shale is ductile or brittle is determined by its original depositional environment and resulting clay content, as well as the maximum depth of burial experienced and resulting degree of induration. The two endmembers differ in mechanical behavior, porewater chemistry, and thermal and hydrologic properties.

**Natural Barrier System (Section 3)**—The ductile shale endmember is characterized by a high clay mineral content, low mechanical strength, low thermal conductivity, and very low permeability within intact blocks of rock (over a scale of several hundred meters). The brittle shale endmember is characterized by a higher proportion of strong grains such as quartz, higher mechanical strength, somewhat higher thermal conductivity, and potentially higher bulk permeability due to the presence of interconnected fractures. The ductile shale endmember has experienced shallower burial depths than the brittle endmember, is less indurated, and has relatively dilute porewater, while the brittle shale endmember has experienced deeper burial depths, is more indurated, and has saline porewater.

**Repository Design and Construction (Section 4)**—Repository depths between 300 and 900 m have been proposed for shale host rock (Shurr 1977); a nominal depth of 500 m is assumed, with the repository situated in a flat-lying stratigraphy and built on a single level.

The repository would be constructed in stages, with access drifts intended to remain open for the lifetime of the repository (approximately 100 years) and disposal drifts intended to remain open for less than about 3 years. Immediate support during or after excavation is necessary in shales to control rock deformation and rockfall hazards. The reference concept assumes a minimal support system consisting of rock bolts, which retain welded wire cloth, covered by a layer of low pH shotcrete (10–30 cm thick). Ground support in temporary openings would be limited to shorter rock bolts and thinner shotcrete, while permanent openings may require multiple applications of shotcrete and steel sets (or other heavy lining) to stabilize against large deformations.

The reference concept assumes axial, in-drift emplacement of waste packages containing 21 PWR assemblies or 44 boiling water reactor (BWR) assemblies. Waste emplacement drifts would be backfilled with crushed rock and/or bentonite buffer to provide shielding during the operational phase and to prevent rock fall.

Large waste packages pose a challenge for thermal management in a shale repository. Repository temperature limits may be based on various temperature constraints designed to ensure material integrity of the fuel cladding, waste package materials, a clay-based buffer, and/or the host rock itself. Waste package and drift spacings are selected to be reasonably large (20 m and 70 m, respectively), and waste packages are assumed to be loaded and aged (through surface storage) such that the power output at the time of emplacement is less than about 4 kW/waste package. Such a strategy meets potential temperature



limits of 250°C at the waste package surface and 100°C at the drift wall or a short distance into the wall rock. The strategy (depending on the engineered thermal properties of the backfill) includes a zone of “sacrificial” backfill surrounding each waste package for which maintenance of favorable mechanical, chemical, and hydrological properties of the backfill/buffer cannot be assumed without site-specific study.

**Disturbed Rock Zone (Section 5)**—The mechanical properties of shale, whether more ductile or brittle, impact the coupled thermal-hydrological-mechanical evolution of the host rock, including the potential for mechanical damage and associated changes in transport properties. In the host rock immediately adjacent to drift walls, both excavation-induced fracturing and thermal spalling are expected. A ductile shale is expected to experience creep (visco-plastic) deformation around excavations and to self-seal fractures on relatively short time scales, while a brittle shale may sustain durable damage. In a high-temperature repository, thermally induced mechanical damage to the host rock may extend beyond the immediate environment of the drift wall if thermal pressurization of porewater is sufficient to cause hydraulic fracturing or activation of pre-existing natural fractures in the host rock. The potential for near-field hydraulic fracturing depends on coupled feedback between permeability, thermal conductivity, and mechanical strength of the host rock.

**Engineered Barrier System (Section 6)**—Two options are proposed for in-drift emplacement of waste packages: (1) waste packages are emplaced on the floor of the drift and (2) waste packages are emplaced on a plinth of compacted bentonite. The first option is operationally simpler, and may be suitable in a self-sealing, low-permeability host rock. The second option presents additional engineering and design challenges, but may be desirable if flow in connected fractures cannot be ruled out.

Several backfill/buffer emplacement concepts are proposed for further study for a high-temperature shale repository. The first concept is for crushed rock backfill to be emplaced in the high-temperature zone around each waste package and compacted bentonite buffer or an admixture of crushed rock and bentonite pellets to be emplaced in the disposal drifts between waste packages. In the second concept, compacted bentonite buffer is emplaced throughout the disposal drifts. For the latter, the high heat load of the waste packages may be managed by (1) enhancing the thermal conductivity of the buffer with additives such as quartz sand, graphite, graphene, or copper wire mesh; or (2) determining for a given set of conditions (including clay mineralogy and porewater composition) that a higher temperature limit is acceptable in the bentonite buffer. Additional research is needed to characterize some of these materials.

The potential reference waste packages are comprised of a stainless steel canister that may serve multiple purposes including transportation, aging, and disposal; canister internals supporting the fuel assemblies and providing criticality control; and a disposal overpack. Carbon steel, stainless steel, and copper are possible overpack materials that have been studied in a variety of repository programs (e.g., Andra 2005; SKB 2010).

The waste form is spent uranium oxide (UO<sub>2</sub>) fuel, a polycrystalline ceramic material stable to high temperatures and likely slow to degrade in the disposal environment (Shoesmith 2007). In spent oxide fuels, the radionuclide inventory is usually considered to consist of two parts: (1) a part that resides in the fuel rod gap and grain-boundary region and (2) a part that is embedded in the fuel matrix and released only upon degradation of the fuel matrix.

Nominal and bounding initial radionuclide inventories and waste package power outputs as functions of time are constructed using assembly and fuel characteristics from the Unified Database.

**Corrosion Behavior of Candidate Waste Package Materials (Section 7)**—Corrosion mechanisms of Fe-based alloys and Cu-based materials are discussed. In the reducing porewater environment of a shale repository, carbon steel would experience general corrosion via reaction with water; copper would experience general corrosion if reduced sulfur species are present; and stainless steel is likely to form a passive, stable oxide film on the surface that slows general corrosion and leads to localized (less predictable) pitting or crevice corrosion. Corrosion rates and stability of passivation films depend on environmental factors, including concentrations of chemical species, temperature, pH, and radiation flux. Structural damage to waste packages may occur due to extensive general corrosion, stress corrosion cracking, or hydride embrittlement.

**Chemical Changes at Interfacial Areas (Section 8)**—Steel corrosion, cement degradation, and host rock/bentonite interactions have the potential to cause wide-ranging effects on the physical and chemical properties of the bentonite buffer where it contacts other materials (e.g., Caporuscio et al. 2019). Changes to physical properties may include dissolution/recrystallization of montmorillonite, loss of bentonite swelling capacity (due to cementation or recrystallization to nonswelling phases), and development of porosity due to the formation denser mineral phases (e.g., zeolites). Such changes depend on bulk system chemistry and temperature.

**Summary of High-Temperature Effects**—High temperatures in the near field of a shale repository may drive hydrological, mechanical, and chemical changes. Three avenues of future R&D are apparent from the concepts proposed in this report: characterization of materials engineered for thermal management (e.g., buffer materials), development of conceptual models, and investigation of the temperature dependence of coupled processes.

This is the first time that SFWST generic disposal research has made a clear distinction between more ductile and more brittle shales. Each may require a different approach to defense in depth with a different degree of reliance on, for instance, corrosion resistance of the waste package or ability of the buffer/backfill to retard radionuclide transport. Depending on the characteristics of the natural and engineered systems, different processes may play a greater or lesser role, including, for instance, (1) creep deformation, rockfall, or hydrofracturing of the host rock; (2) illitization, porewater chemistry changes, or precipitation of secondary phases in the buffer; and (3) general corrosion, local corrosion, or mechanical damage due to corrosion processes in the overpack.

Conceptual models for some of these processes will include a temperature dependence. This report identifies the potential for (1) development of thermal overpressures and possibility of hydrofracturing in the near field; (2) influence on drift closure processes such as an accelerated rate of creep or thermal spalling; (3) depending on the geochemical environment, enhanced chemical alteration of the bentonite buffer resulting in alteration of swelling capacity or other bentonite properties; (4) faster corrosion rates; and (5) temperature-dependent diffusion, radionuclide solubilities, and sorption. Further evaluation of these and other temperature-dependent coupled processes will enable preliminary material choices and contribute to development of a reference case for a high-temperature repository in shale.

This report fulfills the GDSA Repository Systems Analysis Work Package Level 3 Milestone – *Disposal Concepts for a High-Temperature Repository in Shale*, M3SF-21SN010304064.

## **ACKNOWLEDGEMENTS**

This report captures ideas generated in a two-day workshop that took place in February 2020 in Albuquerque, NM. Thanks to all who took part: presenters, report writers, and question askers. Participants included most of the authors as well as many additional subject matter experts, including Dave Sevougian, Laura Price, Paul Mariner, Tara LaForce, Michael Nole, Pat Brady, K-Won Chang, Geoff Freeze, Chris Camphouse, Michael Gross, Erika Swanson, Glenn Russell, and Prasad Nair. Thanks to Prasad Nair, Tim Gunter, and Jorge Monroe-Rammsy at the Department of Energy, Office of Nuclear Energy for their support of this work. Thanks to Lindsay McCabe for her help assembling the document. Particular thanks to Dave Sevougian (retired), who instigated the workshop, and Laura Price, whose careful technical review improved the document.

This page is intentionally left blank.

## CONTENTS

1.	INTRODUCTION.....	19
1.1	Background Information.....	19
1.1.1	History of Shale/Argillite Repository Studies.....	19
1.1.2	Summary of Conclusions and Recommendations from the SFWST Roadmap Update.....	22
1.2	Objective and Process.....	22
1.3	Postclosure Technical Basis.....	23
2.	GEOLOGIC SETTING OF MAJOR SHALE DEPOSITS IN THE U.S. ....	25
2.1	Overview of Shale Deposits in the U.S.....	25
2.2	Depth and Thickness of U.S. Shale Formations.....	26
2.3	Overview of Shale Diagenesis, Burial Depth and Mechanical Properties.....	27
3.	NATURAL BARRIER SYSTEM.....	29
3.1	Stratigraphic Framework for Ductile and Brittle Shales.....	29
3.2	Properties of Ductile and Brittle Shales.....	30
3.2.1	Relationship of Mineralogy to Mechanical Properties.....	30
3.2.2	Relationship of Mineralogy to Mechanical Properties.....	33
3.2.3	Hydrologic Properties.....	38
3.2.4	Thermal Properties.....	39
3.2.5	Porewater Chemistry.....	39
3.2.6	Summary of Properties for Ductile and Brittle Shale.....	49
3.3	Properties of Ductile and Brittle Shales.....	50
4.	REPOSITORY DESIGN AND CONSTRUCTION.....	53
4.1	Assumed Repository Depth and Host Ground Conditions.....	53
4.1.1	Available Repository Area.....	54
4.1.2	Hydrologic Conditions.....	54
4.2	Preclosure Performance Criteria.....	55
4.2.1	Accommodating Clay/Shale Rock Characteristics.....	55
4.2.2	Facility Lifetime.....	56
4.2.3	Service/Access Opening Operational Duration.....	57
4.2.4	Waste Package Shielding.....	58
4.3	Postclosure Performance Criteria.....	58
4.3.1	Opening Support Criteria.....	58
4.3.2	Ground Support Material Criteria.....	59
4.3.3	Buffer and Backfill Performance Criteria.....	59
4.4	Excavation and Ground Support Options.....	60
4.4.1	Shaft and Ramp Options.....	61
4.4.2	Mechanized Excavation Methods.....	61
4.5	Thermal Management in a Shale Repository.....	62
4.5.1	Clay/Shale Formation Thermal Properties.....	64
4.5.2	Calculated Generic Emplacement Power Limits.....	64

4.5.3	Backfill and Formation Temperatures .....	70
4.6	Repository Layout Considerations .....	70
4.6.1	Shaft/Ramp Phase .....	70
4.6.2	TBM Phase.....	74
4.6.3	Emplacement Drifts .....	75
4.6.4	Ventilation and Other Services .....	76
5.	DISTURBED ROCK ZONE.....	77
5.1	Thermally Induced THM Processes at Tunnel and Repository Scale.....	77
5.2	Excavation-Induced Damage in Ductile Versus Brittle Shale .....	78
6.	ENGINEERED BARRIER SYSTEM.....	81
6.1	Ground Support/Cementitious Liners .....	81
6.2	Buffer .....	83
6.2.1	Buffer Emplacement .....	83
6.2.2	Buffer Material Options .....	84
6.2.3	Processes in the Buffer Material .....	87
6.2.4	Buffer Material Properties .....	91
6.2.5	Radionuclide Transport.....	92
6.3	Waste Packages for Spent Nuclear Fuel .....	98
6.3.1	Waste Package Functional Requirements .....	98
6.3.2	Waste Package Canister and Internals .....	99
6.3.3	Waste Package Material Options .....	101
6.4	Reference Internal Canister Design .....	103
6.5	Waste Form.....	105
6.5.1	Spent Fuel Types and Characteristics .....	105
6.5.2	Radionuclide Inventories and Heat of Decay.....	105
6.5.3	Cladding.....	111
6.5.4	Neutron Absorbers .....	112
6.6	Spent Fuel Degradation Model and In-package Chemistry .....	114
7.	CORROSION BEHAVIOR OF CANDIDATE WASTE PACKAGE MATERIALS.....	117
7.1	Corrosion of Iron Alloys and Copper Under Oxic and Anoxic Conditions .....	117
7.1.1	Fe-Based Alloys.....	117
7.1.2	Cu-Based Materials.....	118
7.2	Corrosion Mechanisms .....	120
7.2.1	General Corrosion .....	121
7.2.2	Localized Corrosion.....	123
7.3	Summary of Copper and Steel Corrosion Behavior.....	127
8.	CHEMICAL CHANGES AT INTERFACIAL AREAS.....	129
8.1	High-Temperature Waste Canister Overpack-Bentonite Interactions.....	129
8.1.1	Steel-Bentonite Interaction .....	129
8.1.2	Clay-Copper Interaction.....	131
8.2	Additional Interactions.....	132
9.	SUMMARY AND CONCLUSIONS.....	135



---

10. REFERENCES ..... 139

**LIST OF FIGURES**

Figure 1-1. Components of a Generic Disposal System ..... 23

Figure 2-1. Shale Provinces in the U.S. .... 26

Figure 2-2. Selected Shale Formations and Sedimentary Basins showing Depth to Top of Shale..... 27

Figure 3-1. Schematic Representation of the Stratigraphic Columns in Representative Areas of the Northern Great Basin, Illinois, and Michigan Basins ..... 30

Figure 3-2. Mineral Compositions of Well-Characterized Shale by Intended or Proposed Use ..... 31

Figure 3-3. Conceptual Model for Shale Microstructure ..... 32

Figure 3-4. (A) Compressive Strength, (B) Log Permeability, and (C) Porosity Versus Clay Content for Well-Characterized Shales ..... 32

Figure 3-5. Mineral Compositions of the Pierre Shale, Paleozoic Shales of the Eastern Interior Basins, and European Shales Considered for HLW Disposal ..... 33

Figure 3-6. Fracture Aperture-Size Distribution for Selected Shales ..... 36

Figure 3-7. Examples of Fracture Layer (bed) Boundedness and Fracture Stratigraphy in Shales ..... 37

Figure 3-8. Chloride Concentration Profile as a Function of Reported Maximal Borehole or Perforation Depths..... 42

Figure 3-9. Piper Plot of Groundwater Major Cation/Anion Solutes (in percent mEq/L units) for the Considered Paleozoic Shales ..... 43

Figure 3-10. Piper Plot of Groundwater Major Cation/Anion Solutes (in percent mEq/L units) for Cretaceous and Jurassic Shales..... 44

Figure 3-11. Plot of Total Dissolved Solids Versus Chloride Concentration for Paleozoic and Cretaceous Shale Formation Waters..... 45

Figure 3-12. Plot of Concentration Ratios Ca/SO<sub>4</sub> Versus Na/Cl for Paleozoic and Cretaceous Shale Formation Waters ..... 46

Figure 4-1. Illustration of Two Types of Backfill: Crushed Rock from the Host Shale around Waste Packages and Low Permeability, Clay Admixture between Waste Packages ..... 60

Figure 4-2. Peak Temperature Versus Package Spacing for Values of Depth into the Rock (32-PWR size packages, 40 GW-d/MT burnup) ..... 66

Figure 4-3. Peak Temperature Versus Package Spacing for Values of Depth into the Rock (32-PWR size packages, 60 GW-d/MTU burnup, 70 m and 90 m drift spacing) ..... 67

Figure 4-4. Conceptual Layout for the Shale Repository: Shaft/Ramp Construction Phase ..... 71

Figure 4-5. Conceptual Layout for the Shale Repository: TBM Phase ..... 72

Figure 4-6. Conceptual Drift Layout for a High-Temperature Shale Repository ..... 73

Figure 4-7. Conceptual Drift Layout for the Shale Repository with Transport Routes for Moving Waste Packages Underground to Emplacement Drifts..... 74

Figure 5-1. Schematic of Repository-Scale Coupled Thermo-Hydro-Mechanical Responses and Their Impact on Emplacement Tunnels..... 78

Figure 5-2. Extensions of (a) Hydraulic Permeability and (b) Fracture Zones Measured around a Tunnel in the Callovo-Oxfordian Claystone..... 79

Figure 5-3. Relationship between Depth of Failure and the Maximum Tangential Stress at the Boundary of a Tunnel ..... 80

Figure 6-1. Components of the EBS for a High-Temperature Shale Reference Case ..... 81

Figure 6-2. Geometry of a Cross-Section of a Drift for Two Emplacement Options: Option 1 (waste package with overpack sits on a concrete floor) and Option 2 (waste package with overpack sits on a buffer pedestal) ..... 84

Figure 6-3. Enhancement of Thermal Conductivity of Bentonite Buffer Materials with Copper Wires/Meshes ..... 86

Figure 6-4. Schematic of the Temporal Evolution of THMC Processes in Bentonite Buffer ..... 87

Figure 6-5. Thermal Conductivity of Compacted Bentonite as a Function of Dry Density and Water Content..... 88

Figure 6-6. Illustration of (A) Clay Layering and (B) Clay Stacks under Various Degrees of Compaction..... 93

Figure 6-7. Rendering of a 21 PWR/44 BWR Fuel Assembly Waste Package Configuration..... 100

Figure 6-8. Thermal Power for a 21-PWR Waste Package Assuming Nominal Radionuclide Inventory..... 108

Figure 6-9. Thermal Power for a 21-PWR Waste Package Assuming Burnup-Bounded Assemblies..... 111

Figure 7-1. Schematic Diagram of Pitting Corrosion, Illustrating the Relationship between the Cathode and Anode, the Reactions That Occur for Each, and the Effect on pH at Each Location..... 124

Figure 8-1. Image of Altered Bentonite and X-ray Fluorescence Results from a Bentonite Block adjacent to the Steel Heater ..... 130

Figure 8-2. Scanning Electron Microscope Image of the Surface of a Reacted Low Carbon Steel Coupon Showing the Formation of Fe-Saponite and Secondary Pyrrhotite ( $Fe_{1-x}S$ )..... 131

**LIST OF TABLES**

Table 3-1. Summary of Major Aqueous Ion Chemistries of Cretaceous and Paleozoic Waters from Shale Formations ..... 48

Table 3-2. Summary of Properties of the Pierre (Ductile) and Paleozoic (Brittle) Shales..... 50

Table 4-1. Ventilation Time Results for Additional Cases ..... 65

Table 4-2. Calculated Temperatures for 40 GW-d/MT Burnup ..... 67

Table 4-3. Calculated Temperatures for 60 GW-d/MT Burnup ..... 68

Table 4-4. Peak Drift Wall and Waste Package Surface Temperature Results for the Sedimentary Open Backfilled Concept (70 m drift spacing, 20 m package spacing)..... 69

Table 6-1. Mineral Composition of Various Bentonite Buffer Options ..... 85

Table 6-2. Influence of Hydraulic, Temperature, and Chemical Gradients on Liquid, Heat, and Solute Fluxes ..... 89

Table 6-3. Thermal, Hydrological, and Mechanical Parameters for Bentonite Buffer ..... 92

Table 6-4. Upper Bound on Effective Diffusion Coefficients for Radioelements in Compacted Bentonite..... 94

Table 6-5. CEC and Exchangeable Cations for MX-80 Bentonite and FEBEX Bentonite ..... 95

Table 6-6. Cation Exchange Reaction and Corresponding Selectivity Coefficients ( $K_c$ ) for Montmorillonite..... 95

Table 6-7. Linear Distribution Coefficients for MX-80 Bentonite ( $K_d$  in  $m^3/kg$ )..... 97

Table 6-8. Recommended Radioelement Solubilities..... 98

Table 6-9. Waste Canister/Package Characteristics..... 101

Table 6-10. Waste Canister/Package Material Parameters ..... 103

Table 6-11. Temperature-Dependent Thermal Properties of Stainless Steel 316 ..... 104

Table 6-12. Initial Characteristics of Some Internal Components of the Conceptual 21-PWR/44-BWR Canister ..... 105

Table 6-13. Nominal Radionuclide Inventory at Emplacement for 21-PWR Waste Package..... 107

Table 6-14. Selected Bounding Assemblies Characteristics..... 109

Table 6-15. Radionuclide Inventory 50 years OoR for 21-PWR Waste Package Assuming Burnup-Bounded Assemblies ..... 110

## ACRONYMS

3D	three-dimensional
Andra	Agence Nationale pour la Gestion des Déchets Radioactifs (National Radioactive Waste Management Agency [France])
ALC	name of one of the experiments for DECOVALEX 2019, Task E; acronym definition unknown
BWR	boiling water reactor
CAD	computer-aided design
CASH	Ca-rich aluminosilicate hydrate
CEA	Atomic Energy Commission (France)
CEC	cation exchange capacity
COBECOMA	COrrOsion BEhavior of COntainer MAterials
CRWMS M&O	Civilian Radioactive Waste Management System Management and Operating Contractor
DECOVALEX	DEvelopment of Coupled models and their VALdation against EXperiment
DOE	U.S. Department of Energy
DOE-NE	DOE Office of Nuclear Energy
DPC	dual-purpose canister
DRZ	disturbed rock zone
EBS	engineered barrier system
EDZ	excavation-damaged zone
EdZ	excavation-disturbed zone
EIA	U.S. Energy Information Administration
EIG EURIDICE	Economic Interest Grouping for the European Underground Research Infrastructure for Disposal of nuclear waste In Clay Environment
ENRESA	Empresa Nacional de Residuos Radioactivos S.A. (Radioactive Waste Management Agency [Spain])
FEBEX	Full-scale Engineered Barrier EXperiment
FE test	proof-of-concept test
GDSA	Geologic Disposal Safety Assessment
HADES	High-Activity Disposal Experimental Site
HLW	high-level radioactive waste

HotBENT	High Temperature Effects on Bentonite Buffers
HPC	high-performance computing
HTO	tritiated water
HZDR	Helmholtz-Zentrum Dresden-Rossendorf
IAEA	International Atomic Energy Agency
IRF	instant release fraction
IRSN	Institut de Radioprotection et de Sûreté Nucléaire (Radioprotection and Nuclear Safety Institute [France])
KBS	kärnbränslesäkerhet (nuclear fuel safety); acronym used for KBS-3, a disposal concept developed in Sweden
LANL	Los Alamos National Laboratory
LBNL	Lawrence Berkeley National Laboratory
MGR	monitored geologic repository
MIC	microbially influenced corrosion
MT	metric tons
MTU	metric tons of uranium
Nagra	National Cooperative for the Disposal of Radioactive Waste (Switzerland)
NATCARB	National Carbon Sequestration Database and Geographic Information System
NBS	natural barrier system
NEA	Nuclear Energy Agency
NEA-TDB	Nuclear Energy Agency Thermochemical Database Project
NGSAM	Next Generation System Analysis Model
NRC	U.S. Nuclear Regulatory Commission
NUMO	Nuclear Waste Management Organization of Japan
NWTRB	Nuclear Waste Technical Review Board
ONDRAF/NIRAS	French: Organisme National des Déchets Radioactifs et des matières Fissiles enrichies / Dutch: Nationale Instelling voor Radioactief Afval en verrijkte Splijtstoffen  (National Agency for Radioactive Waste and Enriched Fissile Materials [Belgium])
ORNL	Oak Ridge National Laboratory
OoR	out of the reactor



---

PAMINA	Performance Assessment Methodologies IN Application
PFLOTRAN	Parallel subsurface FLOW and reactive TRANsport
PWR	pressurized water reactor
RES <sup>3</sup> T	Rosendorf Expert System for Surface and Sorption Thermodynamics
SCC	stress corrosion cracking
SCK·CEN	Belgian Nuclear Research Centre
SCM	surface complexation model
SEM	scanning electron microscope
SFWST	Spent Nuclear Fuel and Waste Science and Technology
SKB	Svensk Kärnbränslehantering AB (Swedish Nuclear Fuel and Waste Management Company)
SNF	spent nuclear fuel
SNL	Sandia National Laboratories
SS	stainless steel
TAD	transportation, aging and disposal canister
TBM	tunnel-boring machine
TDS	total dissolved solids
TED	name of one of the experiments for DECOVALEX 2019, Task E; acronym definition unknown
TEV	transport-emplacement vehicle
THC	thermal, hydrologic, and chemical
THCMBR	thermal, hydrologic, chemical, mechanical, biological, and radiological
THM	thermal, hydrologic, and mechanical
THMC	thermal, hydrologic, mechanical, and chemical
TO or TOT	clay layer combinations: T = tetrahedral Si–O sheet and O = octahedral Al–O or Mg–O sheet
TSPA	total system performance assessment
UCS	unconfined compressive strength
UDB	Unified Database
UFD	used fuel disposition
UNF-ST&DARDS	Used Nuclear Fuel – Storage, Transportation, & Disposal Analysis Resource and Data Systems

UNS	Unified Numbering System
URL	underground research laboratory
U.S.	United States
USGS	United States Geological Survey
WATSTORE	National WATer data STOrage and REtrieval system
WIPP	Waste Isolation Pilot Plant
XRD	X-ray diffraction

# DISPOSAL CONCEPTS FOR A HIGH-TEMPERATURE REPOSITORY IN SHALE

## 1. INTRODUCTION

The U.S. (United States) Department of Energy (DOE) is investigating the possibility of disposing of spent nuclear fuel (SNF) and high-level radioactive waste (HLW) in mined repositories in a variety of host rocks including salt, crystalline rocks such as granite, and clay-rich (argillaceous) sedimentary rocks such as shale. One goal of this investigation has been to develop and demonstrate the capability to conduct assessments of the potential postclosure performance of “generic” repositories based on a “reference case” description of the natural system and the engineered barrier system (EBS) design. The purpose of this report is to describe disposal concepts that can be applied to a high-temperature reference case for a generic SNF/HLW repository in shale.

Disposal of large, heat-generating waste packages containing the equivalent of 21 pressurized water reactor (PWR) assemblies or more is among the disposal concepts under investigation for a future repository for SNF in the United States. Without a long (>200 years) surface storage period, disposal of 21-PWR or larger waste packages (especially if they contain high-burnup fuel) would result in in-drift and near-field temperatures significantly higher than considered in previous generic reference cases that assume either 4-PWR or 12-PWR waste packages (Jové Colón et al. 2014; Mariner et al. 2015; 2017). Sevougian et al. (2019c) identified high-temperature process understanding as a key research and development (R&D) area for the Spent Fuel and Waste Science and Technology (SFWST) Campaign.

A two-day workshop in February 2020 brought together campaign scientists with expertise in geology, geochemistry, geomechanics, engineered barriers, waste forms, and corrosion processes to begin integrated development of a high-temperature reference case for disposal of SNF in a mined repository in a shale host rock. The results of the workshop as well as the concepts and processes forming the basis for a high-temperature shale repository reference case are described in this report.

### 1.1 Background Information

The disposal of SNF and HLW in clay-rich sedimentary rock formations has been analyzed in the U.S. and especially internationally for nearly 50 years, because such rock types are characterized by potentially favorable waste isolation properties, including low permeability, geochemically reducing conditions, and widespread geologic occurrence in generally stable tectonic environments. Shale and argillite rock formations contain a high content of clay minerals such as smectites and illites, which create conditions in which diffusive transport and chemical sorption phenomena predominate. These attributes could help impede radionuclide mobility. Although the U.S. has not conducted detailed site characterization testing in shale or argillite formations, these types of formations have been comprehensively studied through international nuclear waste repository programs as part of siting studies and underground research laboratory (URL) programs in Switzerland, France, Belgium, and Japan. These investigations, beginning several decades ago, have produced a large and fundamental body of information including site characterization data (geological, hydrogeological, geochemical, and geomechanical properties), and extensive, long-term, process testing experiments in both the natural system, and in the EBS, including clay barriers and seal materials.

#### 1.1.1 History of Shale/Argillite Repository Studies

The evaluation of nuclear waste disposal in shale formations in the United States began in the mid to late 1970s and continued until the early 1980s, when the process defined in the Nuclear Waste Policy Act of

1982 eventually resulted in the identification and selection of Yucca Mountain, and the abandonment of the second repository program. The studies were generally regional in scale and nationwide, although a number of specific sites were recommended for additional evaluation. They included extensive examinations of Mesozoic formations such as the Pierre Shale in the northern Great Plains (e.g., Shurr 1977), and Paleozoic shale formations within the Illinois, Michigan and Appalachian Basins of the Eastern U.S. (e.g., Droste and Vitaliano 1976).

The United States Geological Survey (USGS) conducted regional evaluations for DOE of potential repository host rocks on lands that were controlled by the federal government, such as the Nevada Test Site, the Hanford Reservation in Washington State, Idaho National Laboratory, and numerous other areas (Schneider et al. 1979). The USGS also performed an evaluation of clay-rich sedimentary rocks (and their slightly to moderately metamorphosed equivalents) throughout the state of Nevada (Simpson et al. 1981). Among the geologic units they identified as a potential host rock was the Eleana Formation, which also occurs on the Nevada Test Site. In one of the first U.S. field tests related to the possible disposal of HLW in shale, Sandia National Laboratories performed a Heater Experiment at a shallow depth in the Eleana Formation on the Nevada Test Site, to examine the thermomechanical response to emplacement of a heat source (Lappin et al. 1981).

U.S. studies of potential nuclear waste repositories in shale were largely suspended in the early 1980s, but siting studies, and R&D programs in URLs, continued in several international repository programs. The Swiss radioactive waste program, the National Co-operative for the Disposal of Radioactive Waste (known as Nagra) began examining disposal of SNF/HLW in clay-rich rock formations such as the Opalinus Clay in the late 1970s. The Mt. Terri Project is an international URL project focused on characterization and testing of the Opalinus Clay; it began in the 1990s and is still active today (Vomvoris et al. 2013). The underground facility is located in the Jura mountains of northwestern Switzerland.

In France, repository siting studies began in 1982, when the National Radioactive Waste Management Agency, an agency of the French Atomic Energy Commission (CEA) known as Andra, began to work with other countries (e.g., Belgium, Germany and Switzerland) to evaluate the potential for geologic disposal in various host rocks, including clay-rich shale and argillite formations. By the late 1980s, Andra scientists were conducting investigations at four sites in France in different host rocks. In December 1991, France's National Assembly adopted a law that changed Andra's status, making it independent from the CEA, and defining the process and criteria for conducting a feasibility study to determine the location and suitability of a deep geological disposal facility. Andra was given fifteen years to complete this study (Andra [no date], History). In response, Andra initiated a major research program to study disposal in a clay formation, specifically the study of the Meuse/Haute-Marne site in a Jurassic age argillaceous host rock (clay rock) known as the Callovo-Oxfordian, which is approximately 155 million years old and lies at a depth of 400 to 600 m. Andra began construction of a URL (the Meuse/Haute-Marne Centre) in 1999 near the town of Bure in parallel with the ongoing geological exploration programs.

After more than 20 years of detailed site and underground research studies, Andra published a series of documents that concluded that a repository could be safely constructed, operated and closed at the site (Andra 2015). Continuing work at the site is focused on completing the analyses required to obtain a license to construct and operate a repository at the Bure site.

In addition to Andra's extensive programs, France's independent Institut de RadioProtection et de Sûreté Nucléaire (IRSN) has operated a URL at the Tournemire experimental station in southern Aveyron for over 20 years (IRSN 2020). Located in a former railway tunnel built over 120 years ago, this station provides access to a clay formation that has similar geological characteristics to the site chosen by Andra. The facility enables IRSN to independently assess hydrologic and geochemical processes that play an important role in ensuring the long-term safety of a geological repository.

Belgium has studied the safety of a potential repository in clay-rich rocks since 1974. The Boom Clay, a poorly indurated clay of Oligocene age (approximately 30 million years old), was and still is regarded as a

potentially suitable host formation. The formation is found at a depth of 190 to 290 m below the Belgian Nuclear Research Centre (SCK·CEN) research site in Mol. In 1980 SCK·CEN began construction of the High-Activity Disposal Experimental Site (HADES) URL at a depth of about 225 m. The laboratory was extended, with the excavation of a second shaft (1997-1999) and a connecting gallery (2001–2002). Since 1995, the URL has been operated by the Economic Interest Grouping for the European Underground Research Infrastructure for Disposal of nuclear waste In Clay Environment (EIG EURIDICE), an entity formed by SCK·CEN and the Belgian National Agency for Radioactive Waste and Enriched Fissile Materials (ONDRAF/NIRAS) (EIG EURIDICE 2020).

Japan has been conducting R&D related to geologic disposal of HLW since the late 1970s. In 2000, the government passed the “Act on Final Disposal of Specified Radioactive Waste” (Final Disposal Act), which specifies deep geologic disposal of HLW, together with a stepwise site-selection process. The Nuclear Waste Management Organization of Japan (NUMO) was established to implement the siting, construction, and operation of a repository. NUMO is currently in the preliminary phases of conducting literature and geological studies to identify potential sites, and initiate the siting process. Japan also constructed the Horonobe URL (JAEA 2005) in northern Hokkaido to study and conduct R&D activities in sedimentary rocks. Surface activities at Horonobe began in 2001, with construction of the underground facilities starting in 2005. The URL host rocks are described as argillaceous, siliceous, and diatomaceous mudstones of the Miocene and Pliocene Wakkanai and Koetoi Formations (Hama et al. 2007), approximately 350 m below the surface. An extensive R&D program of geologic, hydrologic, geochemical, geomechanical, and thermal testing and coupled process modeling continues today, with numerous collaborations with other international projects (e.g., Hanamuro 2016).

In addition to Switzerland, France, Belgium and Japan, numerous other countries have considered locating a repository in clay-rich rocks. In this context, the Nuclear Energy Agency (NEA) established an international working group on argillaceous media in 1990, informally known as the Clay Club (NEA 2014). The role of the Clay Club is to examine those rock formations that are being considered for the deep disposal of radioactive waste, which range from ductile clays to brittle shales. Members include Canada, Germany, Hungary, the Netherlands, Spain, the United Kingdom, and the U.S. The Clay Club emphasizes the sharing of resources, and the synthesis and communication of knowledge, experience, and findings to various audiences.

In the U.S., DOE formed the Used Fuel Disposition (UFD) Campaign in the Office of Nuclear Energy (DOE-NE) in 2010 to evaluate alternative strategies for the storage, transportation and disposal of SNF and HLW. The alternatives included disposal in host rocks other than volcanic tuffs, specifically including salt, crystalline rocks, and clay-rich sedimentary rocks. Scientific and engineering expertise for these studies was drawn from multiple national labs, universities, and commercial sources. The first description and analysis of the performance of a generic repository in shale in the U.S. was published by Hansen et al. (2010). The performance analysis was based on a relatively simplistic model implemented in Microsoft Excel. A more detailed demonstration of performance assessment methodology for a generic repository in clay was conducted using the GoldSim modeling tool, with inputs based on the European Commission Performance Assessment Methodologies IN Application (PAMINA) project benchmark parameters, and on Andra’s Dossier 2005 Argile safety analysis (Clayton et al. 2011). A safety case for a generic deep geologic repository in argillite and other potential host rocks was described by Freeze et al. (2013).

A detailed description of a reference case for a generic U.S. repository in shale (with design and input parameters derived from the U.S. waste management program) was presented and analyzed in Jové Colón et al. (2014). Jové Colón et al. (2014) included extensive description of the data collection, experimental testing programs, and coupled process model development efforts that were being conducted to improve the performance assessment models. Mariner et al. (2015) introduced the Geologic Disposal Safety Assessment (GDSA) Framework for evaluating the performance of a range of disposal options. GDSA Framework employs PFLOTRAN (Parallel subsurface FLOW and reactive TRANsport; Lichtner et al.

2019) for multiphysics simulation and Dakota (Adams et al. 2020) for uncertainty and sensitivity analysis. The analysis included numerical simulations of a shale reference case derived from the description in Jové Colón et al. (2014). Mariner et al. (2017) presented an updated description of the reference case that included numerous model modifications and major advances in the capabilities and testing of GDSA Framework. More recently, Sevougian et al. (2019b) and Mariner et al. (2019) described several additional modifications to the reference case, as well as improvements in GDSA modeling capability, the Geologic Framework Model, and analyses of EBS configurations based on emplacement of large waste packages containing 24 and 37 PWR assemblies.

### 1.1.2 Summary of Conclusions and Recommendations from the SFWST Roadmap Update

After DOE formed the UFD Campaign in 2010, and to prepare for a future repository siting process, the Campaign formulated an R&D Roadmap that defined and prioritized R&D activities to develop, for demonstration purposes, a suite of defensible performance assessment models for generic repositories in the U.S. (DOE 2012). The Roadmap also identified the importance of re-evaluating priorities in future years. Since 2012, significant knowledge has been gained from R&D activities in the U.S. and via international collaborations, especially with countries that operate URLs. The 2019 R&D Roadmap Update (Sevougian et al. 2019c) summarized the progress of ongoing activities, re-assessed R&D priorities, and identified new activities of high priority.

For a generic repository in shale, many of the current highest priority issues (and activities) relate to the effects of introducing large, hot waste packages to the design. The higher temperatures could impact several aspects of barrier performance, including for instance, mineralogical, and geochemical changes to the EBS (the bentonite buffers) and thermal-hydrologic-mechanical changes to the shale host rocks. Testing and validation of complex coupled thermal-hydrologic-mechanical-chemical (THMC) models is more difficult at high temperatures, where multiple fluid phases are present, and reliable thermodynamic data may not be available. Such models are important for enhancing understanding of processes in the EBS such as spent fuel and waste package degradation and transport out of the waste package, and in the natural system, such as radionuclide transport. The behavior and performance of Portland cement in a high-temperature repository is also an important uncertainty (Sevougian et al. 2019c).

Many high priority activities involve collaborations with international partners, and high-temperature testing and modeling in several of the URLs, such as the DECOVALEX program (DEvelopment of COupled Models and their VALidation Against EXperiment), which is performing tests and modeling studies at the Mont Terri, Meuse/Haute-Marne and Horonobe URLs.

## 1.2 Objective and Process

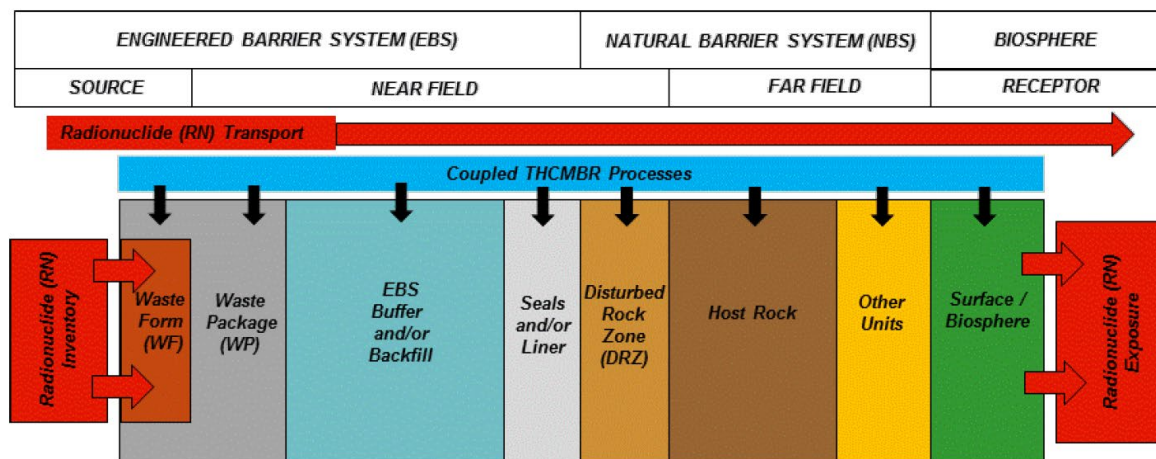
In developing concepts for a new high-temperature shale repository reference case, several objectives are accomplished. Most importantly, by bringing together scientists from across the campaign, shared concepts are developed to inform future modeling and experimental programs. Additionally, (1) the range of shale properties considered has been expanded to be more inclusive of the shale formations extant in the U.S., (2) waste package design and waste package loading consistent with Used Nuclear Fuel-Storage, Transportation & Disposal Analysis Resource and Data Systems (UNF-ST&NDARDS) database have been integrated, and (3) descriptions of features and processes have been updated to draw upon recent studies. The report systematically describes the physical system, including both the natural and engineered barriers. In describing the processes that may influence the performance of the repository, the report focuses on processes occurring in the near field and those potentially influenced by temperature. Where alternatives exist for a given feature (e.g., materials used in the EBS, such as buffers, or the waste package), the alternatives are discussed and evaluated. It is hoped that future consideration of alternatives will drive development of simulation capability and motivate experimental design to expand



understanding of the potential influence of temperature on repository performance and understanding of material and design choices that can mitigate the influence of temperature.

### 1.3 Postclosure Technical Basis

A reference case description of a generic deep geologic repository system and the processes acting within the system forms the technical basis for a generic post-closure performance or safety assessment (OECD 2004). A deep geologic repository system consists of an EBS, the natural barrier system (NBS) and the biosphere (Figure 1-1). A barrier is any feature that prevents, limits, or delays the release of water and/or radionuclides to the biosphere. The EBS includes the waste form, the waste package and the engineered features that are relied on to contain or limit radionuclide releases. The NBS consists of the host rock in which the geologic repository is located and the geologic units above and below the host rock.



NOTE: THCMBR = thermal, hydrologic, chemical, mechanical, biological, and radiological.

Source: Freeze et al. 2013, Figure 2-1.

**Figure 1-1. Components of a Generic Disposal System**

The disturbed rock zone (DRZ) is the portion of the host rock that experiences durable (but not necessarily permanent) changes due to excavation and emplacement of heat-generating waste. Examples of phenomena that could impact the performance of the system at a high level include waste form and waste package degradation; coupled thermal, hydrologic, chemical, mechanical, and biological processes occurring in the subsurface; and radionuclide transport through the EBS and the NBS to the biosphere (Freeze et al. 2013). The biosphere, which is not addressed in this report, is where the receptor lives, the receptor’s lifestyle and the characteristics of that environment.

Defense in depth is provided by the multiple barriers in the repository system. Engineered barriers are designed to complement the natural barrier system so that the repository system as a whole contains multiple, layered defenses preventing or limiting radionuclide transport to the biosphere. This report provides alternatives to be considered for both the NBS and the EBS, including a spectrum of host rock properties, alternative backfill/buffer materials, alternative overpack materials, and alternative waste package loading schemes. Depending on specific choices made in building a reference case for demonstration of performance assessment methodology, different features of the reference concept may be called upon to perform differently. For instance, in an endmember ductile shale, creep deformation would be expected to heal fractures, thus minimizing the permeability of the host rock and reducing reliance on the overpack and the backfill to contain or retard radionuclides. In a host rock with some

ability to sustain fractures, the repository concept may have greater reliance on a corrosion-resistant overpack and a low-permeability, swelling buffer to provide defense in depth.

Both siting and design of the repository system are expected to contribute to the performance of a high-temperature repository in a shale host rock. A number of criteria exist for assessing the suitability of a shale location, including depth and thickness of the host rock horizon, seismic inactivity, structural simplicity, minimal topographic relief (which minimizes hydraulic gradients), and minimal exploitable natural resources in the subsurface (Shurr 1977). Intact shale has low permeability and high-sorption capacity, both of which retard radionuclide transport. At depth, a geochemically reducing environment limits metal corrosion rates, SNF dissolution rates, and reduces radionuclide solubility. Although the specifics of the EBS design will depend on the characteristics of the host rock, the waste package, waste form (fuel and cladding), and backfill/buffer will perform to some degree the following functions. The waste package will prevent water from contacting the waste form until the package fails, and then may provide some means of delaying the release of radionuclides depending on the failure mode. The waste form cladding may limit the amount of water contacting the waste form and the slow dissolution rate of the waste form will limit radionuclide releases to the buffer. Resistance to flow and sorption within a clay-rich backfill/buffer will retard radionuclide transport. Backfill/buffer also serves to protect waste packages from mechanical damage due to rock fall or ground motion.

## 2. GEOLOGIC SETTING OF MAJOR SHALE DEPOSITS IN THE U.S.

Conceptual models of the geologic environment and host rock for the shale reference case have been based primarily on properties of the Mesozoic Pierre Shale of the Northern Great Plains and European formations (Jové Colón et al. 2014; Perry and Kelley 2017; Mariner et al. 2017; Sevougian et al. 2019b). Shales in the U.S. encompass a wide range of mineralogical composition, mechanical properties, and fracture characteristics. Compared to other shales in the U.S., the Pierre Shale has higher clay content, low compressive strength and behaves as a more ductile rock that is resistant to fracturing. In terms of these properties, it can be considered a shale endmember.

A second shale endmember can be conceptualized as stronger shale that is more brittle and prone to fracturing. Examples of the second endmember are the regionally extensive Paleozoic shales found in sedimentary basins in the eastern and midwestern U.S. interior (Eastern Interior region of Gonzales and Johnson 1985). As a group, these shales have lower clay content and higher compressive strength than the Pierre Shale. Consideration of both ductile and more brittle shale in the shale reference case is intended to better represent the range of mineralogical and material properties found in shale formations of the U.S.

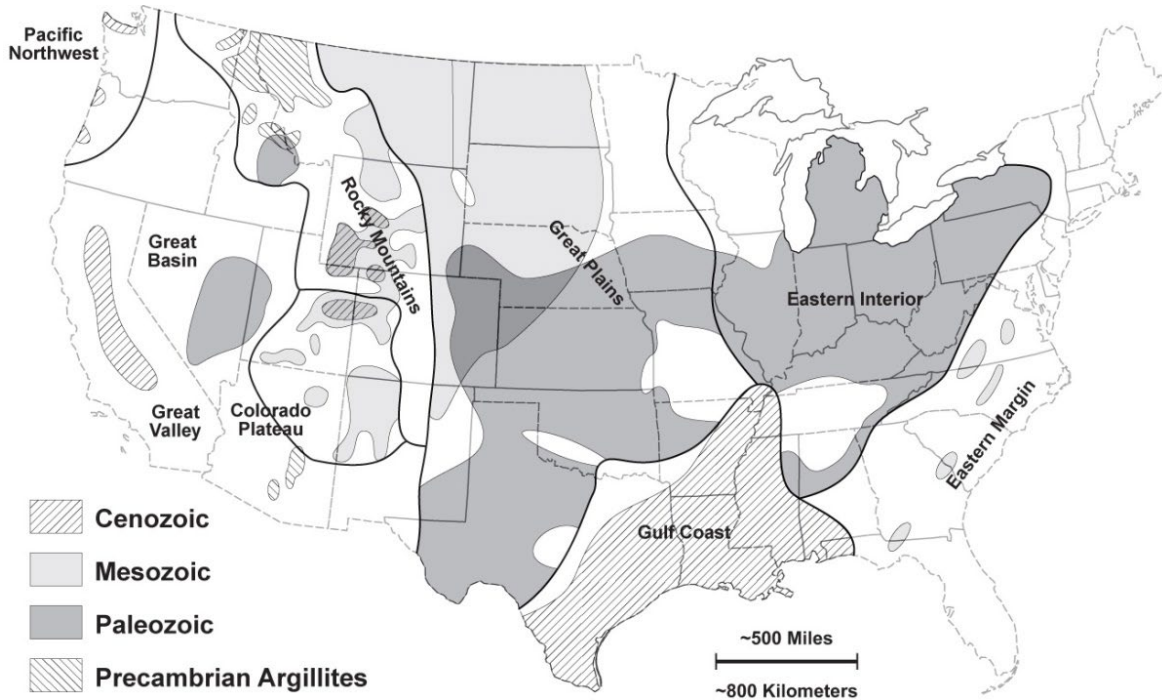
### 2.1 Overview of Shale Deposits in the U.S.

Shale is the most common type of sedimentary rock and occurs throughout the U.S. (Figure 2-1). The distribution of shale largely reflects the paleogeography of continents and seas over the last several hundred million years of geologic time. Shale deposits that are flat lying or with low dips generally indicate a region that has undergone limited tectonic activity (Gonzales and Johnson 1985). Tectonically stable areas often coincide with large sedimentary basins that preserve thick shale deposits over long periods of geologic time.

For the shale reference case, we focus on two major shale populations of the U.S: Mesozoic (Cretaceous) shale of the northern Great Plains and Paleozoic (mostly Devonian-Mississippian) shale of the Eastern Interior region (Figure 2-1). The Mesozoic Pierre Shale has historically been a focus of repository shale studies in the U.S. because of its large regional extent, great thickness, and high clay content (Shurr 1977). Because of its high clay content and low degree of induration, the Pierre Shale has low compressive strength and behaves as a ductile material with fracture-sealing properties (Nopola, 2013; Bourg 2015).

Paleozoic shale formations within the Illinois, Michigan, and Appalachian Basins of the Eastern Interior region comprise the second regionally extensive population of shales that have been considered as potential repository host rocks (Droste and Vitaliano 1976; Lomenick et al. 1983; Gonzales and Johnson 1985; Figure 2-2). In contrast to the Pierre Shale, these shales have lower clay content and higher strength, and they behave as a more brittle material as indicated by natural fracture systems.

A feature of shale formations not heavily emphasized in previous conceptual models is that shales are anisotropic layered systems. Differences in the mineralogy (sometimes subtle) and mechanical properties of different layers can control the fracture frequency and characteristics within individual layers (Gross 1995; Gale et al. 2014). The observation that fracture systems are influenced by layering within shale deposits indicates the need to model flow and transport using modeling methods that take these features into account.



Source: Gonzales and Johnson 1985; figure taken from Hansen et al. (2010).

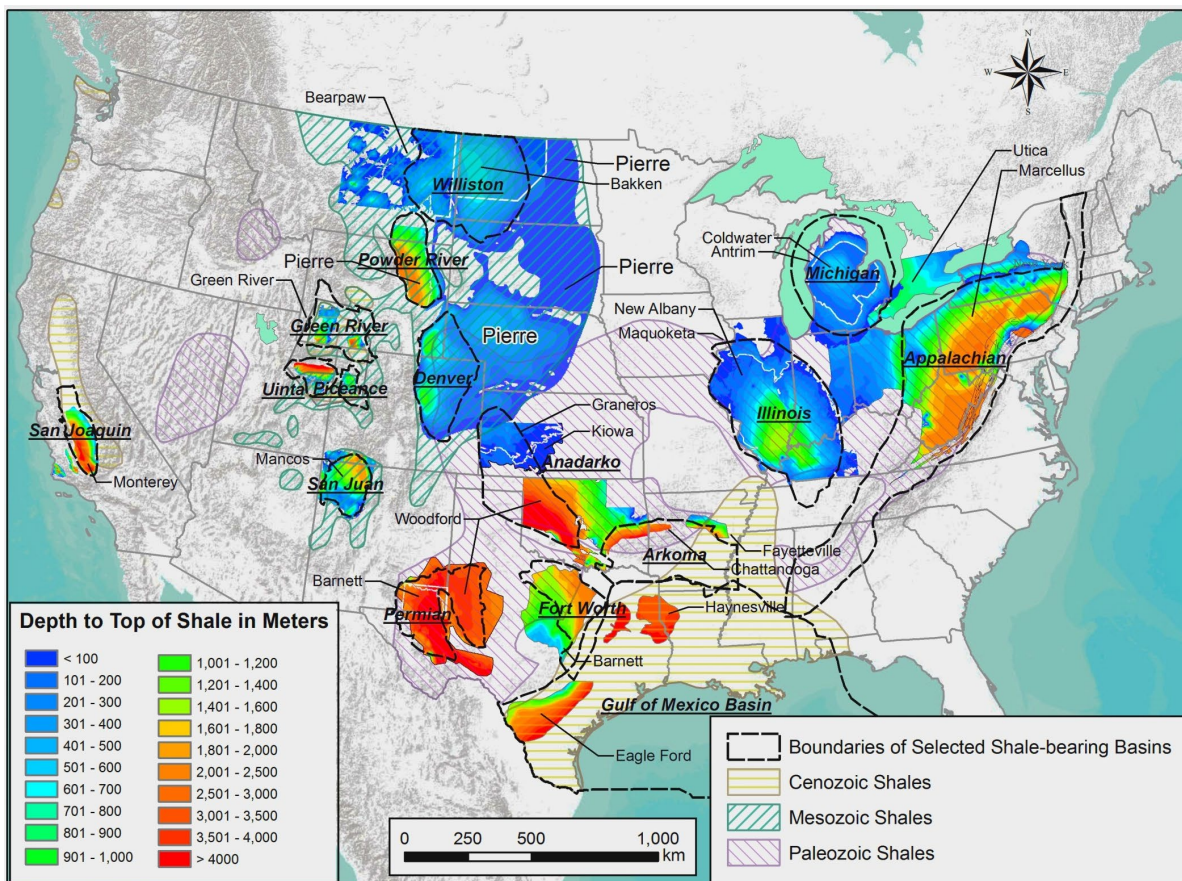
**Figure 2-1. Shale Provinces in the U.S.**

## 2.2 Depth and Thickness of U.S. Shale Formations

Shale formations are typically deepest in basin interiors and shallowest near basin margins (Figure 2-2). The largest regional extents of shale formations with tops that lie at or near the surface (<100–200 m) are the Mesozoic shales of the northern Great Plains (which includes the Pierre) and the Colorado Plateau and the Paleozoic shales of the Eastern Interior region (Figure 2-2; Perry and Kelley 2014). Based on a repository reference depth of  $500 \pm 200$  m, these regions contain shale formations (especially at basin margins) within an appropriate depth range. The depth of shales in both regions can approach or exceed 1,000 m in the deepest parts of basins (Figure 2-2). Paleozoic and Mesozoic shales of the southern Great Plains and Gulf Coast region typically lie at depths of 1,000 to >3,000 m, effectively ruling out these shales as potential host rocks.

The Pierre Shale is one of the thickest shale formations in the U.S. with a thickness of 200–600 m over large areas of its extent (Perry and Kelley 2014). Paleozoic shales in comparison are typically between 100–150 m thick (maximum ~300 m) in areas where the formations are at an appropriate depth of <700 m (Droste and Vitaliano 1976; Gonzales and Johnson 1985; Perry and Kelley 2014). The thickness of the Paleozoic shales is similar to shale formations being considered as repository host rocks in France, Switzerland and Belgium, which range from 100–160 m (Hansen et al. 2010).





Source: Modified from Perry and Kelley (2014).

Figure 2-2. Selected Shale Formations and Sedimentary Basins showing Depth to Top of Shale

### 2.3 Overview of Shale Diagenesis, Burial Depth and Mechanical Properties

Shale forms through complex geologic and geochemical processes that begins with deposition of clay and clastic particles in marine basins followed by compaction and induration by burial and cementation (Gonzales and Johnson 1985; Bock et al. 2010). Uplift and erosion of overlying sediments brings shale to a shallower depth (<1,000 m) that is appropriate for disposal of SNF and HLW.

The burial, compaction and uplift/erosion history of shale, along with their mineralogy, dictates in large part the degree of induration, mechanical properties and ductile/brittle behavior (Bock et al. 2010). In general, shale that has been deeply buried during compaction and diagenesis will be more indurated and brittle at a shallower depth following uplift and erosion.

Shale that is currently at a shallower depth than its maximum burial depth in the past is referred to as overconsolidated. The overconsolidation ratio is the ratio of the past maximum vertical stress (maximum burial depth) to the present vertical stress. The state of stress in overconsolidated shale can lead to brittle failure at a lower confining stress (Bock et al. 2010). Therefore, a shale formation that has experienced a greater maximum burial depth would be expected to behave as more brittle shale at typical repository depths. This has been well documented through comparison of shales studied in European repository programs where maximum burial depth is correlated with degree of induration, density and compressive strength (Bock et al. 2010, Table 2-3).

Analysis of geologic relationships between the Pierre Shale presently near the surface and the reconstructed thickness of overlying sediments indicates erosion and removal of 180–340 m of overburden in the Northern Great Plains (Rice 1987). In comparison, the maximum burial depths of Paleozoic shales indicate a higher degree of overconsolidation. Maximum burial depths are estimated at >600 m for the New Albany Shale and 1,800 m for the Antrim Shale (Thomas et al. 1980; Apotria et al. 1994). This is consistent with greater induration, compressive strength and brittle behavior of the Paleozoic shales compared to the Pierre Shale.



### 3. NATURAL BARRIER SYSTEM

The NBS includes the lithologic, mineralogical and hydrologic properties of the host rock and the properties of the stratigraphic sequence that lies above and below the host rock. As discussed in the previous section, the variations in properties of shales in the U.S. can be framed as two shale endmembers: a weak ductile shale with high clay content and fracture-sealing properties, and a strong brittle shale with lower clay content that is able to sustain fractures. Although this approach may oversimplify the possible range of properties found in shale, it provides a framework to conceptualize a wide range of observed shale properties for the shale reference case.

#### 3.1 Stratigraphic Framework for Ductile and Brittle Shales

Representative stratigraphic columns for the Pierre Shale and Paleozoic shales of the Eastern Interior Province are shown schematically in Figure 3-1 (Noger and Drahovzal 2005; Ellis 2013; Sevougian et al. 2019b). The main differences between the stratigraphic columns associated with the two shale populations are the thicknesses of the shale formations and the proportions of carbonate rocks.

The thickness of the Pierre Shale represented in the stratigraphic column in Figure 3-1 is between 400 and 600 m (Sevougian et al. 2019b). Shale formations below the Pierre Shale have a cumulative thickness similar to the Pierre. Shale units of interest in the Illinois Basin (New Albany) and the Michigan Basin (Antrim and Ellsworth) have typical thicknesses of between 75 and 150 m, similar to the thicknesses of shales being considered for disposal in Europe (Hansen et al. 2010).

Carbonate formations make up a larger proportion of the stratigraphic column in the Illinois and Michigan Basins. Aquifer-bearing formations therefore make up a more significant portion of the overall stratigraphic sequences. The proportion of carbonates in the upper 1,500 m of the stratigraphic column of the Pierre Shale is approximately 10%, while the proportion of carbonates in the upper 1,500 m in the northern Michigan Basin and southern Illinois basin is 50% and 80%, respectively (Figure 3-1).

A detailed description of the stratigraphic column associated with the Pierre Shale is presented in Perry and Kelly (2017) and Sevougian et al. (2019b). A more detailed description of the stratigraphy and groundwater systems associated with Paleozoic shales is presented in LaForce et al. (2020).

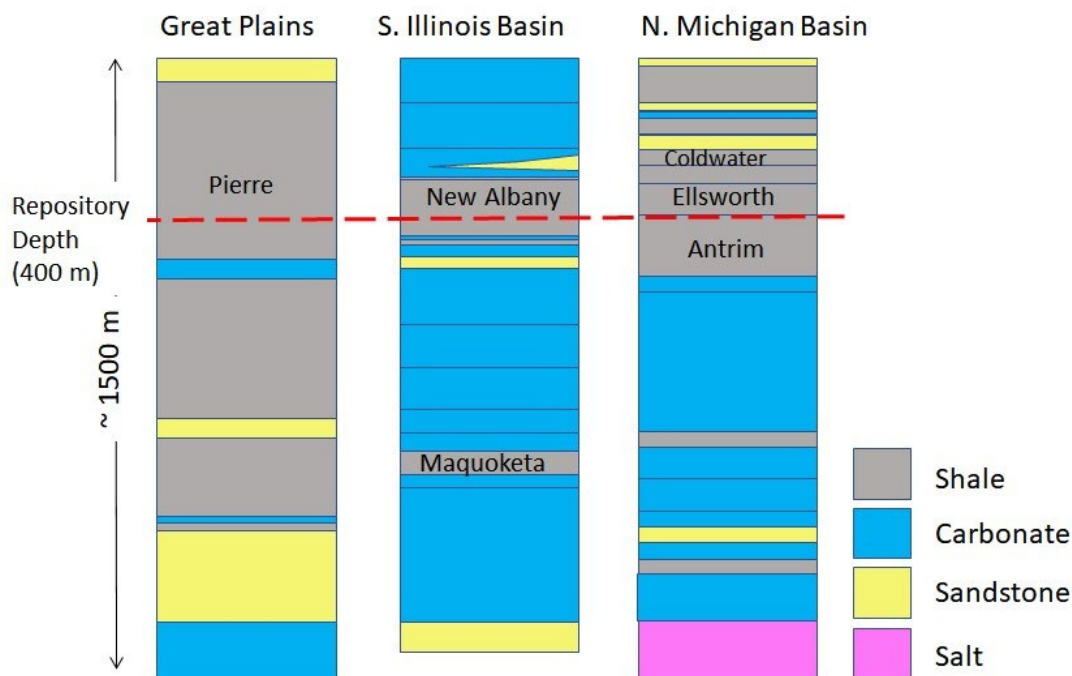


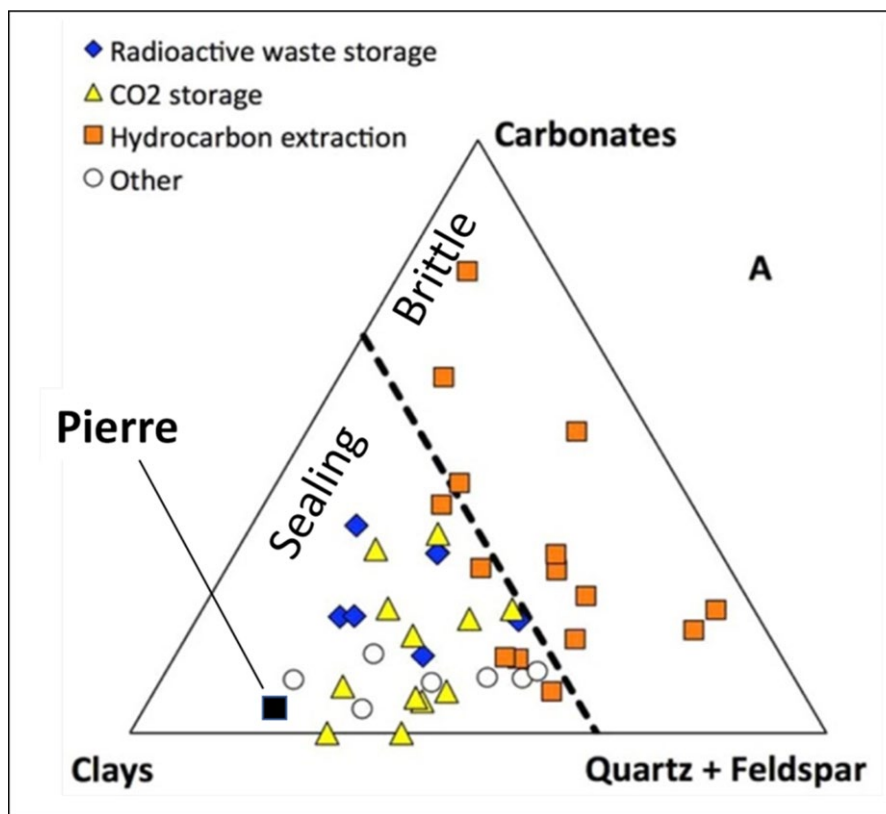
**Figure 3-1. Schematic Representation of the Stratigraphic Columns in Representative Areas of the Northern Great Basin, Illinois, and Michigan Basins**

## 3.2 Properties of Ductile and Brittle Shales

### 3.2.1 Relationship of Mineralogy to Mechanical Properties

The broad term “shale” is defined as a fine-grained sedimentary rock composed of clay- and silt-sized mineral grains (Hansen et al. 2010; Crandell 1958; Schultz et al. 1980). While shale is fissile or laminated, we do not distinguish it from nonlaminated mudstone and claystone in the context of a host rock for the shale reference case.

Major mineral constituents of shale are clay, quartz/feldspar, and carbonate (often as intergranular cement), each of which can constitute from 20% to 80% of the rock (Figure 3-2). This illustrates the wide range of mineral compositions found in different shale formations. Depending on clay content and sealing behavior, shale formations are suitable for hydrocarbon extraction, carbon capture and storage seals, or radioactive waste disposal (Bourg 2015). Shales considered for radioactive waste disposal typically contain greater than 40% clay minerals, 20%–55% quartz/feldspar and 0%–30% carbonate (Figure 3-2). High clay content in shales contributes to low permeability, high sorption capacity, and sealing of fractures (Hansen et al. 2010). Higher quartz content indicates lower sorption capacity, higher compressive strength, and greater brittleness. Note that mineralogy of a shale formation can be highly variable (data points on Figure 3-1 are intended to portray “typical” or “average” values) and that lithologic subunits within a shale formation therefore can have variable mechanical properties.



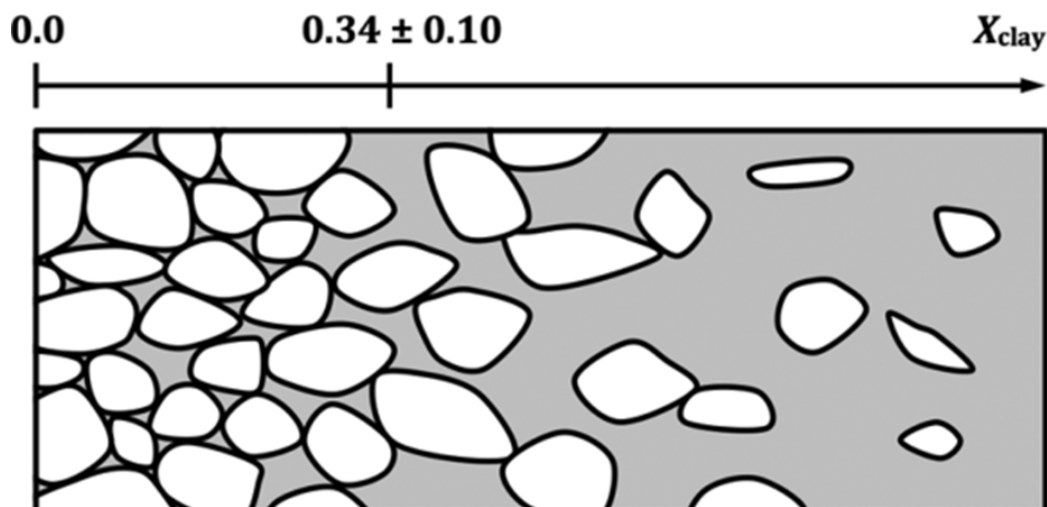
NOTE: The composition of the Pierre Shale is shown for comparison.

Source: Bourg 2015.

**Figure 3-2. Mineral Compositions of Well-Characterized Shale by Intended or Proposed Use**

Bourg (2015) presents a conceptual model of shale properties based on whether the shale microstructure consists of a load-bearing matrix of quartz and feldspar (strong minerals) in grain-to-grain contact or a weaker load-bearing matrix with a higher clay content (Figure 3-3.). Based on a world-wide sampling of well-characterized shales, Bourg (2015) showed that, above a clay content of approximately 1/3, shales show a sharp decrease in compressive strength and a transition to ductile deformation and sealing behavior over brittle deformation (Figure 3-4). This transition is accompanied by a decrease in permeability and an increase in porosity (Figure 3-4).

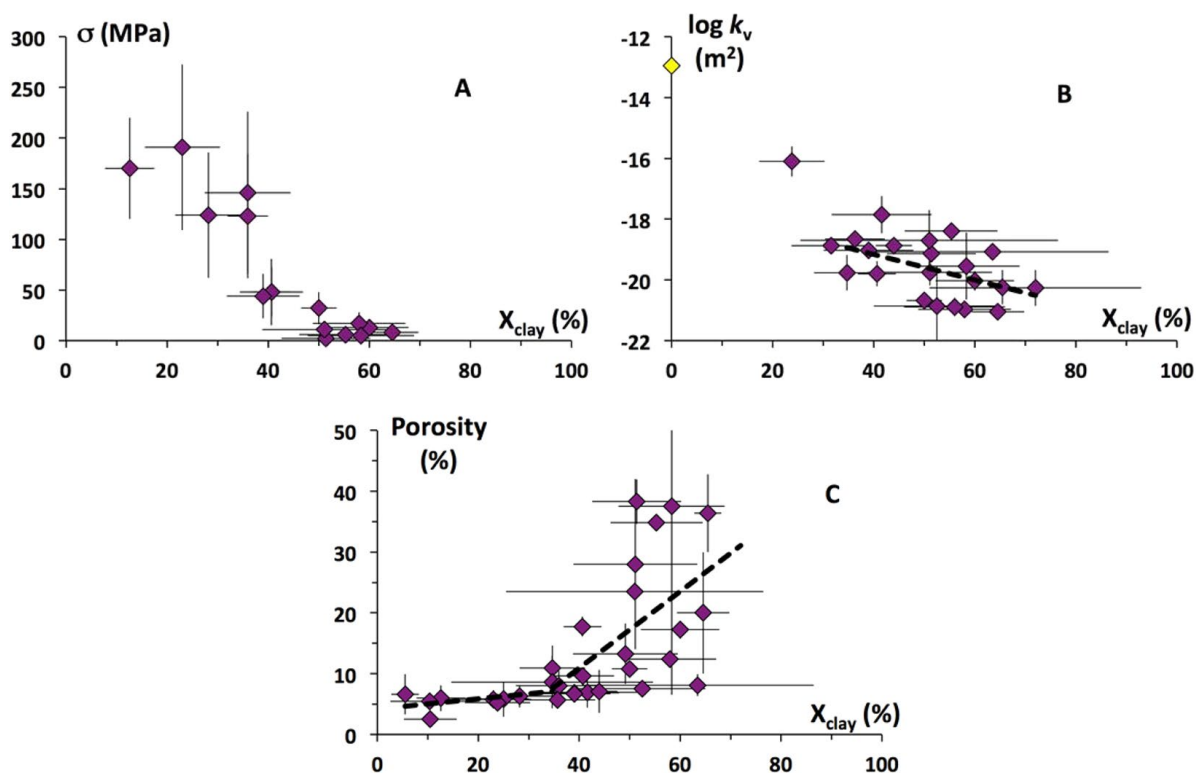
Shale formations in the U.S. show the same relationship between clay content and compressive strength (Figure 3-5). The main lithologic type of the Pierre Shale has between 70% and 80% clay that is primarily smectite (Schultz et al. 1980). Quartz and feldspar make up about 20% of the rock and carbonate about 5% (Figure 3-5). The high clay content of the Pierre Shale places it at the 90<sup>th</sup> percentile of all shales (Neuzil 2000). Paleozoic shales have lower clay content ranging from about 40% to 50%. Combined quartz and feldspar range from 45% to 55% and carbonate from 5% to 10% (Figure 3-5).



NOTE: The structure is made of strong grains such as quartz (white) and weaker clay (gray). Clay fraction increases from left to right.

Source: Bourg 2015.

Figure 3-3. Conceptual Model for Shale Microstructure



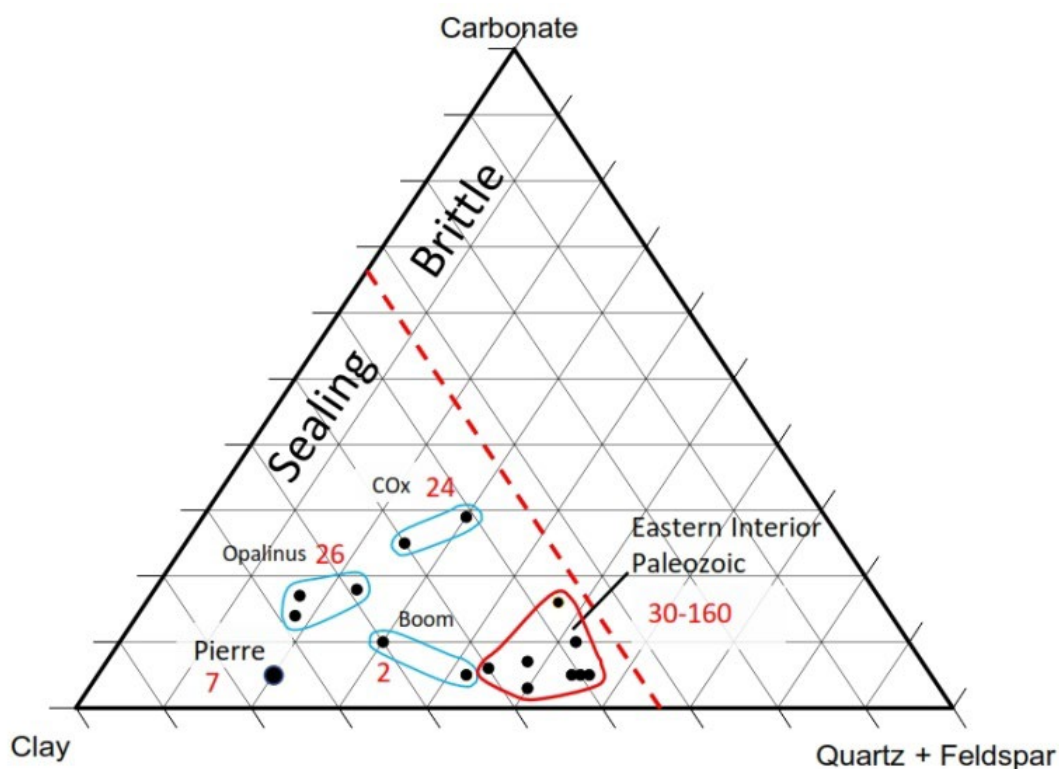
Source: Bourg 2015.

Figure 3-4. (A) Compressive Strength, (B) Log Permeability, and (C) Porosity Versus Clay Content for Well-Characterized Shales

The difference in compressive strength for the two shales correlates to clay content. Hansen et al. (2010) report the compressive strength of the Pierre Shale as 7 MPa (see also Nataraj 1991). Abel and Gentry (1975) report the range of compressive strength for the Pierre Shale as 0.5–18 MPa. In more recent laboratory studies, Zhou et al. (2010) suggest values of 30–40 MPa for the Pierre Shale may represent an upper boundary of compressive strength due to biased sampling of only the most indurated rock.

The Paleozoic shales with lower clay content have compressive strength ranging from approximately 55 to 160 MPa (Kim 1978; Nuttal 2013; Pena 2015). Measurements of the compressive strength of 33 core samples from the Antrim Shale encompass this entire range of values demonstrating the wide variation in mechanical properties that is possible within a single shale formation (Kim 1978).

By comparison, European shales (Boom, Opalinus and Callovo-Oxfordian) have clay contents that are lower than the Pierre Shale but, except for the Callovo-Oxfordian Claystone, higher than the Paleozoic shales (Figure 3-5). The Boom Clay is unconsolidated and behaves as a ductile material while both the Opalinus Clay and Callovo-Oxfordian are brittle shales that still have capacity for fracture sealing over long time periods (Volckaert et al. 2004).



NOTE: Numbers in red are values for unconfined compressive strength.

Source: The boundary between sealing shales and brittle shales at 33% clay content is from Bourg (2015).

**Figure 3-5. Mineral Compositions of the Pierre Shale, Paleozoic Shales of the Eastern Interior Basins, and European Shales Considered for HLW Disposal**

### 3.2.2 Relationship of Mineralogy to Mechanical Properties

Understanding the characteristics of fracture systems and potential sealing behavior of ductile and more brittle shales is key to understanding flow and transport in fractured shale. This section summarizes the key characteristics of fracture systems in shales.

### 3.2.2.1 Fracture Systems in Shales

Fractures are present in most shale formations with fracturing more common in shales with lower clay content (Gale et al. 2014; Bourg 2015). Most shale formations have lithologic subunits with different mineralogical compositions. These differences can lead to differences in mechanical behavior and fracture abundance within the subunits (members) of a shale body (Gross 1995; Gale et al. 2014). Differential tectonic stresses within the regional extent of a shale formation can also lead to differences in fracture abundance at different locations.

#### The Pierre Shale

Few studies address fracturing in the Pierre Shale. Although fractures and fracture zones have been documented, the formation is generally considered to be relatively unfractured compared to other shales in the U.S. At a site in central South Dakota, Nichols and Collins (1986) documented two subhorizontal fracture zones in the Pierre Shale in a 180 m deep borehole at depths of 70 and 90 m. No fractures were observed between depths of 39 and 70 m and eight isolated fractures were observed between depths of 22 and 39 m (below the depth of the weathered zone). Most of the isolated fractures had dips of greater than 45° as opposed to the more horizontal fractures in the fracture zones. The fractures show no evidence of alteration or interaction with water indicating that they are not transmissive, even though the shale at these depths is saturated (Nichols 1992). The subhorizontal fracture zones are interpreted as rebound-induced unloading fractures caused by erosion of overlying overburden (Nichols 1992).

In the same study area, Neuzil (1993) measured a low-pressure fluid anomaly in the Pierre Shale centered within the middle of the formation at a depth of ~150–175 m. Preservation of the anomalous pressure requires the shale to have maintained very low permeability for a long time period as the formation underwent unloading from erosion of the overlying rock. Although the extent of the area affected by the pressure anomaly is not certain, it is probably on the scale of at least hundreds of meters. This indicates that the shale volume does not have transmissive fractures (which would allow fluid movement and equilibration of the pressure) and that fluid flow is predominantly by matrix flow in very low permeability rock.

Prior to the work of Neuzil (1993), Bredehoeft et al. (1983) presented a regional groundwater flow model and concluded that vertical leakage from the underlying sandstone aquifer into the overlying shale constituted the dominant flow within the groundwater system. Hydraulic conductivity estimated from the model indicated a regional permeability of the shale confining layer that is 2–3 orders of magnitude higher than permeability measured at the core or borehole scale (Bredehoeft et al. 1983). These differences were reconciled by hypothesizing that flow through the shale was primarily through widely separated vertical fracture zones (scale of kilometers), while lower permeability measured at smaller scales indicated intervening blocks of intact shale (scale of hundreds of meters) that do not contain transmissive fractures.

#### Paleozoic Shales of the Eastern Interior Region

The Paleozoic shales of the eastern interior basins are more extensively fractured than the Pierre Shale, consistent with their lower clay content and higher quartz content (Gale et al. 2014). Fracture frequency and other fracture properties vary considerably within brittle shale formations resulting in large variations in permeability (Gale et al. 2014). Higher fracture frequency and permeability in a brittle shale formation is closely tied to areas of high gas and oil production, while the converse is true for parts of the shale formation that are less fractured (Ryder 1996; Gale et al. 2014). For purposes of the shale reference case and repository siting, we assume that the most fractured and permeable regions of shale formations would be avoided in favor of less fractured shale with permeability values that fall within the lower part of the range.

Like the Pierre Shale, fractures are likely not uniformly distributed throughout the shale formations but concentrated in particular areas due to tectonic stresses or within stratigraphic horizons of different



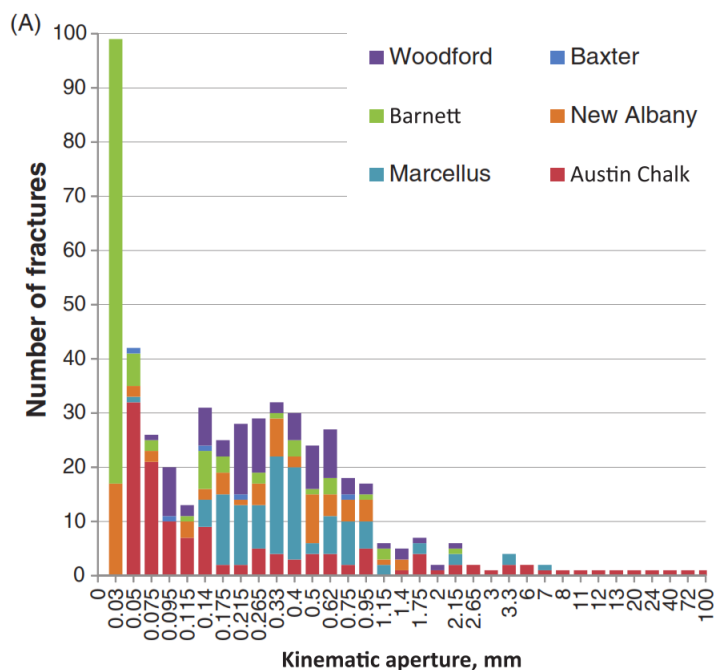
mineralogy and mechanical properties (Nichols et al. 1994; Gale et al. 2014). For example, the main gas-producing area of the Antrim/Ellsworth Shale, in a relatively small region of the northern Michigan Basin, coincides with a region of the formation that is highly fractured and at relatively shallow depth (~300–600 m; Ryder 1996). Vertical wells drilled into the producing zone typically produce water for a short period of time indicating interconnected fractures at depth.

Fracture permeability in shales depends primarily on fracture intensity, connectivity, length, and aperture (Gale et al. 2014). These characteristics are generally hard to estimate from subsurface data (particularly connectivity and length), and it cannot be assumed that fracture characteristics observed in outcrops correspond to characteristics in the deep subsurface (Gale et al. 2014).

Gale et al. (2014) present new observations and a review of previous studies concerning natural fractures in shales. These shales include Paleozoic formations in the Illinois, Michigan, and Appalachian Basins. We focus on the Antrim/Ellsworth (Michigan Basin) and New Albany Shales (Illinois Basin) as representative of brittle and fractured shales of appropriate depth and thickness to be considered for SNF and/or HLW disposal. Briefly, the characteristics of fractures in these shales are as follows:

- The dominant fracture sets are vertical or subvertical, but horizontal or subhorizontal bedding plane fractures are also relatively common (Gale et al. 2014). In the Antrim Shale, for example, 95% of fractures are vertical or subvertical (Ryder 1996).
- In both the New Albany and Antrim Shales, the most prominent vertical fracture sets are often present as near-orthogonal pairs, thereby increasing the likelihood of fracture connectivity (Ryder 1995; Gale et al. 2014).
- Fracture length, which is difficult to ascertain because of limitations of outcrop exposures or core dimensions, is on the order of tens of meters or more (Gale et al. 2014).
- Based on core measurements, fracture height for the New Albany Shale ranges from 10–25 cm, although the true height may be much greater (Gale et al. 2014).
- Fracture aperture in the New Albany Shale ranges from 0.03 to 1 mm (Gale et al. 2014; Figure 3-6). Fracture aperture in the Antrim Shale is similar ranging from 0.001 to 0.75 mm (Ryder 1996).
- Fracture spacing in both the Antrim Shale and the New Albany Shale is typically between 0.5 and 2 m (Ryder 1996; Gale et al. 2014).

Shale formations are anisotropic with bedding planes and lithologic layering. Lithologic layering reflects different mineral compositions that can impart different mechanical behavior and fracture characteristics (Gross 1995; Laubach et al. 2009; Gale et al. 2014). Fracture systems often display a fracture stratigraphy, wherein fracture frequency, length, and terminations are influenced by the mechanical properties of layers and the interfaces between layers (Figure 3-7). Characterizing a particular shale in terms of fracture stratigraphy may be difficult without detailed site studies. If fracture stratigraphy is present in shale formations, incorporating vertical changes in fracture characteristics will be important in modeling groundwater flow through the fracture system. A method for modeling discrete fracture systems in layered media has been described in Jové Colón et al. (2014; Section 3.2, Part II). Such methods may be appropriate for simulating flow and transport in shale with fracture stratigraphy.

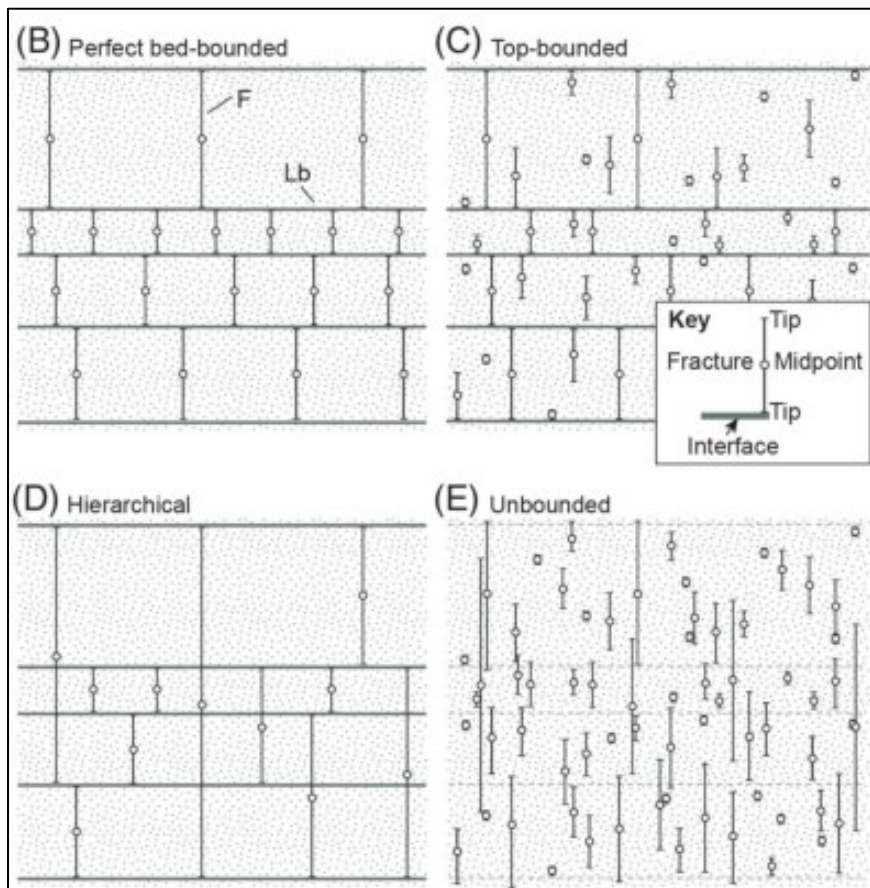


Source: Gale et al. 2014.

**Figure 3-6. Fracture Aperture-Size Distribution for Selected Shales**

Large variations (both vertically and horizontally) in fracture frequency are characteristic of Paleozoic shale formations. Localized areas of higher fracture frequency and permeability are manifested as zones of high gas production (Ryder 1996; Gale et al. 2014). Most producing natural gas zones have been identified by the oil and gas industry and can be avoided for potential repository siting in favor of areas of less permeable shale. The presence of vertical fracture stratigraphy also presents the possibility that less permeable stratigraphic horizons could be targeted for repository siting as discussed in LaForce et al. (2020).





NOTE: Panel B is an example of fracture heights perfectly bounded within mechanically distinct layers. Panel E is an example of fracture heights that are independent of layering. Panels B (bed bounded) and D (Hierarchical) are the most commonly observed patterns in shale.

Source: Gale et al. 2014.

**Figure 3-7. Examples of Fracture Layer (bed) Boundedness and Fracture Stratigraphy in Shales**

### 3.2.2.2 Fracture Self-Sealing

Self-sealing refers to the capacity of transmissive fractures to become closed and nontransmissive over time (Bock et al. 2010). Self-sealing of fractures in shale can occur in both natural fractures and fractures induced by repository construction. Fractures sealing occurs by four main mechanisms (Bock et al. 2010):

1. Mechanical closure of fractures due to lithostatic stress acting normal to the fracture or to ductile creep of fracture walls
2. Swelling of clays along fracture walls
3. Deposition of colloidal particles that clog fractures, a mechanism thought to have limited sealing potential
4. Precipitation of minerals on fracture walls (mineral fracture fillings)

It is generally accepted that shales with high clay content like the Pierre Shale will self-seal on relatively short time scales (decades) because of their weaker clay-supported matrix (Bock et al. 2010; Nopola 2013; Bourg 2015). One caveat to this generalization is that widely spaced vertical fracture zones have been proposed to account for cases in which regional-scale permeability is apparently several orders of magnitude higher than values measured for intact shale (Bredehoeft et al. 1983; Neuzil 1993).

Self-sealing of shales with the properties of the Paleozoic shales is less certain. Over long time frames, some fractures are clearly sealed by mineral precipitation (Gale et al. 2014). Over shorter time frames, swelling or ductile creep of fracture walls is a more likely sealing mechanism (Bock et al. 2010). It is not clear at exactly what threshold of physical parameters (e.g., clay content, mechanical strength) the sealing of fractures will occur. Undoubtedly, sealing behavior depends on the clay content of the shale. Bourg (2015) suggests a threshold at about  $33\% \pm 10\%$ , which places some of the Paleozoic shales within the field of sealing shales (Figure 3-5). Bock et al. (2010), based on studies at European URLs, suggests a threshold of 40% clay for self-sealing to occur. The Opalinus and Callovo-Oxfordian Clays are within the sealing field (40%–70% clay content) and yet deform in a brittle manner. Tunnels that pass through the Opalinus Clay show no water inflow where the overburden is greater than 200 m even though faults are present, indicating that fractures have sealed at depth, probably because of lithostatic stresses (Bock et al. 2010). The Paleozoic shales considered here have clay content of 35%–50%, placing them near the proposed threshold for expected capacity to self-seal based on clay content and ductility (Figure 3-5). Both open and closed fractures are observed in most of the Paleozoic shales, although closed fractures are typically sealed because of mineralization (Gale et al. 2014). As described previously, gas production differs among the members of the Antrim Shale, correlating with fracture frequency, transmissivity, and connectivity (Ryder 1996).

### 3.2.3 Hydrologic Properties

#### 3.2.3.1 Permeability

Permeability of shales in the absence of fractures decreases with increasing clay content (Bourg 2015; Figure 3-4). Based on a large body of previous work, Neuzil (2000) states that the permeability of the Pierre Shale in central South Dakota is between  $10^{-20}$  and  $10^{-21}$  m<sup>2</sup> (see review in Perry and Kelley 2017). Numerous measurements of shale permeability from localities around the world indicate a range from  $10^{-18}$  to  $10^{-21}$  (Bourg 2015; Neuzil 2019).

Bourg (2015) presented a relationship between clay content and permeability using data from 23 shales and siltstones (not including the Pierre Shale). A linear fit to these data yields the formula  $\log k_v = -17.5 - 0.042 (X_{\text{clay}})$ , where  $X_{\text{clay}}$  is the estimated percent clay in the formation. Using this relationship, the Pierre Shale, with clay content of between 65% and 85% (Schultz et al. 1980), has a calculated permeability of between  $10^{-20}$  and  $10^{-21}$  m<sup>2</sup>, consistent with numerous measurements from laboratory or borehole experiments (e.g., Neuzil 1993). For Paleozoic shales with clay content of 40% (Figure 3-4), this linear relationship predicts a permeability of  $10^{-19}$  m<sup>2</sup>.

Estimating the permeability of fractured shale is challenging because of uncertainty in the characteristics of fracture systems at depth (Gale et al. 2014). It is evident that fractures in Paleozoic shales can be either transmissive or closed because of mechanical processes (lithostatic confining stress, creep) or mineralization. Open or closed fractures can be present in different parts of the same formation, with closed fractures typically mineralized (Gale et al. 2014). From observations and studies of a number of fractured shales, Gale et al. (2014) conclude that fractures are likely to be concentrated in clay-poor, mechanically strong horizons and that there may be considerable variability in abundance and size of fractures in different layers (members) of a single shale formation. Ryder (1996) describes different members of the Antrim Shale where higher quartz content is correlated with higher fracture frequency, permeability, and gas production (see discussion in LaForce et al. 2020).

Experimental studies aimed at understanding fracture and sealing processes in the excavation-damaged zone (EDZ) indicate that upon initial fracturing, the permeability of a shale can increase by 3–5 orders of magnitude to values in the range of  $10^{-15}$  to  $10^{-16}$  m<sup>2</sup> (Bernier et al. 2007; Zhang and Rothfuchs 2008). Based on fracture density and mean aperture, Richards et al. (1994) estimated the permeability associated with fracture sets in the Ellsworth Shale (immediately overlying the Antrim) at  $\sim 10^{-15}$  m<sup>2</sup>. Fracture density is highest in the lowermost Norwood Member ( $\sim 4$  m) and permeability associated with fracture sets is estimated at  $\sim 10^{-11}$  m<sup>2</sup> (Richards et al. 1994; Ryder 1996). Given that the Norwood Member is the

most highly fractured member of the Antrim Shale and a primary gas producer (Ryder 1996), the estimated permeability value is considered to represent an upper bound for the most fractured and transmissive zones within fractured shale. Shale intervals associated with these zones would be avoided during repository siting. Based on both experimental and field studies, we consider a permeability in the range of  $10^{-15}$  to  $10^{-16}$  m<sup>2</sup> to be representative of a typical fractured shale.

### 3.2.3.2 Porosity

Porosity is correlated with both permeability and clay content, with porosity increasing with higher clay content and higher permeability (Bourg 2015; Neuzil 2019). Schultz et al. (1980) reported a porosity range of 9%–30% for all rock units in the Pierre Shale (shale, siltstone, marl) with an average of 20% for the most prevalent marine shale. Paleozoic shales are typically more indurated and have lower porosity in the range of 5%–10%. Mastalerz et al. (2013) reports porosity of ~5% for two samples of the New Albany Shale at a depth of 700–800 m. The U.S. Energy Information Administration (EIA 2011) reports a porosity of 9% for the Antrim Shale at a depth of 400 m. These values are consistent with values from other Paleozoic shales reported by Bourg (2015). For comparison, the Opalinus and Callovo-Oxfordian Clays have porosity between 11% and 17% and the Boom Clay, with higher clay content, has porosity of 39% (Volckaert et al. 2004).

### 3.2.4 Thermal Properties

The thermal conductivity of shale is dependent on mineralogy, porosity, and saturation (Robertson 1988). The dependence on shale mineralogy is primarily a function of the proportion of clay (low thermal conductivity) and quartz (high thermal conductivity). From this relationship, one would expect the Paleozoic shales to have higher thermal conductivity based on their higher quartz content (20% versus ~50%; Figure 3-5).

Determinations of the thermal conductivity of the Pierre Shale from core measurements or heat flow analysis range from 0.7 to 1.2 W/(m·K) with the range probably representing variability inherent in different sampling and study locations (Sass and Galanis 1983; Gilliam and Morgan 1987; Förster and Merriam 1997). Previous iterations of the shale reference case used a value of 1.2 W/(m·K) (Mariner et al. 2017; Sevougian et al. 2019b).

Characterization of thermal properties and response were carried out in a series of experiments in the Paleozoic Conasauga Shale (southern Appalachian Basin), considered representative of Paleozoic shales in the eastern U.S. (Smith 1978). Measurements of thermal conductivity in three core samples of the Conasauga Shale were variable with thermal conductivities ranging from 1.0 to 2.1 W/(m·K) (Smith 1978). A similar range of thermal conductivities (1.5–2.3 W/(m·K)) was derived from analysis of the results of the Conasauga Near-Surface Heater Experiment (Krumhansl 1979a, 1979b). The higher range of values for the Paleozoic shales compared to the Pierre Shale is consistent with higher quartz content in the Paleozoic Shale although the values for both shales vary by about a factor of two. Section 5 describes the factors influencing thermal expansion of the host rock, thermal overpressure of pore fluids, and thermal spalling at excavation walls.

### 3.2.5 Porewater Chemistry

Groundwater chemistry of deep clay rock (shale, argillite) formations is of interest to (1) oil and gas field operations (e.g., drilling fluid composition) for prevention of corrosion and scale formation (Stewart et al. 2015; Thyne and Brady 2016) and for hydraulic fracturing fluid strategies (Chapman et al. 2012), and (2) the potential development of a nuclear waste repository using shale as a host rock (von Damm 1987). Porewater chemistry in low permeability argillaceous host rock can be variable and hard to obtain in sufficient quantities for analysis of aqueous solutes due to the low extractable amounts and difficulties in fluid retrieval from rock samples (e.g., squeezing). The porewater chemistry in clay/shale/argillaceous rock formations should preferably be constrained to extractions from samples relevant to repository depths. Moreover, fluid samples should be very well characterized and sampled at various formation

depths to resolve chemical variability (major elements and isotopic compositions) and to determine the extent of mixing with either shallower groundwaters or other members of the shale formation. Such detailed level of sampling is difficult to achieve even at URL sites with dedicated monitoring boreholes. The studies by Turrero et al. (2006) and Tournassat et al. (2015) provide a comprehensive chemical characterization of porewaters for Oligocene-Miocene Clay rock from Spain and Opalinus Clay rock from the Mont Terri URL, Switzerland. Tournassat et al. (2015) describes direct and indirect methodologies for obtaining porewater compositions such as sampling from seeps in boreholes, extractions from rock samples, and leaching and cation exchange experiments.

Relatively few sources relevant to porewater chemistry of clay rock formations in the U.S. at the depth of interest ( $\sim 500 \pm 200$  m in nuclear waste repositories) can be found. They are mostly limited to waters extracted from shale samples in deep weathered zones (e.g., Cody Shale; Brantley et al. 2013), groundwater collected from wells (including shallow seeps and springs), and production waters and/or brines from oil and gas field wells (e.g., USGS produced water database [Blondes et al. 2018] and the National Carbon Sequestration Database and Geographic Information System [NATCARB; Bauer et al. 2018] database; Engle et al. 2016). Geochemical databases of produced waters from oil and gas wells provide a substantial amount of water chemistry data for shale formations, but it is still considered an indirect form of sampling with potential artifacts. Using the WATSTORE (national WATER data STORage and REtrieval system) database from the USGS, von Damm (1987) evaluated shale groundwater chemistry. WATSTORE provides groundwater chemistry data for various geographical areas, but those of interest are the Northern Great plains (Pierre and Bearpaw Shales, which are late Cretaceous) and a few from the Midcontinent group comprising Mississippian and Pennsylvanian shales. The USGS produced water database (Blondes et al. 2018) provides water chemistry data for the Antrim (upper Devonian), Maquoketa (late Ordovician), Chattanooga (Devonian), Mancos (upper Cretaceous), New Albany (Devonian), Monterey (Miocene), Stanley (Mississippian), and Wolfcamp/Cline (Pennsylvanian) Shales. From this USGS data set, the shale formations of interest for a nuclear waste repository are the Antrim, Maquoketa, Chattanooga, Mancos, and New Albany Shales based on their thicknesses and relatively shallow stratigraphic depths compared to other Paleozoic-Cretaceous shales. Note that evaluation of water chemistries of these shale formations does not imply a potential siting target. Instead, these serve as the basis for geochemical evaluation of potential porewaters observed in this type of host clay rock based on geologic, stratigraphic, and mineralogic similarities between these formations.

Given the geological complexity in many of these shale/clay rock formations, there is the potential for situations such as mixing of porewaters between member units (e.g., sandstone units) within the formation itself or chemical reactions during flow in the wellbore, all of which can lead to changes in the fluid chemistry. A large portion of produced waters are saline brines sampled from oil and gas field operations as the result of hydraulic fracturing activities where water flooding (with some additives) can induce the above-mentioned processes in the formation units (Engle et al. 2016; Thyne and Brady 2016). Moreover, gaps in the analyzed solutes (cations, anions) and absence of details for both sampling and analytical methods can impact the quality and reliability of the water chemistry data. Still, even with these potential artifacts and data quality issues, these water chemistry databases can at least provide reasonable bounds for constraining porewater compositions of potential shale host rock formations.

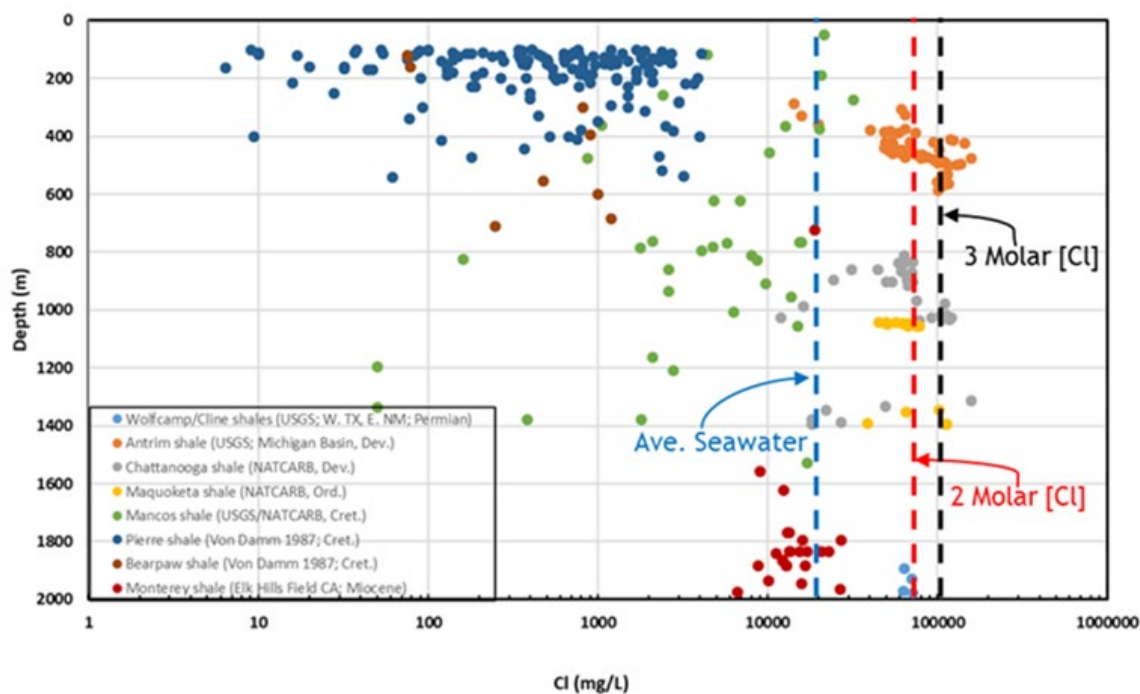
For this analysis we selected representative porewater compositions from the resources described above based on the completeness of analyzed cations and anions, screening out water with charge imbalances greater than 5% and 10%, and data outliers deemed reasonably off trend. For the charge imbalance criterion, we started by screening out all data with charge imbalances greater than 5%. When this threshold resulted in relatively large sets of data for a given shale formation being discarded, a change in charge imbalance tolerance to 10% was investigated with consideration towards the potential data quality issues. In some cases, the more relaxed charge imbalance approach allowed for the evaluation of trends in major solute chemistry.



Even with the geologic and stratigraphic heterogeneities, the bulk mineralogy of these Paleozoic shales tends to be similar between these formations: illitic clay, quartz, kaolinite, and chlorite with some carbonate, minor feldspar, and pyrite. The Antrim Shale has been described as a thin-bedded, dark, carbonaceous shale composed of illite (20%–35%), quartz (50%–60%), and kaolinite (5%–10%), with minor occurrences of chlorite (0%–5%) and pyrite (0%–5%). The Chattanooga has been also characterized as a black shale with silt-size grains of quartz, clay, and micaceous (chlorite) phases with some pyrite. The Maquoketa Shale sequence contains mainly illitic clay, quartz, chlorite, kaolinite, and an abundant clay-rich dolomitic component. The Permian Wolfcamp/Cline also has a similar bulk mineral assemblage, but this formation lies stratigraphically deeper than the Cretaceous shales and Paleozoic shales. The Cretaceous shales are represented by the Mancos, Pierre, and Bearpaw formations. The Pierre and Bearpaw (late Cretaceous) shales have overall mineralogical compositions of illite-smectite clay (60–80%), mainly present as mixed-layer clay, quartz, kaolinite, chlorite, and some feldspars (Schultz 1980; von Damm 1987). The Mancos Shale has similar bulk mineralogy as the Pierre and Bearpaw Shales with variable levels of illite and quartz plus calcite.

Figure 3-8 shows a plot of chloride concentration from oil and gas field produced waters and groundwaters from various shale formations as a function of reported maximal borehole or perforation depths. Even though the depths assigned to these waters are rather uncertain, the figure provides a general relation of the chloride concentration ranges expected for these shales. In particular, the Antrim, Chattanooga, and Maquoketa Paleozoic shales show very similar range of chloride concentrations. Peak chloride concentrations for these Paleozoic shales are roughly between 70,000 and 100,000 mg/L (~2–3 Molar). The Cretaceous Pierre and Bearpaw Shales have similar range of chloride concentrations although there is much less data for the latter. According to von Damm (1987), peak chloride concentrations in the porewaters of the Cretaceous Pierre Shale are ~5,000 mg/L (0.14 M), which are much less saline than those of the Paleozoic shales. Neuzil (1993) reports on porewater salinities from borehole investigations (down to 180 m) and core samples showing a trend of increasing salinity with depth. The Mancos Shale shows a large degree of scatter with maximum chloride concentrations in the neighborhood of ~20,000 mg/L (0.56 M), close to average seawater.

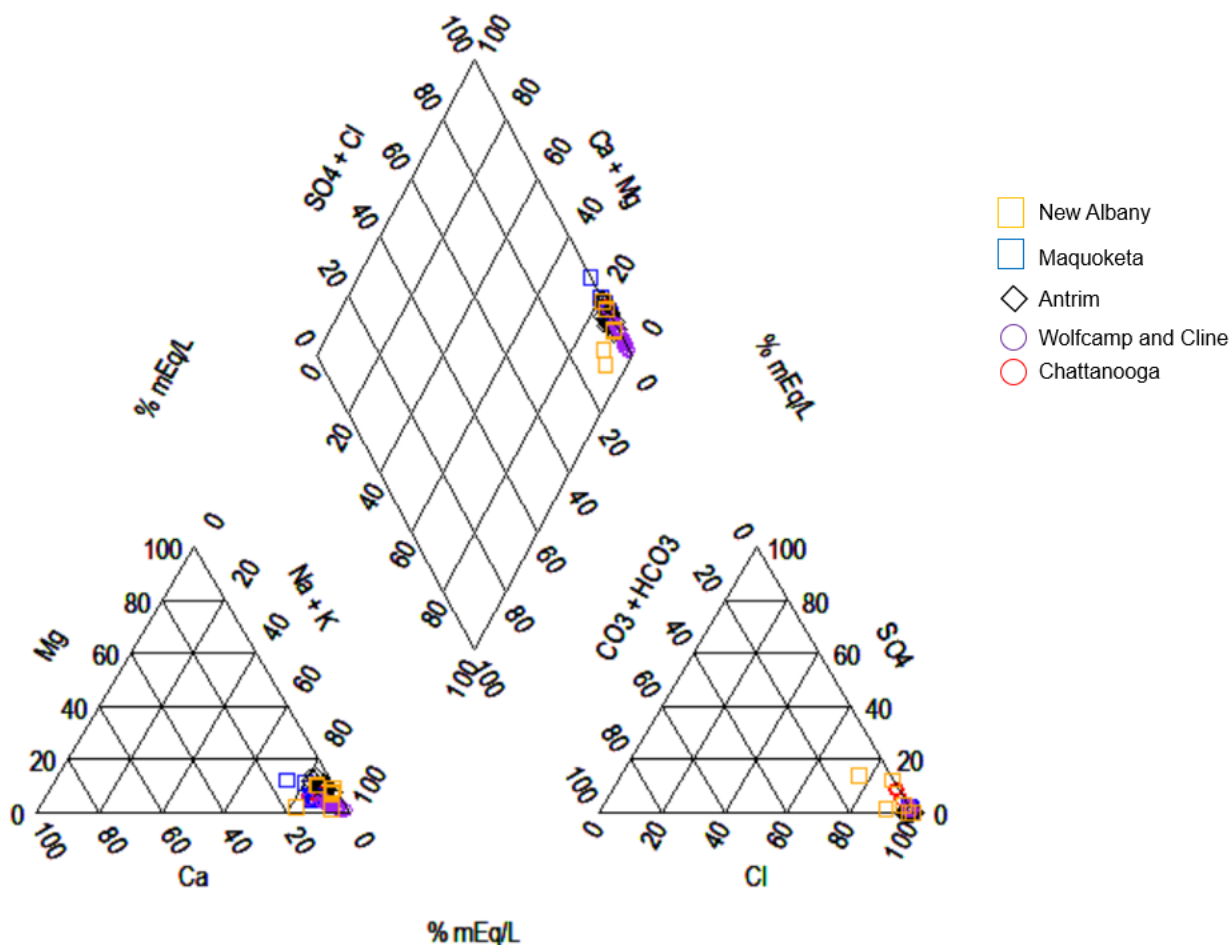
The Antrim, Pierre, Bearpaw, and Mancos Shale formations have depths within the ranges of interest for a deep geological nuclear waste repository. The Chattanooga, Maquoketa, Monterey, and Wolfcamp/Cline Shales are stratigraphically too deep for consideration. Despite being so deep, the Wolfcamp/Cline Shale is of interest due to an extensive set of data that can be used for comparison purposes. Engle et al. (2016) evaluates the geochemistry of porewaters for the Wolfcamp/Cline Shale including the major solutes and some isotopic data for this formation. This information will be used for evaluation purposes of porewater chemistries with the assumption that the results are relevant to porewater analyses for other shale formations even when considering differences in geologic history, stratigraphic complexity, pressure/temperature conditions, bulk mineralogy, and geochemical evolution of fluids.



NOTE: Data obtained from water chemistry databases for oil and gas field produced waters and groundwaters.

**Figure 3-8. Chloride Concentration Profile as a Function of Reported Maximal Borehole or Perforation Depths**

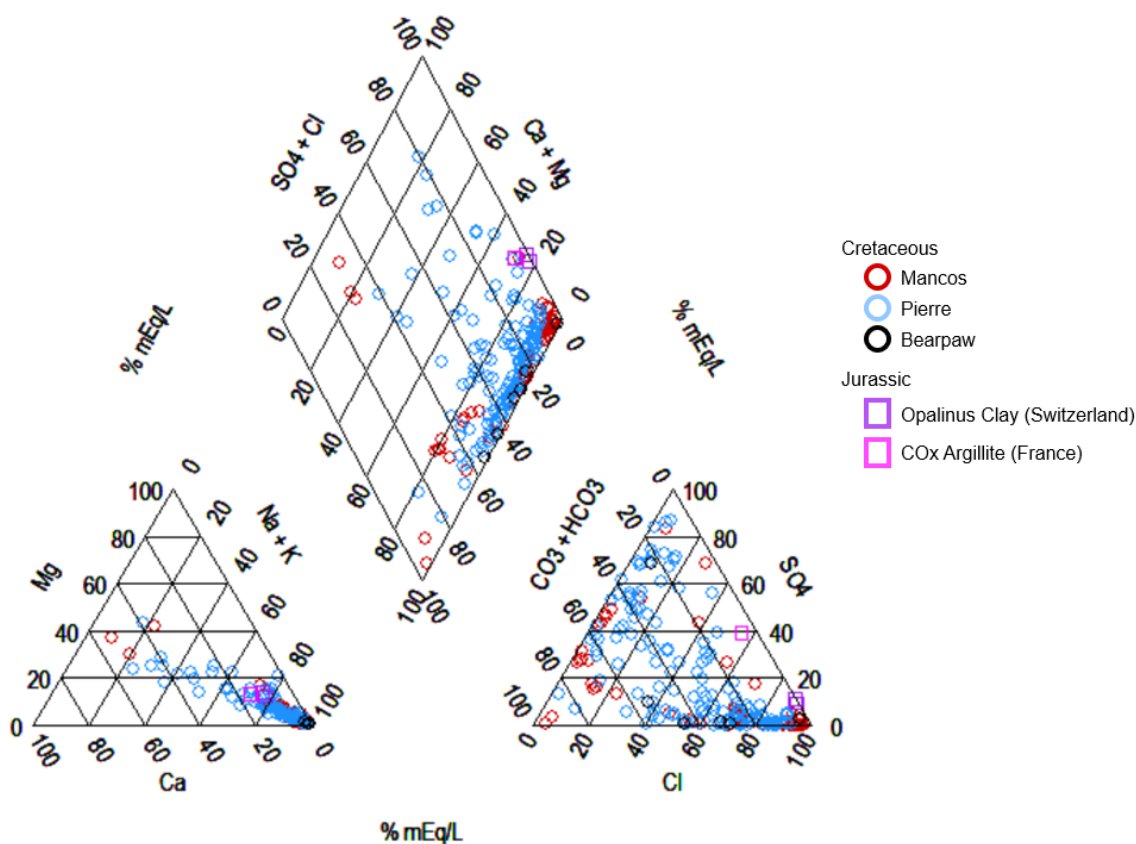
As seen in Figure 3-9, a Piper plot of these Paleozoic shales graphically reveals nearly overlapping water chemistries for major cations and anions. Overall, the trends produced in these plots mirror those given by Thyne and Brady (2016) for the oil and gas field produced waters from the Bakken Shale. Such an observation is expected since the major solute porewater chemistries in these Paleozoic shales share the commonality of being rich in Na and Cl with some Ca (Thyne and Brady 2016, Kharaka et al. 2019). These shale porewaters are also characterized by interactions with evaporites or salt mineral precipitates from seawater evaporation, and residual deep-seated water from this process (Kharaka et al. 2019). Also, interactions with other minerals common in argillaceous/clay rock such as mixed-layer clays, carbonates (e.g. calcite), quartz, and feldspars add to the complexity of porewater geochemical evolution. Furthermore, interactions with organic matter and organic-bearing fluids particularly in oil-rich shales with aqueous pore solutions could have an effect on redox reactions and observed alkalinities (Kharaka et al. 2019).



NOTE: Data obtained from USGS/NATCARB databases.

**Figure 3-9. Piper Plot of Groundwater Major Cation/Anion Solutes (in percent mEq/L units) for the Considered Paleozoic Shales**

In general, the porewater chemistry of Cretaceous shales like the Pierre, Bearpaw, and the Mancos have similar major solute compositions as shown by the Piper plot in Figure 3-10. However, there is a significant level of data scatter for porewater chemistries of the Pierre and Mancos Shales due to the larger amount of data and inherent variability. Even with the data scatter, some compositional trends common to the Mancos, Pierre, and Bearpaw Shales can be discerned particularly for the Na, Cl, and SO<sub>4</sub> content. The Jurassic argillaceous formations represented by the Opalinus Clay (Switzerland) and the CO<sub>x</sub> argillite in France have porewater chemistries with relatively higher Ca, Mg, and SO<sub>4</sub> content than the Cretaceous shales. These Jurassic porewater compositions are shown for comparison purposes only. Although there are some similarities with the water chemistry of the Paleozoic shales, this situation only seems to apply for the most concentrated Na-Cl waters with lower Ca content. The Cretaceous porewater concentrations can be as concentrated as those from the Paleozoic shales. However, in general, Cretaceous porewaters exhibit much more dilute concentrations plus much more variable carbonate and SO<sub>4</sub> contents. Still, the level of data spread on sulfate and carbonate concentrations for the Pierre and Mancos Shale waters raises some questions about data quality and any geochemical processes that could contribute to such high variability. Further evaluation is needed to conduct culling of data based on additional screening arguments and geochemical modeling to test potential solution-mineral interactions mechanisms that describe the observed trends.



NOTE: The Mancos Shale water chemistry data is for oil and gas field produced waters (USGS databases). The porewaters for the Jurassic shale formations are for the Opalinus Clay argillite at the Mont Terri URL (Switzerland) and the COx argillite (Bure site) in France (Tournassat et al. 2015).

Source: von Damm 1987.

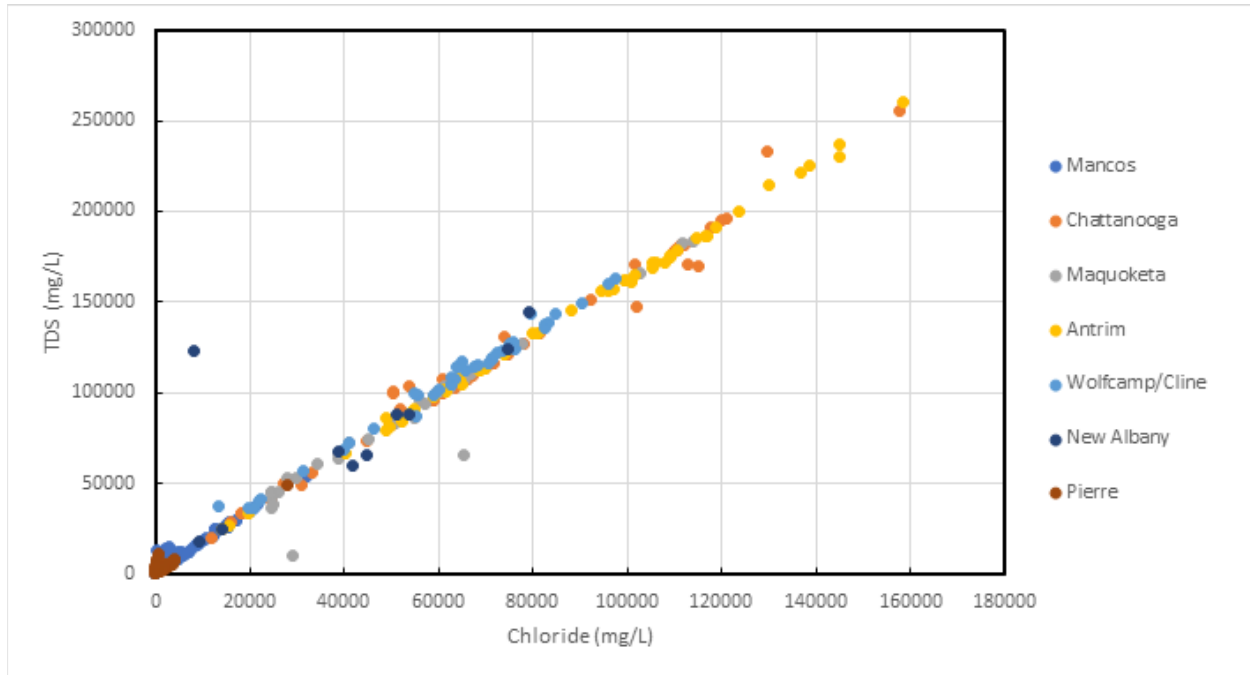
**Figure 3-10. Piper Plot of Groundwater Major Cation/Anion Solutes (in percent mEq/L units) for Cretaceous and Jurassic Shales**

Figure 3-11 shows a plot of total dissolved solids (TDS) as a function of chloride concentration, displaying a strong correlation over a widespread range of values. Kharakha et al. (2020) suggested that TDS values exceeding  $\sim 100,000$  mg/L may represent waters that have undergone interactions with salt evaporite sequences or evaporation in the subsurface. A relatively large population of data from the Antrim, Chattanooga, and the Maquoketa Shales fall within the  $>100,000$  TDS concentration whereas the Cretaceous shales consistently plot below this value. There could be a large uncertainty on TDS values since fluid mixing—e.g., dilution due to water injection and “flowback” before produced water compositions stabilize—can cause a shift in the TDS distribution. Still, the correlation is valuable to assess potential target porewaters particularly with high Cl concentrations.

Figure 3-12 shows a plot of Ca/SO<sub>4</sub> versus Na/Cl concentration ratio for all the considered shale porewaters. Even with the data scatter, a common feature of this plot is the “vertical” trend of Ca/SO<sub>4</sub> ratio at a Na/Cl ratio of  $\sim 0.6$ . The bulk of Paleozoic shale waters plot within this vertical trend whereas the Cretaceous shale waters plot at higher Na/Cl ratios trending toward more dilute concentrations. Such behavior was also described by Engle et al. (2016) where the increase in Ca/SO<sub>4</sub> is likely due to a decrease in SO<sub>4</sub> that appears not to be related to the evaporation of late Permian seawater. Instead, Engle et al. (2016) suggests that such a “vertical” trend may be achieved by equilibrium with anhydrite and exchange of Na and Ca in clay phases. Geochemical modeling could offer an opportunity to evaluate

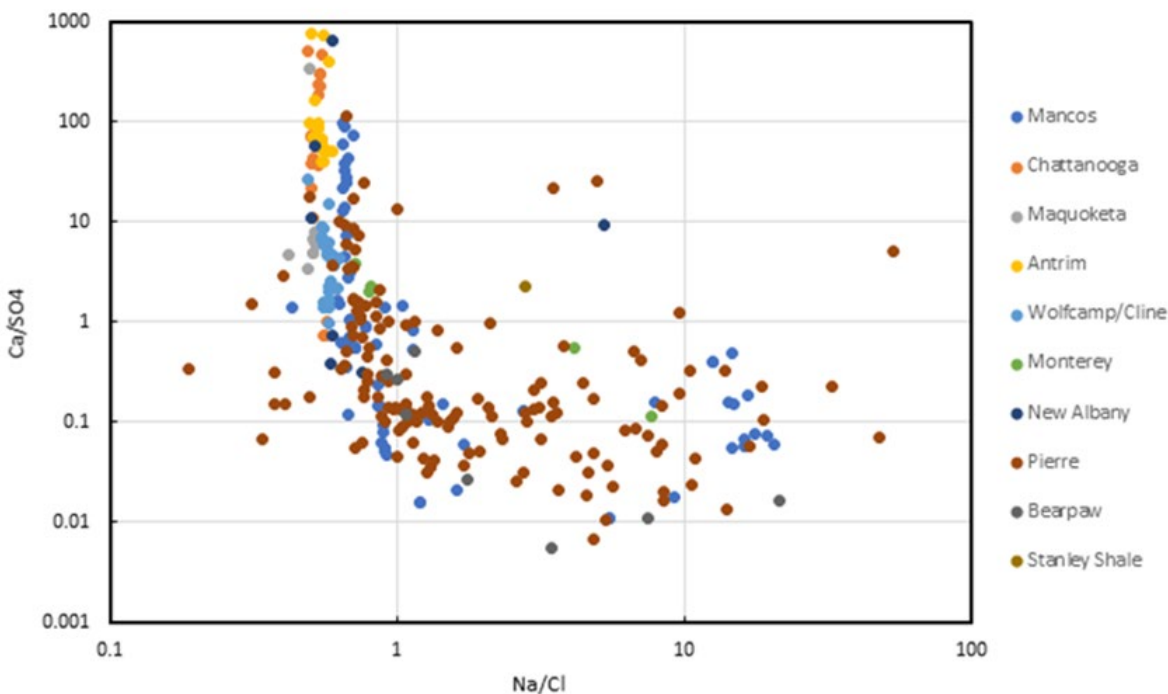


these trends on the basis of equilibria between mineral and porewater with reactions that involve Ca-bearing sulfates (e.g., gypsum), illitic clay, halite, carbonates, and silicate phases (quartz, feldspar). Such an analysis was conducted by Thyne and Brady (2016) on the Bakken porewaters, for which assumptions regarding mineral saturation state, temperature effects, and solution chemistry could be tested.



NOTE: The Paleozoic shale formations are the Chattanooga, Maquoketa, Antrim, Wolfcamp/Cline, and New Albany Shales. The Cretaceous shale formations are the Mancos and Pierre Shales.

**Figure 3-11. Plot of Total Dissolved Solids Versus Chloride Concentration for Paleozoic and Cretaceous Shale Formation Waters**



NOTE: The Paleozoic shale formations are the Chattanooga, Maquoketa, Antrim, Wolfcamp/Cline, New Albany, and Stanley Shales. The Cretaceous shale formations are the Mancos, Pierre, and Bearpaw Shales. The Monterey Shale is from the Miocene epoch, making it younger than the other shales.

**Figure 3-12. Plot of Concentration Ratios  $\text{Ca}/\text{SO}_4$  Versus  $\text{Na}/\text{Cl}$  for Paleozoic and Cretaceous Shale Formation Waters**

Table 3-1 summarizes the major ion water chemistries for Cretaceous and Paleozoic shales from the considered databases. The table lists the lowest, highest, and average values considered for each formation noting the large variability for solutes like Na and Cl. The Paleozoic shales seem to be more consistent in terms of the ranges of groundwater major solute concentrations and overall consistency in the bulk concentrations among different formations. However, for both the Paleozoic and the Cretaceous shales, the wide range in values reflects the potential for these waters to have been affected by fluid mixing during oil and gas well operations and/or during production, including mixing of waters within units (or subunits) from the same formation. Moreover, the potential for other processes like evaporation and interactions with salt phases (e.g., dissolution) or other mineral phases in the formation also precludes an accurate analysis of the shale porewater chemistry. All of these processes are very difficult to assess from major ion water composition alone, requiring detailed studies based on isotopic analysis using state-of-the-art pore fluid sampling and extraction methodologies.

Given the wide range of compositions and depths reported for sampled fluids, the Paleozoic Antrim Shale groundwater chemistry is the best candidate at this point for a representative porewater composition for the brittle shale endmember. A preliminary geochemical speciation of these porewaters at 25°C was conducted using the EQ3/6 (Wolery and Jarek 2003) software. The results of this preliminary analysis indicate that  $\text{SiO}_2(\text{aq})$  concentrations are either close to saturation, saturated, or super supersaturated with respect to quartz. Given the high quartz content in these shales, it is reasonable to suggest that this phase controls dissolved silica in these porewaters. Most of the shale porewaters are also saturated with respect to calcite, which probably exert controls on Ca and its relatively high concentration. Some Antrim Shale members contain carbonate minerals (e.g., calcite, dolomite), and calcite is present as fracture fillings in the formation (Budai et al. 2002). Activity phase diagrams were used to evaluate the stability relations of

clay minerals (kaolinite, illite) reported in the Antrim formation. Analysis of  $K^+$  activities and related activity ratios obtained from the EQ3/6 speciation results indicate supersaturation with respect to illite, which is the second most abundant phase (after quartz) in the shale formation. More work is needed to conduct further geochemical analysis up to higher temperatures to evaluate fluid/mineral equilibria relations.

In terms of salinity, the Antrim Shale is similar to the New Albany Shale of the Illinois Basin (Parris et al. 2010). These can be considered potential candidates for a representative porewater composition for the brittle shale endmember. Groundwaters from the Cretaceous Pierre, Bearpaw, and Mancos can be considered potential candidates for a representative porewater composition for the ductile shale endmember. In comparison to a brittle shale endmember, the groundwaters of a ductile shale endmember have a seemingly more complex geochemical evolution, are depleted in Cl, and tend to be more enriched in carbonate, which could result in less sorption on clay particularly at above-neutral pH. Given the large uncertainties and data quality gaps, careful culling of these data based on screening criteria and geochemical modeling assessments should be conducted to improve constraints on porewater compositions to be used in the shale reference case analyses.

**Table 3-1. Summary of Major Aqueous Ion Chemistries of  
Cretaceous and Paleozoic Waters from Shale Formations**

		Cretaceous Formations			Paleozoic Formations		
		Mancos <sup>a,b</sup>	Pierre <sup>c</sup>	Bearpaw <sup>c</sup>	Chatanooga <sup>a</sup>	Maquoketa <sup>a</sup>	Antrim <sup>a</sup>
pH	Lowest Reported Value	5.63	3.8	8.1	6	5.8	5.44
	Highest Reported Value	8.9	9.6	8.9	7.9	8	7.37
	Average	7.95	7.90	8.39	6.78	6.95	6.42
	Standard Deviation	0.64	0.49	0.30	0.44	0.53	0.42
[Na] (mmol/L)	Lowest Reported Value	0.13	0.52	24.79	403.31	706.66	404.09
	Highest Reported Value	868.68	782.95	73.95	3,379.38	1,764.85	3,849.50
	Average	209.50	45.60	43.55	1,812.05	1,317.28	1,976.27
	Standard Deviation	176.52	64.45	14.02	827.00	319.03	733.91
[Ca] (mmol/L)	Lowest Reported Value	0.10	0.03	0.09	28.22	25.30	9.31
	Highest Reported Value	204.60	17.22	1.30	413.54	253.26	235.29
	Average	4.93	1.63	0.29	174.97	113.28	106.86
	Standard Deviation	22.93	2.13	0.41	90.50	48.54	56.66
[Mg] (mmol/L)	Lowest Reported Value	0.12	0.00	0.05	6.99	12.84	12.10
	Highest Reported Value	21.15	11.52	0.41	122.65	216.42	228.76
	Average	2.16	1.20	0.12	62.92	43.45	117.79
	Standard Deviation	4.02	1.56	0.12	31.22	28.73	55.08
[K] (mmol/L)	Lowest Reported Value	0.31	0.02	0.05	—	—	2.56
	Highest Reported Value	14.07	5.63	0.08	—	—	18.72
	Average	1.87	0.39	0.07	—	—	11.02
	Standard Deviation	2.98	0.48	0.01	—	—	4.14

**Table 3-1. Summary of Major Aqueous Ion Chemistries of Cretaceous and Paleozoic Waters from Shale Formations (continued)**

		Cretaceous Formations			Paleozoic Formations		
		Mancos <sup>a,b</sup>	Pierre <sup>c</sup>	Bearpaw <sup>c</sup>	Chatanooga <sup>a</sup>	Maquoketa <sup>a</sup>	Antrim <sup>a</sup>
[Cl] (mmol/L)	Lowest Reported Value	0.20	0.18	2.14	457.04	640.34	403.39
	Highest Reported Value	1,410.44	789.84	33.85	4,448.15	4,936.53	4,465.44
	Average	198.81	32.00	16.94	2,312.96	1,730.59	2,415.32
	Standard Deviation	231.54	66.72	12.35	989.50	1028.11	960.62
[SO <sub>4</sub> ] (mmol/L)	Lowest Reported Value	0	0	0.12	0	0.18	0.02
	Highest Reported Value	82.68	51.01	33.31	25.51	22.38	1.11
	Average	5.80	4.64	6.45	5.20	8.89	0.45
	Standard Deviation	13.64	7.38	11.35	7.48	4.10	0.29
[SiO <sub>2</sub> ] (mmol/L)	Lowest Reported Value	—	0.07	0.10	—	—	0.10
	Highest Reported Value	—	0.87	0.18	—	—	0.31
	Average	—	0.41	0.15	—	—	0.21
	Standard Deviation	—	0.09	0.03	—	—	0.06

Source: <sup>a</sup>USGS produced water database (Blondes et al. 2018).

<sup>b</sup>NATCARB (Bauer et al. 2018).

<sup>c</sup>von Damm (1987).

### 3.2.6 Summary of Properties for Ductile and Brittle Shale

The contrasting properties of the ductile and brittle shale populations discussed in this report are summarized in Table 3-2. The Pierre Shale is chosen as representative of a ductile shale endmember. The Antrim and New Albany shales are chosen as representative of a brittle shale endmember.

Key features of a brittle shale are fracture characteristics and fracture permeability. Interconnected fractures increase the permeability of the shale by several orders of magnitude, from typical values of  $\sim 10^{-20}$  to values of  $\sim 10^{-16}$ , consistent with permeability increases measured in the EDZ of European URLs. Because most shales have some degree of lithologic layering, fracture systems may be characterized by fracture stratigraphy, where fracture frequency, height and terminations are controlled by the mechanical properties of different layers within a shale formation. The variability in fracture frequency (and hence permeability) of brittle shale emphasizes the need for repository siting that avoids the most fractured zones within shale formations.

**Table 3-2. Summary of Properties of the Pierre (Ductile) and Paleozoic (Brittle) Shales**

Property	Pierre Shale (ductile)	Paleozoic Shales (brittle; primarily New Albany and Antrim)
Typical thickness (m)	400–600	75–150
Clay Content (%)	65–80	35–50
Quartz Content (%)	~20	~50
Compressive Strength (MPa)	5–10 (range of 0.5–18)	30–160
Fracture Characteristics	Widely spaced vertical fracture zones (high transmissivity features) proposed at regional scale.	Dominated by vertical fractures at low to high frequency. Vertical variations in mechanical properties of rock influence fracture stratigraphy.
Thermal Conductivity (W/[m·K])	0.7–1.2	1.0–2.1
Porosity (%)	~20 (range of 10–30)	5–10
Permeability (m <sup>2</sup> )	~10 <sup>-20</sup> – 10 <sup>-21</sup> ; 3–4 orders of magnitude higher proposed at regional scale.	~10 <sup>-19</sup> based on clay content; ~10 <sup>-15</sup> – 10 <sup>-16</sup> for typical fractured shale
Salinity (Cl <sup>-</sup> concentration) (mg/L)	10–4,000	10,000–160,000

### 3.3 Properties of Ductile and Brittle Shales

The transport of radionuclides from a repository in shale to potential receptors in the accessible environment is controlled by complex coupled THMC processes that evolve over time as a result of the impact of the repository on the natural host rock, the EBS, and the aqueous and gas species that are present. The effects of higher temperatures on the engineered barriers are described in detail in Section 4 through Section 8 of this report. The higher temperature environment contemplated now (compared to previous shale reference case analyses) may also have long lasting, durable effects on the natural system, particularly in the near-field environment where the host rock may be mechanically, chemically and mineralogically affected. For the past several years, the SFWST program has been conducting R&D activities designed to advance and refine our understanding of coupled THMC processes, including hydrothermal experiments on barrier clay and natural host rock interactions, thermodynamic database development, and repository-scale underground testing (in international URLs) and reactive transport modeling of the near-field and host rocks under nonisothermal conditions. Many of these activities were described in detail by Jové Colón et al. (2019).

The SFWST Campaign developed the GDSA computational framework to analyze and assess the potential performance of generic reference case repositories. The primary codes of the framework are PFLOTRAN and Dakota. PFLOTRAN is a multiphase transport code designed for simulating flow and reactive transport in the subsurface (Hammond et al. 2014). Dakota is an uncertainty quantification and

sensitivity analysis code (Adams et al. 2020). To date, PFLOTRAN has been used to assess the effects of large, hot waste packages by analyzing the transport of heat away from the repository, changes in water density caused by nonisothermal conditions, and the effect of density changes on flow and transport processes (Sevougian et al. 2019b).

Continued improvement of high-temperature (approximately 100°C to 300°C) geochemistry and flow and transport models will require the collection and incorporation of improved thermodynamic data in our models. The SFWST Campaign utilizes SUPCRT92, a software package for calculating the standard thermodynamic properties of minerals, gases, aqueous species, and reactions at elevated temperatures and pressures. An ongoing effort is underway to update the databases embedded in SUPCRT92 (maintained at Lawrence Livermore National Laboratory), and to integrate them with the international Nuclear Energy Agency Thermochemical Database Project (NEA-TDB). The purpose of the NEA-TDB is to develop and make available a comprehensive, internally consistent, quality-assured and internationally recognized chemical thermodynamic database of selected chemical elements to meet the modeling requirements for safety assessments of radioactive waste disposal systems. These activities are undertaken in coordination with international partners and organizations. New versions of these databases will be made available in several formats for use by the SFWST-relevant codes (PFLOTRAN, PhreeqC, Geochemists WorkBench, etc.).

Planned updates also include revisions of the Equation-of-State (EoS) model for water to include the capability to compute thermal conductivity, surface tension, and dielectric constant (Jové Colón et al. 2019). The updated version of EoS would then be incorporated into a modified SUPCRT92 code.

The SFWST Campaign is also working to develop a database framework that is aligned with that of Rossendorf Expert System for Surface and Sorption Thermodynamics (RES<sup>3</sup>T), a thermodynamic sorption database developed by Helmholtz-Zentrum Dresden-Rossendorf (HZDR). This effort includes a comprehensive compilation of raw sorption data and fitting strategies to a surface complexation model (SCM) coupled to optimization software. The research is needed to integrate different data sets, to obtain self-consistent reaction stability constants, and to assess model uncertainties. Future plans include developing strategies to include temperature dependence for adsorption and solubility in the models.

An extensive program of experimental hydrothermal geochemistry studies at Los Alamos National Laboratory (LANL) is designed to analyze mineral stability and phase equilibria at elevated temperatures (up to 200°C to 300°C; see Section 8). The experiments are focused on hydrothermal interactions of shale host rock, bentonite clay used as a barrier, cementitious materials, and steel. Characterization studies (compositional, structural, geochemical) of experimental run products will be integrated with thermodynamic modeling to evaluate the occurrence of secondary mineralization and clay phase stability at elevated pressures and temperatures.

The experimental program results will also be coordinated and integrated with characterization studies of clay-rich host rock and bentonite samples and with large-scale heating experiments conducted by international repository programs (such as Mont Terri and Bure) in which SFWST participates. Because the U.S. has no research facilities in shale host rocks, it is especially important that SFWST collaborate to ensure that our models are tested and validated to the extent possible. As an example, the Mont Terri FE experiment undertaken by Nagra, is a long-term, large-scale test of the potential performance of geologic disposal in Opalinus Clay, with focus on both the EBS components and the host-rock behavior. The FE experiment is conducted in a tunnel at Mont Terri, extending 50 m in length and 2.8 m in diameter. Heating from emplaced waste is simulated by three heat-producing canisters of 1,500 W maximum power each. The temperature is expected to exceed 100°C, with a target temperature of 125°C to 135°C at the inner part of the buffer.

DOE is one of the experimental partners for the FE heater experiment, and Lawrence Berkeley National Laboratory (LBNL) is one of the modeling teams. The results of the modeling effort have been described

in a series of status reports since 2013, and they include comparisons to measured monitoring results for temperature, pressure, humidity and other parameters (Rutqvist et al. 2020).

LBNL is also participating in modeling of an in-situ heater experiment, conducted in Callovo-Oxfordian Claystone (COx) at the Meuse/Haute-Marne URL in Bure, France. This experiment is one of the tasks of the DECOVALEX-2019 project. The task is coordinated by Andra, and involves modeling of two in-situ tests performed at the URL:

- The TED experiment, a small-scale heating experiment focused on the claystone THM behavior of the undisturbed rock mass in the far field
- The ALC experiment, a one-to-one scale heating experiment focused on the interaction between the surrounding rock and the support (steel casing in this case) in the near field

In both the Mont Terri and Bure experiments, LBNL is utilizing the TOUGH2 and FLAC3D codes to simulate the coupled thermal, hydrologic, and mechanical (THM) response of the NBS and EBS to the introduction of heat caused by waste emplacement. These studies will help scientists assess (and develop models for) the evolution of the excavation-disturbed zone (EdZ) and the EDZ (excavation-damaged zone) in the near-field environment as a function of temperature (Section 5).

The SFWST Campaign also participated in the heater test at the Full-scale Engineered Barrier Experiment (FEBEX) in the URL at the Grimsel Test Site and is a partner in the newly initiated High Temperature Effects on Bentonite Buffers (HotBENT) heater test at the Grimsel Test Site. The FEBEX heater test ran for 18 years; temperatures never exceeded 100°C. Two periods of dismantling yielded samples of the heated bentonite buffer for analysis of water saturation, porewater chemistry, and mineralogy (e.g., Zheng et al. 2020). The HotBENT heater test will sustain temperatures of up to 200°C in various combinations of waste package material and bentonite buffer from different sources with the goal of learning more about bentonite parameter characterization above 100°C (Grimsel Test Site [Switzerland] 2020).

In addition to collaborating on model development, international programs can provide site characterization data and parameter estimates that may be useful in developing generic (reference case) models of potential repository performance. For example, Nagra has published a series of reports that provide values of important host rock and regional transport related parameters such as radionuclide sorption coefficients ( $K_d$ ), effective diffusion coefficient, and solubility limits in Opalinus Clay, as well as other formations above and below it, and MX-80 bentonite. These include

- Nagra Technical Report 12-03 (Van Loon 2014), which describes effective diffusion coefficients in argillaceous rocks and bentonite
- Nagra Technical Report 12-04 (Baeyens et al. 2014), which describes sorption data ( $K_d$ ) in argillaceous rocks and bentonite
- Nagra Technical Report 14-06 (Berner 2014a), which describes radionuclide solubility calculations in a bentonite environment
- Nagra Technical Report 14-07 (Berner 2014b), which describes radionuclide solubility calculations in a cementitious environment



## 4. REPOSITORY DESIGN AND CONSTRUCTION

A generic high-temperature shale repository reference case will be used primarily across generic performance assessment and criticality consequence investigations, and in support of field and laboratory testing activities (Section 1.2). Conceptual aspects of repository design and construction are relevant to ensure that the generic case is realistic, likely to achieve preclosure and postclosure safety objectives, and can be readily constructed using existing technology at reasonable cost.

### 4.1 Assumed Repository Depth and Host Ground Conditions

Criteria for assessing the suitability of a shale or similar clay-rich formation for geologic disposal of radioactive waste have been proposed, including (e.g., Shurr 1977; Mariner et al. 2017 and references therein):

- **Depth**—The isolation horizon should be from 300 to 900 m below surface.
- **Shale Thickness**—Maximum thickness of the isolation medium is desired, and a minimum thickness of 150 m is preferred.
- **Overburden Thickness**—Minimal thickness of overlying geologic units is preferred.
- **Lithology and Mineralogy**—The repository interval should be a reasonably uniform shale or other clay-rich unit with few or no interbeds of more permeable lithology.
- **Penetrations (boreholes)**—Boreholes of any kind are undesirable, particularly if they penetrate to rocks below the disposal horizon. It is recognized that some holes are necessary to provide geologic information at depth.
- **Structure**—The disposal zone should have nearly horizontal bedding and the surrounding region should be structurally simple (e.g., no folding or faulting).
- **Seismicity**—Seismically inactive regions are preferred.
- **Topography**—Minimal topographic relief is desirable to limit the influence of topography on subsurface hydraulic gradients.
- **Mineral and Water Resources**—Regions with minimal exploitable mineral and water resources, at or below the surface, are preferred.

In a ductile shale, repository depth may be optimized to promote reconsolidation of excavation damage or disturbance in a few decades without requiring extreme ground support measures to maintain opening stability during repository construction and operations. Repository depth great enough to activate creep deformation in ductile shale, over the desired timeframe of repository evolution, will be on the order of 200 to 500 m depending on formation characteristics (Nopola and Roberts 2013; 2016).

For ductile shales the unconfined compressive strength (UCS) can be compared to overburden stress (e.g., 5 MPa UCS equates to about 225 m depth) to estimate the potential for creep. Note that UCS is defined from high-strain rate tests and is only an index of stress magnitude that could result in long-term creep. Creep in shales does occur, as reported by Nopola (2013) and Nopola and Roberts (2013; 2016). To promote sealing of fractures from excavation in ductile shale, the depth could be great enough that the overburden stress approximates the UCS. For highly indurated shales the UCS will likely be greater than the overburden stress at the repository depth (e.g., 20 MPa UCS equates to about 900 m depth). Thus, these shales will fail in a brittle manner from stress concentration around excavated openings.

The feasibility of repository construction and operation in shale media is related to burial depth, the state of stress, environmental conditions in situ, and the rock response to those conditions. A ductile clay subject to loading from hundreds of meters of overburden could require complicated excavation and

ground support measures. A brittle shale would require construction and opening ground support designed to manage cohesion in the near-field wall rock while reducing its stiffness and transferring stress to intact rock farther from the opening.

The depth of the repository must accommodate unit thickness and depth, while maintaining the desired characteristics of geologic stability and waste isolation. For example, the ductile Boom Clay is a candidate host medium for construction of a repository at a depth of approximately 250 m (ONDRAF/NIRAS 2001). Were it to occur at much greater burial depths, this clay could be less porous and more indurated (diagenetically modified).

Where practical, the repository would be located in a host formation that extends to the surface or nearly so, and extends at least 100 m or more below the repository, to promote waste isolation. The interposition of different rock units, for example sandstone, limestone, or other clay/shale units that might serve as conduits or barriers to radionuclide migration, is possible for generic sensitivity studies but beyond the scope of this discussion.

The repository is assumed to be situated in flat-lying stratigraphy so that it resides within a particular stratigraphic unit, and ground conditions are the same (or nearly so) throughout the layout. The repository would be built on one level, selected as the optimum on multiple criteria. Multilevel waste emplacement has been shown to exacerbate heat dissipation over tens to hundreds of years, producing average or peak temperatures greater than for single-level waste emplacement (Hardin et al. 2012a).

Previous shale reference cases have assumed a single-level repository at a depth of 400 m (Sevougian et al. 2019b) or 500 m (Mariner et al. 2017), with the host horizon located within a flat-lying thick shale unit to optimize waste isolation.

#### **4.1.1 Available Repository Area**

A typical 21-PWR waste package would contain 9.5 metric tons (MT) heavy metal (as uranium, or MTU, at 0.45 MTU per fuel assembly) and a typical 44-BWR package would contain 7.9 MTU (0.18 MTU per assembly). The inventory of U.S. spent fuel is expected to grow to approximately 135,000 MTU considering the existing fleet of operating and decommissioned reactors, plus current new-builds. The fraction of BWR fuel will be approximately 35% of the total, based on simulations (Hardin et al. 2012a, Table E-1). Using these values, the numbers of 21-PWR/44-BWR waste packages would be about 6,000 (BWR) and 9,000 (PWR). Previous shale reference case analyses (Mariner et al. 2015; 2017; Sevougian et al. 2019b) assume an inventory of 70,000 MTU for the repository, approximately half of the 135,000 MTU projected inventory. The discussion in this report assumes co-located disposal of 135,000 MTU.

Previous scoping studies of thermal management options for repositories in clay/shale and other media (Hardin et al. 2012a; 2013) have focused on drift–drift and package–package spacings needed to dissipate heat from waste packages with a given capacity, containing spent fuel with given enrichment, burnup, and age out-of-reactor. Drift spacings can be increased more economically than package spacings because the impact on total excavated volume is smaller. However, both spacings contribute equally and directly to the needed repository layout area.

A thermal management approach is recommended in Section 4.5. This approach covers spacings and aging requirements, based on scoping thermal calculations. With a drift spacing of 70 m and package spacing of 20 m, the overall emplacement area would be 35 km<sup>2</sup>, comprising 25 km<sup>2</sup> for emplacement drifts and an additional 10 km<sup>2</sup> for access and service drifts associated with each 10,000 MTU panel (Hardin and Kalinina 2016).

#### **4.1.2 Hydrologic Conditions**

The principal advantages of clay/shale media are the low hydraulic conductivity of the host rocks and the potential to attenuate radionuclide migration in groundwater through adsorption. A repository would ideally be located in a formation with low hydraulic head gradient (e.g., on the order of 10<sup>-4</sup> or less),

which might be associated with arid or semi-arid recharge conditions, limited occurrence of surface water (or snow and ice), and flat terrain. These conditions are favorable to construction, operation, closure, and postclosure performance of a repository.

Clay/shale media are hydrologically saturated, in that all interstices (macropores, nanopores, and inter-layer spaces) are fully occupied by water. Clay minerals are water sensitive, and loss of water during construction and operations can be destabilizing. At the same time, clay/shale media with low permeability may be very slow to produce groundwater into excavated openings, and much of the water in the undisturbed material apparently does not behave as mobile, free water. What this means for excavation and ground support is that water inflow and hydraulic loading are secondary concerns, at least for time scales on the order of years to decades.

That said, slight water inflow is observed in a few boreholes at the Meuse/Haute-Marne URL (Callovo-Oxfordian) and at the Mont Terri URL (Opalinus), demonstrating that channel flow can and does occur in shale media. This means that design, preparation for construction activities, and performance analyses should accommodate the potential for water inflow from discrete zones, over a wide range of flow rates. Moreover, investigation of water inflow during repository development should support determination of source characteristics (e.g., reservoir size) as well as the use of engineered plugs and seals to isolate groundwater pathways in the host rock from the waste emplacement areas of the repository.

## 4.2 Preclosure Performance Criteria

Preclosure performance encompasses worker safety, construction, emplacement operations, maintenance, closure operations, safety of the public, and the costs associated with achieving each of these items. Constructability and operability are addressed by design activities, while preclosure safety is evaluated using risk analysis. The present study is a conceptual prelude to design and preclosure safety analysis, with the objective being to describe a plausible, generic disposal system in a shale host rock, so that the postclosure performance can be modeled by GDSA.

### 4.2.1 Accommodating Clay/Shale Rock Characteristics

Excavations in shale media are designed to accommodate rock characteristics: strength, creep, and sensitivity to drying or wetting (slaking; Hardin 2014). Strength and creep behavior determine the type of ground support needed to support openings. Immediate support during or after excavation is necessary in shales to control rock deformations and rockfall hazards. Large opening-closure displacements can occur, which may require special ground support measures such as phased support installation, delayed support installation, compliant support components, robust and/or thick rigid liner systems, and/or extended bolting radius. The goal is to have ground support that continues to apply confinement even with large closure pressures and/or displacements. In the case of creep, it may be possible to apply enough confinement so that the stress condition proximal to the opening is similar to the undisturbed in-situ condition (slowing creep and increasing loading of ground support). In summary, with the assumption that openings must serve for more than a few weeks or months and cannot be allowed to fail without support, two general approaches are used: (1) systems that apply confining pressure while accommodating large displacements, and (2) rigid systems that apply sufficient confining pressure to arrest closure displacements.

Shotcrete is intolerant of large displacements and where cracking occurs, steel sets may be added for additional, compliant support. In some shale media with time-dependent deformation response, shotcrete may be applied in stages that extend until the closure rate has decreased (a few months or years).

For the present study a minimal support system is selected consisting of rock bolts (length and anchorage determined by support requirements), which retain welded wire cloth, covered by a layer of shotcrete (thickness typically 10 to 30 cm). For permanent openings (i.e., at least 100 years service life, including service openings, shafts, ramps, etc.), ground support may involve multiple layers of shotcrete and steel

sets, or a heavy lining to stabilize creep. For temporary openings (i.e., up to approximately 3 years), ground support is limited to shorter rock bolts and thinner shotcrete, depending on site characteristics.

Slaking is decrepitation of shales that are sensitive to moisture, in response to drying and wetting that occur on exposure to the changing mine atmosphere. Where slaking is a concern, all exposed surfaces in shafts, ramps, drifts and other openings must be covered to prevent interaction with the humidity changes. Covering or coating of exposed surfaces is also needed to inhibit direct contact with unexpected ground water inflow or water sprayed for dust control. Covering options include cast-in-place concrete, metal liners, and shotcrete which may be fiber reinforced or applied over wire cloth. The shotcrete option is relatively fast and inexpensive; it is selected for the present study. Similarly, for the present study the invert roadbed would be constructed from fiber-reinforced shotcrete.

Finally, the liner system may be required to control the influx of flammable methane gas production, in combination with ventilation.

#### **4.2.2 Facility Lifetime**

The shale repository will have a minimum 100-year operational period, after construction, not including licensing periods or closure operations. Three waste emplacement strategies resulting in facility lifetimes of 100 to 150 years are discussed below. Projections of percent waste emplaced are relative to the projected total inventory of 135,000 MTU (Section 4.1.1) and do not account for measures such as emplacement of de-rated or smaller waste packages that would be employed to expedite closure.

##### **4.2.2.1 Co-located Repositories for BWR and PWR SNF**

Emplacement of waste packages containing BWR spent fuel, which tend to be cooler than waste packages containing PWR spent fuel of a similar age, could begin around 2050 with a thermal power limit of 4 kW, with thermal blending of fuel from dual-purpose (storage and transportation) canisters (DPCs) into 44-BWR size waste packages (interpreted from analysis of projected DPC cooling, Hardin et al. 2013, Figure 9-1). Emplacement of BWR waste packages would proceed for up to 100 years, controlled by thermal aging and blending considerations. Further studies using updated logistical simulators could be used to detail how much acceleration of the loading schedule may be possible with thermal blending.

To emplace all PWR fuel within a prescribed period one approach (not recommended in Section 4.5) would be to stagger the BWR and PWR emplacement campaigns by 50 to 75 years. This is because PWR fuel tends to require more thermal aging (and there is more tonnage in a 21-PWR size package). If PWR fuel emplacement begins around 2100, then the operation could be completed in 100 to 150 years, with heavy dependence on thermal blending. This approach would essentially involve two co-located but separate repositories with some common facilities.

The Next Generation System Analysis Model (NGSAM), a capability for simulating waste management options (Joseph et al. 2019), was used to explore the discussion in the previous two paragraphs. If the monitored geologic repository (MGR) that accepts BWR SNF opens in 2050 and the MGR that accepts PWR SNF opens in 2100, then nearly 91% of the BWR SNF is projected to be emplaced by 2150 and nearly 79% of the PWR SNF is projected to be emplaced by 2200. Additionally, nearly 94% of the PWR SNF is projected to be emplaced by 2250.

##### **4.2.2.2 Increased Power Limit**

Another possible approach (also not recommended) is to increase the emplacement package thermal power limit to 6 kW. A repository for BWR and PWR fuel could be opened by around 2050, and the operating lifetime limited to around 125 years (interpreted from DPC cases in Hardin et al. 2013). This outcome would also rely heavily on thermal blending particularly for disposition of PWR fuel.

An NGSAM simulation was performed to explore the discussion in the previous paragraphs. If the MGR opens in 2050 with an emplacement package thermal power limit of 6 kW, all of the SNF is projected to be emplaced by 2170. Additionally, over 99.6% of the SNF is projected to be emplaced by 2150.

#### **4.2.2.3 Delayed Opening**

A simpler approach (recommended in Section 4.5 as a reference concept) would be to delay opening of the repository to approximately 2100, and operate it for another 100 to 150 years for disposal of both BWR and PWR spent fuel. This approach would tend to extend the storage time for spent fuel in DPCs to 150 years or longer, which is plausible but well beyond the original design life. DPC containment longevity can be managed for 100 years (NRC 2014) and may not be a significant issue.

To summarize the lifetime recommendation, if repository development is delayed to 2100, then the operating lifetime could be limited to around 100 years for both BWR and PWR fuel with an emplacement thermal power limit of 4 kW/package. Thermal blending would be critical for disposition of younger, hotter spent fuel, and smaller packages or de-rated packages would be employed to complete emplacement of the hottest fuel in this timeframe. Note that the delay identified here is approximate, being based on simulation of DPCs which are generally larger than 21-PWR/44-BWR capacity. Further discussion is provided in Section 4.5.

A 100-year facility lifetime (repository opening around 2100) is long compared to industrial manufacturing or energy production facilities that are decommissioned or replaced after about 50 years due to obsolescence. However, it compares to public works such as dams, bridges, transport tunnels, and aqueducts that have remained in service for decades and are expected to serve for 100 years or longer. Note that emplacement openings can be excavated just-in-time and closed after just a few years, as recommended in Section 4.6, so this operational lifetime requirement applies mainly to underground access and service tunnels (Section 4.2.3) as well as repository handling and packaging facilities at the surface.

An NGSAM simulation was performed to explore the discussion in the previous three paragraphs. If the MGR that accepts SNF opens in 2100, then nearly 87% of the BWR SNF is projected to be emplaced by 2200 and nearly 79% of the PWR SNF is projected to be emplaced by 2200. Additionally, nearly 94% of the PWR SNF is projected to be emplaced by 2250. De-rating (short loading) of waste packages for hotter fuel could be used to reduce the duration of operations to 100 years, as noted below in the discussion of NGSAM capabilities.

Information about the NGSAM simulations to keep in mind includes the following:

- A significant amount of effort to optimize the waste package packing algorithm in NGSAM has not yet been undertaken. Improving the waste package packing algorithm is an area of potential future work.
- Waste packages are not short-loaded to allow for earlier emplacement. This could potentially be added as a capability in NGSAM to allow for earlier emplacement of additional packages.
- Linear interpolation is performed to estimate heat values in between the dates when assembly heat values are estimated. If an alternative interpolation method is implemented in NGSAM, it could potentially result in improved accuracy in estimating heat values. Additionally, the more dates where heat values can be estimated will definitely result in improved accuracy in estimating heat values.

#### **4.2.3 Service/Access Opening Operational Duration**

Underground access and service openings for a shale repository will have nominal operating lifetimes of 100 years, with additional time for construction, licensing, and closure. Additional durations of 10 years



have been assumed for these additional activities, bringing the total nominal service lifetime to 120 years (to support 100 years of waste emplacement operations).

Several aspects of repository facilities and functionality will make it easier to achieve 120-year service lifetime. Perhaps most important, with the recommended layout and construction sequence (Section 4.6) most of the long service life features of the disposal system would be located in nonradiation areas, and could be more readily maintained than emplacement drifts. Modularity of subsurface emplacement is important because it can facilitate early closure of emplacement panels, decreasing the extent of underground openings and facilities that require continued maintenance. Some facilities such as shafts and ramps would be designed to serve for the full lifetime of the repository, with allowance in the design for replacement if needed.

Modularity and redundancy are correlated since multiple independent facilities for packaging, transport, ventilation, etc., permit maintenance and upgrades without shutting down operations. Another aspect of redundancy is the extensive layout area assumed to be available for repository construction, which means that the layout can be adapted if there is a need for underground facilities to be replaced or redesigned. For example, extra room in the repository layout can be provided for additional ramp or shaft pillars, and for replacement ventilation drifts.

#### **4.2.4 Waste Package Shielding**

Waste package concepts currently under consideration for GDSA modeling do not include permanent radiological shielding of individual packages. This is aligned with some international disposal concepts (e.g., KBS-3, SKB 2011; Andra 2005) while other concepts may provide partial shielding due to package wall thickness (Nagra 2002). Gamma and neutron shielding can be provided as parts of package handling and transport equipment. Shielding around emplaced packages would be needed in the off-normal event that human activity is required in the disposal areas, such as to inspect waste packages or to repair remotely operated equipment. Gamma shielding would typically require 15 cm of additional steel thickness in the disposal overpack (or shielding equivalent in other materials) which would substantially increase the cost and weight of waste packages, and equipment for package handling and transport (see shielding analysis in SNL 2019). Neutron shielding is lighter and cheaper but bulky especially combined with gamma shielding. In addition, shielding materials have thermal insulating properties, and eventually could complicate the chemical evolution of the EBS. In general, providing shielding on a reusable platform such as a waste package transport-emplacment vehicle (TEV) is more cost effective than incorporating shielding into individual packages.

### **4.3 Postclosure Performance Criteria**

Disposal system design is focused on waste packaging and other engineered barriers (backfill, plugs, and seals), other construction details (e.g., ground support and invert construction), and repository layout, all of which are engineered to ensure postclosure waste isolation performance that meets safety objectives and complies with regulatory performance criteria.

#### **4.3.1 Opening Support Criteria**

Service/access openings would be designed to perform with minimal or limited maintenance for the full service life of the underground repository (e.g., 120 years). Separate designs, with different requirements, would be used for the service/access openings vs. the emplacement areas. For service/access openings service life is the principal requirement. Whatever methods are used for construction and ground support, access is maintained and the environment is nonradiological, so the openings can be reworked when the repository is closed. For example, the liner can be removed using a retreat strategy, as the openings are backfilled.

For emplacement openings there are postclosure performance criteria. In the repository layout (Section 4.6) relatively short, blind emplacement drifts are used, which reduces the number of possible

transport pathways through the EBS. Emplacement openings would be as small as possible consistent with ground support and waste package emplacement, which reduces the potential damaged rock zone. Ground support would be designed to function only until waste emplacement, backfilling, and plugging of the drift were complete.

Backfill would be used to limit “chimney” formation, which can occur by fracturing in the roof as the opening consolidates over time. Extensive fracturing in the roof could produce permeable channels parallel to the emplacement drifts, through which ground water and released radionuclides could be transported.

### 4.3.2 Ground Support Material Criteria

Portland cement-based materials (such as shotcrete) and steel are the most readily available and practical materials. Considering the overall scale of a shale repository for U.S. commercial SNF (more than 300 km of drifts) material procurement and installation will be important to overall project cost, and there are no realistic alternatives to cementitious materials and steel.

For all underground drifts, ground support would consist of steel rock bolts, steel wire cloth (welded), shotcrete, and steel sets (as needed). This system can be used with either excavation method considered below. These would be committed materials (i.e., not removed). The composition and quantity of shotcrete would be evaluated in preclosure and postclosure performance evaluations. Ground support materials would not be aggressive toward waste packaging materials such as low-alloy steel or stainless steel (Section 5). The principal interactions would be between cementitious materials, the waste package overpack, and buffer or host rock (Section 8.2).

A pre-cast concrete segment liner system is often used with excavation by tunnel-boring machine (TBM) and could be applied to runs of the service/access drifts with few planned drift intersections. However, where a large number of drift intersections are planned such as the access drifts (Section 4.6) a segmented liner system could become complex and even hazardous during assembly of intricate block arrangements (vaults, arches, “windows,” etc.). A system with thick shotcrete and steel elements would be used instead.

### 4.3.3 Buffer and Backfill Performance Criteria

Following Lenhard et al. (2011), buffer and backfill are distinguished by function in this report. Buffer protects the waste packages and minimizes radionuclide release from the repository; functions may include physical, chemical, hydrologic, and biological isolation of the waste, protecting the waste package from rock movement, and retarding radionuclide transport. Backfill is emplaced to provide hydrologic isolation, and to maintain the mechanical stability of drifts and shafts (Lenhard et al. 2011). Repository concepts commonly describe buffer emplaced alongside waste canisters and backfill emplaced in access drifts and tunnels (e.g., SKB 2011; Andra 2005). In this section, a concept for backfilling waste disposal drifts with crushed host rock is presented. In Section 6.2, concepts involving emplacement of engineered bentonite buffer in waste disposal drifts are discussed.

The backfill performance concept is integrated with thermal management (Section 4.5). Repository concepts relying on bentonite buffer to protect the waste package typically impose a temperature limit between 100°C and 130°C (e.g., SKB 2011; Andra 2005; Nagra 2002) in the buffer to avoid uncertainty regarding thermal alteration that could decrease swelling and degrade hydrologic and radionuclide retention properties. If bentonite performance is to be discounted at temperatures >100°C, then one solution is to not rely on bentonite at all around waste packages, but maintain the peak temperature below 100°C between packages. Backfilling would be done immediately after emplacement of each waste package, using remotely operated equipment.

Backfill derived from processing of the host shale could be used around the waste packages, since its function would be limited to roof support. Then a backfill with an admixture of crushed shale and compacted pellets of dehydrated, swelling clay (bentonite) would be used between packages (Figure 4-1).



The augmented backfill would also have the function of inhibiting ground water flow in the drift, once hydrated. The approach would reduce the amount of clay admixture by about half, thereby lowering cost and the number of trainloads of material needed (approximately one large rail car of admixture material would be needed per waste package backfilled).

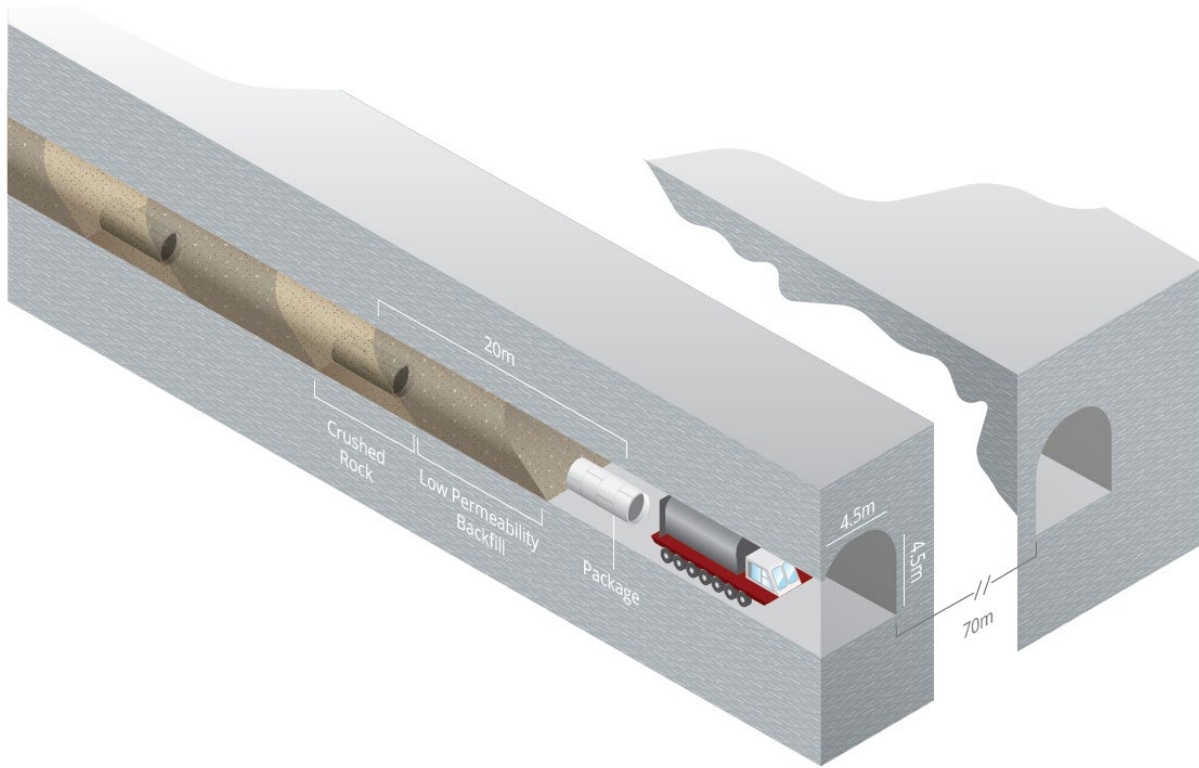


**Figure 4-1. Illustration of Two Types of Backfill: Crushed Rock from the Host Shale around Waste Packages and Low Permeability, Clay Admixture between Waste Packages**

#### 4.4 Excavation and Ground Support Options

The underground repository would consist of several large arrays, each consisting of approximately ten modular disposal panels arranged around a central support area (Section 4.6). Each panel within an array would consist of an access drift roughly 3 km long, connected at each end to service and ventilation drifts. For each panel, there would be approximately 40 blind emplacement drifts spaced 70 m apart. Each emplacement drift would be about 230 m long, including an entry curve and room to emplace 10 waste packages on 20 m centers. Drift details and construction sequence would be optimized using workflow studies that include long-term stability of openings. Some or all of the access drifts could be used for waste emplacement after the adjacent emplacement drifts are loaded, and after their operational support functions are no longer required.

Service and access drifts would complete a perimeter around each array of ten panels, and they would be constructed before the emplacement drifts. Exploring the emplacement area this way would allow reconnaissance of the host rock before starting construction of each panel. It would also develop immediate and redundant access to both the intake and exhaust sides of the ventilation system. Other service drift and ventilation arrangements are possible such as the reticulated array of tunnels proposed for the Salt Repository Project by Fluor (1987) and implemented at the Waste Isolation Pilot Plant

(WIPP). The reticulated arrangement is flexible but has certain disadvantages such as routing options in the event of radioactive material release, and the central locations of service tunnels that need to be maintained for many decades.

#### 4.4.1 Shaft and Ramp Options

Access to the repository for transport of waste packages and other heavy items, could be provided by a shaft or ramp. A waste transport shaft may be preferred in media such as bedded salt with high potential for anomalous ground water pressure, but this would require a heavy shaft hoist that would be the largest of its kind by at least a factor of 2 (SNL 2019). For ductile or brittle shale, it is more likely that ground water inflow will not be a problem during initial construction or final plugging/sealing, so a ramp could provide a more practical access. A similar conclusion was reached by a shaft vs. ramp feasibility conducted by the Canadian waste management program, which recommended use of a ramp for any geologic setting to be considered (e.g., crystalline or sedimentary) (Lee and Heystee 2014).

Typical repository concepts include waste transport ramps with 10% grade suitable for rubber-tire transporters. A ramp may be spiral (e.g., for diesel power) or linear (which may be configured as a funicular with power produced at the surface) (Fairhurst 2012). They have high-strength concrete floors suitable for loading at 12,000 lb or more per tire. A funicular if selected, could be steeper than 10% and would have steel rails and a separate track for a large counterweight. The waste transport ramp and transporter system would be capable of transferring up to three waste packages to the repository horizon per 10-hour shift, and could handle an emplacement throughput rate of at least 3,000 MTU per year (Hardin et al. 2012a).

All types of ramps would be decommissioned and closed the same way: by removing the conveyance, and removing ground support for installation of plugs and seals, in a retreat strategy. For this study, the type of ramp may not be critical since the differences relate mostly to preclosure configuration, while the postclosure configuration after plugging and sealing would be essentially the same.

In addition to the ramp, a shale repository would be accessed by at least three vertical shafts. A single ventilation exhaust shaft would be needed with finished diameter of up to approximately 9 m, air flow capacity of up to 500,000 cfm, and filtration capability at the surface. Additional, smaller diameter shafts (approximately 5 to 7 m finished diameter) would be constructed for personnel (and emergency egress), waste rock removal, and ventilation air intake. The first shafts to be constructed would be the personnel and waste rock shafts, followed by the ventilation exhaust, and ventilation intake shafts. The first shaft would be excavated by drill-and-blast, and subsequent shafts could be raise-bores. Shaft liners would be designed to meet the site geological and hydrological conditions, and would include sections of cast iron, reinforced concrete, and nonreinforced concrete or other materials as appropriate (to be removed for plugging and sealing, at repository closure). Shaft collars and stations would be constructed from reinforced concrete. Headframes, hoist houses, and related facilities would be designed to withstand site-related design-basis seismic and weather loads.

Over the operational lifetime of the repository additional intake and exhaust shafts could be constructed to serve construction and emplacement operations on the different headings.

#### 4.4.2 Mechanized Excavation Methods

Given the extent of excavations for any repository for commercial SNF, mechanized mining of some type would be used wherever possible. A reasonable choice would be to excavate the initial headings with a TBM. Drill-and-blast methods are not necessary, and would cause additional excavation damage especially in more brittle shale. The TBM would provide for initial ground support using rock bolts, wire cloth, and shotcrete (Hardin 2014). This would be supplemented later with steel sets (as needed) and additional shotcrete. Circular openings are preferred because of the inherent stability, and because they are readily excavated by TBM.

During construction of the three shafts, the operations area (Section 4.6) would be constructed using a roadheader (a heavy tracked vehicle with a boom and mechanized cutter head, and provision for removing waste rock typically including a conveyor). The waste transport ramp would then be constructed, and used to transport the parts of a TBM. After assembly of the TBM underground, excavation of the access drifts (about 40 km per array of panels) would begin. Temporary rail would be installed in all TBM-excavated drifts, to support and move the TBM and its trailing gear. The rail would be supported by pre-cast concrete invert segments, which would be left in place after construction, and would underpin the shotcrete floor.

Additional excavation using a roadheader would create ventilation and haulage crosscuts where needed. Temporary rail would be removed, final ground support would be installed, and the final floor constructed. For the ramp, access drifts for waste transport, and emplacement drifts the final floor would consist of compacted crushed rock ballast covered by a thin layer (e.g., 10 cm) of fiber reinforced shotcrete. For other drifts the floor could consist of a thin layer of shotcrete applied over and between the invert segments, followed by a thicker layer of compacted crushed rock ballast. The array of ten panels would then be ready for excavation of the first blind drift for waste emplacement.

For emplacement drifts, mailbox-shaped openings (nominal finished size 4.5 m wide by 4.5 m high) would be excavated by roadheader (Hardin et al. 2013). The roof would be arched to promote stability and limit excavated volume, while the invert (floor) would have a squared cross section to provide width for travel of the TEV. Ground support would be designed to function for only a few years during which time all construction, waste emplacement, and backfilling activities would be completed and the drift plugged and sealed. Minimal ground support would consist of rock bolts and wire cloth, with a thin covering of shotcrete. If more support is needed or large displacements are expected, then steel sets could be used.

Assuming reasonable rock quality with sufficient bearing strength for the TBM, the most difficult aspect of construction and ground support design will be the drift intersections. Generally, a TBM cannot proceed through a previously excavated tunnel, but it can be backed up and repositioned for the next drift to be excavated. However, the TBM will require a “launch chamber” excavated by roadheader, with ground support, each time it is repositioned to begin a new drift. At drift intersections there will be larger spans and wedge pillars created, which may require additional support using steel arches, beams, etc. The layout can be modified during design to minimize the number of difficult-to-construct intersections, for example by extending the blind emplacement drifts to accommodate more than 10 waste packages.

## 4.5 Thermal Management in a Shale Repository

International repository projects in clay/shale media have much smaller capacity waste packages than the 21-PWR/44-BWR packages for this study. The Swiss concept (Nagra 2002) would dispose of four PWR assemblies per package, while the French Cigéo concept (Andra 2005) would dispose of HLW glass or spent fuel equivalent to approximately 2 MTU per package. U.S. spent fuel management practice has tended toward larger capacity because of economies of scale, starting with multipurpose disposable canister concepts developed in the 1990s, and the evolution of DPCs (the majority of which have greater capacity than 21-PWR/44-BWR), and the Yucca Mountain License Application (DOE 2008).

Larger waste packages pose a challenge for thermal management strategy in a shale repository, because (1) both the shale host rock and clay-based backfill materials are temperature sensitive; and (2) waste packages containing significantly more than 2 MTU of spent fuel can develop temperatures well above 100°C in the repository near field. The solution recommended here is to space waste packages relatively far apart, and to manage peak temperatures in the near field so that while temperatures may exceed 250°C near waste packages, other regions of the drift backfill remain below 100°C.

Repository temperature limits may be based on any or all of the following types of constraints:

- Cladding protection limits of 350°C to 400°C (Nuclear Regulatory Commission [NRC] Interim Staff Guidance #11 Rev. 3)
- Waste package material limits (e.g., 200°C < T ≤ 300°C for not longer than 500 years for Alloy 22)
- Clay-based buffer/backfill alteration (possible at temperature greater than 100°C)
- Shale host rock temperature sensitivity (>100°C)
- Repository thermal-hydrology and far-field coupled processes (e.g., dilatancy deformation of shale media discussed in Section 5)
- Waste package handling equipment limits (e.g., 18 kW/package for TEV)

For shale media and repository concepts that rely on clay-based buffer/backfill materials, maximum buffer/backfill temperature and maximum host rock temperature are more constraining than other limits listed above (cladding, packaging materials, repository coupled processes, and handling equipment are associated with higher limits).

The following repository design features are available to modify thermal management to comply with thermal limits:

- Waste package capacity (for this study 21-PWR/44-BWR)
- Fuel burnup and age out-of-reactor (repository opening date and duration of operations)
- Waste package spacing and drift spacing
- Engineered backfill (if used) or natural collapse rubble, and its thermal conductivity
- Host rock heat dissipation properties (primarily thermal conductivity)
- Emplacement sequencing and segregation of waste types (e.g., alternate hotter and cooler packages during emplacement; tailor thermal management to specific waste forms)
- Fuel basket thermal design (heat rejection for cladding protection)
- In-drift vs. borehole emplacement (efficiency of thermal coupling to the host rock)
- “Open-mode” preclosure long-term repository ventilation (similar to aging fuel at the surface)

For this study the repository-opening date and duration of operations are flexible, as discussed in Section 4.2.2 and in the thermal management strategy below. Fuel basket heat rejection would affect internal waste package temperatures, but not external temperatures. In-drift emplacement is selected to ensure feasibility of operations, and “open-mode” ventilation is not used so that emplacement drifts can be excavated, loaded, and closed on an as-needed basis to minimize ground support.

Waste package and drift spacings are selected to be reasonably large (20 m and 70 m, respectively). In the concept engineered backfill composition is varied according to its proximity to waste packages, and whether its function includes control of groundwater flow (Section 4.3.3). Thermal properties are controlled by host rock geology, designated to be either ductile or brittle shale. Note that variability in shale thermal properties is significant and details of the concept could be changed in response to site

characteristics. Emplacement sequencing is represented in the concept by blending fuel into packages and emplacing most of them at or near 4 kW.

#### 4.5.1 Clay/Shale Formation Thermal Properties

Thermal conductivity of clay/shale media has been well studied, and different geologic formations exhibit widely different behaviors. A review and summary (Hardin et al. 2012b) reported average thermal conductivity of  $1.73 \pm 0.61$  W/(m·K), and identified transverse anisotropy up to about 2:1 for some units (greater thermal conductivity parallel to bedding). Heat capacitance (volumetric) was reported at  $2.5 \pm 0.3 \times 10^6$  J/(m<sup>3</sup>·K).

The same study looked at which parameters contribute most to calculated temperature vs. time at the waste package surface, and found that thermal conductivity has the greatest contribution at all times, followed by geometry (ratio of backfill-filled drift radius to package radius), with heat storage effects contributing relatively little.

Backfill thermal conductivity is also important to predicting near-field temperatures. Typical (dry) granulated geologic media have low thermal conductivity on the order of 0.3 W/(m·K) (handbook value for quartz sand; Weast and Astle 1981) because conductive heat flow is impeded due to sparse contacts between grains. Dehydrated, compacted smectite clay has a nominal conductivity of 0.6 W/(m·K) (Hardin et al. 2012b) while addition of even a few percent moisture can increase conductivity to 0.9 W/(m·K) or greater (Jobmann and Buntebarth 2009). For the near-field arrangement described in Section 4.6, it is likely that the backfill closest to the waste packages will heat up rapidly and expel moisture as steam, that condenses in the backfill further away. Thus, the region of backfill between packages will have greater thermal conductivity that couples more effectively to the host rock, while the region closest to packages will be hotter than if thermal conductivity is assumed to be constant.

For scoping thermal calculations discussed below, backfill thermal conductivity is assumed to be a constant 0.6 W/(m·K). For the reasons given above this could tend to underestimate peak temperature at the waste package surface while overestimating backfill temperature between waste packages. This is acceptable for scoping calculations that show backfill temperature can be limited, provided that predicted waste package peak temperature is below levels of concern for longevity of waste package materials and spent fuel cladding (i.e., less than 300°C limits de-alloying and sensitization of waste package barrier materials, and limits cladding degradation by creep rupture; SNL 2008a).

#### 4.5.2 Calculated Generic Emplacement Power Limits

Published thermal scoping calculations that are available for evaluating the shale repository concept include the following:

- ***Repository Reference Disposal Concepts and Thermal Management Analysis. FCRD-USED-2012-000219 Rev. 2 (Hardin et al. 2012a)***—This study considered a range of media and some analyses with 21-PWR size waste packages, but generally used small packages (4-PWR/12-BWR) for shale repository cases.
- ***Collaborative Report on Disposal Concepts. FCRD-UFD-2013-000170 Rev. 0 (Hardin et al. 2013)***—This study included an analysis of peak host rock temperature sensitivity to drift and package spacings, mostly for 32-PWR size packages (bounding 21-PWR results) with in-drift axial emplacement, and including clay/shale media. It also introduced the over-temperature design that heats up the host rock peak temperature to exceed 100°C for some distance beyond the drift wall and preserves a region of backfill between drifts at peak temperature less than 100°C.
- ***Temperature-Package Power Correlations for Open-Mode Geologic Disposal Concepts. SAND2013-1425 (Hardin 2013)***—This study presents tables of cases for open mode (preclosure



ventilation) whereby fuel is aged at the surface (10, 50 or 100 years), then aged underground with preclosure ventilation (40, 90, 100, 150, or 200 years), then closed over a 10-year period, and finally backfilled at closure. Waste package capacity of 4, 12, 21 and 32 PWR assemblies as well as drift/package spacings of 70 m/20 m were considered for clay/shale media. This study also showed that thermal results are relatively insensitive to the exact diameter of a waste package, but directly depend on fuel capacity. Calculated peak temperatures after closure can be used to bound temperatures for waste that is aged on the surface without preclosure ventilation (add the surface aging, preclosure ventilation, and closure durations to determine fuel age at emplacement/backfilling/closure in the present study).

The approach taken here for thermal management strategy development is to use the work on 32-PWR size packages to select aging time (a range, starting at about 100 years) and center-to-center spacings (drift/package spacings of 70 m/20 m), and estimate the resulting peak temperatures at the waste package surface, drift wall, and within the host rock. These results are then compared to package surface and drift wall temperatures after closure, for 21-PWR waste package capacity, calculated for the sedimentary backfilled open concept with the same age range at closure.

A more direct and explicit calculation approach would simulate surface aging and enclosed-mode emplacement with 21-PWR and 44-BWR size packages, and a range of burnup, to verify the more approximate approach taken here. However, the approach here gives acceptable scoping results because uncertainty on generic shale thermal properties ( $1.73 \pm 0.61 \text{ W/(m}\cdot\text{K)}$ ), plus variable anisotropy; see Section 4.5.1) is likely more than the differences between open-mode and enclosed-mode thermal scoping results.

The first application of previous work with 32-PWR size packages is to evaluate the selected spacings (Hardin et al. 2013). Calculations for fuel burnup of 40 GW-d/MTU and drift/package spacing of 60 m/20 m show that 196 year fuel age at closure maintains drift wall temperature at 100°C, or 113 years age maintains 120°C (Table 4-1). Decreasing capacity to 21 PWR assemblies and increasing drift spacing to 70 m, reduces the aging time to maintain drift wall temperature at 100°C, to approximately 100 to 175 years which is consistent with the shale repository concept (see Section 4.2.2). There is some flexibility in these results and the repository schedule to accommodate higher burnup, as discussed below.

**Table 4-1. Ventilation Time Results for Additional Cases**

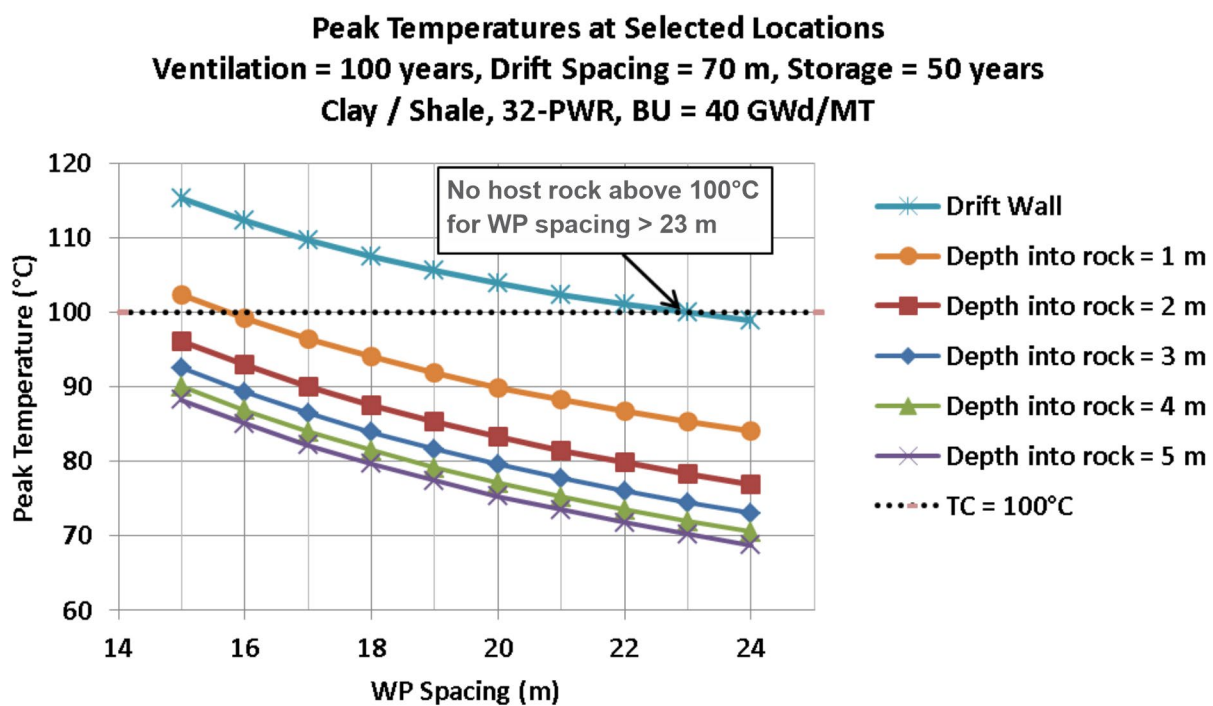
50 yr Decay Storage 32-PWR-Size Package 40 GW-d/MT Burnup			Needed Ventilation Time (yr) <sup>a</sup>		
			Waste Package Spacing <sup>b</sup> (m)		
	Drift Wall Peak Temp. Target (°C)	Drift Spacing (m)	10	20	30
Sedimentary (Clay/Shale)	100	30	1450	513	236
	100	60	660	146	86
	100	90	335	106	80
	120	30	950	270	81
	120	60	347	63	46
	120	90	148	57	44
	140	30	662	116	35
	140	60	156	34	24
	140	90	83	32	23

NOTE: <sup>a</sup> Fuel age is the sum of 50-yr decay storage + ventilation time. Ventilation times longer than 150 yr are shaded.

<sup>b</sup> Waste package spacing is center to center.

Source: Hardin et al. 2013.

The next application is to evaluate temperature rise within the host rock adjacent to waste packages (Hardin et al. 2013). Calculations for fuel age of 150 years (ventilation plus storage), 40 GW-d/MT burnup, and drift spacing of 70 m show that peak temperature at distance of 1 m into the drift wall, can be maintained at 100°C or less, with package spacing on the order of 20 m, with some allowance for higher burnup, etc. (Figure 4-2). This is a scoping result that shows how the radial dissipation of heat limits elevated temperatures within the host rock.



Source: Hardin et al. 2013.

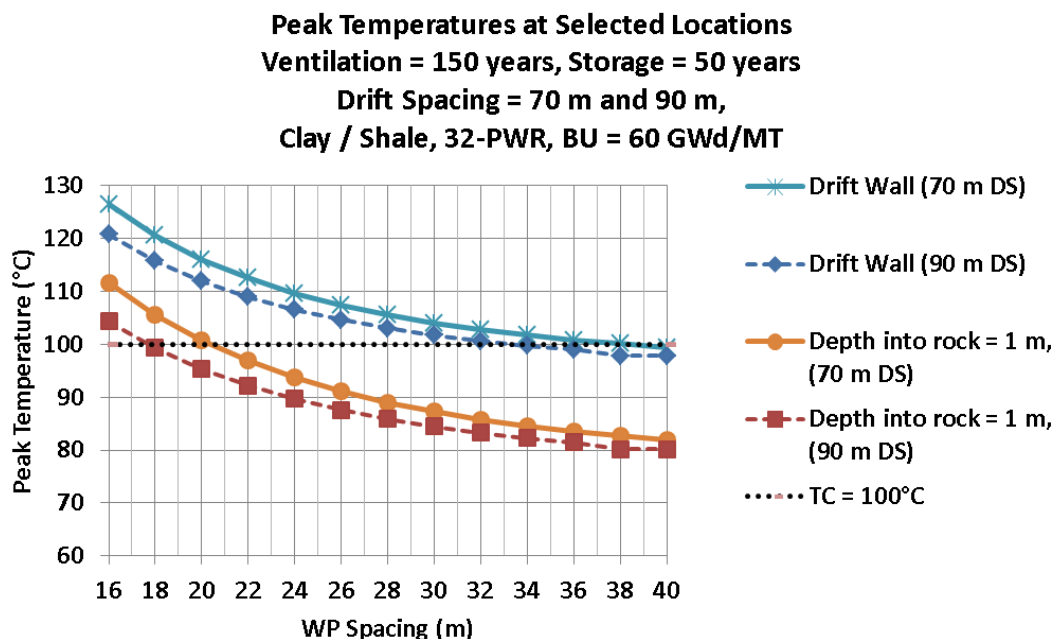
**Figure 4-2. Peak Temperature Versus Package Spacing for Values of Depth into the Rock**  
**(32-PWR size packages, 40 GW-d/MT burnup)**

The next application evaluates the impact of larger drift and package spacings (Hardin et al. 2013). Calculations for fuel age of 200 years (ventilation plus storage), and 60 GW-d/MTU high burnup show only small differences between drift spacings of 70 and 90 m. Increasing the package spacing (up to 40 m) can further reduce near-field temperatures, but package spacing of 20 m is sufficient to maintain peak drift-wall temperature at 120°C or less (Figure 4-3).

The last application of previous calculations is to compare results for 32-PWR and 21-PWR size waste packages (Hardin 2013). The calculations were for open modes, with preclosure ventilation, but the application will use postclosure peak temperature differences to conclude about temperatures for 21-PWR size packages in the shale repository. Presented in Table 4-4, the 10/90/10 case (nominal 110-yr fuel age at closure) and the 50/150/10 case (nominal 210-yr age) roughly bracket the range of fuel age for the



shale repository opening in 2100 and closing 100 years later. For 40 GW-d/MT burnup, the temperature differences between 32-PWR and 21-PWR sizes taken from Table 4-4 are summarized in Table 4-2.



Source: Hardin et al. 2013.

**Figure 4-3. Peak Temperature Versus Package Spacing for Values of Depth into the Rock (32-PWR size packages, 60 GW-d/MTU burnup, 70 m and 90 m drift spacing)**

**Table 4-2. Calculated Temperatures for 40 GW-d/MT Burnup**

Calculated Temperatures	Case Description: Fuel Age at Closure and WP Capacity			
	110 yr		210 yr	
	21 PWR	32 PWR	21 PWR	32 PWR
Peak Waste Package T (°C)	280	352	178	221
Peak Wall T (°C)	97	134	72	95
Difference (°C)	183	218	106	126

Source: Excerpted from Hardin 2013.

Calculations discussed above showed that a 32-PWR size package with 40 GW-d/MT fuel burnup and age 150 years out-of-reactor would produce peak drift wall temperature of approximately 105°C with drift/package spacings of 70 m/20 m (Figure 4-2). This is midway between the estimates for 110 and 210 years tabulated above. The corresponding temperature range for 21-PWR size packages is 97°C to 72°C (110 to 210 years). Linearly interpolating, the drift wall temperature would be about 85°C adjacent to a 21-PWR package at 150 years.

For the 21-PWR package size the tabulated range of waste package surface temperatures is 280°C to 178°C. Linearly interpolating the differences and adding to the interpolated drift wall temperature, gives a package surface temperature of about 238°C at 150-year fuel age. This result is consistent with the peak

temperature limit for the shale repository concept (250°C). Where necessary, thermal blending of younger fuel would draw heavily on lower burnup fuel, and fuel with age greater than 110 years.

Temperature differences for high burnup (60 GW-d/MT) fuel for the 110-year and 210-year cases taken from Table 4-4 are summarized in Table 4-3.

**Table 4-3. Calculated Temperatures for 60 GW-d/MT Burnup**

Calculated Temperatures	Case Description: Fuel Age at Closure and WP Capacity			
	110 yr		210 yr	
	21 PWR	32 PWR	21 PWR	32 PWR
Peak Waste Package T (°C)	395	500	227	284
Peak Wall T (°C)	130	183	86	116
Difference (°C)	265	317	141	168

Source: Excerpted from Hardin 2013.

The drift-wall temperature range for 21-PWR size packages is 130°C to 86°C (110 to 210 years). Linearly interpolating, the drift wall temperature would be about 112°C adjacent to a 21-PWR package at 150 years. This is consistent with the shale repository concept (peak drift wall temperature 120°C) discussed previously (Table 4-1).

For the 21-PWR package size the tabulated range of waste package surface temperatures is 395°C to 227°C (Table 4-4). Linearly interpolating the differences and adding to the interpolated drift wall temperature, gives a package surface temperature of about 327°C at 150-year fuel age. These results are hotter than assumed for the shale repository concept (maximum package surface temperature 250°C) so it is clear that higher burnup fuel must be blended with lower burnup, and loading of high-burnup fuel should be deferred to start midway through the repository lifetime. Note that the heat output for a 21-PWR size package with 60 GW-d/MT burnup and 110-year age, is 4,956 W (Table 4-4), which is significantly greater than the 4 kW repository loading limit. Further reduction in heat output could be achieved by (1) de-rating waste packages (short loading); (2) designing special fuel baskets that accept both high-burnup fuel and damaged fuel (which typically has lower burnup); and (3) using older fuel (repository start date later than 2,100, such that average fuel age is greater than 110 years). Cooler conditions could also be achieved by (1) smaller emplacement drifts (less than 4.5 m diameter), or (2) greater backfill thermal conductivity (> 0.6 W/(m·K)).

Disposal Concepts for a High-Temperature Repository in Shale

October 2020

69

Table 4-4. Peak Drift Wall and Waste Package Surface Temperature Results for the Sedimentary Open Backfilled Concept (70 m drift spacing, 20 m package spacing)

UOX20, Clay, 70-m drift spacing, backfilled																									
~50 yr (store/vent/close = 10/40/10 total=60 yr)					~100 yr (store/vent/close = 10/90/10 total=110 yr)					~150 yr (store/vent/close = 50/100/10 total=160 yr)					~200 yr (store/vent/close = 50/150/10 total=210 yr)					~300 yr (store/vent/close = 100/200/10 total=310 yr)					
WP size	Peak Wall T (°C)	Time of Peak (yr OoR)	Power at Empl. (W)	Power at Closure (W)	Power at Peak T (W)	Peak Wall T (°C)	Time of Peak (yr OoR)	Power at Empl. (W)	Power at Closure (W)	Power at Peak T (W)	Peak Wall T (°C)	Time of Peak (yr OoR)	Power at Empl. (W)	Power at Closure (W)	Power at Peak T (W)	Peak Wall T (°C)	Time of Peak (yr OoR)	Power at Empl. (W)	Power at Closure (W)	Power at Peak T (W)	Peak Wall T (°C)	Time of Peak (yr OoR)	Power at Empl. (W)	Power at Closure (W)	Power at Peak T (W)
4	37	59	1156	520	527	34	115	1156	319	304	33	241	592	238	188	32	280	592	202	150	32	515	341	164	126
12	57	59	3468	1560	1580	47	116	3468	956	907	43	244	1776	715	560	42	380	1776	606	450	40	532	1024	492	369
21	80	59	6069	2730	2765	62	116	6069	1674	1587	54	257	3108	1252	955	52	380	3108	1061	788	49	532	1791	861	646
32	107	59	9248	4160	4214	79	116	9248	2550	2418	68	257	4736	1907	1455	65	380	4736	1616	1200	60	532	2730	1312	985
WP size	Peak Wall T (°C)	Time of Peak (yr OoR)	Power at Empl. (W)	Power at Closure (W)	Power at Peak T (W)	Peak Wall T (°C)	Time of Peak (yr OoR)	Power at Empl. (W)	Power at Closure (W)	Power at Peak T (W)	Peak Wall T (°C)	Time of Peak (yr OoR)	Power at Empl. (W)	Power at Closure (W)	Power at Peak T (W)	Peak Wall T (°C)	Time of Peak (yr OoR)	Power at Empl. (W)	Power at Closure (W)	Power at Peak T (W)	Peak Wall T (°C)	Time of Peak (yr OoR)	Power at Empl. (W)	Power at Closure (W)	Power at Peak T (W)
4	79	61	1156	520	513	60	111	1156	319	313	52	161	592	238	236	48	211	592	202	201	45	312	341	164	166
12	159	61	3468	1560	1540	109	111	3468	956	939	89	161	1776	715	709	80	211	1776	606	603	71	313	1024	492	496
21	227	61	6069	2730	2695	152	111	6069	1674	1643	121	161	3108	1252	1240	107	211	3108	1061	1055	94	317	1791	861	863
32	284	61	9248	4160	4107	187	111	9248	2550	2503	147	161	4736	1907	1889	130	212	4736	1616	1603	113	322	2730	1312	1304
UOX40, Clay, 70-m drift spacing, backfilled																									
~50 yr (store/vent/close = 10/40/10 total=60 yr)					~100 yr (store/vent/close = 10/90/10 total=110 yr)					~150 yr (store/vent/close = 50/100/10 total=160 yr)					~200 yr (store/vent/close = 50/150/10 total=210 yr)					~300 yr (store/vent/close = 100/200/10 total=310 yr)					
WP size	Peak Wall T (°C)	Time of Peak (yr OoR)	Power at Empl. (W)	Power at Closure (W)	Power at Peak T (W)	Peak Wall T (°C)	Time of Peak (yr OoR)	Power at Empl. (W)	Power at Closure (W)	Power at Peak T (W)	Peak Wall T (°C)	Time of Peak (yr OoR)	Power at Empl. (W)	Power at Closure (W)	Power at Peak T (W)	Peak Wall T (°C)	Time of Peak (yr OoR)	Power at Empl. (W)	Power at Closure (W)	Power at Peak T (W)	Peak Wall T (°C)	Time of Peak (yr OoR)	Power at Empl. (W)	Power at Closure (W)	Power at Peak T (W)
4	49	58	2680	1104	1135	41	113	2680	648	624	37	190	1272	462	404	36	288	1272	378	309	35	470	700	296	228
12	91	58	8040	3312	3406	67	113	8040	1944	1872	56	187	3816	1385	1225	53	288	3816	1134	927	49	470	2100	889	684
21	139	58	14070	5796	5960	97	113	14070	3402	3276	78	187	6678	2423	2143	72	288	6678	1985	1623	65	470	3675	1556	1198
32	197	58	21440	8832	9082	134	113	21440	5184	4992	104	198	10176	3693	3242	95	288	10176	3024	2473	84	470	5600	2371	1825
WP size	Peak Wall T (°C)	Time of Peak (yr OoR)	Power at Empl. (W)	Power at Closure (W)	Power at Peak T (W)	Peak Wall T (°C)	Time of Peak (yr OoR)	Power at Empl. (W)	Power at Closure (W)	Power at Peak T (W)	Peak Wall T (°C)	Time of Peak (yr OoR)	Power at Empl. (W)	Power at Closure (W)	Power at Peak T (W)	Peak Wall T (°C)	Time of Peak (yr OoR)	Power at Empl. (W)	Power at Closure (W)	Power at Peak T (W)	Peak Wall T (°C)	Time of Peak (yr OoR)	Power at Empl. (W)	Power at Closure (W)	Power at Peak T (W)
4	138	61	2680	1104	1089	93	111	2680	648	635	74	161	1272	462	457	66	211	1272	378	376	58	311	700	296	295
12	307	61	8040	3312	3267	193	111	8040	1944	1904	146	161	3816	1385	1370	126	211	3816	1134	1128	105	311	2100	889	885
21	452	61	14070	5796	5717	280	111	14070	3402	3331	208	161	6678	2423	2397	178	211	6678	1985	1975	145	313	3675	1556	1543
32	571	61	21440	8832	8711	352	111	21440	5184	5076	259	161	10176	3693	3653	221	211	10176	3024	3009	179	316	5600	2371	2338
UOX60, Clay, 70-m drift spacing, backfilled																									
~50 yr (store/vent/close = 10/40/10 total=60 yr)					~100 yr (store/vent/close = 10/90/10 total=110 yr)					~150 yr (store/vent/close = 50/100/10 total=160 yr)					~200 yr (store/vent/close = 50/150/10 total=210 yr)					~300 yr (store/vent/close = 100/200/10 total=310 yr)					
WP size	Peak Wall T (°C)	Time of Peak (yr OoR)	Power at Empl. (W)	Power at Closure (W)	Power at Peak T (W)	Peak Wall T (°C)	Time of Peak (yr OoR)	Power at Empl. (W)	Power at Closure (W)	Power at Peak T (W)	Peak Wall T (°C)	Time of Peak (yr OoR)	Power at Empl. (W)	Power at Closure (W)	Power at Peak T (W)	Peak Wall T (°C)	Time of Peak (yr OoR)	Power at Empl. (W)	Power at Closure (W)	Power at Peak T (W)	Peak Wall T (°C)	Time of Peak (yr OoR)	Power at Empl. (W)	Power at Closure (W)	Power at Peak T (W)
4	60	58	4480	1696	1748	47	111	4480	944	921	41	172	1980	643	598	39	255	1980	500	430	36	423	1028	371	296
12	126	58	13440	5088	5244	86	111	13440	2832	2764	67	171	5940	1930	1802	61	249	5940	1500	1312	54	423	3084	1114	887
21	200	58	23520	8904	9178	130	111	23520	4956	4837	97	170	10395	3377	3171	86	249	10395	2625	2296	73	423	5397	1949	1551
32	290	58	35840	13568	13990	183	111	35840	7552	7371	133	170	15840	5146	4832	116	249	15840	4000	3498	97	423	8224	2970	2364
WP size	Peak Wall T (°C)	Time of Peak (yr OoR)	Power at Empl. (W)	Power at Closure (W)	Power at Peak T (W)	Peak Wall T (°C)	Time of Peak (yr OoR)	Power at Empl. (W)	Power at Closure (W)	Power at Peak T (W)	Peak Wall T (°C)	Time of Peak (yr OoR)	Power at Empl. (W)	Power at Closure (W)	Power at Peak T (W)	Peak Wall T (°C)	Time of Peak (yr OoR)	Power at Empl. (W)	Power at Closure (W)	Power at Peak T (W)	Peak Wall T (°C)	Time of Peak (yr OoR)	Power at Empl. (W)	Power at Closure (W)	Power at Peak T (W)
4	197	61	4480	1696	1671	122	111	4480	944	921	93	161	1980	643	636	79	211	1980	500	497	66	311	1028	371	369
12	458	61	13440	5088	5013	269	111	13440	2832	2764	193	161	5940	1930	1907	158	211	5940	1500	1490	125	311	3084	1114	1107
21	680	61	23520	8904	8773	395	111	23520	4956	4837	279	161	10395	3377	3336	227	211	10395	2625	2608	175	311	5397	1949	1938
32	864	61	35840	13568	13370	500	111	35840	7552	7371	351	161	15840	5146	5084	284	211	15840	4000	3974	218	313	8224	2970	2939

Source: Hardin 2013.

### 4.5.3 Backfill and Formation Temperatures

A waste package emplacement thermal power limit of  $\leq 4$  kW would be applied at emplacement (i.e., at backfilling and drift closure). With a shale repository opening in calendar year 2100, the range of fuel age at that time would be from 45 years (assuming current reactors are decommissioned in 2055) to about 125 years (e.g., fuel discharged in 1975). Fuel discharged from current new-builds would be aged for at least 100 years before disposal later in the 22<sup>nd</sup> century.

Center-to-center drift spacing would be 70 m, and center-to-center waste package spacing 20 m. These are conservatively large spacings, but they do not approach a point of diminishing returns (e.g., compare 70 and 90 m drift spacings in Figure 4-3).

An over-temperature strategy would be used for peak host-rock temperature. Temperature at the drift wall would be limited to 120°C, while temperature a short distance into the host rock would be limited to 100°C. The maximum backfill temperature would occur at the waste package surface, and would be limited to approximately 250°C. Backfill at locations this hot would be limited to crushed host rock, while clay-based backfill properties would be credited only in cooler regions between waste packages. Other potential temperature limits (package material, fuel cladding) are significantly higher but are not expected to exceed applicable limits.

Scoping thermal calculations discussed here use a backfill thermal conductivity of 0.6 W/(m·K), which may be challenging to attain with large-scale implementation (several million cubic meters). Cooler conditions could be achieved using the changes identified in the previous section (see also Section 6.2.2.1).

## 4.6 Repository Layout Considerations

A conceptual layout for the shale repository, and the construction sequence (shaft/ramp phase and TBM phase) are shown in Figure 4-4, Figure 4-5, and Figure 4-6.

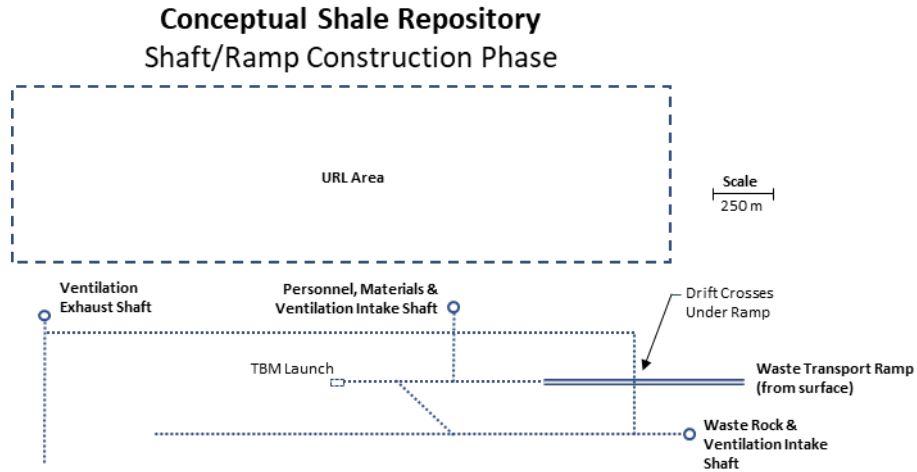
An important constraint on the repository layout is the need to limit the length of time that drifts need to stay open. Service drifts would be mined first, then access drifts, then emplacement drifts starting with those most distant from the central support area. When all the emplacement drifts are loaded and backfilled, the access drifts would be backfilled back to the operations area. Emplacement along that heading would then be complete, and a new set of panels would be excavated on a new heading. The sequence should be designed so that any mishap in a disposal tunnel (e.g., roof collapse, or radiation leak) could be isolated with backfilling and ventilation control, so that further emplacement and other underground operations could continue elsewhere in a “clean” environment.

A repository for 140,000 MTU of commercial SNF in 21-PWR size packages would require approximately 368 km of disposal tunnels and 200 km of service tunnels. The total excavated volume, not including shafts, ramps, or service areas, would be on the order of  $11 \times 10^6$  m<sup>3</sup>. These estimates scale approximately to the capacity, so a repository for only 70,000 MTU would require about half as many drifts and half as much excavated volume (but the same number of shafts). Note that estimates of this nature are for scoping purposes only and should be compared only at the level of one significant figure, pending more advanced design.

### 4.6.1 Shaft/Ramp Phase

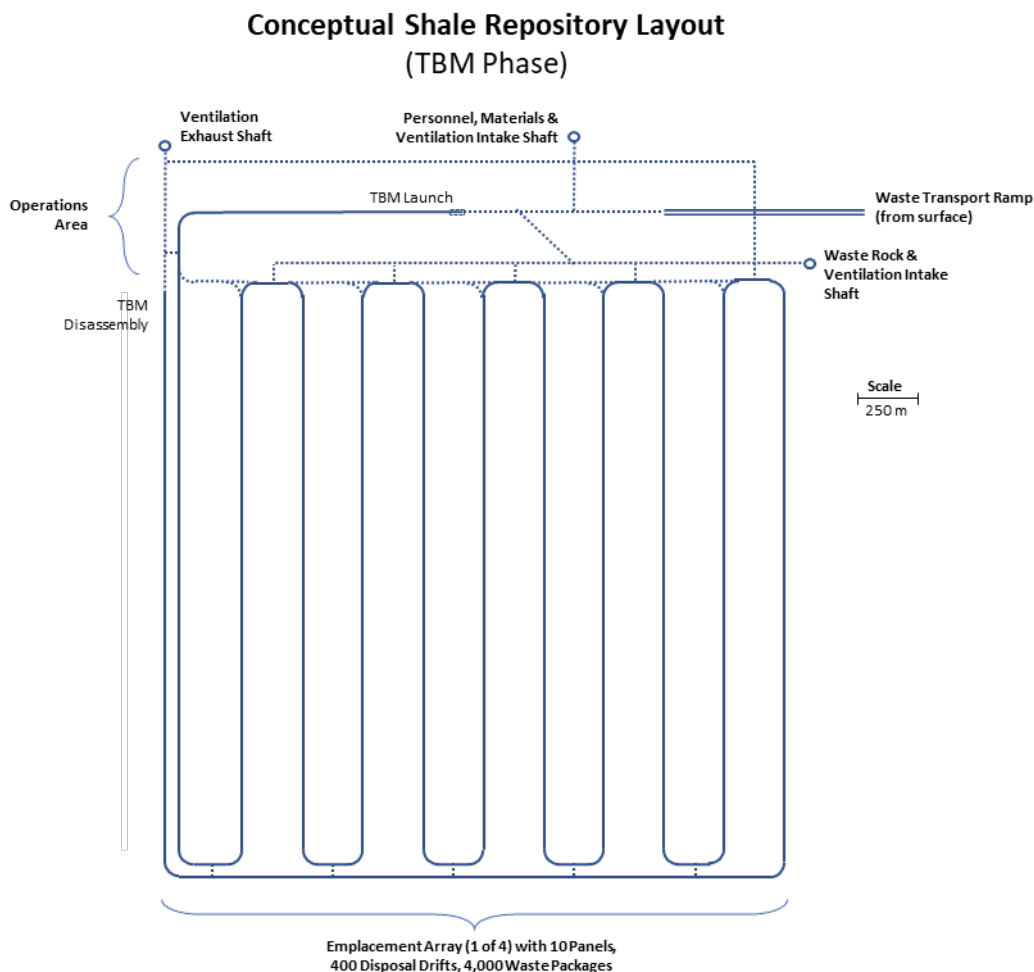
The first shaft to be constructed would be the personnel/materials shaft, followed by the waste rock and ventilation exhaust shafts. The first shaft would be excavated by drill-and-blast, and subsequent shafts by either drill-and-blast or raise boring, following local practice. Following the selections of Hardin and Kalinina (2016, Concept 15) and consistent with the general description in Section 4.4.1, the personnel and waste rock shafts would have finished diameters of 5.5 m, and the ventilation exhaust shaft would have finished diameter of 8 m. These values are provided as reference values for generic modeling studies

that depend in some way on shaft diameter. Shafts would be lined with nonreinforced concrete, following local practice. Nonreinforced concrete is readily removed at closure for plugging and sealing. Service drifts would be excavated mostly during the shaft/ramp phase (Figure 4-4). The service drifts would be excavated by roadheader, and lined with rock bolts, wire cloth, and shotcrete to finished diameter of 8 m. Site characterization URL activities could be performed after completion of the shaft/ramp phase (Figure 4-4).



NOTE: While the ramp shown in the figure is linear, a spiral ramp is also a design option.

**Figure 4-4. Conceptual Layout for the Shale Repository: Shaft/Ramp Construction Phase**



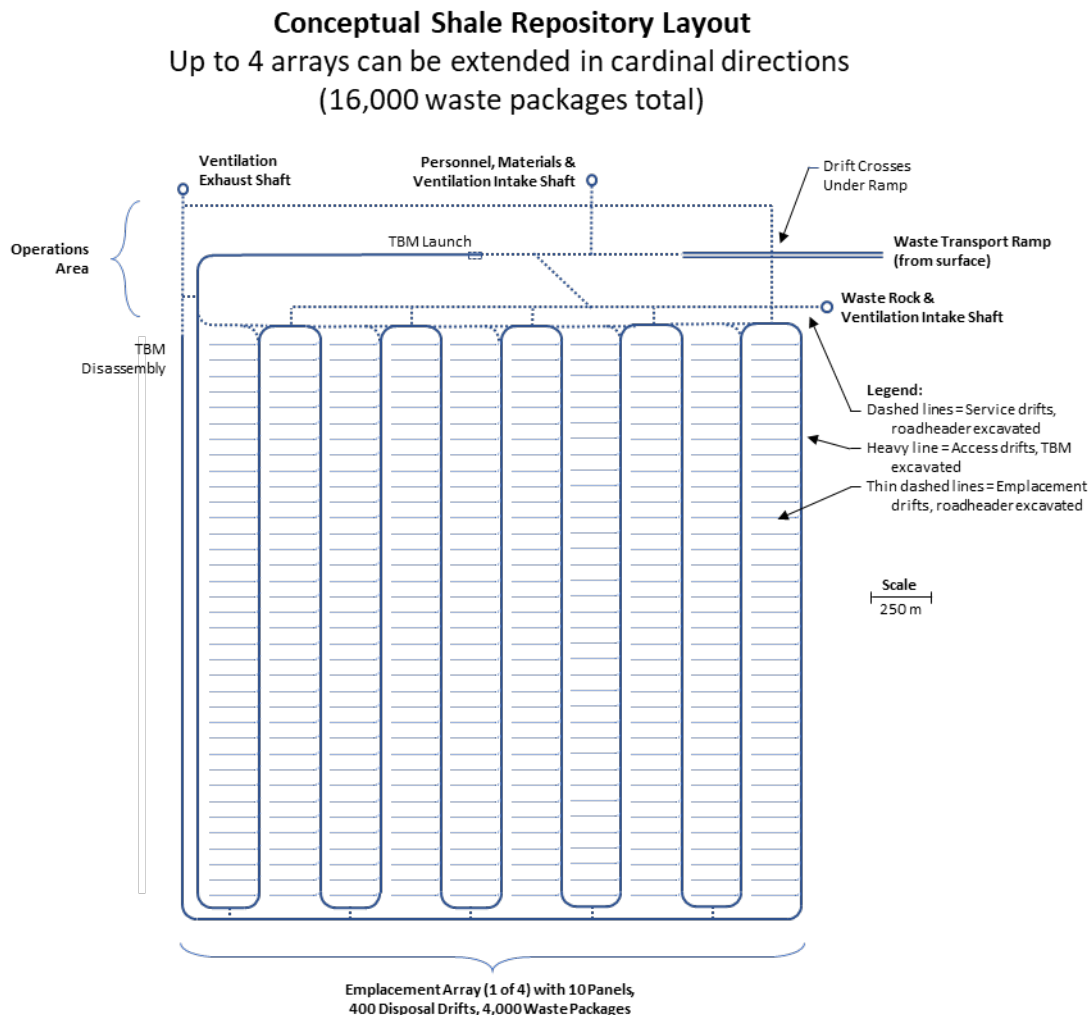
NOTE: While the ramp shown in the figure is linear, a spiral ramp is also a design option.

**Figure 4-5. Conceptual Layout for the Shale Repository: TBM Phase**

When the project is ready for repository construction, the waste transport ramp would be excavated using a roadheader, starting at the surface with grade of 7.5%. The ramp would have a nominal diameter of 6.5 m with a roadway at least 4.5 m wide, and length of 6.7 km. Although less than the 10% maximum grade for rubber-tire vehicles suggested by Fairhurst (2012), the lower grade would improve operational safety (assuming that layout room is available and hydrologic conditions are consistent with ramp selection).

The ramp could be linear or spiral depending on site conditions and other planning considerations. A linear ramp permits installation of a very high payload capacity funicular with the power center at the surface, eliminating a potential cause of underground fire (Fairhurst 2012). However, it would likely require a transfer station underground in the operations area for off-loading waste packages from the funicular to a TEV for underground transport and emplacement. On the other hand, a spiral ramp collocates the ramp surface facilities with shafts and other support. It requires a self-powered waste transporter, which would deliver waste packages all the way from the surface to emplacement. Such a transporter would likely be diesel powered unless regenerative battery-electric technology could be developed (the fire hazard would be different, but present either way). Electric power distribution by pantograph could be used along the waste transport routes (Figure 4-7) in the ramp and access drifts, but

it would create additional hazards, and it would not be suitable for emplacement drifts so that secondary battery power would be needed anyway.

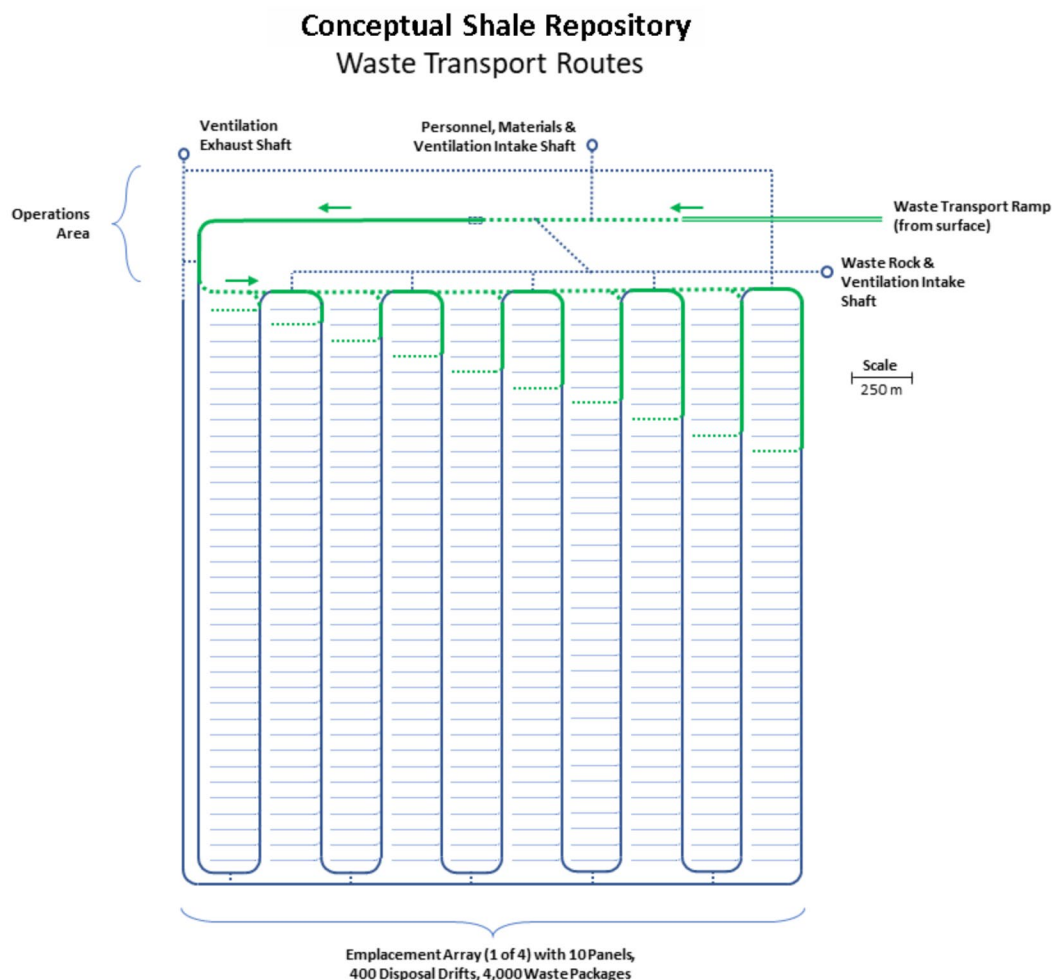


NOTE: While the ramp shown in the figure is linear, a spiral ramp is also a design option.

**Figure 4-6. Conceptual Drift Layout for a High-Temperature Shale Repository**

The TEV would have independent hydraulically driven and steered tandem wheel trucks, with solid rubber tires, similar to Wheelift® hauling equipment ([www.wheelift.com](http://www.wheelift.com)). A TEV loaded with a canister weighing 50 MT in a disposal overpack weighing 30 MT, plus a radiation shield weighing approximately 60 MT (SNL 2019, Appendix A), yields a total payload weight of 140 MT. The dose rate would be less than 50 mrem/hour at the surface of the shield (45 GW-d/MT burnup, approximately 40-year age out of the reactor [OoR]) and heat output of 10 kW. Allowing an additional 100 MT for the transporter yields a total driven loaded TEV mass of 240 MT (more than 500,000 lb). This estimate is comparable to the bounding loaded weight of 273 MT estimated for the Yucca Mountain TEV (BSC 2008). Loaded weight, dose rate, and heat output calculated here are operationally feasible and greater than what would be expected for the reference 21-PWR waste package containing SNF with a 100-year age OoR.





NOTE: While the ramp shown in the figure is linear, a spiral ramp is also a design option.

**Figure 4-7. Conceptual Drift Layout for the Shale Repository with Transport Routes for Moving Waste Packages Underground to Emplacement Drifts**

At approximately 12,000 lb per tire, 48 tires would be used in 24 tandem trucks, 12 on each side. The layout of a TEV would be similar to the Cometto hauler tested in Sweden (Fairhurst 2012) but wider with wheels as small as practical given the running surfaces, and configured around a shield so that it can drive over the top of a waste package and hoist it up into the shield.

#### 4.6.2 TBM Phase

Based on characterization, a heading would be selected for excavation of the first emplacement array (Figure 4-5 and Figure 4-6). TBM components would be transported down the ramp and assembled in the TBM launch section of the operations area (Figure 4-5). Access drifts would then be excavated by TBM to a finished diameter of 7.2 m, lined with rock bolts, wire cloth, and shotcrete. Locations in the access drifts where intersecting service drifts or emplacement drifts are planned, would have special limits placed on ground support so it can be readily removed (e.g., rock bolts and shotcrete only). Interconnections between drifts required for waste rock handling and storage, ventilation, and personnel access, would be constructed using a roadheader, to complete the TBM phase and prepare the array for construction and loading of emplacement drifts.

The access drift layout constructed during the initial TBM phase (Figure 4-5) would explore a region of approximately 3 km by 3 km for the first array of emplacement panels. Mapping and characterization investigations would be used to verify ground conditions for waste emplacement.

### 4.6.3 Emplacement Drifts

Emplacement drifts would accommodate 10 packages, each approximately 5 m long, on 20 m centers (185 m aggregate length), plus a turnout at the access end that takes up about 45 m (230 m total length in the direction of the drift). The unexcavated pillar at the distal end would be at least 20 m. Adjacent access drifts would thus be 250 m apart on centers (Figure 4-6). With emplacement drifts spaced 70 m apart (center-center) the extraction ratio would be less than 7%. The width and radius of the turnout on each emplacement drift would be enough for clearance of the TEV, which would be at least 4 m wide and 10 m long. Turnouts would be designed to intersect access drifts at an angle that promotes stability of the V-shaped pillar between them. Emplacement drift cross section would be mailbox shaped, 4.5 m wide and 4.5 m high (or slightly larger as needed to accommodate the TEV), excavated by roadheader with temporary ground support consisting of bolts, wire cloth, and shotcrete. The floor would be a thin layer (e.g., 10 cm) of fiber-reinforced shotcrete to prevent slaking of the shale and provide a temporary running surface for equipment, especially the loaded TEV. The emplacement drifts would be “blind” which is favorable for waste isolation and requires only one plug/seal to isolate each drift.

The development sequence for each blind emplacement drift (of 1,600 total in the full repository) would consist of: (1) excavation, invert construction, and ground support; (2) emplace each waste package directly on the floor or on a plinth and cover with backfill using remotely operated equipment; and (3) construct the plug/seal in the emplacement drift entry.

Placing each waste package directly on the floor is the simplest mode of emplacement. If the host rock is brittle enough to sustain transmissive fractures, it may be desirable to emplace low permeability bentonite around the entire circumference of the waste package. Elevating the waste package and installing compacted buffer material beneath it would be significantly more expensive and time consuming to construct and would use more expensive materials. In a proof-of-concept test (“FE test”) at the Mont Terri URL (Nagra 2019), the scaled waste package was initially elevated on a “plinth” of compacted, dehydrated clay surrounded by a pelletized clay backfill. The test was hydrated artificially and heated, then examined afterward by excavation, from which it was determined that the package had moved during hydration. Results from the FE test are not directly applicable to a disposal concept with waste packages weighing approximately 10 times as much. Operational safety, engineering feasibility, and postclosure performance concerns would need to be addressed.

The waste isolation performance of a shale repository depends heavily on the natural barriers including low-permeability host rock (whether ductile or brittle shale). Emplacing waste packages in high-permeability host rock, or in high-permeability zones within the host rock, would be avoided. Allocating isolation performance to the host rock, there should be no need for an enclosing buffer of clay-based material around each waste package. This is reflected in the use of backfill that is less dense than compacted clay, and also in the selection of the waste package emplacement mode. Elaboration of the concept to include completely enclosing each package in temperature-sensitive buffer material, would depend on site-specific or project-specific factors to justify the additional cost and risk. Solutions such as elevating waste packages on blocks of clay, would be weighed against other remedies to supplement natural barrier performance such as a more corrosion resistant waste package.

Each package would immediately be buried with processed, crushed shale up to the roof. This would be done using portable shielding, remotely controlled equipment, and handling the backfill pneumatically or with augers. A 5-m-or-so length in the middle between packages would be backfilled with a mixture of crushed shale and dehydrated, pelletized bentonite (a clay consisting predominately of smectite minerals). Stacking of backfill materials would be loosely controlled; the angle of repose is about 35° (Figure 4-1).

Shielding for in-drift human access starts to become effective when the waste package has 2 m or so of backfill covering (SNL 2019).

Backfill materials would be stacked as high as practicable but not necessarily to the roof. The void volume within the stacked material (porosity 30% or greater, a difficult parameter to control in stacking operations) far exceeds the volume of a reasonable head space. The backfill will expand when hydrated, by an amount that is maximized volumetrically by the presence of void space. The clay-augmented backfill would be designed to expand enough to achieve the void reduction, and loading pressure on the host rock, set by requirements. Eventually the opening will close in on the backfill further increasing the loading pressure. There could be some penetration of hydrated backfill into open fractures in the host rock, but this effect would not be credited with reducing water flux because the clay would be readily mobilized in flowing fractures.

At the entrance to each emplacement drift a plug/seal would be constructed, consisting of two barrier walls (e.g., prefabricated concrete) with a plug of dehydrated, compacted bentonite blocks between. The roof, ribs, and invert in the plug interval would be cut away to improve sealing against intact shale. Backfill would be stacked against the barrier walls for mechanical support. Thickness of the entire plug would be about 5 m, roughly equal to the width and height. Design of the plug/seal would be tailored to the hydrologic environment of the repository. In a shale with the possibility of channel flow, analysis could show that plugging/sealing is needed throughout the repository to limit flow along repository openings.

#### **4.6.4 Ventilation and Other Services**

The ventilation plan during emplacement operations would always direct air flow from emplacement areas toward the outside of the array, and toward the ventilation exhaust shaft. This would make it possible to seal off any emplacement area where contamination occurred and continue disposal operations. For emplacement drift development, temporary ventilation would be accomplished using positive pressure vent tubes, with blowers located in the access drifts. The equipment would be moved to each successive emplacement drift developed. During excavation of each emplacement drift, muck would be stored if necessary, and used for backfilling of the previous emplacement drift.

Since forced ventilation would not be used for waste cooling, a minimal number of shafts is needed for ventilation throughout construction and operations. As each waste panel is completed, its ventilation requirement would be minimized. As each array of panels is completed, it would be backfilled and isolated from the rest of the underground facilities by plugging/sealing.

Mine water, electric, and compressed air utilities would be provided throughout the service and access drifts, but only temporarily in emplacement drifts as needed during construction. Water, electric, and compressed air connections and equipment would be removed completely from each emplacement drift before waste handling operations and backfilling.

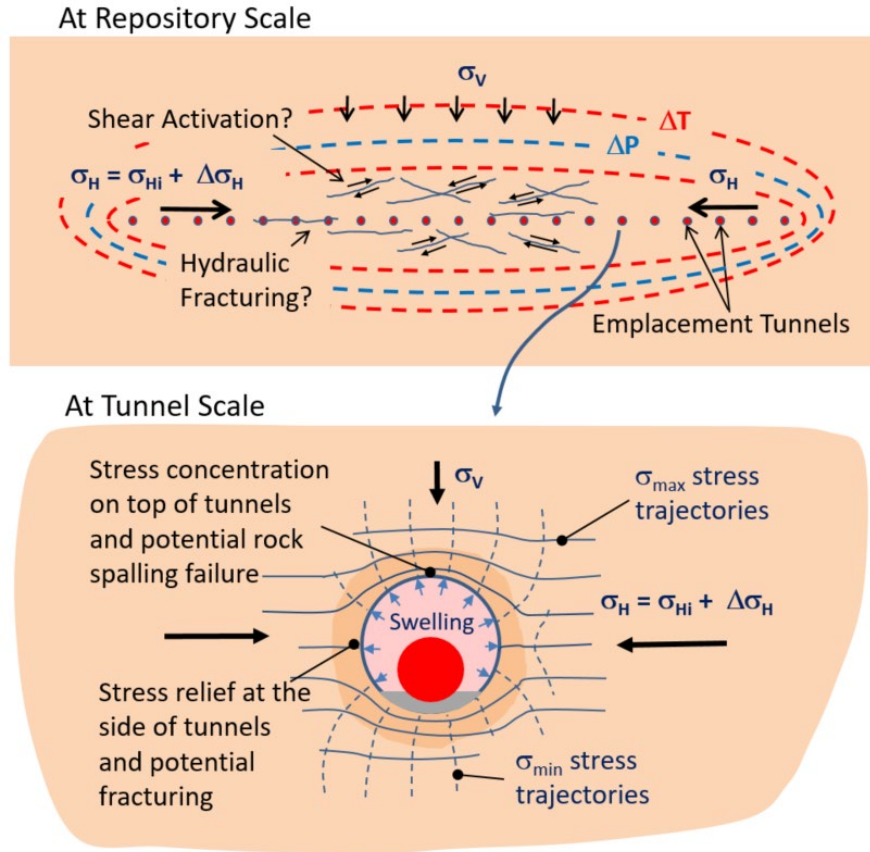
## 5. DISTURBED ROCK ZONE

The shale host rock, whether ductile or brittle, will experience mechanical deformation and alteration of hydrologic properties due to excavation and thermal pressurization. Previous shale reference cases (Mariner et al. 2017; Sevougian et al. 2019a) considered alteration of host rock properties in the DRZ immediately adjacent to drift walls. However, emplacement of large, hot waste packages has the potential to cause thermal pressurization and hydrofracturing at larger scales.

### 5.1 Thermally Induced THM Processes at Tunnel and Repository Scale

Simulation studies have demonstrated the importance of repository temperature in creating thermal stress and thermal pressurization that, if not managed, could potentially lead to formation fracturing or shear activation, as well as high stress concentration and damage around emplacement tunnels (Figure 5-1; Rutqvist 2020). Because the vertical stress remains constant and equal to the weight of the overburden, thermally induced horizontal stress will result in an increased shear stress that will be the driver for potential activation of fractures (Figure 5-1). Such shear activation could result in an increased permeability and could also potentially induce small seismic events. Finally, the increasing horizontal stress will act on the repository tunnels and that stress concentration around the tunnel openings could cause compressive spalling failure or tensile failure to different parts of the tunnel walls (Figure 5-1b). These thermally induced coupled THM processes need to be evaluated in the thermal management of a high-temperature shale repository until the conditions favoring thermally induced shear activation or fracturing have abated, i.e., over a postclosure period of approximately 10,000 years (Rutqvist 2020).

The mechanical properties of shale, whether more ductile or brittle, will likely have a significant impact on the coupled THM evolution, including the potential for mechanical damage and associated changes in transport properties. As discussed in Section 3.2.1, more brittle shales are stiffer (higher Young's modulus and lower Poisson's ratio), stronger (higher compressive strength), and more permeable. Thermal stress is generally proportional to the stiffness of the rock, meaning that a higher Young's modulus and a lower Poisson's ratio tend to increase horizontal thermal stress changes. That situation may tend to increase the shear stress across the repository and could also tend to increase the horizontal stress impact on the repository emplacement tunnels. On the other hand, a higher permeability may reduce the potential for thermal pressurization, and therefore lessen the likelihood of hydraulic fracturing within the repository horizon. The potential for hydraulic fracturing and activation of natural fractures in the host rock should be considered in the thermal design of the repository to avoid such damaging effects on the repository host rock. Over time, damage and brittle fracturing in shale formations is typically followed by fracture self-sealing once the conditions leading to rock failure have abated. The ability of a clay/shale rock to provide a low permeability environment over long time periods is affected by conditions of rock stress and stress history, diagenetic alteration, and pore fluid pressure (Nygård et al. 2006). That is, ductile shale with high clay content is more likely to seal compared to a more brittle shale.



NOTE:  $\sigma$  = stress, where subscript indicates direction (V = vertical, H = horizontal, and Hi = initial horizontal) or relative magnitude (max, maximum; min, minimum); P = pressure; T = temperature;  $\Delta$  indicates change.

Source: Rutqvist 2020.

**Figure 5-1. Schematic of Repository-Scale Coupled Thermo-Hydro-Mechanical Responses and Their Impact on Emplacement Tunnels**

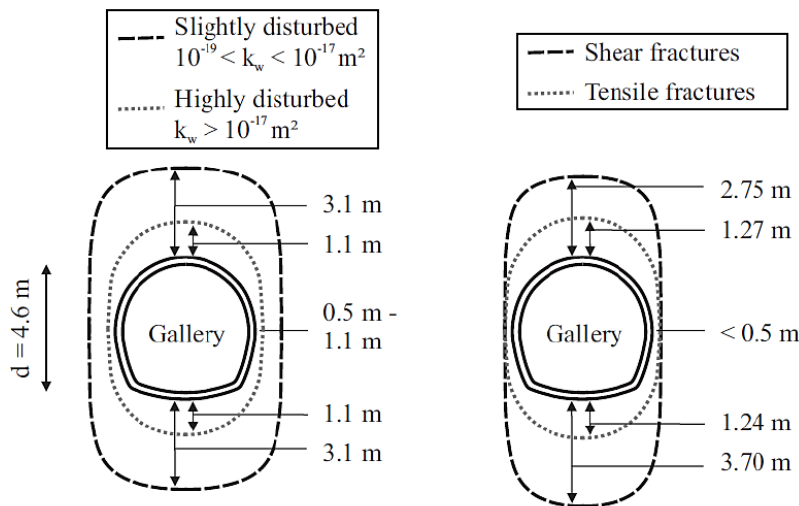
## 5.2 Excavation-Induced Damage in Ductile Versus Brittle Shale

The mechanical properties, whether more ductile or brittle, will also impact the formation and evolution of the disturbed zone around the emplacement tunnels. Generally, the disturbance may be divided into the EdZ and the EDZ (as a reminder, the excavation-disturbed zone and the excavation-damaged zone, respectively). The EdZ is a zone with hydro-mechanical and geochemical modifications, without major changes in flow and transport properties, whereas the EDZ is a zone with hydro-mechanical and geochemical modifications, inducing significant changes in flow and transport properties (Tsang et al. 2005). The formation of the EDZ will be controlled by the initial stress field, the material properties (e.g., material anisotropy), the existence of natural fracture zones or local inhomogeneities of the rock mass and the geometry of the tunnel. Comprehensive investigations at different sites at European URLs have shown that an EDZ occurs in ductile or plastic clays as well as in harder indurated claystones (Blümling et al. 2007).

For the performance assessment it will be necessary to estimate the shape and transport properties of the EDZ as this information can provide insight about potential permeable paths for radionuclide transport. The actual shape and properties of the EDZ in a mined repository will be site specific, depending on the local rock properties and in-situ stresses. However, observations at tunnels in URLs may be used to derive conceptual models of the shapes and properties, the nature of which might differ for more ductile versus more brittle shales. For example, Figure 5-2 illustrates a conceptual model of EDZ in the case of



tunneling along the minimum principal stress direction in indurated Callovo-Oxfordian Claystone at the URL in Bure, France. The site investigation shows that shear fractures extending farthest from the tunnel are not permeable, whereas close to the walls and the crown of the tunnel, mixed shear and extension fractures unloaded against the free-face tunnel wall result in significantly higher permeability, e.g. above  $1 \times 10^{-17} \text{ m}^2$ . This value is a three-orders-of-magnitude increase from the undisturbed permeability, which is about  $1 \times 10^{-20} \text{ m}^2$  for Callovo-Oxfordian Claystone. This highly disturbed zone extends 1.1 m for this particular tunnel, which has a diameter of 4.6 m. Results similar to those in Figure 5-2 would be expected in the case of ductile shale with rock properties similar to those of Opalinus Clay or Callovo-Oxfordian Claystone.

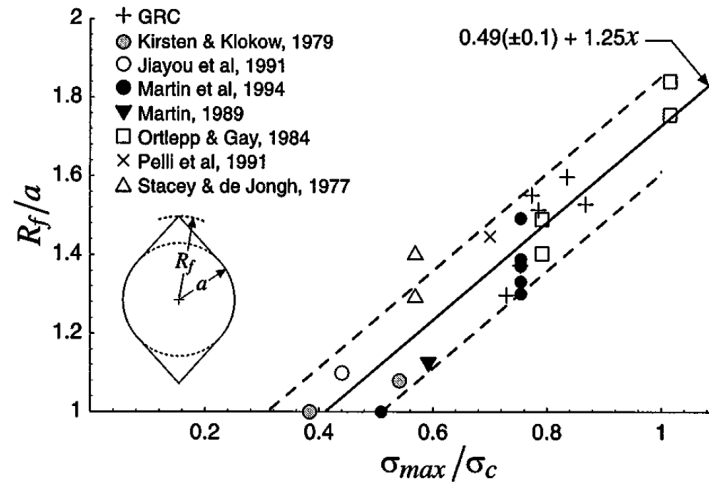


Source: Pardoen 2015.

**Figure 5-2. Extensions of (a) Hydraulic Permeability and (b) Fracture Zones Measured around a Tunnel in the Callovo-Oxfordian Claystone**

For the more brittle Paleozoic shales, there is a lack of systematic field studies on the disturbed zone around excavations in the context of nuclear waste disposal. Instead, analogous situations may be utilized to estimate the expected disturbed zone. Examples include observations of borehole breakout in deep boreholes crossing more brittle shale formation and subjected to anisotropic stress as well as studies in other types of brittle rock. A characteristic of stress-induced failure of tunnels in brittle rock is the notched-shape of the failure region and the associated slabbing and spalling that may occur in a stable manner or violently in the form of strainbursts (Martin et al. 1999). Figure 5-3 presents empirical estimates of the spalling zone in which the spalling starts to appear if the tangential stress at the tunnel wall exceeds 40% of the uniaxial compressive strength measured on laboratory samples (Martin et al. 1999). The data in Figure 5-3 involve various types of brittle rock, including one case of interbedded siltstone-mudstone. If the failure occurs for an open unsupported tunnel, the rock in this notch may fall out. The space could then be filled by a swelling bentonite buffer after emplacement. If this situation occurs behind reinforcement, or during thermal stress increase after waste emplacement, such a rock failure would be expected to increase permeability by orders of magnitude.





NOTE: Prediction is made using brittle failure parameters.

Source: Martin et al. 1999.

**Figure 5-3. Relationship between Depth of Failure and the Maximum Tangential Stress at the Boundary of a Tunnel**

The long-term behavior of the tunnel near field can be significantly influenced by adequate support measures and the time-dependent evolution of the EDZ before the emplacement of the waste and the backfilling. The properties of the initial EDZ alter significantly during the transient phase, when the buffer and rock mass are heated by the heat-producing waste and become saturated due to the flow of formation water from the host rock. Experimental results in the laboratory and in situ clearly show that (self-) sealing leads to a significant reduction in the effective hydraulic conductivity of the EDZ with time, thus reducing the potential flow along underground excavations (Blümling et al. 2007). The processes which are responsible for such a reduction in hydraulic conductivity during saturation and water up-take may be related to accelerated creep, disintegration of the rock, swelling and shear compaction (Blümling et al. 2007). The support of the swelling buffer and backfill on the EDZ can be instrumental in tightening fractures in the EDZ. For example, in-situ experiments on fractures at Mont Terri show a strong dependency of permeability on effective normal stress, with fractures exhibiting transmissivity values close to that of intact rock if effective normal stress is higher than a few MPa. This outcome means that a swelling stress of a few MPa within the buffer could reduce the permeability of the EDZ significantly and may assure sealing in the long term. If fractures are created in more Paleozoic shales, those fractures may stay open for a longer period of time or may never completely seal. Thus, for more ductile or more brittle shale, the EDZ evolution can be significantly different and is best evaluated with site-specific investigations.

## 6. ENGINEERED BARRIER SYSTEM

The EBS includes the waste form (SNF) and its cladding, the waste package, and the backfill or buffer material that surrounds the waste package and fills the emplacement drift (Figure 6-1). The waste package prevents water from contacting the waste form until the package fails, and then may provide some means of delaying the release of radionuclides depending on the failure mode. The waste form cladding may limit the amount of water that can contact the waste form, and a slow dissolution rate of the waste form will limit radionuclide releases to the buffer. The backfill/buffer material surrounding the waste package protects the waste package and may also serve the purpose of limiting radionuclide releases to the natural barrier (Section 4.3.3). As noted in Section 4.3.1, the shale repository concept requires the use of ground support, likely in the form of a concrete liner or rockbolts and shotcrete in the waste package emplacement areas. Although the liner is necessary for preclosure operations and safety, it does not have a postclosure barrier function to limit water contacting the waste form or limit the release of radionuclides. Nonetheless, the materials of construction and their evolution will have to be considered in the coupled thermal, hydrologic, mechanical, and chemical (THMC) evolution of the EBS.

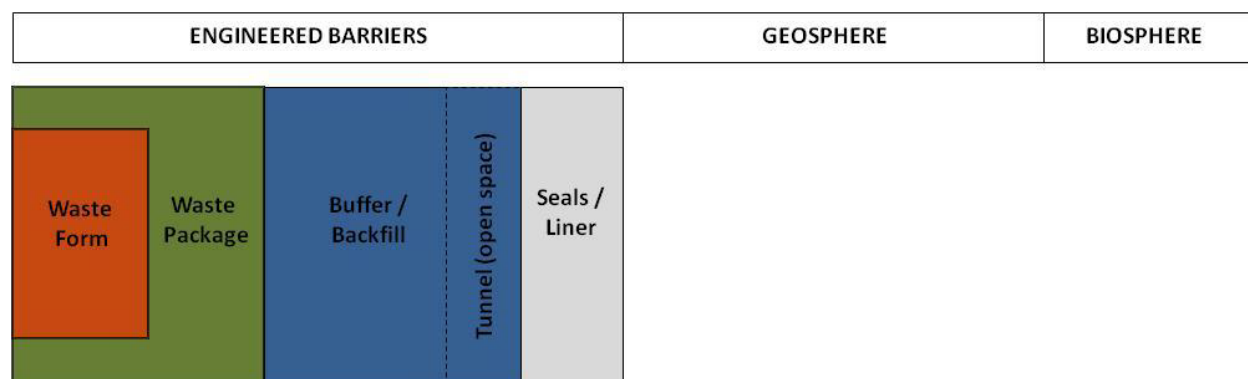


Figure 6-1. Components of the EBS for a High-Temperature Shale Reference Case

### 6.1 Ground Support/Cementitious Liners

In a clay/shale host media, excavations (typically by TBM) will require the inclusion of a ground support. Cementitious liners provide the added reinforcement to keep access and disposal drifts excavations stable during the operational period of the repository. For the most part, tunnel linings will be composed of shotcrete or pre-cast concrete blocks, although metallic structural components (steel or cast iron) may also be used in the form of ribs, sleeves, or panels for certain sections in need of enhanced mechanical support. There is a substantial amount of literature related to constructability, drawn from the experiences and deployment of different techniques in the construction of highway tunnels (Hardin 2014).

Additional research and information, specific to tunneling for nuclear waste repository, exists in various underground tests including those at Mont Terri, KONRAD, and Bure. These resources cover mostly the geomechanics of ground support structures, including interplay between excavated host and the liner structures. While tests and case studies bolster reasonable level of confidence in the constructability and durability during the repository operational period (~100 years), the evolution of deterioration and the ensuing impact of this degradation during the thermal period (~1,000 years) and through the performance period of the repository (~ million years) remains an open question.

There are three general concerns, not necessarily specific to shale/clay, for use of cementitious materials in a repository environment: (1) the perturbation to the base geochemical evolution owing to the extreme alkalinity of cementitious materials, (2) the possibility for the formation of preferential flow pathways due

to large widespread deterioration and/or fracture development, and (3) concerns related to materials sourcing and availability of materials in some ill-defined future time frame. The first two concerns stem immediately from uncertainties regarding the time-dependent and coupled-processes that comprise deterioration of cementitious materials. While it is assumed the cement will degrade completely during over the entire performance period of the repository ( $10^6$  years), in the absence of tests and/or natural analogues, it is harder to understand how the deterioration of cementitious materials will interact with performance assessment. Of particular interest would be development of preferential flow pathways (presumably prior to creep closure of the host rock), and the impact that dissolution/precipitation of cement matrix mineral phases would have on the overall fate and transport of radionuclides.

**Low pH Cement**—The alkalinity of cement matrices was largely addressed by the introduction of so-called “low pH” cements for use in repository settings. Ordinary Portland Cement has a pore solution pH of  $\sim 13$ , since the porewaters are saturated with calcium hydroxide. In low pH cements, silicon-rich additives, like coal fly ash or silica fume, are added to the cement mixture, resulting in a paste that essentially forms no calcium hydroxide and yielding a cement with a pore solution pH  $\sim 10$ – $11$ . An in-depth summary of low pH cements can be found in Dole et al. (2004). The concept of low pH cement, initially developed for the safety assessment for the Yucca Mountain Project, has been widely adopted in repository designs for various host media, including shale/clay host formations.

**Cracking and Advective Pathways**—Widespread cracking and fracture propagation is a well-known damage mechanism in cements, which could be instigated in a repository environment in number of ways; one likely factor in a waste repository containing heat-generating waste is the thermal pulse. Since cementitious materials are a saturated porous material in regular service environments, the dry-out expected during the thermal period in a heat-generating nuclear waste repository could, in theory, lead to widespread dehydration-induced cracking in liner materials. This damage, in turn, could be exacerbated by creep closure induced geomechanical stresses. This is an instance in which further study would be necessary to understand the plausibility of advective pathways forming as a result of drying damage would have an impact of repository performance.

Fiber reinforced concretes have been used to mitigate crack formation in cements and concretes (Li 2019). Specifically, glass or steel fibers can be added to shotcrete to prevent crack formation in tunneling projects (Hardin 2014). That said, there are several chemical processes (alkali silica reaction, sulfate ingress, etc.) that can lead to significant mechanical damage in cementitious materials, and models that can capture important chemo-mechanic coupling under repository conditions are still a much-sought-after capability in the cement research community at large. Lacking such sophisticated three-dimensional (3D) models, cementitious materials have a tendency to be represented in performance assessment models using simplified representations that introduce conservative assumptions into the safety case (NEA 2012). Overall, better understanding of fundamental processes will be needed, together with better modeling tools that can capture such fundamental processes.

**Sourcing, Availability, and Sustainability**—One critical issue facing use of cementitious materials in a repository is ensuring the availability and consistency of supplemental cementitious materials (SCMs), e.g., fly ash, silica fume, etc., into some unknown future timeframe where the material, usually an industrial by-product, may no longer be available. This was well-illustrated during the development of the cementitious seals for WIPP, where several years of research were devoted to developing a specialized expansive salt concrete for the harsh saline environment of the Salado evaporite (Wakeley et al. 1990), only to be derailed due to sourcing difficulties for one of the key constituents, the expansive agent.

For example, fly ash, an extremely common cement additive currently, is derived from the ash produced at a coal-fired power plant. As trends continue towards lowering  $\text{CO}_2$  intensity of cement products, demand for the material has increased. Verifying the proportions of fly ash additive that can safely be added to cement with respect to mechanical and chemical stability, as well as negotiating microstructural and chemical differences in fly ash owing to coal type, etc. were critical challenges that took several years

to solve. Of course, if current trends of sustainability decarbonization continue well into the 21<sup>st</sup> century, some SCMs, like fly ash, may become difficult or impossible to source. This sourcing difficulty would have significant impacts on the ability to verify and validate current low pH cement recipes, potentially nullifying the years of testing and field-scale demonstration that will have gone into the materials' development and technical basis.

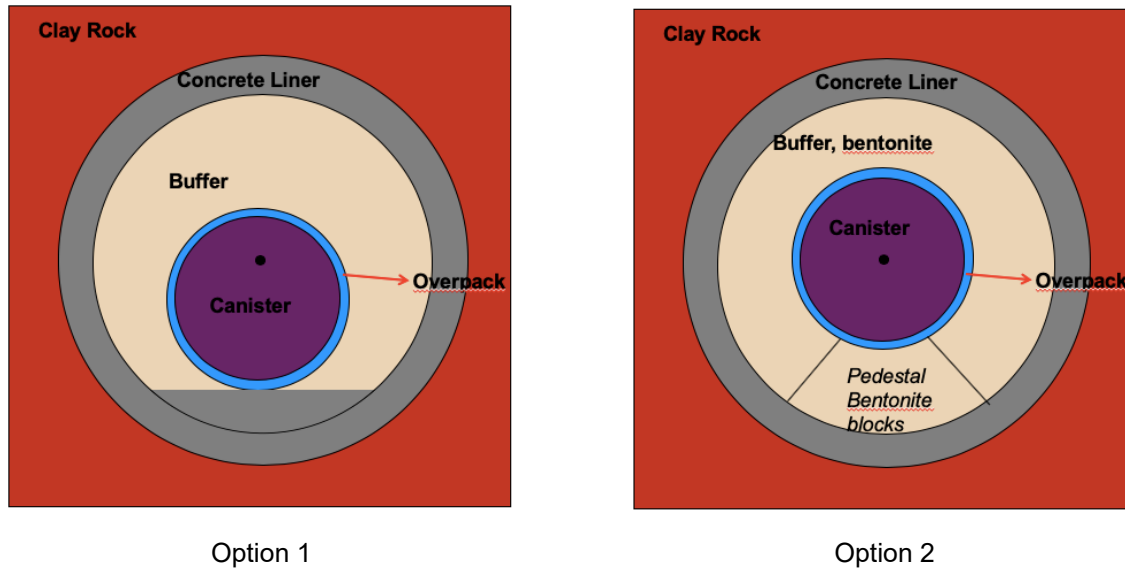
## 6.2 Buffer

The reference concept for a mined repository in a shale host rock assumes that waste emplacement drifts will be backfilled to provide shielding during the operations period, to prevent rock fall and large deformation of the drifts, and to inhibit advection along the drifts postclosure (Section 4.3.3). The emplacement concept presented in Section 4 assumes crushed host rock is emplaced around each waste package and a mixture of crushed host rock and low-permeability, high-sorption capacity bentonite buffer is emplaced between waste packages to prevent flow and retard radionuclide transport. In the case of a repository in a ductile shale, which similar to bentonite has high clay content and sorption capacity, low permeability, and the ability to self-heal, reliance on the backfill to inhibit advective transport may be minimal. In the case of a repository in a more brittle shale (lower clay content and possible fracture-enhanced permeability), reliance on the backfill may be greater. In this case, emplacing a swelling, low-permeability, high-sorption capacity bentonite buffer throughout the waste emplacement drift may be desirable.

This section describes options for emplacing compacted bentonite buffer in waste disposal drifts. It builds on concepts presented in Jové Colón et al. (2014). No further description of crushed rock backfill is given because it has not been widely studied in the literature.

### 6.2.1 Buffer Emplacement

Jové Colón et al. (2014) presented two emplacement options (Figure 6-2). In both cases, the waste package emplacement is coaxial with the drift. In Option 1, the waste package rests on the cement invert that forms the floor of the drift. In Option 2 the waste package rests on a plinth of compacted bentonite. Demonstration tests carried out at Mont Terri URL have demonstrated the constructability of full-scale bentonite plinths capable of supporting up to 1,000 MT ( $10^6$  kg) (Müller et al. 2017), more than 10 times the weight of a loaded 21-PWR waste package (Table 6-9)..



Source: Modified from Jové Colón et al. (2014).

**Figure 6-2. Geometry of a Cross-Section of a Drift for Two Emplacement Options: Option 1 (waste package with overpack sits on a concrete floor) and Option 2 (waste package with overpack sits on a buffer pedestal)**

In either option, a double-layer buffer configuration comprised of two different engineered materials could be used to optimize the physical and chemical properties of the engineered barrier or to create an inner sacrificial layer in which buffer temperature would be allowed to exceed performance-relevant temperature limits and an outer layer in which temperature limits would be met (Jové Colón et al. 2014). Other backfill emplacement strategies in the immediate vicinity of the waste package could include (1) use of a backfill material for which limited credit is taken regardless of temperature (i.e., crushed host rock as in Section 4.3.3), (2) use of amendments designed to increase the thermal conductivity of the bentonite buffer, or (3) use of a buffer material expected to be stable to high temperatures given site-specific geochemical conditions. The latter two options are expanded upon in the next section.

### 6.2.2 Buffer Material Options

The basic buffer material is bentonite, which is an impure clay consisting predominantly of the mineral component montmorillonite (from the smectite group of expansive clay minerals), along with small amounts of other accessory minerals such as quartz, calcite, and pyrite (Table 6-1).

Table 6-1. Mineral Composition of Various Bentonite Buffer Options

Mineral	FEBEX <sup>a</sup> (wt %)	MX-80 <sup>b</sup> (wt %)	MX-80 <sup>c</sup> (wt %)
Smectite	92±3	87	75
Illite	—	1	—
Kaolinite	—	—	<1
Mica	—	4	<1
Chlorite	0.8	—	—
Quartz	2±1	3	15.2
Cristobalite	2±1	—	—
K-Feldspar	Trace	3	5–8
Plagioclase	2±1	—	
Pyrite	0.02	0.25	0.3
Siderite	—	—	0.7
Calcite	Trace	—	0.7
Gypsum	0.14	0.7	—
Organic Carbon	—	—	0.4

NOTE: FEBEX = Full-scale Engineered Barrier EXperiment (in crystalline rock)

Source: <sup>a</sup> ENRESA 2000; Fernández et al. 2004 as reported in Jové Colón et al. 2014.

<sup>b</sup> Borgesson et al. 2006 as reported in Jové Colón et al. 2014.

<sup>c</sup> Baeyens et al. 2014.

Compacted bentonite is fabricated by adding water to dry bentonite powder. Deionized water or a groundwater composition matching that of the host rock may be used. The initial porewater composition of the bentonite blocks or pellets is then a function of the water composition used in fabrication and any reactions between dissolved ions and the minerals in the bentonite (Jové Colón et al. 2014).

Pellets emplaced in drift can achieve an average dry bulk density of 1,450–1,500 kg/m<sup>3</sup> as in Swiss and French repository concepts (Savage 2014; Idiart et al. 2020). Blocks of highly compacted bentonite can achieve an average dry bulk density of 1,600 kg/m<sup>3</sup> as in the FEBEX (Full-scale Engineered Barrier EXperiment) heater test (Zheng et al. 2020). Thermal, hydrologic, and mechanical properties will depend on choice of emplacement method as well as the addition of any amendments used to enhance thermal conductivity.

### 6.2.2.1 Amendments to Enhance Thermal Conductivity

The peak temperature in the buffer can be reduced if the buffer is engineered for high thermal conductivity (Rutqvist et al. 2020; Sevougian et al. 2019a). Higher thermal conductivity reduces the thermal gradient across the buffer, which effectively reduces evaporation near the waste package. This is beneficial for assuring timely resaturation and development of a uniformly distributed buffer swelling to maintain the protective functions of the buffer (Rutqvist 2020).

#### Quartz, Graphite, and Graphene

Mixtures of bentonite with silica (e.g., quartz), graphite, or graphene oxide filler materials have been considered to enhance thermal conductivity (Choi and Choi 2008; Jobmann and Buntebarth 2009; Wang et al. 2015). Laboratory studies have shown that a 50% quartz content increased thermal conductivity of a bentonite-quartz mixture by only a factor of 1.5 whereas a 50% graphite content increased thermal



conductivity by a factor 7.5 (Jobmann and Buntebarth 2009). As a result, much lower percentage of graphite than sand would be needed to increase thermal conductivity by the same margin.

### Copper Mesh or Threads

Use of a high thermal conductivity copper mesh is proposed to transfer heat from the inner to the outer surface of the buffer (Figure 6-3). An alternative to the copper mesh is an admixture of copper wire threads and bentonite. The volume fraction of copper needed for the copper mesh is 1%. The presence of such a small volume fraction of copper presumably would not change the mechanical or hydrological properties of the bentonite buffer. The potential for and rate of copper corrosion would need to be evaluated on a site-specific basis (see Section 7.1.2, Section 7.2.1.1, and Section 7.2.2.1). Additional modeling and experimental work is needed for proof of concept.

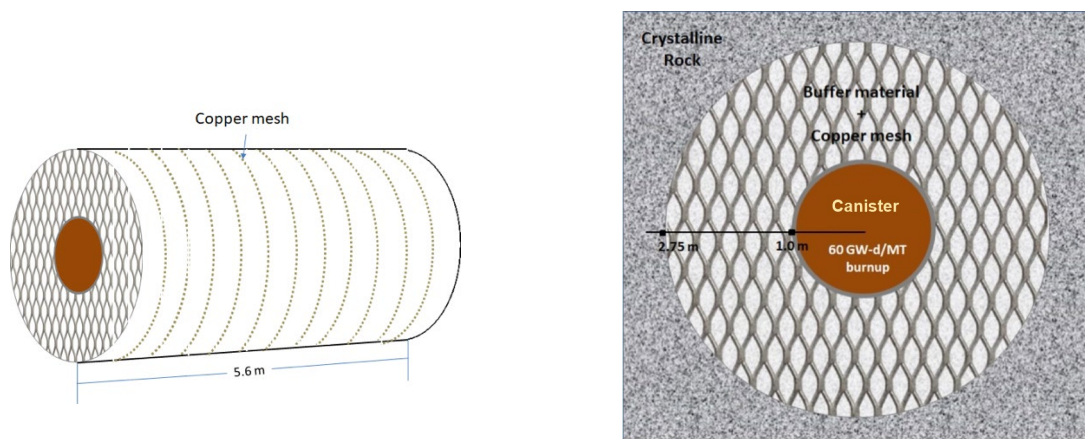


**Figure 6-3. Enhancement of Thermal Conductivity of Bentonite Buffer Materials with Copper Wires/Meshes**

#### 6.2.2.2 High-Temperature Materials

At high temperatures and under certain geochemical conditions, montmorillonite (the smectite phase in bentonite) may be partially replaced with nonswelling phases including illite (given sufficiently high K concentrations; Section 6.2.3.4) and zeolites (in the presence of Portland cement; Section 8). Cheshire et al. (2018) observed interfacial Fe-saponite growth instead of illite in hydrothermal experiments of Wyoming bentonite interactions with steel material (see Section 8).

Tri-octahedral smectites such as natural saponite are known to be less susceptible to alteration under harsh conditions (Eberl et al. 1978; Guven 1990). Recently, Mg-bearing saponite [ $\text{Mg}_3(\text{Si}, \text{Al})_4\text{O}_{10}(\text{OH})_2 \cdot 4\text{H}_2\text{O}$  (saponite-15A)] has been considered as a buffer material (Yang et al. 2014) because of its stability at  $100^\circ\text{C}$ – $200^\circ\text{C}$ , high pH, and high ionic strength (Xiong and Wang 2019). The X-ray diffraction (XRD) pattern of this natural saponite indicated greater stability under the same environmental conditions when compared to montmorillonite. At the same compaction/bulk density ( $1,800 \text{ kg/m}^3$ ), saponite had higher swelling capacity than montmorillonite, thus the saponite can be a good alternative to bentonite. The stability of Mg-rich saponite in multicomponent brines that are expected to be present in clay formations and the stability in the presence of anticipated corrosion products from waste packages/overpacks are currently being studied (Xiong and Wang 2019).

### 6.2.3 Processes in the Buffer Material

After emplacement adjacent to heat-generating waste, the buffer will experience coupled THMC processes, illustrated schematically in Figure 6-4. As temperature in the buffer increases then decreases with time, the buffer, which is initially partially saturated, will experience desaturation followed by resaturation and experience changes in stress due to swelling and thermal expansion. Alteration of minerals with high solubility may occur at early times, followed by alteration of clay minerals at later times. Physical and chemical properties of the buffer evolve in response, potentially affecting fluid flow, solute transport, porewater chemistry, and the stresses experienced by the waste package and at the drift wall.

The following description of bentonite buffer and of the processes acting within it is largely derived from measurements and modeling of compacted bentonite at temperatures of up to 90°C to 120°C. To simplify the discussion, only two bentonite materials are considered in any degree of detail: blocks of FEBEX Ca-bentonite and pellets of MX-80 Na-bentonite. The material properties and behavior of alternative buffer and backfill materials, such as crushed rock, amended bentonite, or saponite would be different.

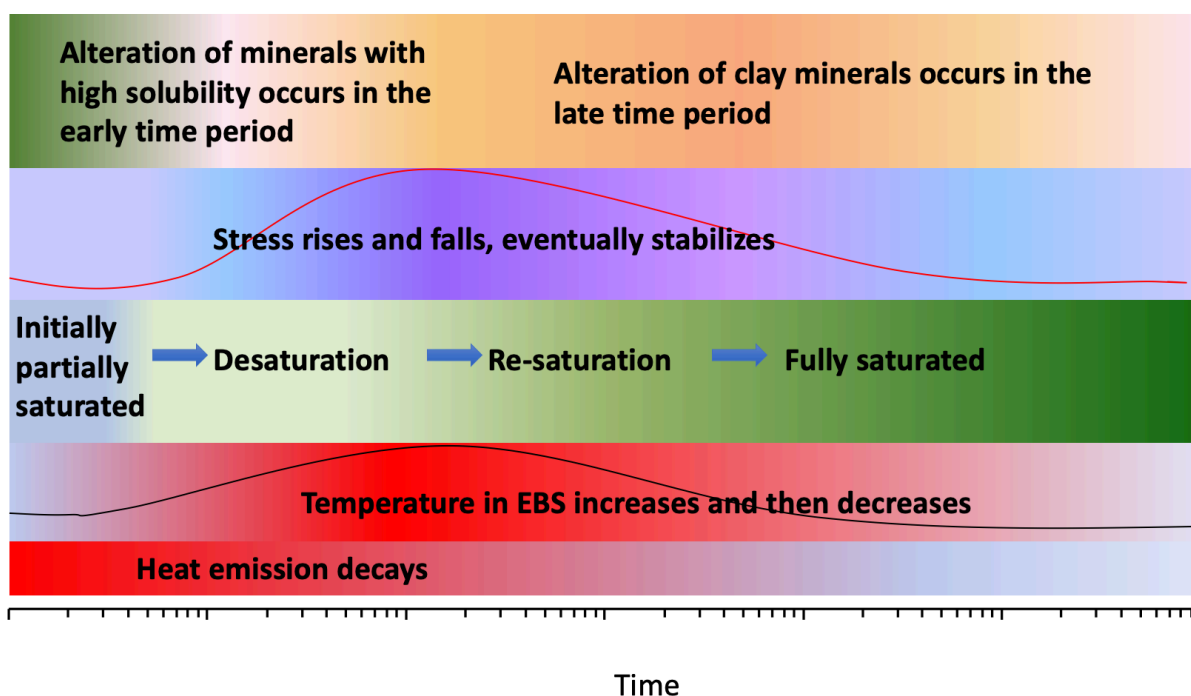


Figure 6-4. Schematic of the Temporal Evolution of THMC Processes in Bentonite Buffer

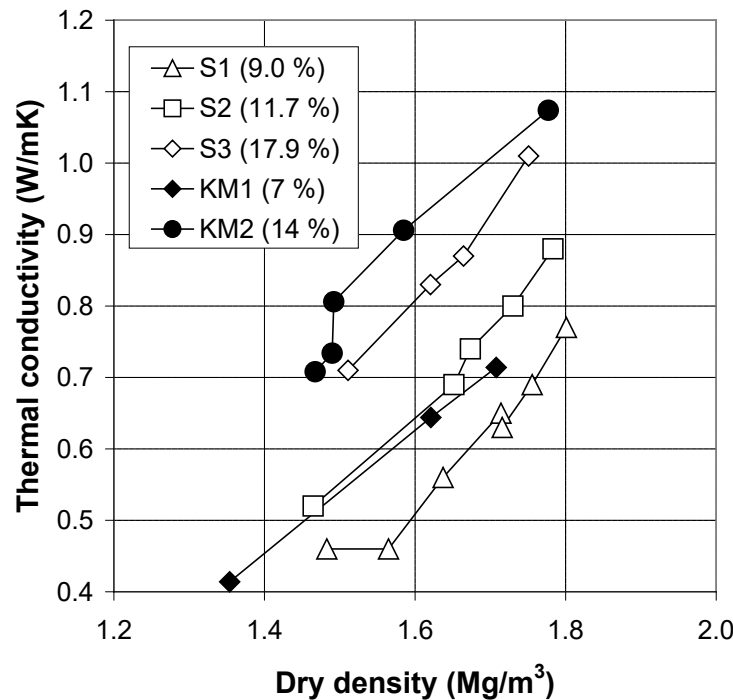
#### 6.2.3.1 Thermal Processes

Thermal processes are conductive and advective heat transport, and phase changes (evaporation and condensation). Key parameters include thermal conductivity and heat capacity. Thermal conductivity is usually specified for the bulk material, while heat capacity is specified for the solid (mineral) phase because liquid and gas equations of state account for the heat capacity of the fluid phases.

Thermal evolution affects pore pressure and stresses in the rock, flow of liquid and gas, and chemical equilibria and reaction rates. An adequate understanding of the temperature evolution in the EBS is important for understanding processes affecting radionuclide mobilization and transport, including waste package corrosion, dilation and compression of fractures, evolution of porosity and permeability, and

radionuclide solubility and sorption; understanding these processes is necessary to ensure that temperature limits will not be exceeded.

The thermal conductivity of compacted bentonite depends on bulk density, water saturation, and temperature. Figure 6-5 illustrates the change of thermal conductivity as a function of dry density and water content for various samples of MX-80 bentonite (Tang et al. 2008). With the exception of having a much higher plasticity index, the samples S1 to S3 tested by Tang et al. (2008) have similar properties to the bentonite used in the FEBEX project (ENRESA 2000). For the compacted bentonite blocks (dry density = 1.7 Mg/m<sup>3</sup>) used in the FEBEX project, the buffer thermal conductivity varies from 0.45 W/(m·K) when completely dry to 1.1 W/(m·K) when completely wet. The effect of saturation can be represented as a nonlinear function, such as a power law function and a variety of empirical relationships relating bulk density and saturations to thermal conductivity have been proposed. THM models validated against data collected at the FEBEX heater test suggest a relatively linear relationship (Zheng et al. 2020).



NOTE: The percentages in parentheses in the legend are water content values. Samples S1 to S3 are original to the study documented in Tang et al. (2008). Samples KM1 and KM2 (Kahr and Müller-Vonmoos 1982) are provided for comparison purposes.

Source: Tang et al. 2008.

**Figure 6-5. Thermal Conductivity of Compacted Bentonite as a Function of Dry Density and Water Content**

Thermal conductivity of common silicate mineral phases and rock types decreases with increasing temperature (Clauser and Huenges in Ahrens 1995; Vosteen and Schellschmidt 2003), while specific heat capacity increases with increasing temperature (Vosteen and Schellschmidt 2003). At temperatures up to 80°C, Lee et al. (2016) observed little effect of temperature on thermal conductivity of compacted bentonite. Xu et al. (2019) observed an increase in the apparent thermal conductivity of compacted bentonite at temperatures between 60°C and 90°C, which they attribute to transfer of latent heat by movement of water vapor and an increase in the thermal conductivity of water with increase in

temperature. A similar increase was not observed in dry bentonite. High-temperature disposal concepts may benefit from improved understanding of the effect of temperature on (apparent) thermal conductivity.

### 6.2.3.2 Hydrological Processes

Primary hydrological processes are liquid and gas flow driven by a pressure gradient. Secondary processes to consider in a high-temperature repository system include thermal osmosis, i.e. fluid flow across a membrane (low-permeability porous medium) driven by temperature gradient, and non-Darcy flow after liquid saturation is achieved (Zheng et al. 2020). Key parameters include intrinsic permeability, relative permeability and capillary pressure functions, compressibility, porosity, thermal osmotic permeability and vapor diffusion constant. A threshold pressure below which flow does not obey Darcy's Law may also be relevant in saturated systems.

Hydrological processes in the buffer affect transport of heat and solutes, mechanical processes including buffer swelling and creep deformation, and chemical reactions.

Zheng et al. (2020) performed numerical modeling of the FEBEX heater test and associated mock-up and small-scale experiments to evaluate the importance of non-Darcy flow, coupled hydro-mechanical processes, and thermal osmosis to bentonite hydration. The FEBEX heater test was designed to maintain a temperature less than 100°C at the contact between the bentonite buffer and the heater; at a radius of 1 m, temperatures reached a maximum less than half this value.

Simulation results suggest that a two-phase Darcy-type flow model adequately simulates bentonite hydration when accounting for changes in porosity and permeability due to bentonite swelling (Zheng et al. 2020). In the unsaturated system, the phenomenon of non-Darcy flow (i.e., a threshold pressure gradient at which Darcy flow initiates) was not distinguishable from parameter uncertainty in relative permeability curves. How best to relate permeability to mechanical behavior (e.g., swelling) remains an open question. Zheng et al. (2020) found that expressing permeability as a function of dry density resulted in a better fit to data than expressing permeability as a function of effective stress. Before the bentonite homogenizes (at full liquid saturation), it may also be relevant to capture spatial heterogeneity in bentonite permeability.

Thermal, hydraulic, and chemical gradients may all influence heat, liquid, and solute fluxes as depicted in Onsager's matrix (Table 6-2) (Horseman and McEwen 1996; Soler 2001). In particular, the temperature gradient across the buffer may be large enough to drive liquid flow by thermal osmosis thus slowing down hydration of the buffer near the heat source (Zhou et al. 1999). For the case in which water is infiltrating the bentonite from the outer circumference of the disposal drift, the effect of adding a thermal osmosis term is the same as decreasing the permeability of the buffer. In simulations of the FEBEX heater test, Zheng et al. (2020) constrained the influence of thermal osmosis to be equivalent to a 30% decrease in permeability. Because the bentonite buffer hydraulic conductivity has some 20%–30% uncertainty, the model was unable to distinguish whether thermal osmosis is a relevant process.

**Table 6-2. Influence of Hydraulic, Temperature, and Chemical Gradients on Liquid, Heat, and Solute Fluxes**

Flux	Gradient		
	Hydraulic	Temperature	Chemical
Liquid	Hydraulic flow Darcy's law	Thermo-osmosis	Chemical osmosis
Heat	Convection flow	Thermal conduction Fourier's law	Dufour effect
Solute	Hyperfiltration	Thermal diffusion or Soret effect	Diffusion Fick's law

Capillary pressure and relative permeability curves may be impacted by changes in fluid properties with temperature. Jacinto et al. (2009) measured decreasing suction pressures in dry, compacted bentonite with increasing temperatures up to 120°C; they proposed that the observed decreases were due not only to decreases in surface tension and contact angle (e.g., She and Sleep 1998) but also to migration of interlayer water in the clay particles to macropores. Better understanding of the effects of temperature on capillarity, water retention, and relative permeability would benefit the development of a reference case for a high-temperature repository in shale.

### **6.2.3.3 Mechanical Processes**

The primary mechanical process occurring in the bentonite buffer is swelling upon rehydration. Thermal expansion (of fluid and mineral phases) will contribute to overall stress conditions in the drift. Other potential processes that may require evaluation include creep deformation, piping and erosion, and transient creation of fractures or dilatant pathways due to buildup of H<sub>2</sub> gas overpressure. Mechanical processes affect porosity, permeability, and pore pressure, and thus affect flow of liquid and gas.

During the dehydration and rehydration process, bentonite buffer nearest the heat source may initially experience shrinking due to dry-out (Zhou et al. 1999). Further from the heat source and eventually throughout, the buffer will swell as it hydrates. Swelling is a chemo-mechanical process. Interlayer water pushes the layers of active clay minerals further apart, causing expansion of the bulk material (e.g., Rutqvist et al. 2020, Section 4). Swelling forms a tight seal with and exerts pressure on the waste package (which must be able to withstand it) and on drift walls (shotcrete). It can contribute to sealing fractures in the DRZ by compressing them. The swelling capacity depends on the mineralogy and initial dry bulk density of the bentonite, the ionic composition of the porewater and the space available for expansion. Jové Colón et al. (2014) cites a swelling capacity of 5–8 MPa for FEBEX bentonite and a swelling capacity of around 1 MPa for Kunigel-VI bentonite.

Swelling behavior of compacted bentonite can be emulated in coupled models using formulations ranging from simple to complex. These include a linear dependence on liquid saturation (as in Zheng et al. 2017); a state surface equation (as in Zheng et al. 2020); and the Barcelona Expansive Model (BExM), a mechanistic model accounting for the coupling between micro- and macro-structural deformation (as in Rutqvist et al. 2020).

Creep deformation of a ductile shale host rock (Chen et al. 2014; Nopola and Roberts 2013; 2016) may occur over the long term and high temperatures could accelerate it. Although it can be argued that bentonite emplaced at a high bulk density will experience minimal creep (Börgesson and Hernelind 2006), bentonite emplaced at lower bulk density may be susceptible to creep deformation after saturation. This behavior has not been evaluated.

Buffer erosion is a process that must be evaluated for mined repositories in fractured crystalline rock (e.g., Neretnieks et al. 2009). It can occur during rehydration where the inflow rate from a fracture exceeds the hydration rate of the buffer; preferential flow paths form (piping) and clay particles are carried away by the focused, flowing water (erosion). Given a sufficiently high flow rate, erosion can also occur after the buffer is fully saturated if changes in ground water composition decrease electrostatic forces between clay particles (for instance, upon infiltration of fresh glacial meltwater). Because a ductile shale would not sustain fractures, erosion under either of these circumstances is unlikely. To develop a reference concept for a repository in a more brittle shale host rock, it may be useful to evaluate the potential for buffer erosion on the basis of fracture flow rates.

Hydrogen generated by anoxic corrosion of metals (and radiolysis of water) may result in a discrete gas phase if the rate of generation exceeds the rate at which it can diffuse through the pores of the bentonite buffer. In this case, the gas phase is hypothesized to migrate through transient fractures or dilatant pathways created by the gas overpressure rather than by viscocapillary (two-phase) flow through the



existing pore network (Rutqvist et al. 2020, Section 7). SFWST participation in the DECOVALEX-2023 task that will involve modeling of the Large-Scale Gas Injection Test in the Äspö Hard Rock Laboratory in Sweden will help further understanding of gas migration.

#### **6.2.3.4 Chemical Processes**

Chemical processes altering bentonite mineralogy and swelling capacity are considered in this section. The effect of chemical processes on radionuclide transport and retention are considered in the following section.

Coupled THMC models have been developed (e.g., Liu et al. 2013; Zheng et al. 2014; 2015; 2017) to evaluate the impact of chemical processes on mechanical behavior, specifically the effect of illitization, pore-water chemistry changes, and cation exchange on the swelling of EBS bentonite.

Given geochemical conditions conducive to replacement of the swelling clay mineral montmorillonite with the nonswelling clay mineral illite, a process known as illitization, bentonite could lose some percent of its swelling capacity (Liu et al. 2013; Zheng et al. 2015; 2017). The potential for illitization depends on many factors including the availability of potassium in the aqueous phase or through dissolution of potassium-rich minerals (e.g., K-feldspar) and temperature (Zheng et al. 2015; 2017). The extent of change in swelling pressure additionally depends on the initial swelling capacity of the bentonite in question and changes in porewater composition (ionic strength). Zheng et al. (2017) performed a numerical modeling study of geochemically induced changes in swelling stress over a period of 100,000 years for Kunigel bentonite and FEBEX bentonite for two scenarios: a “low T” scenario in which temperature peaks at 100°C at the surface of the canister and a “high T” scenario in which the temperature at the surface of canister peaks at 200°C. In the “high T” scenario, models show more stress reduction due to dissolution of smectite and increase in ionic strength than in the “low T” model. The percent reduction in swelling stress due to each process was presented at two points: (1) near the heater (Point A) and (2) near the buffer-host rock interface (Point B). In the “high T” scenario assuming FEBEX bentonite, the increase in ionic strength and the decrease in smectite volume reduced the swelling stress at Point A (near the heater) by 0.1% and 3.4%, respectively, and at Point B (the buffer-host rock interface) by 1.1% and 12%, respectively. For the corresponding Kunigel-VI bentonite study, the values at Point A were 7% and 9%, and at Point B were 8% and 45%, respectively. The larger change at Point B is due to interactions with the host rock. Clearly, there is a significant difference between the two bentonites. Given the initial 92% montmorillonite in the FEBEX case and the swelling pressure of 7–8 MPa, a 10% loss of smectite is unlikely to compromise its performance.

Liu et al. (2013, Section 5.2) provides a review of natural analogue, experimental, and modeling studies investigating bentonite alteration over a range of temperatures up to 300°C. In addition to illitization, a number of other clay mineral alterations have been observed (also see Section 8), some of which are associated with changes in swelling pressure or permeability. Mineralogical changes may also affect radionuclide sorption capacity. Certainly, coupled THMC modeling to inform choice of temperature limits in the buffer and host rock and to improve understanding of the evolution of properties in the EBS is warranted when site- and design-specific data are available.

#### **6.2.4 Buffer Material Properties**

Table 6-3 presents values for THM parameters for two representative bentonites: FEBEX Ca-bentonite emplaced as blocks, and MX-80 Na-bentonite emplaced as pellets. The reader is referred to the cited sources and references therein for additional discussion of these choices, expressions for porosity and permeability as a function of swelling/hydration, specific implementations of relative permeability functions, and parameterization of various geomechanical models.



**Table 6-3. Thermal, Hydrological, and Mechanical Parameters for Bentonite Buffer**

Parameter	FEBEX Blocks, Emplaced <sup>a</sup>	MX-80 Pellets, Emplaced <sup>b</sup>	MX-80 Column emulating Emplaced Pellets <sup>c</sup>
Average dry bulk density (emplaced)	1,600	1,500	1,530
Grain density (kg/m <sup>3</sup> )	2,780	—	2,750
Porosity (—)	0.41	0.45	0.44 to 0.45
Initial liquid saturation (—)	0.55–0.59	0.22	0.22
Saturated permeability (m <sup>2</sup> )	2.15×10 <sup>-21</sup>	1.0×10 <sup>-18</sup>	1×10 <sup>-21</sup> – 9.5×10 <sup>-20</sup>
Relative permeability, $k_{rl}$	$k_{rl} = S^3$	$k_{rl} = S_e^3$	Various
Van Genuchten 1/α (1/Pa)	1.1×10 <sup>-8</sup>	5.6×10 <sup>-8</sup>	3.5 × 10 <sup>-8</sup>
Van Genuchten $m$	0.45	0.41	0.512
Residual liquid saturation	0.1	0.15	Various
Compressibility (1/Pa)	5.0×10 <sup>-8</sup>	—	—
Thermal expansion coefficient (1/K)	1.5×10 <sup>-4</sup>	—	10 <sup>-6</sup> – 10 <sup>-5</sup>
Dry specific heat (J/[kg·K])	1,091	—	950
Thermal conductivity (W/[m·K]) dry/wet	0.47/1.15	—	0.3–0.4/1.0–1.2
Effective vapor diffusion coefficient	7.03×10 <sup>-5</sup>	—	—
Thermal osmosis coefficient (m <sup>2</sup> /[K·s])	1.2×10 <sup>-12</sup>	—	—

NOTE: Values not listed are either not reported or not needed as modeled.  
For relative permeability,  $S$  = liquid saturation and  $S_e$  = effective liquid saturation.

Source: <sup>a</sup> Zheng et al. 2020.

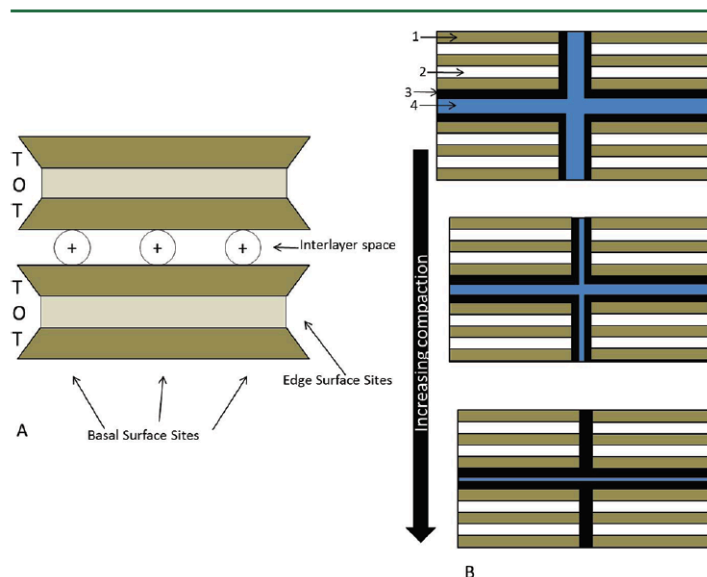
<sup>b</sup> Idart et al. 2020.

<sup>c</sup> Graupner et al. 2018.

### 6.2.5 Radionuclide Transport

In the absence of erosion, bentonite permeability is sufficiently low that radionuclide migration through the buffer will occur via diffusion. Adsorption (surface complexation, cation exchange) will retard transport of some radionuclides. Precipitation of mineral phases may also limit migration.

Miller and Wang (2012), Van Loon (2014), and Tinnacher et al. (2016) each present a useful overview of the dual porosity nature of clay-rich materials. A brief summary is given here. Clays are sheet silicates comprised of tetrahedral and octahedral layers. Swelling clays have interlayer space between that holds cations and electrostatically bound interlayer water (Figure 6-6). A stack of layers forms a platelet, and platelets act as particles to form the bulk porous medium, which is characterized by a dual porosity structure: intra-particle porosity and interparticle porosity. The intra-particle porosity is where the interlayer water resides. The interparticle porosity contains both electrostatically bound water in the diffuse double-layer and free water at greater distance from the charged clay surfaces.



NOTE: In (A), T sheets are tetrahedral Si–O sheets; O sheets are octahedral Al–O (or Mg–O) sheets. Image shows a 2:1 clay. A 1:1 clay would only have one T sheet and one O sheet comprising a TO layer. As pictured, there are cations in the interlayer space denoted by the circles with + symbols. In certain clays the interlayer is only filled with water. Also shown are the physical locations of the basal and edge surfaces. In (B), (1) refers to TOT clay layer, (2) refers to interlayer water, (3) refers to diffuse double layer water, and (4) refers to free water.

Source: Miller and Wang 2012.

**Figure 6-6. Illustration of (A) Clay Layering and (B) Clay Stacks under Various Degrees of Compaction**

### 6.2.5.1 Diffusion

Diffusion of charged species is constrained by charge-balance and is affected by the charged surfaces of clay particles (e.g., McDuff and Ellis 1979; Miller and Wang 2012; Tinnacher et al. 2016). For diffusion of trace species (i.e., radionuclides), charge balance in the aqueous phase can be neglected. Anions are repelled, resulting in less pore space available for diffusion and effective diffusion coefficients smaller than that of a neutral species; this phenomenon is known as “anion exclusion.” Cations that participate in cation exchange reactions will diffuse faster than a neutral species due to cation transfer within the electrostatically bound water on clay sheet surfaces; a phenomenon known as “surface diffusion.” Typically, as ionic strength increases, the width of the diffuse double layer becomes smaller, decreasing the effect of anion exclusion (Van Loon 2014).

Temperature dependence of diffusion can be represented with Arrhenius relationship (Lichtner et al. 2019):

$$D(T) = D_0 \times e^{\frac{E_D}{R} \left( \frac{1}{T_0} - \frac{1}{T} \right)} \quad \text{Equation 6-1}$$

Where  $D_0$  is the diffusion coefficient at the reference temperature,  $T_0$ ;  $E_D$  is the diffusion activation energy,  $R$  is the ideal gas constant ( $8.317 \times 10^{-3}$  kJ/[mol·K]), and  $T$  is in Kelvin. For diffusion of iodide in aqueous solution at temperatures up to 300°C, the value of  $E_D$  is between 15 and 17 kJ/mol (Trevani et al. 2000). The diffusion activation energy for tritiated water (HTO),  $^{36}\text{Cl}^-$ , and  $^{22}\text{Na}^+$  in Opalinus Clay at temperatures between 25°C and 70°C was found to be approximately 20 kJ/mol (Van Loon 2014).

Van Loon (2014) calculated reference upper and lower bounds on effective diffusion coefficients ( $D_e$ ) for radioelements in compacted bentonite. The values associated with an upper bound on total porosity of

0.48 and on anion-accessible porosity of 0.145 are reproduced in Table 6-4. These values are consistent with other properties listed in this report for compacted MX-80 bentonite with an average, emplaced dry bulk density of 1450–1500 kg/m<sup>3</sup>. Surface diffusion is accounted for in the effective diffusion coefficients for cations that participate in ion exchange reactions (Section 6.2.5.2), the alkaline metals (K, Cs), and the alkaline earth metals (Ca, Sr, Ra).

**Table 6-4. Upper Bound on Effective Diffusion Coefficients for Radioelements in Compacted Bentonite**

Element	Species	$D_e$ (m <sup>2</sup> /s)	Element	Species	$D_e$ (m <sup>2</sup> /s)
Be(II)	Cation	1.8E-10	I(-I)	Anion	4.4E-11
Cinorg	Anion	2.7E-11	Cs(I)	Cation	1.5E-09
Corg	Neutral	4.7E-10	Sm(III)	Cation	1.8E-10
Cl(-I)	Anion	4.4E-11	Eu(III)	Cation	1.8E-10
K(I)	Cation	1.2E-09	Ho(III)	Cation	1.8E-10
Ca(II)	Cation	2.8E-10	Pb(II)	Cation	1.8E-10
Co(II)	Cation	1.8E-10	Po(IV)	Neutral	1.8E-10
Ni(II)	Cation	1.8E-10	Ra(II)	Cation	3.2E-10
Se(IV)	Anion	1.8E-11	Ac(III)	Cation	1.8E-10
Sr(II)	Cation	4.2E-10	Th(IV)	Neutral	1.8E-10
Zr(IV)	Neutral	1.8E-10	Pa(V)	Neutral	1.8E-10
Nb(V)	Neutral	1.8E-10	U(IV+VI)	Neutral	1.8E-10
Mo(VI)	Anion	1.8E-11	Np(IV)	Neutral	1.8E-10
Tc(IV)	Neutral	1.8E-10	Pu(III+IV)	Cation	1.8E-10
Pd(II)	Neutral	1.8E-10	Am(III)	Cation	1.8E-10
Ag(I)	Cation	4.7E-10	Cm(III)	Cation	1.8E-10
Sn(IV)	Neutral	1.8E-10	—	—	—

NOTE: Diffusion data for compacted bentonite; values above are for upper bound on porosity and T=25°C.

Source Van Loon 2014, Table 28.

### 6.2.5.2 Adsorption

Adsorption occurs through cation exchange reactions in which cations are adsorbed by electrostatic interaction with the negatively charged mineral surface and through surface complexation reactions in which aqueous species complex with surface sites on mineral edges [or faces]. Mechanistic modeling of either of these requires a full aqueous speciation model, which can be difficult to parameterize and expensive to run. Adsorption is frequently modeled using empirical isotherms of various forms. The most commonly used isotherm in performance and safety assessment of deep geologic repositories is the linear isotherm (Lichtner et al. 2019):

$$C_{sorb} = K_d C_{aq} \quad \text{Equation 6-2}$$

where C is concentration and  $K_d$  is the ratio of sorbed concentration (mass element/mass solid phase) to aqueous concentration (mass element/volume H<sub>2</sub>O). The linear isotherm is valid for trace radionuclide concentrations (Baeyens et al. 2014). The concept can also be used as an approximation for reactions that

are not strictly sorption, such as isotopic substitution of radioactive <sup>14</sup>C in carbonate minerals (Baeyens et al. 2014).

**Cation Exchange**

Isomorphous substitution of lower valence cations into the mineral lattice creates a permanent negative charge on the surface of a clay mineral. The negative charge is balanced by electrostatic attraction of cations in solution to the negatively charged surfaces. The total permanent negative charge is the cation exchange capacity (CEC; Bradbury and Baeyens 2011). Alkaline (K, Cs) and alkaline earth (Ca, Sr, and Ra) cations participate in cation exchange reactions (Baeyens et al. 2014).

As seen in Table 6-5, Bradbury and Baeyens (2002) report a CEC of pure montmorillonite equal to 870 meq/kg and of MX-80 bentonite equal to 787 meq/kg. Fernandez et al. (2001) report a CEC of FEBEX bentonite equal to 1,020 meq/kg. Baeyens et al. (2014) presents selectivity coefficients (K<sub>c</sub>) for cation exchange reactions on montmorillonite (Table 6-6) as well as a method to convert these values to K<sub>d</sub> for clay-rich materials.

**Table 6-5. CEC and Exchangeable Cations for MX-80 Bentonite and FEBEX Bentonite**

Cations and CEC (meq/100 g)	MX-80 Bentonite <sup>a</sup>	FEBEX Bentonite <sup>b</sup>
Ca <sup>+2</sup>	6.6	34.6
Mg <sup>+2</sup>	4.0	34.0
Na <sup>+</sup>	66.8	31.1
K <sup>+</sup>	1.3	1.94
CEC	78.7	102

NOTE: CEC = cation exchange capacity.

Source: <sup>a</sup> Bradbury and Baeyens 2002 as cited in Jové Colón et al. 2014.

<sup>b</sup> Fernández et al. 2001 as cited in Jové Colón et al. 2014.

**Table 6-6. Cation Exchange Reaction and Corresponding Selectivity Coefficients (K<sub>c</sub>) for Montmorillonite**

Cation Exchange Reaction	Log K <sub>c</sub>
Na-mont + K <sup>+</sup> ⇌ K-mont + Na <sup>+</sup>	0.6
Na-mont + Cs <sup>+</sup> ⇌ Cs-mont + Na <sup>+</sup>	1.18
2 Na-mont + Mg <sup>2+</sup> ⇌ Mg-mont + 2 Na <sup>+</sup>	0.34
2 Na-mont + Ca <sup>2+</sup> ⇌ Ca-mont + 2 Na <sup>+</sup>	0.41 <sup>a</sup>

NOTE: <sup>a</sup> Ca<sup>2+</sup> = Sr<sup>2+</sup> = Ra<sup>2+</sup>

Cation exchange capacity (CEC) for montmorillonite = 870 meq/100 g.

Source: Baeyens et al. 2014.

**Surface Complexation**

Other cations, including heavy metals, rare earth elements and actinides, sorb by surface complexation. Some anions (e.g., UO<sub>2</sub>(OH)<sub>3</sub><sup>-</sup>) can sorb by surface complexation as well (Baeyens et al. 2014). Surface

complexation is modeled using self-consistent thermodynamic data for aqueous and surface complexation reactions (e.g., Bradbury and Baeyens 2011; Tournassat et al. 2018). Fox et al. (2019) observed a 30%–50% reduction in sorption of U(VI) in samples of FEBEX bentonite that had been heated to 90°C compared to unheated samples. Because U(VI) is known to form surface complexes at edge sites, they hypothesize that formation of opal nodules seen in scanning electron microscope (SEM) images of heated samples decreased the availability of edge sites.

### **Linear Isotherm ( $K_d$ )**

$K_d$  values depend on mineralogy and porewater composition including pH and aqueous speciation of the sorbing radioelement, and must be measured at or calculated for specific conditions. Baeyens et al. (2014, Section 2) provides a method for calculating generic  $K_d$ s for argillaceous rock and bentonite buffer from  $K_d$ s measured in pure illite, montmorillonite, and calcite systems using conversion factors that account for mineral mass fractions, pH, predicted aqueous speciation, and estimated available surface area in the field. This method could probably be extended to account for the effect of temperature by performing aqueous speciation calculations for radioelements of interest over the relevant temperature range, and is applicable to any argillaceous system for which mineralogy and porewater composition can be constrained.

$K_d$ s calculated for MX-80 bentonite, assuming 75 wt % montmorillonite and several porewater scenarios relevant to disposal in the Swiss Opalinus clay formation (Baeyens et al. 2014, Table 8.6) are presented in Table 6-7. These values are consistent with other properties of MX-80 bentonite listed in this report, and could be used instead of previous shale reference case choices including values used in reference case simulations in Mariner et al. (2015; 2017) and Sevougian et al. (2019a).

Table 6-7. Linear Distribution Coefficients for MX-80 Bentonite ( $K_d$  in  $m^3/kg$ )

MX-80 bentonite	Reference	High porosity	High salinity	High pCO <sub>2</sub>	Low pCO <sub>2</sub>
Porosity [%]	36	48	36	36	36
pH	7.27	7.28	7.08	7.07	7.79
2:1 clay content [wt.-%]	75	75	75	75	75
Be(II)	2.29E+00	2.29E+00	1.46E+00	1.40E+00	4.66E+00
C <sub>inorg</sub>	6.40E-05	6.30E-05	1.40E-04	3.90E-05	2.10E-04
C <sub>org</sub>	0.00E+00	0.00E+00	0.00E+00	0.00E+00	0.00E+00
Cl(-I)	0.00E+00	0.00E+00	0.00E+00	0.00E+00	0.00E+00
K(I)	7.13E-03	7.43E-03	3.53E-03	7.05E-03	1.01E-02
Ca(II)	2.33E-03	2.55E-03	7.50E-04	2.25E-03	5.59E-03
Co(II)	4.15E-01	4.13E-01	2.78E-01	2.95E-01	1.05E+00
Ni(II)	1.28E+00	1.26E+00	1.01E+00	7.97E-01	3.21E+00
Se(-II)	0.00E+00	0.00E+00	0.00E+00	0.00E+00	0.00E+00
Sr(II)	2.33E-03	2.55E-03	7.50E-04	2.25E-03	5.63E-03
Zr(IV)	1.02E+03	1.03E+03	9.48E+02	9.48E+02	9.38E+02
Nb(V)	1.00E+00	1.00E+00	1.00E+00	1.00E+00	1.00E+00
Mo(VI)	1.33E-02	1.32E-02	1.52E-02	1.53E-02	9.30E-03
Tc(IV)	3.38E+00	3.38E+00	3.54E+00	2.97E+00	3.70E+00
Pd(II)	5.78E+01	5.87E+01	5.52E+00	5.51E+01	5.99E+01
Ag(I)	0.00E+00	0.00E+00	0.00E+00	0.00E+00	0.00E+00
Sn(IV)	8.13E+02	8.20E+02	8.21E+02	8.17E+02	5.12E+02
I(-I)	0.00E+00	0.00E+00	0.00E+00	0.00E+00	0.00E+00
Cs(I)	2.93E-02	3.08E-02	1.35E-02	2.93E-02	4.03E-02
Sm(III)	3.16E+01	3.14E+01	4.22E+01	1.58E+01	1.50E+02
Eu(III)	1.31E+01	1.31E+01	1.29E+01	6.47E+00	5.25E+01
Ho(III)	2.51E+01	2.51E+01	3.52E+01	1.19E+01	1.08E+02
Pb(II)	9.54E+00	9.84E+00	2.52E+00	8.40E+00	1.69E+01
Po(IV)	1.20E+00	1.20E+00	1.20E+00	1.20E+00	1.20E+00
Ra(II)	1.28E-03	1.43E-03	5.48E-04	1.28E-03	3.68E-03
Ac(III)	7.56E+01	7.68E+01	7.26E+01	4.03E+01	1.45E+02
Th(IV)	7.69E+01	7.43E+01	2.78E+02	3.45E+01	2.69E+02
Pa(V)	7.53E+01	7.46E+01	7.48E+01	7.48E+01	7.49E+01
U(IV)	3.71E-01	3.60E-01	3.90E+00	1.14E-01	5.06E+00
U(VI)	9.06E-05	8.57E-04	1.21E-02	5.57E-04	5.45E-03
Np(IV)	3.75E+02	3.75E+02	3.75E+02	3.72E+02	3.75E+02
Pu(III)	6.24E+01	6.30E+01	6.68E+01	3.09E+01	1.50E+02
Pu(IV)	9.38E-02	9.38E-02	7.50E-02	3.30E-02	1.35E+00
Am(III)	7.56E+01	7.68E+01	7.26E+01	4.03E+01	1.45E+02
Cm(III)	7.56E+01	7.68E+01	7.26E+01	4.03E+01	1.45E+02
	source data for montmorillonite				
	chemical analogue (see Table 4.3)				
	set to zero				
	special cases (see section 8.4.4)				
	cation exchange				



**6.2.5.3 Radioelement Solubility**

Berner (2014a) calculated radioelement solubility limits in MX-80 bentonite assuming porewater compositions resulting from 10,000-year reaction of Opalinus Clay porewater. The presence of an optional 0.15-m thick low-pH shotcrete liner was neglected in the porewater evolution calculations, because it was not found to have much effect. Recommended radioelement solubilities thus calculated are reproduced in Table 6-8. Berner (2014a) provides guidance for upper and lower limits and discusses solubility-limiting phases. As with  $K_{ds}$ , these values are consistent with other properties of MX-80 bentonite listed in this report, and could be used instead of previous shale reference case choices.

**Table 6-8. Recommended Radioelement Solubilities**

Element	Solubility (mol/kg)	Element	Solubility (mol/kg)
Be	9.1E-7	I	9.0E-7 <sup>a</sup>
Cinorg	8.9E-4	Cs	Unlimited
Cl	Unlimited	Sm	1.5E-7
K	1.2E-3	Eu	2.2E-7
Ca	9.1E-3	Ho	2.5E-6
Co	2.0E-5	Pb	8.8E-7
Ni	5.5E-5	Po	6.6E-7
Se	5.3E-9	Ra	3.4E-10
Sr	5.6E-5	Ac	2.8E-6
Zr	1.0E-7	Th	4.1E-9
Nb	7.1E-5	Pa	4.6E-9
Mo	2.1E-5	U	2.2E-7
Tc	4.1E-9	Np	9.9E-9
Pd	5.7E-8	Pu	6.8E-10
Ag	1.0E-5	Am	2.8E-6
Sn	9.2E-8	Cm	2.8E-6

NOTE: <sup>a</sup> Limiting solid is AgI(s). Solubility is not limited when Ag not present.  
Source: Berner 2014a.

**6.3 Waste Packages for Spent Nuclear Fuel**

**6.3.1 Waste Package Functional Requirements**

Containers for SNF provide structural integrity and support to the used fuel, criticality control, heat dissipation, containment during handling and repackaging, and containment after permanent disposal. The waste package system also performs the following:

- Preclosure functions assigned to overpack
  - Containment for >100 yr or until repository closure
  - Structurally robust to withstand handling and drops
  - Unshielded
- Postclosure functions assigned to overpack

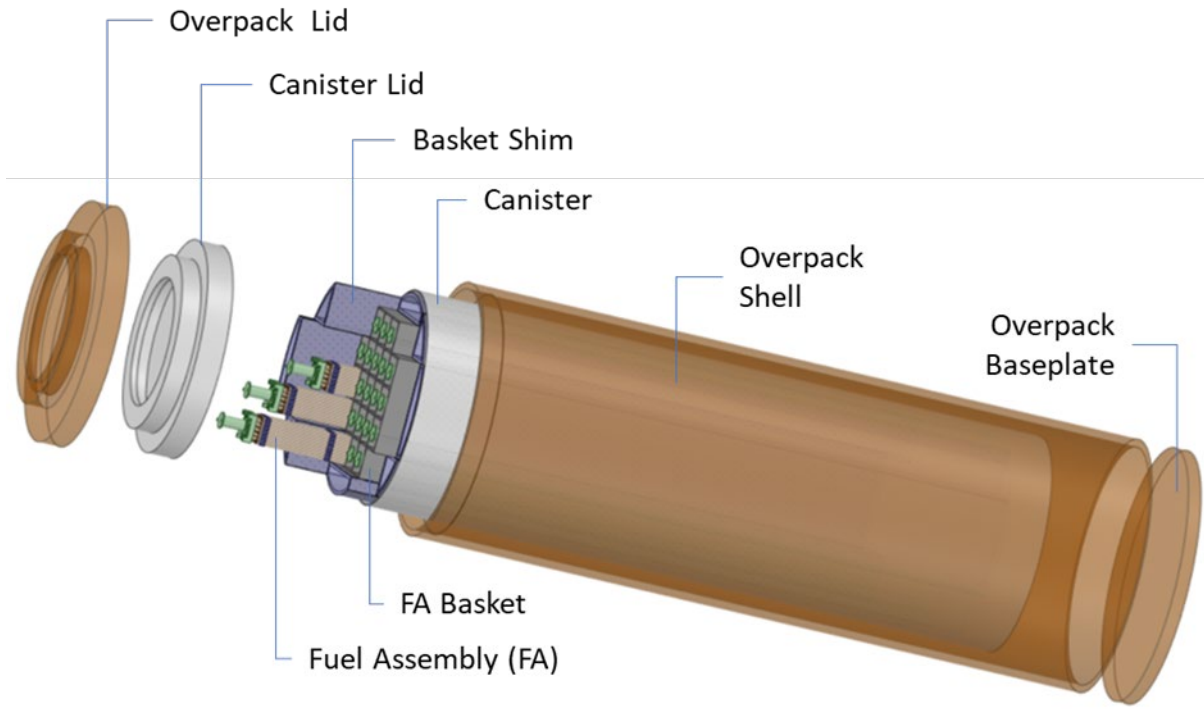
- Containment consistent with disposal concept (100 yr to >10,000 yr)
- Corrosion allowance or resistance – Carbon steel is easier to predict. Ductile versus brittle shale might make a difference in choice.
- Resist impact from rockfall, and crushing from ground water, backfill, and rock pressures during containment period

These functions are met using internal features such as racks for fuel support, thermal shunts, moderator exclusion features, neutron absorbers, flux traps, and inserts or fillers. These internal features have impact on the effective (homogenized) physical and thermal parameters of the waste package.

### **6.3.2 Waste Package Canister and Internals**

Typical containers for SNF are stainless steel structures, with internal stainless-steel racks or “baskets” to hold fuel assemblies and provide strength and rigidity. Containers can have external features such as flanges, rings, or trunnions to facilitate handling. They also typically have neutron absorbing structures made from borated stainless steel, or other materials with protective coatings. Some of these containers may likely use filler materials to fill their internal voids in order to exclude moderators such as water collecting in the voids during a container breach.

Waste package design for commercial SNF in a high-temperature shale repository would likely have three or four key components: waste canister/container, a basket or lattice structure inside the canister for holding spent fuel assemblies in place for criticality control, inner shell (vessel) and an outer corrosion barrier, and if necessary, an inner shell between the waste canister and the outer barrier (Figure 6-7). A waste canister/container is generally sealed permanently at the point of origin, thereby avoiding any further exposure of the waste during successive handling and repackaging operations. The combination of the inner shell (if used) and the outer corrosion barrier constitute what is generally referred to as the disposal overpack for the waste container. Overpacks provide economical means to meet different requirements such as heat dissipation, impact damage limits, handling during emplacement and corrosion resistance. Together the canister/container and disposal overpack are often referred to as a waste package. The generic dimensional characteristics of a waste package in different configurations are listed in Table 6-9.



Rendering of a 21 PWR FA Waste Package Components

Figure 6-7. Rendering of a 21 PWR/44 BWR Fuel Assembly Waste Package Configuration

**Table 6-9. Waste Canister/Package Characteristics**

Container Type	Mass <sup>f</sup> (kg [lb])	Outside Diameter (m [in.])	Overall Length (m [in.])	Wall Thickness (m [in.])	Heat Output (W/pkg)	Void Volume <sup>d,g,h</sup> (m <sup>3</sup> )	Void Fraction <sup>g,h</sup>	Density (g/cm <sup>3</sup> )	Source
Canister 4P/9B	7,000 (15,432)	0.79 (31.1)	5.03 (198)	0.013 (0.51)	2,200	0.970	0.518	7.9	a,b,h
Canister 12P/24B	20,000 (44,093)	1.1 (43.3)	5.03 (198)	0.016 (0.63)	5,500	2.150	0.524	7.9	a,b
Canister 21P/44B	33,000 (72,753)	1.68 (66.1)	5.38 (212)	0.025 (1)	10,000	6.314	0.594	7.9	c
Canister 37P/89B	52,798 (116,400)	1.92 (75.5)	4.6 (181)	0.013 (0.51)	10,000	6.090	0.479	7.9	e
Overpack 4P/9B	6,142 (13,539)	0.92 (36.22)	5.69 (224)	0.05 (2)	—	0.539	0.179	7.9	c
Overpack 12P/24B	8,614 (18,985)	1.27 (50)	5.69 (224)	0.05 (2)	—	1.337	0.219	7.9	c
Overpack 21P/44B	13,627 (30,035)	1.98 (77.95)	5.69 (224)	0.05 (2)	—	3.869	0.245	7.9	c
Overpack 37P/89B	15,251 (33,614)	2.21 (87)	5.69 (224)	0.05 (2)	—	4.319	0.217	7.9	c

NOTE/Source: <sup>a</sup> Hardin and Kalinina 2015.

<sup>b</sup> Areva Federal Services LLC 2013.

<sup>c</sup> SNL 2007b.

<sup>d</sup> SNL 2007a.

<sup>e</sup> NWTRB 2016.

<sup>f</sup> Note that canister masses represent as loaded with SNFs; mass for all overpacks were estimated from dimensions.

<sup>g</sup> All void volumes between can and overpack were estimated using canister external and overpack internal diameters and heights.

<sup>h</sup> Canister void volumes were estimated using 3D computer-aided design (CAD) model of specific canister.

### 6.3.3 Waste Package Material Options

There is a wide range of considerations that will ultimately go into the selection of materials used to fabricate the waste package canister, its internals, and any canister overpack. These considerations include the following:

- Mechanical performance
- Thermal performance
- Neutronic performance
- Chemical (including corrosion) performance
- Predictability of performance
- Compatibility with other materials
- Fabricability
- Cost
- Previous experience

All of the above considerations will need to be evaluated as part of iterative performance assessments (including analyses of features, events, and processes) for repository designs.

Common materials suitable for repositories in reducing environments include carbon steel, stainless steel, copper and titanium (Shoesmith 2006; Rebak and McCright 2006). Corrosion performance (discussed in Section 7) of waste package materials is also a function of temperature, ionic strength, pH, and concentrations of halide ions.

### **6.3.3.1 Steel and Copper**

Steel has a number of attributes that make it a suitable candidate as a canister for SNF and HLW disposal. It is widely available at relatively low cost. Because steel is relatively easy to weld, waste packages made of steel will be easy to seal. Carbon steel and low-alloy steels have been extensively tested in ground water environments for several decades. Researchers in the Swedish repository program have studied the anoxic corrosion behavior of carbon steel and cast iron in ground water at 50°C and 85°C and the impact of the presence of copper on the type and the mechanical properties of the films formed on the iron alloys (Smart et al. 2006). Andra has specified the use of carbon steel for SNF container overpacks, in the Callovo-Oxfordian argillite formation (Andra 2005). Nagra has identified carbon steel as the primary candidate waste package material for the Swiss repository concept in Opalinus Clay (Nagra 2009).

Carbon steel has also been identified as a candidate waste package material for salt repositories in Germany (Weber et al. 2011). Note that performance assessment models may take no significant containment credit for steel containers, particularly for long-term (i.e.,  $>10^5$  years) assessments.

Copper could be a suitable waste package material because it is thermodynamically stable under anoxic conditions and it has a tendency to undergo slow, uniform corrosion rather than localized corrosion in reducing environments. The SNF waste package planned for use in crystalline rock repositories in Sweden and Finland will consist of a nominally 50 mm thick layer of copper over an insert of cast nodular iron which will provide mechanical strength (SKB 2006). The Canadian reference concept for a crystalline repository calls for a copper outer vessel that resists corrosion enclosing an inner steel vessel that provides mechanical strength (NWMO 2012). Note that copper is a ductile metal, and these designs call for a load-bearing component interior to the copper. Since similar anoxic conditions will likely exist in clay/shale repositories after repository closure, copper may be an appropriate material for those systems as well (see Section 7.2.1.1 for discussion of copper corrosion). For this reason, copper is identified as an alternative to steel in the Swiss repository concept (Nagra 2003).

### **6.3.3.2 Alternative Materials**

As alternatives to active (corrosion allowance) canister materials such as copper and carbon steel, passive materials such as alloys of nickel and titanium, and stainless steel, have been considered as waste package materials. Such materials could be selected for either oxidizing or reducing repository environments. These materials form a passive, stable oxide film on the surface, and the chemical inertness of this film limits the general corrosion rate of the material. Passive materials may undergo localized corrosion (e.g., pitting or crevice corrosion) if the oxide film breaks down. The behavior of stainless steel has been studied in the Boom Clay, and it is a candidate material for the Belgium repository concept (Kursten et al. 2004).

Titanium alloys have also been studied as candidate waste package materials in Canada, Japan, and Germany. Titanium alloys were selected as potential alternatives because of their excellent performance in more aggressive brine solutions compared, for example, to stainless steels (Kursten et al. 2004; Rebak 2007).

### **6.3.3.3 Innovative Internal and Overpack Materials**

Amorphous metal and ceramic thermal spray coatings have been developed with excellent corrosion resistance and neutron absorption. These coatings, with further development, could be cost-effective options to enhance the corrosion resistance of waste packages and other EBS components, and to limit nuclear criticality in canisters for transportation, aging, and disposal of SNF. Iron-based amorphous metal

formulations with chromium, molybdenum, and tungsten have shown the corrosion resistance believed to be necessary for such applications. Rare earth additions enable very low critical cooling rates to be achieved. The boron content of these materials and their stability at high neutron doses enable them to serve as high efficiency neutron absorbers for criticality control. Another corrosion resistant option, ceramic coatings, may provide even greater corrosion resistance for EBS applications, although the boron-containing amorphous metals are still favored for criticality control applications. These amorphous metal and ceramic materials have been produced as gas-atomized powders and applied as nonporous coatings with nearly full density, using the high-velocity oxy-fuel process. Blink et al. (2009) summarize the performance of these coatings as corrosion-resistant barriers and as neutron absorbers, and also present a simple cost model to quantify the economic benefits possible with these new materials (Hardin et al. 2011).

### 6.4 Reference Internal Canister Design

A reference internal canister design is selected based on the 21-PWR/44-BWR concept described in Oak Ridge National Laboratory (ORNL 2015a). It is similar to the transportation, aging, and disposal (TAD) canister system proposed for a repository concept in volcanic tuff (DOE 2008). Given the wide range of industrial experience with stainless steel and the reasonable availability of corrosion and other performance data in a range of environments, the canister will consist of a 316 stainless steel. Nominal dimensions can be found in Table 6-9 and Table 6-12.

The mechanical and physical properties are summarized in Table 6-10. The temperature-dependent thermal properties values for the 316L stainless steel are shown in Table 6-11. (Candidate overpack materials are discussed in Section 7.)

The characteristics of some of the internal components of the conceptual 21-PWR/44-BWR canister are shown in Table 6-12. The surface areas and volumes of these component were extracted from a 3D computer-aided design (CAD) model to compute the internal void volume and fraction of the canister. The references for the source of the dimensions used for the 3D CAD model are specified under Table 6-9.

**Table 6-10. Waste Canister/Package Material Parameters**

Parameter	Value
Material Type	316L SS
Density (g/cm <sup>3</sup> )	7.9
Tensile Strength (MPa)	485
Thermal Conductivity (W/[m·K])	14.6
Heat Capacity (J/[kg·K])	450
Thermal Expansion (1/°F)	9.20E-06
Young’s Modulus (N/m <sup>2</sup> )	2.00E+11
Corrosion Rate (Mils/yr [mm/yr] <sup>a</sup> )	36
Rockwell B (HD#)	95

NOTE: SS = stainless steel

Source: <sup>a</sup> SNL 2004.



**Table 6-11. Temperature-Dependent Thermal Properties of Stainless Steel 316**

Temperature		Thermal Conductivity (Btu/[hr·ft·°F])	Thermal Diffusivity (ft <sup>2</sup> /hr)	Thermal Conductivity (W/[m·K])	Specific Heat (J/[kg·K])
°F	°C				
70	21.11	7.7	0.134	13.33	481.68
100	37.78	7.9	0.136	13.67	486.92
150	65.56	8.2	0.138	14.19	498.09
200	93.33	8.4	0.141	14.54	499.38
250	121.11	8.7	0.143	15.06	509.98
300	148.89	9.0	0.145	15.58	520.29
350	176.67	9.2	0.148	15.92	521.07
400	204.44	9.5	0.151	16.44	527.38
450	232.22	9.8	0.153	16.96	536.92
500	260.00	10.0	0.156	17.31	537.34
550	287.78	10.3	0.159	17.83	543.02
600	315.56	10.5	0.162	18.17	543.31
650	343.33	10.7	0.164	18.52	546.91
700	371.11	11.0	0.167	19.04	552.14
750	398.89	11.2	0.170	19.38	552.26
800	426.67	11.5	0.173	19.90	557.22
850	454.44	11.7	0.176	20.25	557.25
900	482.22	12.0	0.178	20.77	565.11
950	510.00	12.2	0.181	21.11	565.01
1,000	537.78	12.4	0.184	21.46	564.91
1,050	565.56	12.7	0.186	21.98	572.35
1,100	593.33	12.9	0.189	22.33	572.14
1,150	621.11	13.1	0.191	22.67	574.92
1,200	648.89	13.3	0.194	23.02	574.68
1,250	676.67	13.6	0.196	23.54	581.64
1,300	704.44	13.8	0.199	23.88	581.30
1,350	732.22	14.0	0.201	24.23	583.86
1,400	760.00	14.2	0.203	24.58	586.36
1,450	787.78	14.4	0.206	24.92	585.96
1,500	815.56	14.6	0.208	25.27	588.39

Source: CRWMS M&O 1996.

**Table 6-12. Initial Characteristics of Some Internal Components of the Conceptual 21-PWR/44-BWR Canister**

Container Type	Component	Mass <sup>f</sup> kg (lb)	Outside Diameter m (in)	Overall Length m (in)	Wall Thickness m (in)	Total Surface Area m <sup>2</sup> (in <sup>2</sup> )	Total Volume m <sup>3</sup> (in <sup>3</sup> )	Volume Fraction
Canister 21P/44B	Canister Assembly	33000 (72753)	1.68 (66.1)	5.38 (212)	0.025 (1)			
	Fuel Assy					895.86(1388446.92)	1.68(99358.77)	0.158043274
	Basket					115.95(179721.40)	0.75(45737.40)	0.070555033
	Shell (interior)					30.14(46862.45)	10.63(648682.40)	1
	Canister Lid					5.40(8362.23)	0.51(31122.12)	0.047977422
	Shims					103.07(159757.65)	1.30(79471.62)	0.12229539
	FA Height Spacers					16.38(25467.33)	0.076(21220.60)	0.007149577
	Void Volume						6.31(385059.8)	0.593979304

## 6.5 Waste Form

### 6.5.1 Spent Fuel Types and Characteristics

Commercial SNF includes irradiated fuel discharged from PWRs and BWRs. The fuel used in these reactors consists of polycrystalline ceramic uranium dioxide (UO<sub>2</sub>) pellets in cladding tubes. Cladding protects the fuel from degradation in the reactor, and likely also in the repository. Cladding is generally made from Zircaloy, an alloy that is chemically stable and resistant to corrosion. A small number of early fuel designs used stainless steel tubes. The fuel assemblies vary in physical configuration, depending upon reactor type and manufacturer. The fuel assemblies also vary in initial enrichment and burnup.

### 6.5.2 Radionuclide Inventories and Heat of Decay

Reference radionuclide inventories assume the waste form is commercial PWR SNF assemblies. Nominal and bounding radionuclide inventories and power outputs are constructed using assembly and fuel characteristics (e.g., assembly-specific initial enrichment and uranium mass, irradiation history information, and discharge burnup) to calculate assembly-specific isotopic concentrations and decay heat. The assembly and fuel characteristics are from the Unified Database (UDB), which is the database system at the heart of the UNF-ST&NDARDS database at ORNL (Clarity et al. 2017; Banerjee et al. 2016). Radiation source terms can also be calculated from this information, but they are not reported here.

#### 6.5.2.1 Nominal Waste Package Loading

The nominal radionuclide inventory per 21-PWR waste package 50 years after discharge from the reactor is provided in Table 6-13. Nominal inventories were assembled using characteristics of the assemblies in the storage canister TSC-37-TSC-03, which contains the most reactive assemblies in the UDB record for Zion, a decommissioned nuclear power plant. The total decay heat in this 37-PWR storage canister was 13.8 kW after 50 years of discharge. Reported radionuclides were selected based on the justification provided in the following references:

- Table 4-4 of Advances in Geologic Disposal System Modeling and Shale Reference Case, 2017. SFWD-SFWST-2017-000044, SAND2017-10304R
- Table 7-1 of Radionuclide Screening, Sandia 2007. ANL-WIS-MD-000006 REV 2
- Table 3-1 of Disposal Criticality Analysis Methodology Topical Report, OCRWM 2003. YMP/TR-004Q Rev. 02

The nuclide inventory was calculated using the ORIGAMI module of the SCALE code (Hu and Ilas 2018). ORIGAMI is a SCALE 6.2.3 sequence dedicated to calculating nuclide inventories, decay heat, and radiation source terms for SNF assemblies with axial and radial burnup variations.

Two methods were used to calculate two options for nominal radionuclide inventory: sorting on decay heat, and sorting on reactivity. For the “Decay Heat Sorted” column in Table 6-13, the 37 fuel assemblies in the TSC-37-TSC-03 were sorted in the order of their decay values after 50 years of discharge. For the

21-PWR disposal canister, the first 21 assemblies in the sorted list were selected as those loaded into the 21-PWR disposal canister. For the “Reactivity Sorted” column, a similar approach was used to sort the 37 assemblies, the difference being that the assemblies’ reactivity values were used for the sorting.

The thermal power for a 21-PWR waste package for the two different inventories is presented in Figure 6-8. The reactivity-sorted 21-PWR waste package could be emplaced 50 years OoR. The decay heat-sorted 21-PWR waste package would need approximately 50 years additional surface storage (a total of 100 years) before emplacement to meet the 4 kW power limit discussed in Section 4.5.

Table 6-13. Nominal Radionuclide Inventory at Emplacement for 21-PWR Waste Package

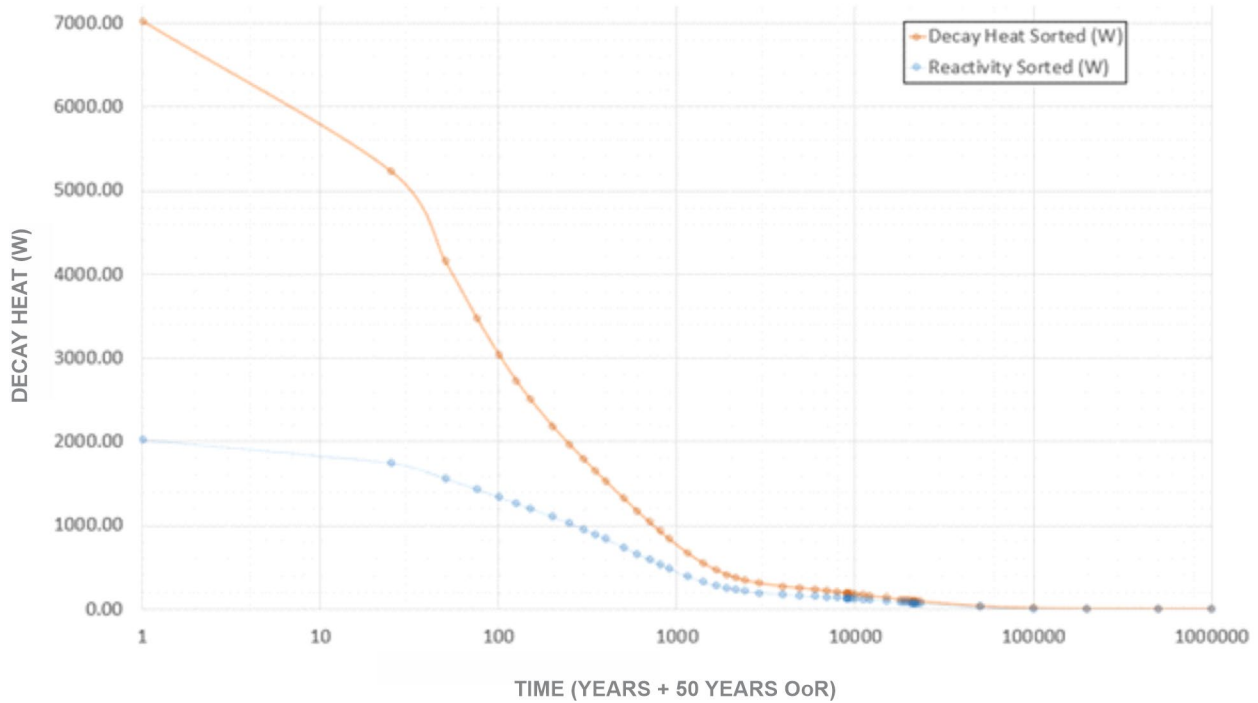
Nuclide	Notes	Decay Heat Sorted (gm)	Reactivity Sorted (gm)	Nuclide	Notes	Decay Heat Sorted (gm)	Reactivity Sorted (gm)
<sup>227</sup> Am		4.92E-06	7.60E-06	<sup>138</sup> Pu		2.24E+03	3.40E+02
<sup>109</sup> Ag	a	1.17E+03	5.22E+02	<sup>239</sup> Pu		6.67E+04	5.54E+04
<sup>241</sup> Am		1.75E+04	1.01E+04	<sup>240</sup> Pu		2.96E+04	1.64E+04
<sup>242</sup> Am		1.26E-04	3.73E-05	<sup>241</sup> Pu		1.04E+03	4.48E+01
<sup>243</sup> Am		2.56E+03	4.53E+02	<sup>242</sup> Pu		8.45E+03	2.65E+03
<sup>137m</sup> Ba	b	6.04E-04	8.77E-05	<sup>226</sup> Ra	d	9.41E-05	3.14E-04
<sup>14</sup> C		1.25E+00	6.09E-01	<sup>228</sup> Ra		4.74E-11	5.28E-11
<sup>144</sup> Ce		2.06E-20	0.00E+00	<sup>101</sup> Ru	a	1.02E+04	5.27E+03
<sup>36</sup> Cl		2.47E-24	8.60E-26	<sup>125</sup> Sb		4.00E-05	1.41E-10
<sup>242</sup> Cm		2.54E-02	7.53E-03	<sup>79</sup> Se		5.88E+01	3.19E+01
<sup>244</sup> Cm		1.29E+02	1.24E+00	<sup>147</sup> Sm		2.92E+03	2.03E+03
<sup>245</sup> Cm		1.04E+02	5.23E+00	<sup>149</sup> Sm	a	3.65E+01	3.22E+01
<sup>133</sup> Cs	a	1.41E+04	7.89E+03	<sup>150</sup> Sm	a	3.90E+03	1.91E+03
<sup>134</sup> Cs		3.55E-06	1.64E-13	<sup>151</sup> Sm		9.79E+01	4.57E+01
<sup>135</sup> Cs		5.94E+03	3.01E+03	<sup>152</sup> Sm	a	1.17E+03	8.05E+02
<sup>137</sup> Cs		3.95E+03	5.74E+02	<sup>126</sup> Sn		2.99E+02	1.38E+02
<sup>151</sup> Eu	a	5.77E+01	6.52E+01	<sup>90</sup> Sr		1.48E+03	2.30E+02
<sup>153</sup> Eu	a	1.61E+03	7.29E+02	<sup>99</sup> Tc		9.92E+03	5.44E+03
<sup>154</sup> Eu		3.29E+00	1.52E-02	<sup>229</sup> Th		5.72E-05	4.61E-05
<sup>155</sup> Gd	a	1.25E+02	4.69E+01	<sup>230</sup> Th		3.68E-01	6.28E-01
<sup>129</sup> I		2.15E+03	1.04E+03	<sup>232</sup> Th		1.29E-01	1.31E-01
<sup>95</sup> Mo	a	9.85E+03	5.39E+03	<sup>232</sup> U		2.60E-02	3.35E-03
<sup>143</sup> Nd	a	9.66E+03	6.03E+03	<sup>233</sup> U		1.69E-01	1.59E-01
<sup>145</sup> Nd	a	8.17E+03	4.62E+03	<sup>234</sup> U		2.72E+03	2.15E+03
<sup>237</sup> Np		7.65E+03	4.53E+03	<sup>235</sup> U		6.61E+04	1.14E+05
<sup>231</sup> Pa		1.02E-02	1.51E-02	<sup>236</sup> U		4.50E+04	3.02E+04
<sup>210</sup> Pb	d	5.03E-07	2.40E-06	<sup>238</sup> U		8.96E+06	9.13E+06
				<sup>90</sup> Y	c	3.76E-01	5.84E-02

NOTE: <sup>a</sup> Stable (except <sup>153</sup>Eu with half-life >10<sup>18</sup> y)

<sup>b</sup> In secular equilibrium with <sup>137</sup>Cs

<sup>c</sup> In secular equilibrium with <sup>90</sup>Sr

<sup>d</sup> Initial inventory is less significant to biosphere dose than contribution from ingrowth.



NOTE: Time scale starts at 50 years OoR, where OoR = out of the reactor.

**Figure 6-8. Thermal Power for a 21-PWR Waste Package Assuming Nominal Radionuclide Inventory**

**6.5.2.2 Burnup-Bounded Waste Package Loading**

Past reference cases (e.g., Mariner et al. 2015; 2017; Sevougian et al. 2019a) have assumed an inventory comprised entirely of high-burnup (60 GWd/MTU) SNF as a means of bounding thermal power in the repository. Selecting high burnup assemblies discharged from the commercial reactor fleet in the United States provides another method of developing a burnup-bounded waste package loading inventory. For this case, 21-PWR assemblies were selected from different sites using filters from the UDB. There are some assemblies in the UDB with a burnup greater than 63 GWd/MTU; these were filtered out for this analysis. The top 21 assemblies from the UDB as filtered are shown in Table 6-14. The burnup-bounded radionuclide inventory at 50 years OoR is shown in Table 6-15.

The decay heat from the burnup-bounded assemblies is shown in Figure 6-9. The burnup-bounded 21-PWR waste package has a lower power output than the reactivity-sorted 21-PWR at 50 years OoR. Like the reactivity-sorted 21-PWR, the burnup-bounded 21-PWR would require approximately 50 years additional aging (to 100 years OoR) before emplacement to meet the 4 kW power limit.

Table 6-14. Selected Bounding Assemblies Characteristics

assembly_id	initial_enrichment	initial_uranium_kg	max_burnup_mwd_per_mthm	reactor_name
2TW01	4.26	388.356	62788	CalvertCliffs1
2TW04	4.26	384.125	62711	CalvertCliffs1
2TF3	4.27	411.949	62611	CalvertCliffs1
2TF1	4.26	412.276	62598	CalvertCliffs1
K35	3.98	416.919	62487	Summer
M11E	4.46	416.444	60301	Byron1
M10E	4.46	416.501	60091	Byron1
M12E	4.46	418.245	59884	Byron1
M09E	4.46	418.137	59650	Byron1
JJ62	4.39	394.837	59224	PointBeach2
JJ63	4.4	394.745	59011	PointBeach2
JJ60	4.4	395.065	58894	PointBeach2
JJ61	4.39	395.061	58837	PointBeach2
P3J408	4.25	439.134	58745	PaloVerde3
W50R	3.7456337	351.556	58616.9	PrairieIsland1
CC70R	4.6	351.105	58599	PointBeach2
FF73	4.95	453	58598.108	IndianPoint3
V-72	4.95	453.5	58463	IndianPoint2
V-91	4.95	453.5	58458	IndianPoint2
V-77	4.95	453.5	58421	IndianPoint2
LMOB6M	3.59	459.1	58417	NorthAnna1



**Table 6-15. Radionuclide Inventory 50 years OoR for  
21-PWR Waste Package Assuming Burnup-Bounded Assemblies**

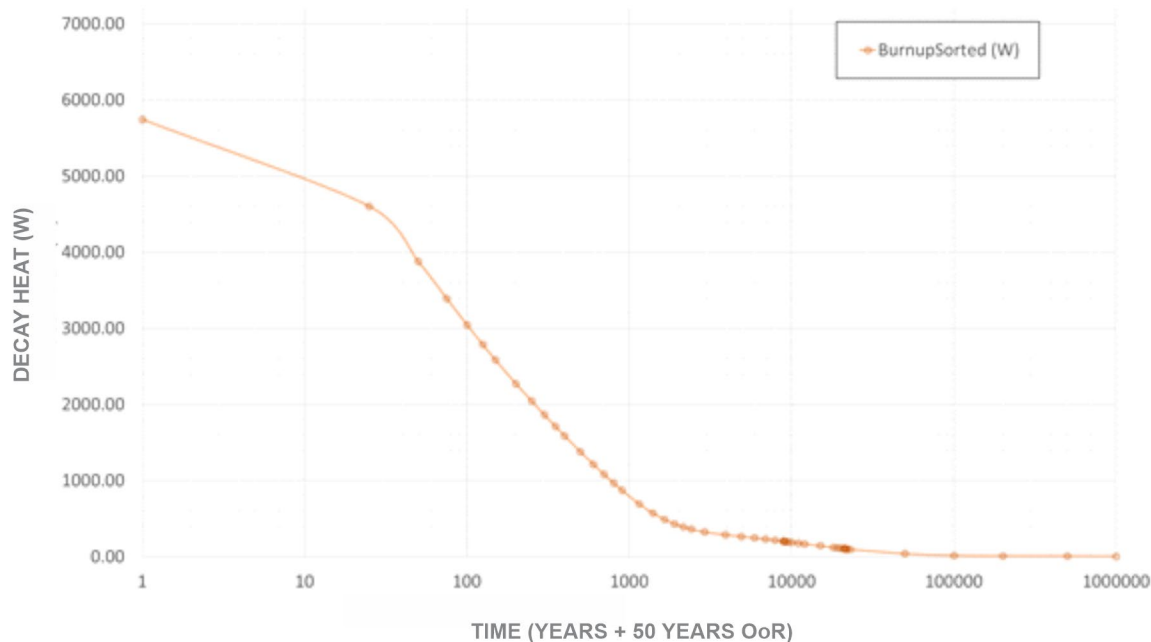
Nuclide	Notes	Burnup Sorted (gm)	Nuclide	Notes	Burnup Sorted (gm)
<sup>227</sup> Ac		3.77E-07	<sup>138</sup> Pu		1.17E+02
<sup>109</sup> Ag	a	6.30E+01	<sup>239</sup> Pu		3.08E+03
<sup>241</sup> Am		8.89E+02	<sup>240</sup> Pu		1.46E+03
<sup>242</sup> Am		6.05E-06	<sup>241</sup> Pu		9.53E+00
<sup>243</sup> Am		1.55E+02	<sup>242</sup> Pu		4.79E+02
<sup>137m</sup> Ba	b	1.51E-05	<sup>226</sup> Ra	d	1.45E-05
<sup>14</sup> C		6.39E-02	<sup>228</sup> Ra		4.22E-12
<sup>144</sup> Ce		0.00E+00	<sup>101</sup> Ru	a	5.73E+02
<sup>36</sup> Cl		2.35E-25	<sup>125</sup> Sb		2.76E-10
<sup>242</sup> Cm		1.22E-03	<sup>79</sup> Se		3.31E+00
<sup>244</sup> Cm		2.19E+00	<sup>147</sup> Sm		1.53E+02
<sup>245</sup> Cm		7.88E+00	<sup>149</sup> Sm	a	1.86E+00
<sup>133</sup> Cs	a	7.73E+02	<sup>150</sup> Sm	a	2.20E+02
<sup>134</sup> Cs		1.50E-12	<sup>151</sup> Sm		3.86E+00
<sup>135</sup> Cs		3.25E+02	<sup>152</sup> Sm	a	6.01E+01
<sup>137</sup> Cs		9.87E+01	<sup>126</sup> Sn		1.65E+01
<sup>151</sup> Eu	a	4.20E+00	<sup>90</sup> Sr		3.62E+01
<sup>153</sup> Eu	a	8.89E+01	<sup>99</sup> Tc		5.49E+02
<sup>154</sup> Eu		1.10E-02	<sup>229</sup> Th		6.63E-06
<sup>155</sup> Gd	a	7.13E+00	<sup>230</sup> Th		3.85E-02
<sup>129</sup> I		1.22E+02	<sup>232</sup> Th		1.05E-02
<sup>95</sup> Mo	a	5.55E+02	<sup>232</sup> U		1.24E-03
<sup>143</sup> Nd	a	5.29E+02	<sup>233</sup> U		1.57E-02
<sup>145</sup> Nd	a	4.57E+02	<sup>234</sup> U		1.98E+02
<sup>237</sup> Np		5.09E+02	<sup>235</sup> U		2.83E+03
<sup>231</sup> Pa		6.78E-04	<sup>236</sup> U		2.68E+03
<sup>210</sup> Pb	d	9.72E-08	<sup>238</sup> U		3.78E+05
			<sup>90</sup> Y	c	9.18E-03

NOTE: <sup>a</sup> Stable (except <sup>153</sup>Eu with half-life >10<sup>18</sup> y)

<sup>b</sup> In secular equilibrium with <sup>137</sup>Cs

<sup>c</sup> In secular equilibrium with <sup>90</sup>Sr

<sup>d</sup> Initial inventory is less significant to biosphere dose than contribution from ingrowth.



NOTE: Time scale starts at 50 years OoR, where OoR = out of the reactor.

**Figure 6-9. Thermal Power for a 21-PWR Waste Package Assuming Burnup-Bounded Assemblies**

### 6.5.3 Cladding

Commercial SNF integrity, in large part, depends on the material that encases the actual fuel, the cladding. A typical assumption in performance assessment calculations is that cladding does not protect the UO<sub>2</sub> fuel from contact with water or inhibit radionuclide transport after a waste package has failed.

In the postclosure repository, intact cladding will prevent water or moist air from contacting the fuel pellets. The cladding is a metallic seal around the fuel pellets (generally a zirconium alloy) and only after cladding fails (e.g., creep rupture or pinholes), can the fuel react with ground water or moist air. Cladding breach and fluid entry can release labile radionuclides in an instant release fraction and initiate degradation of the fuel pellets (Section 6.6) The fuel degradation alteration products increase the volume inside the cladding because they are less dense phases than the fuel itself. This volume increase can lead to further opening of the cladding breach, potentially unzipping the length of the cladding over time. Failed cladding will still somewhat retard radionuclide mobilization by limiting the amount of fluid contact with the pellet and by reducing the diffusion area for radionuclide release. In such a diffusion-dominated regime, the reduced water flux with the fuel pellet would also allow the fluid composition inside the cladding to become dominated by reaction with the fuel.

Although some spent fuel cladding (e.g., zircaloy cladding) is likely to be durable under a wide range of repository conditions, data and models are needed to establish the initial condition of the cladding and to support credible assessments of its long-term behavior in repository environments where a large number of degradation processes are to be considered (see below).

#### 6.5.3.1 Materials

Most commercial SNF in the United States (existing and projected inventories of PWR and BWR fuel) consists of assemblies of Zircaloy tubing filled with UO<sub>2</sub> fuel pellets (e.g., Teague et al. 2019). Zircaloy is used because it is resistant to corrosion and has favorable neutronic properties. It has good mechanical properties that enable it to be made into long thin-walled tubing. Long-term storage testing, with supporting cladding characterization, modeling and analyses in the SFWST Campaign Storage and

Transportation R&D program (Hanson and Alsaed 2019; Teague et al. 2019; EPRI 2019) are providing enhanced understanding of the condition of high-burnup fuel cladding after long storage times.

### 6.5.3.2 Failure Mechanisms

Commercial fuel cladding may be degraded at the time of disposal in the repository. Possible situations or conditions for degradation of cladding include during reactor operation, during wet spent fuel pool storage, during dry storage, and during shipping (e.g., from creep and from vibration and impact) and fuel handling. Models and data are currently under development as part of research being conducted in support of long-term extended storage and subsequent transportation (Hanson et al. 2012; Hanson and Alsaed 2019; Teague et al. 2019; EPRI 2019) that could be used to develop models for cladding initial condition at the time of emplacement in the repository.

Cladding may degrade in the repository as a result of many degradation processes. Waterlogged fuel rods (i.e., previously breached/damaged) may contain residual water after drying which could lead to fuel-side cladding degradation. Cladding may also degrade from creep failure and several external corrosion processes including general corrosion, microbially influenced corrosion (MIC), localized corrosion (including pitting and crevice corrosion), fluoride-enhanced corrosion, creep rupture, internal over pressurization due to helium or fission gasses, stress corrosion cracking (SCC), hydride cracking, mechanical impact, mechanical crushing, and diffusion-controlled cavity growth. Many of these mechanisms have been previously constrained with data from experiments and models of their thermal dependence (e.g., Siegmann et al. 2000; Siegmann 2000; Siegmann and Rechard 2001; BSC 2005). More recently, Hardin et al. (2019) reviewed for zircaloy cladding the initial clad failures (i.e., perforated clad at disposal) and postclosure failure mechanisms including creep rupture and corrosion mechanisms. Hardin et al. (2019) concluded the primary postclosure failure mechanisms for further consideration were identified as creep failure and localized corrosion, either pitting or cracking, in aggressive fluids (e.g., concentrated dissolved constituents such as fluoride). Once cladding is failed, alteration of the SNF will drive splitting/unzipping of the cladding relatively quickly, expanding the direct fluid interface to the fuel inside.

Cladding degradation may happen in stages, with cladding failure (perforation) followed by axial splitting of the cladding. “Axial splitting” is sometimes referred to as “unzipping” in some publications, but “axial splitting” is widely used in the nuclear industry. Cladding failure is the formation of cracks or holes in the cladding from various sources. The cracks and holes can be formed during reactor operation and subsequent storage (including other operations before being received at the repository) and mechanical failure (breaking of the cladding). Cladding failure permits the fuel inside the cladding to begin to react with water or moist air and potentially leads to the splitting of the cladding. In the splitting stage, the cladding is axially split open by the formation of secondary mineral phases (higher oxides of  $\text{UO}_2$ , commonly called rind on the fuel, or by fuel-side oxidation of the Zircaloy), making the radionuclides available for release. The split widens as the rind forms and radionuclides diffuse through the split opening.

For the high-temperature shale reference case, all of the SNF cladding is assumed to be failed at the time of the waste package failure, which allows the SNF uranium oxide waste form to be available for degradation and dissolution (Section 6.6 below). For estimates of radionuclide release and source-term evolution, this is a conservative assumption resulting in overestimates of dose consequence and risk.

### 6.5.4 Neutron Absorbers

The 21-PWR/44-BWR waste packages in a shale repository will likely require neutron absorbers for criticality control for both preclosure and postclosure safety. That said, analyses conducted on approximately 700 DPCs indicate that a concentration of about 3 molal NaCl is sufficient for keeping the analyzed DPCs subcritical. According to Table 3-2, some brittle shale formations in the United States may have high enough Cl concentrations to make a criticality event less likely.

The majority of currently loaded DPCs employ aluminum-boron carbide metal matrix composite materials for criticality control (Greene et al. 2013; Lindquist 2009). Other options include borated-stainless steel alloy, which is used in a small number of DPCs, and nickel-gadolinium alloy, a relatively new candidate material. In these materials, either gadolinium or boron function as neutron absorbers.

Neutron absorbers are used in DPCs in both structural and nonstructural contexts. For example, Metamic HT<sup>®</sup>, an Al-B<sub>4</sub>C composite material, forms the basket structure in the Holtec International MPC-89 canister. Stainless steel- and nickel-based materials would also be used to maintain the basket structure. In the Orano TN NUHOMS<sup>®</sup> canister, Boral<sup>®</sup> is attached by intermittent welds to a 304 stainless steel basket and, therefore, is not used as a structural material.

Al-B<sub>4</sub>C composite materials are lightweight and therefore are favorable for transportation; however, aluminum is expected to rapidly corrode in a disposal scenario (Hardin et al. 2015). At low temperatures, pit corrosion occurs at the aluminum surface in dilute chloride solutions (i.e., Szklarska-Smialowska 1999). In elevated temperature (150°C–300°C) and pressure hydrothermal experiments, alteration of the aluminum metal to an oxide hydroxide phase (boehmite, AlOOH) resulted in material expansion and hydrogen gas generation (Sauer et al. 2020). Further, at 400°C–570°C in humidity experiments, almost complete boron loss was observed from aluminum-boron carbide composites (Wierschke 2015; Wang et al. 2015). Because of this, for a purpose-built package, aluminum-based neutron absorbers are not appropriate.

In comparison, more durable neutron absorbers such as borated stainless steel alloy and nickel-gadolinium alloy are more favorable in a disposal scenario. Corrosion tests show that borated stainless steel alloy and nickel-gadolinium alloy experience slightly enhanced corrosion in comparison to nonborated stainless steel and nickel alloy, respectively (e.g., Mizia et al. 2005; Lister et al. 2005; 2008; He et al. 2012). These materials, however, are more likely to maintain their structural and neutron absorbing functions over timescales needed in a disposal environment in comparison to aluminum-based materials (e.g., Bryan et al. 2011; Ilgen et al. 2014).

To meet likely repository objectives for criticality safety, the 21-PWR/44-BWR waste package neutron absorber materials are assumed to have the following characteristics:

1. Neutron absorber plates or tubes shall be made from borated stainless steel produced by powder metallurgy and meeting ASTM A887-89 (2014), “Standard Specification for Borated Stainless Steel Plate, Sheet, and Strip for Nuclear Application”, Grade A alloys.
2. Minimum thickness of neutron absorber plates between SNF assemblies shall be 11 mm (0.4375 in.) assuming single plates. Use of multiple plates between the SNF assemblies (i.e., flux traps) is prohibited.
3. The neutron absorber plate shall have boron content of 1.1–1.2 wt %, a range that falls within the specification range for 304B4 (Unified Numbering System [UNS] S30464) as described in ASTM A887-20 (2020).
4. Neutron-absorbing material shall extend the full length of the fuel basket.
5. Neutron-absorbing plates shall either surround each assembly or extend the full cross section of the canister (in the plane perpendicular to the canister’s long axis).
6. The borated stainless steel plates shall be incorporated into the basket without the use of welding.

This group of six requirements was developed for a previously submitted license application for geologic disposal in an unsaturated tuff geology (DOE 2008). Based on the generic analyses that have been performed thus far for a range of host geologies, there is confidence that this material as specified will perform favorably. Nonetheless, once a site is selected, site-specific analyses coupled

with geologic disposal system performance models will have to be performed to confirm acceptable performance.

Borated stainless steel with 1.1–1.2 wt.% of natural boron and a thickness of at least 6 mm was determined to have the necessary neutron absorption capacity to maintain subcriticality for the TAD canisters based on burnup credit, moderation, and geometry assumptions developed for a previous repository design (DOE 2008). Borated stainless steel offers improved durability and corrosion resistance compared to the commonly used aluminum-based neutron absorber materials. Use of 304B4 plates that are initially 11 mm thick provides a corrosion allowance of 5 mm. The corrosion of borated stainless steel components is expected if both the disposal overpack and the stainless steel inner canister are breached after repository closure. The influx of water vapor or liquid water will promote corrosion of the borated steel under both oxic and anoxic conditions. A literature review of the available experimental data on the modes and rates of corrosion for borated stainless steel and their comparison to corrosion of nonborated stainless steel is presented in Appendix B of ORNL (2015b).

## 6.6 Spent Fuel Degradation Model and In-package Chemistry

The waste form is spent uranium oxide ( $\text{UO}_2$ ) fuel, a polycrystalline ceramic material stable to high temperatures and likely slow to degrade in the disposal environment (Mariner et al. 2017, Section 4.1.3). Prior to waste package breach, the spent fuel and its cladding is expected to be exposed to a benign (or inert) gas-phase environment inside the waste packages. Commercial SNF alteration processes include phase separation, dissolution, leaching, and cracking that can lead to degradation of spent fuel and radionuclide mobilization and release over time. Following its disposal, commercial SNF degradation may occur due to processes that cause alterations within the fuel matrix (e.g. radiation damage, fission gas and decay helium separation) and due to processes that may cause alterations at the interfaces with the gas and aqueous environments to which the waste form may be exposed after breaching of the fuel containment barriers (i.e., the waste package).

Under reducing conditions such as would be expected in a shale repository, the source of oxidants that can cause degradation of the fuel matrix by the oxidative dissolution process is water radiolysis. For sufficiently low radiation doses, a threshold for transition from the oxidative dissolution process to chemical dissolution of the uranium (IV) dioxide matrix has been identified (Shoesmith 2007) beyond which the dissolution of the fuel is controlled by the solubility of the uranium dioxide matrix and is extremely low. Small concentrations of hydrogen have been shown to suppress the oxidative dissolution due to radiolysis; if corrosion of the waste package materials generates hydrogen, then suppression of oxidative dissolution of the fuel due to beta and gamma radiation fields in a reducing environment would limit degradation to very slow dissolution of the fuel matrix under U(IV) near-saturation conditions (Shoesmith 2007).

In spent oxide fuels, the radionuclide inventory is usually considered to consist of two parts: (1) a part that resides in the fuel rod gap and grain-boundary region and (2) a part that is embedded or microencapsulated in the fuel matrix. During its irradiation in the reactor, a fraction of the noble gas and more volatile fission product elements migrates out of the oxide fuel matrix and accumulates at the grain boundaries in the fuel and also in the gas-filled regions of the fuel rod (referred to as the “gap” region) (Johnson et al. 2005; De Pablo et al. 2008; Rondinella 2008). The inventory fraction in these regions can be dissolved rapidly upon breaching of the fuel cladding and water ingress into the fuel pins. The balance of the radionuclide inventory is embedded or microencapsulated in the fuel matrix and can only be dissolved and released following degradation of the fuel matrix. The simplifying assumption is usually made that the gap and grain boundary fraction of the radionuclide inventory dissolves and is

instantaneously mobilized when the cladding fails. For low to moderate burnup fuels this fraction is relatively small (a few percent of the more volatile and soluble radionuclides such as I and Cs (BSC 2004; Johnson et al. 2005)).

Fission products are assumed to concentrate in voids of the waste form, resulting in two radionuclide release fractions: instant-release (upon waste package breach assuming instantaneous failure of the cladding) and slow-release (according to the  $\text{UO}_2$  matrix dissolution rate (Mariner et al. 2017; Mariner et al. 2016, Section 3.2.2)). The instant release fraction (IRF) depends primarily on the burn-up of the spent fuel (e.g., Sassani et al. 2016). The work of Johnson et al. (2005) provides correlations that can be used for IRF estimates for fuels up to 75 MWd/kgHM. The chemical processes (equilibrium and kinetic) affecting the  $\text{UO}_2$  matrix degradation are temperature dependent and the primary radiolytic-oxidant-driven matrix degradation rate controls are assessed in the fuel matrix degradation model (e.g., Sassani et al. 2012; 2013; Jerden et al. 2012; 2013; 2015), which is a coupled version of the mixed potential model (Jerden et al. 2013; 2014) and the radiolysis model (Buck et al. 2013). The temperature sensitivity has been assessed from 25°C to 200°C for this model (see Jerden et al. 2014, Figure 7), as has the chemical boundary conditions showing that the largest potential impact is from the  $\text{H}_2$  pressure in the system. If higher temperatures are expected to generate brines, this would exceed the applicability of the FMDM and it is recommended to apply the empirical models of SNF degradation rates for brines (Sassani, et al. 2016; Mariner et al. 2017).



This page intentionally left blank

## 7. CORROSION BEHAVIOR OF CANDIDATE WASTE PACKAGE MATERIALS

This section discusses corrosion processes that may be relevant to a shale repository. Because no *a priori* choice of disposal overpack has been made, the section first discusses the general properties of iron-based alloys and copper, two likely choices for potential waste package materials. Then, corrosion processes are discussed, including general corrosion and different types of localized corrosion. Possible approaches for incorporating these into a repository performance assessment are considered. Finally, experimental observations are summarized. This discussion is in the context of a repository in a saturated shale host rock and with a compacted bentonite backfill surrounding and in contact with the waste packages. The bentonite is initially unsaturated and oxic due to entrapped oxygen, but over time, the oxygen is consumed by waste package corrosion and reactions with organic material or sulfides in the backfill and host rock, and the system goes anoxic. As the canisters cool, the backfill re-wets, and long-term conditions in the repository are saturated, anoxic bentonite backfill, in intimate contact with the waste package.

### 7.1 Corrosion of Iron Alloys and Copper Under Oxic and Anoxic Conditions

This subsection provides a basic discussion of the corrosion behavior under oxic and anoxic conditions, for two commonly considered metal: Fe-based and Cu-based materials. The summary relies heavily on the 2004 state-of-the-art document on the COrrOSion BEhavior of COntainer MAterials (COBECOMA; Kursten et al. 2004). More recent articles and summaries are also cited.

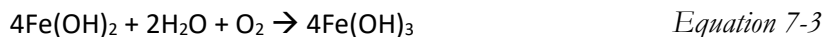
#### 7.1.1 Fe-Based Alloys

##### 7.1.1.1 Failure Mechanisms

Under the oxic conditions that will be present immediately after closure of a repository, iron-based materials such as carbon steel and stainless steel will corrode by reaction of iron with oxygen via two reactions:



The second reaction is fast in carbon steel, but stainless steel forms a passive oxide layer (mostly  $\text{Cr}_2\text{O}_3$ ), inhibiting further reaction. The ferrous hydroxide produced in the second reaction will be further oxidized in the presence of oxygen:



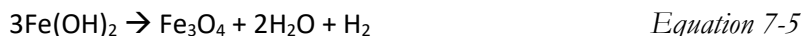
Ferric hydroxide will eventually dehydrate to form more stable oxyhydroxides such as goethite or lepidocrocite.

##### 7.1.1.2 Anoxic Corrosion of Fe-Based Metals

Because of metal corrosion and because of biotic and abiotic reactions with organic material or sulfides in the shale or bentonite buffer, the repository eventually becomes anoxic. Under anoxic conditions, iron corrosion will occur by reaction with water:



$\text{Fe}(\text{OH})_2$  will eventually react to form the more thermodynamically stable magnetite:



This reaction may be kinetically inhibited at low temperatures. Moreover, substitution of ions into the  $\text{Fe}(\text{OH})_2$  (e.g., Mg), can stabilize the hydroxide, inhibiting the reaction to magnetite. In alkaline environments, a dense magnetite layer forms on iron, passivating the surface and greatly slowing further corrosion (Smart et al. 2004).

As indicated above, the anoxic corrosion of steel produces  $\text{H}_2$ . If corrosion is sufficiently fast relative to movement of  $\text{H}_2$  away from the metal surface, the  $\text{H}_2$  may build up. However, it should not significantly inhibit corrosion; thermodynamic calculations indicate that the  $\text{H}_2$  partial pressures necessary to suppress the corrosion reaction are high, i.e., many times the hydrostatic pressure, or even the lithostatic pressure, at a typical repository depth (see discussion in Bryan et al. 2011, p. 59). Telander and Westerman (1993; 1997) performed mild steel corrosion experiments in WIPP-relevant brines, and saw some dependence on  $\text{H}_2$  pressure, with minimum corrosion rates at medium partial pressures (36–70 atm) and more rapid rates at either lower or higher partial pressures. However, their overall conclusion was that even at  $\text{H}_2$  partial pressures equal to WIPP lithostatic pressures (roughly 150 atm), the effect on mild steel corrosion rates was insignificant (Telander and Westerman 1997). This result was confirmed by Werme et al. (2002), who observed no dependence of carbon steel corrosion rate at hydrogen pressures of up to 100 atm. An additional effect of hydrogen gas generation, and of the high partial pressures necessary to suppress the corrosion reaction, is that hydrogen could potentially build up sufficiently to disrupt the buffer material, possibly creating transient fast pathways for flow and transport between the waste package surface and the host rock (see Section 6.2.3.3).

Environmental factors, including concentrations of chemical species, temperature, pH, and radiation flux, affect iron and steel corrosion rates. General corrosion is typically faster under oxic conditions, as oxygen provides an additional electron acceptor. Oxic conditions also generally favor localized corrosion processes. Chloride and fluoride destabilize passive films in stainless steels, resulting in pitting if concentrations are sufficiently high, and increase general corrosion rates as well (Krusten et al. 2004; Smart et al. 2004). Thiosulfate, an intermediate oxidation product of sulfide, stabilizes pits, lowering the pitting potential, and is especially detrimental if present with chloride, which can induce the pitting. Other anions (sulfate, hydroxide, nitrate, carbonate) generally inhibit corrosion, via either competitive sorption or the formation of more protective films. Temperature increases corrosion rate because it is an activation-controlled reaction. However, in an oxic open system, corrosion slows with increasing temperature above 80°C, as the solubility of oxygen decreases to the point that aqueous concentrations are no longer sufficient to support further increases in the corrosion rate. Temperature can also change the corrosion products, affecting their ability to form a protective layer. At elevated pH (>10), iron materials form a passive film and corrode very slowly. However, as the pH drops the corrosion rate increases until passivity is lost. The actual value at which this occurs depends on other environmental parameters (e.g., chloride concentration, temperature, redox potential). For stainless steels, decreasing pH also moves the pitting potential in the active direction, eventually resulting in pitting. However, once a pit forms, pit propagation is independent of external pH, as corrosion in the pit generates its own environment.

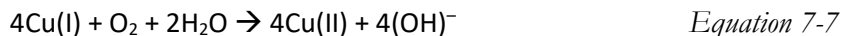
## 7.1.2 Cu-Based Materials

### 7.1.2.1 Oxidic Conditions

Krusten et al. (2004) provide a good general description of copper corrosion behavior under oxic and anoxic conditions. In the presence of oxygen, copper metal corrodes by the overall reaction:



The Cu(I) species further oxidize to form Cu(II) species, via the following schematic reaction:



Under oxic conditions as will persist in a clay or granite repository for a period after closure, the copper metal surface is coated with duplex corrosion product layer of  $\text{Cu}_2\text{O}$  and Cu(II) salts, the actual composition of which depends upon the composition of the backfill porewater. The  $\text{Cu}_2\text{O}$  layer is protective, but the Cu(II) salts are porous and discontinuous, allowing further oxidation of the  $\text{Cu}_2\text{O}$  layer to take place, and corrosion continues to occur. The rate of corrosion depends on the properties of the electrically conducting  $\text{Cu}_2\text{O}$  layer.

The role of chloride in copper corrosion is very complex and varies with concentration, redox conditions, and pH. In oxic conditions, chloride plays an important role in several copper corrosion reactions. It contributes to the anodic oxidation of copper metal via complexation, but can also contribute to the formation of the protective  $\text{Cu}_2\text{O}$  layer via a variety of reactions that involve conversion of cuprous chloride species to  $\text{Cu}_2\text{O}$  species. However, chloride may also contribute to the destruction of the  $\text{Cu}_2\text{O}$  film by supporting formation of a nonprotective cupric chloride-hydroxide layer. Chloride can also aid in reduction of aqueous cupric species at the cathode; this helps preserve the protective layer. Finally, incorporation of chloride ions into the protective  $\text{Cu}_2\text{O}$  layer changes its conductive properties. At high chloride concentrations, the layer can become so defected that it ceases to protect the surface, and copper will corrode by pitting or even corrode actively.

### 7.1.2.2 Anoxic Conditions

The general corrosion rate of copper in anoxic environments is anticipated to be extremely slow because thermodynamic data indicate that copper does not corrode via reaction with water. The generally accepted corrosion reaction for copper by water is



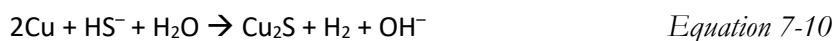
A vanishingly small  $f_{\text{H}_2}$  is required to suppress this reaction ( $\sim 10^{-16}$  bars), so it is not anticipated to occur at a measurable rate.

However, corrosion in anoxic natural waters may be enhanced by the presence of complexing species, especially chloride and sulfide. Under conditions of high chloride content, high temperature, and low pH (<6), chloride can enhance Cu corrosion:



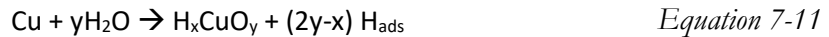
In the absence of another electron acceptor, this reaction is limited by transport of  $\text{H}^+$  to the metal surface or transport of  $\text{CuCl}_n^{1-n}$  away from the surface.

Sulfide is anticipated to be present in clay/shale porewaters as well as granitic porewaters. Sulfide causes corrosion of a copper waste package under anoxic conditions via formation of a copper sulfide corrosion product layer. Similar to the oxide layers that form, sulfides form a duplex corrosion product film, consisting of a thin inner layer of  $\text{Cu}_2\text{S}$ , and an outer layer of  $\text{CuS}$ . The  $\text{Cu}_2\text{S}$  forms by



### 7.1.2.3 “The Copper Controversy”

The discussion above is the classical view of how copper corrodes under anoxic conditions. However, the assumption that copper will not hydrolyze water has been questioned; a group of researchers has reported high measured rates of hydrogen generation in anoxic systems containing only copper and deionized water. These experimental results were first reported in Hultquist (1986), but were dismissed at the time as being experimental artifacts (Simpson and Schenk 1987). However, more recent experimental work verified the elevated  $H_2$  production (Szakálos et al. 2007; Hultquist et al. 2008; Szakálos et al. 2008; Hultquist et al. 2009; Hultquist et al. 2010; Hultquist et al. 2011; Hultquist et al. 2013), and indicated that the  $f_{H_2}$  required to suppress copper corrosion by water is actually on the order of  $10^{-3}$  bars. The research group hypothesized that the observed behavior could be explained by formation of a hydroxide-bearing corrosion product (instead of copper oxide) as in the following schematic reaction:



Moreover, a set of molecular dynamics simulations indicated that formation of stable hydroxide-containing surface complexes may be possible (Belonoshko and Rosengren 2010). If they exist, these surface complexes would lower the energy barrier for  $H_2O$  dissociation.

However, the experimental and modeling work as well as the conclusions in the above papers have been criticized (Johansson 2008; Werme and Korzhavyi 2010). The proposed mechanism for copper corrosion is inconsistent with a large body of experimental work and thermodynamic data. No such copper hydroxide corrosion product has been identified experimentally, and recent molecular dynamics modeling indicates that copper hydroxides or oxyhydroxide are not stable (Korzhavyi and Johansson 2010).

Because of the reliance on the copper waste package in the Swedish and Finnish repository programs, this issue has received a great deal of attention. It has come to be known as “The Copper Controversy.” In 2009, the Swedish repository organization SKB convened a workshop and an expert panel to discuss the issue. The final report of this workshop (Swedish National Council for Nuclear Waste 2009) concluded that further research was needed. In March 2011, the license application was submitted; however, the Swedish Land and Environmental Court required that further research be completed before a construction license could be issued. Since then, SKB and other researchers have carried several studies conclusively showing that copper does not corrode via reaction with water under anoxic conditions and that hydrogen was not generated, so long as carefully degassed copper was used in the tests; this work is summarized in detail in SKB (2019). At the time of this report, a final decision on the construction license has still not been made.

## 7.2 Corrosion Mechanisms

Metals exhibit three general types of behavior—active, passive, or immune—as a function of the redox potential (Eh, or pE), the pH, and the concentrations of other aqueous species in the environment. Active metals corrode readily, and the corrosion products that form are porous or nonadherent and do not act to isolate the underlying metal from further reaction. Passive metals form a dense adherent oxide layer on the surface that restricts mass transfer to and from the metal surface, slowing further corrosion. Some metals are passive in a large range of environments, while others corrode actively over most natural conditions. For instance, copper is generally passive, but behaves actively if reduced sulfur species are present. Carbon steel actively corrodes under most oxic or anoxic conditions, but forms a passivating hydroxide layer at high pH, for instance, when embedded in concrete. Stainless steel is passive under most conditions, because of the formation of a thin, protective chrome oxide-hydroxide layer on the metal surface.

Metals also display two different modes of corrosion, referred to as general and localized corrosion. Both passive and active metals undergo general, or uniform, corrosion, but only passive metals are susceptible

to localized corrosion. To understand the difference between the two modes, it must be recognized that metal corrosion involves two half-reactions, and that those two reactions are not co-located. At the anode, the metal is oxidized. For instance, using iron as an example,



This is the anodic half-cell, and this reaction frequently results in acidification at the anode as the metal ion hydrolyzes, e.g.,



The balancing cathodic reaction involves reduction, generally of oxygen or water. These reactions are



Note that by combining with the water dissociation reaction, the second reaction can also be written as



Both oxygen and water reduction reactions result in hydroxyl production and an increase in pH in the region of the cathode.

### 7.2.1 General Corrosion

In the case of general corrosion, the entire metal surface undergoes attack. Neither the cathode nor the anode is localized; instead, they migrate randomly across the surface. Hence, this type of corrosion has little effect on the surface pH; production of hydroxyl via oxygen or water reduction is balanced by  $\text{H}^+$  generated via metal. Both passive and active metals undergo uniform corrosion. For the active metals, the surface corrosion products do not limit transport of reactants (e.g., oxygen or water) to and from the surface, so metal oxidation continues to occur, although generally slowing with time. In the case of passive metals, a different mechanism takes place. The passive oxide film prevents solution transport, but metal oxidation can still occur via defect migration through the oxide layer. This process has been described as the point defect model (Macdonald 1992). At the metal surface, metal atoms are oxidized and incorporated into the oxide layer with an oxygen defect to balance charge. At the oxide/solution interface, reduction occurs and oxygen is incorporated into the oxide layer along with a metal vacancy to balance charge. The vacancies diffuse together, resulting eventually in thickening of the oxide layer. Note that as the layer thickens, diffusion through the oxide layer slows, and hence corrosion slows. At some point, the rate of corrosion becomes equal to the rate of oxide layer dissolution into the solution. This model is frequently used to describe mineral dissolution processes (e.g., Oelkers 2001) and has also been proposed for carbon steel and iron in anaerobic neutral or alkaline conditions by Werme et al. (2002), based on observations that (1) corrosion rates of these materials decrease over time to a constant low value (Simpson et al. 1985; Grauer et al. 1990; Kreis 1991; Féron et al. 2009), and (2) the rate of corrosion increases with the solubility of iron in the electrolyte (e.g., Davies and Burstein 1980). Application of this model to iron-based materials in alkaline environments, when iron behaves passively due to the formation of a protective, impermeable iron hydroxide layer, seems obvious. It is not clear why



this approach would be valid at neutral pH conditions, when iron corrosion products do not form a passivating layer.

Uniform corrosion rates are relatively slow and are readily measured, making the effects predictable. Hence, for ordinary engineered structures, general corrosion is rarely a concern. However, because of the long time scales involved, general corrosion must be modeled in repository performance assessment calculations. Depending upon the material, a few different approaches can be considered. The simplest is to develop a distribution of general corrosion rates for expected or anticipated repository conditions from experimental or literature data, and then to sample that distribution. Environmental factors such as brine composition will affect corrosion rate, so such data should be repository system-specific. Moreover, since corrosion is a thermally activated process, such a model should include a temperature dependence (e.g., an Arrhenius relationship) for the general corrosion rate.

An alternative approach, for some metals under some conditions, is to limit the general corrosion rate or extent by the availability of reactants. A few examples of this approach are shown below.

### **7.2.1.1 Copper**

Under oxic conditions, copper corrodes rapidly relative to repository regulatory time periods. A common approach, used in Swedish and Canadian performance assessments for copper canisters, is to assume that oxic corrosion occurs very quickly and is uniform on the canister surfaces. The total amount of oxic corrosion that can occur is then assessed based on estimates of the amount of oxygen present. As long as the remaining wall thickness is conservatively sufficient to last the remaining duration of the regulatory time period under anoxic conditions, the engineered barrier is sufficient. In the case of the Swedish repository, calculations by King et al. (2011) indicated that corrosion in the form of oxic corrosion occurring shortly after closure would remove on the order of 0.001 mm of copper from the surface of the copper waste packages. Since the Swedish disposal package has a 5 cm thick copper shell (SKB 2019), the copper loss is insignificant. A similar approach of limiting corrosion by the availability of reactants was applied once the repository went anoxic. Copper does not react with water, so corrosion in the absence of oxygen is believed to occur mostly by reactions with hydrogen sulfide or thiosulfate species in the bentonite porewaters. The corrosion rate is hence controlled by the rate of mass transfer of these species from the surrounding formation to the copper surface. Modeling by SKB suggests that in the one million years following the oxic period, limited sulfide transport through the low-permeability bentonite buffer to the metal surface will result in less than 1 mm of copper corrosion to form copper sulfides (King et al. 2011). Estimates of copper waste package lifetime, for wall thicknesses of 2.5–5 cm, are >1,000,000 years (Kursten et al. 2004; King et al. 2010; King et al. 2011; Kwong 2011). King et al. (2011) estimates the total penetration of the package, over a  $10^6$  year assessment period, to be less than 1 mm, with the majority of the penetration occurring under anaerobic conditions by formation of  $\text{Cu}_2\text{S}$ . Kwong (2011) estimates 1.27 mm penetration over that same time period.

The SKB analysis was for a repository in granite, with a bentonite buffer. Because of copper's reactivity with sulfide, use of copper as an overpack material in a shale repository would require evaluating the amount of sulfide in the bentonite backfill and in the host rock porewaters, and demonstrating that sulfide transport to the canister surface would be slow enough for the overpack to survive the regulatory period.

### **7.2.1.2 Iron-Based Alloys**

In contrast to copper, iron and low carbon steels will react with water under both oxic and anoxic conditions. Hence, they will continue to undergo general corrosion at a measurable rate, once the oxygen has been depleted. In experimental testing, measured rates under anoxic conditions are initially high, but rapidly decrease to an approximately steady value (e.g., see examples in Féron et al. 2009; Bryan et al. 2011). For performance assessment calculations, this rate would vary with redox condition, water chemistry, and temperature, and would be based on measured data (for example, Féron et al. 2009, Figure 5).

Stainless steel also undergoes general corrosion under both oxic and anoxic conditions. Rates of general corrosion are generally quite low, much less than carbon steel, and decrease with time to a constant low value. As discussed earlier, this may be consistent with an oxide dissolution model, in which the corrosion rates are limited by diffusion through the chrome oxide passivating layer, which thickens until eventually the rate of diffusion becomes equivalent to the rate of chrome oxide dissolution from the metal surface. If true, then general corrosion of stainless steel would be controlled by the rate of aqueous transport of chrome species from the surface, and the corrosion rate could be evaluated by modeling chrome solubility and reactive transport in the backfill and host rock porewaters.

### **7.2.1.3 Implementing General Corrosion in a GDSA Model**

Evaluating corrosion of all waste package surfaces for thousands of waste packages using a reactive transport model is not possible. But such a model could be used to estimate a possible distribution of general corrosion rates. Implementing that distribution of corrosion rates in performance assessment calculations could be accomplished in several different ways, and each would result in different dose release curves. Assuming that a distribution of corrosion rates is sampled, how is the selected rate applied? Should it be sampled once per realization and applied to all the canisters in the repository for that realization, or, should a different rate be applied to each canister? In the case of Yucca Mountain, a more complex model was used. Each waste package was divided into ~1,400 different regions (SNL 2008b, Section 6.3.5.1.2), and a different corrosion rate was applied to each. The rationale behind this was that the corrosion rate distributions were determined experimentally, using small coupons. Just as the corrosion rate varied for each coupon in the experiment, it is reasonable to assume that rates would vary across the canister surface. Each of these GDSA model implementations would potentially yield very different results in terms of radionuclide release rates.

### **7.2.2 Localized Corrosion**

The second major mode of corrosion is localized corrosion. In localized corrosion, the anodic reaction (metal dissolution) is localized, while the cathodic reaction occurs on the surrounding metal surface. The current generated by the cathode supports dissolution at the anode. Because anodic damage is localized but may be supported by reactions over a large cathode area, localized corrosion can result in relatively rapid penetration of metal plate. A second potentially important effect, in possible repository settings, is that the separation of the anode and the cathode results in major differences in solution composition at the two locations. At the anode, the solution becomes very acidic (pH 1–2) due to metal dissolution and hydrolysis, while at the cathode, hydroxyl production due to oxygen or water reduction may result in significant increases in pH (Figure 7-1), which could promote mineralogical reactions in the adjacent backfill (Marty et al. 2010). Maintaining the highly acidic conditions at the anode is critical, because if the pH rises, the metal will repassivate and corrosion will cease. Types of localized corrosion include pitting, crevice corrosion, and SCC.

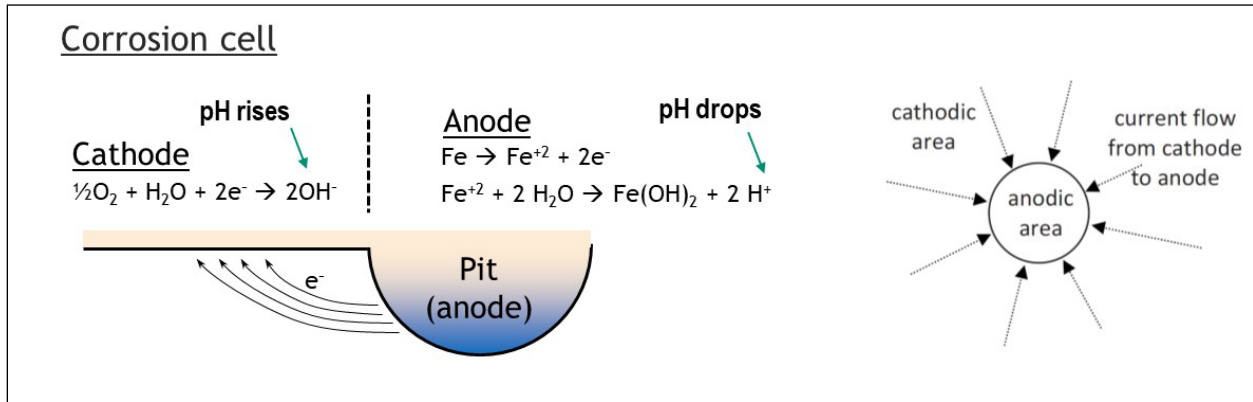


**Figure 7-1. Schematic Diagram of Pitting Corrosion, Illustrating the Relationship between the Cathode and Anode, the Reactions That Occur for Each, and the Effect on pH at Each Location**

In pitting corrosion, a central pit is supported by cathodic reactions on the surrounding metal. The rate of pit growth and possibly the ultimate size of the pit is a function of the available cathodic current, which in turn is limited by ohmic drop in the ionic solution connecting the two regions. Immersed in a concentrated solution, a large cathodic surface area might be able to support rapid pit growth (as discussed later, it may be possible to build a pitting model around this concept). For the surface of a waste package embedded in a saturated clay backfill, the available area supporting pit growth will be controlled by the electrical conductivity of the wet, compacted clay; experimental measurements suggest that this material is an excellent electrical conductor, with conductivities only slightly lower than the pure porewater (Stoulil et al. 2018). This suggests that pitting and other forms of localized corrosion must be seriously considered as potential canister penetration mechanisms in a shale repository.

The aggressive acidic conditions at the anode are a function of two offsetting processes—the rate of metal corrosion and hence  $\text{H}^+$  production, and the rate of diffusive equilibration between the pit and the surrounding area. A large cathode region, supporting a large cathode current, can maintain rapid metal dissolution and acidic conditions at the anode. Or, occluded conditions can support continued corrosion by slowing diffusive equilibration between the anode and the cathode. Localized corrosion initiating in occluded regions on the metal surface is called crevice corrosion, and crevice corrosion is both easier to initiate than pitting, and easier to maintain. In engineered structures, it commonly initiates between components in contact with each other, or under failed coatings (e.g. paint) on the metal. In the case of a metal waste package embedded in a clay backfill, it is possible that the intimate contact between the waste package and the backfill itself would constitute a crevice, or that precipitation of secondary minerals on the metal surface could create a crevice. Stoulil et al. (2019) found that the presence of bentonite, even in a slurry form, seemed to promote crevicing by providing a sorption sink for iron in solution and destabilizing the oxide layer on the carbon steel surface.

If tensile stresses are present in the waste package, some metals may undergo SCC in corrosive environments. Tensile stresses may be due to loading or pressurization, or may be due to residual stresses in the metal caused by welding or fabrication processes. Stress corrosion cracks are capable of penetrating a canister wall very quickly (essentially instantaneously) relative to regulatory performance time periods; hence, incorporating them into performance assessment model does not require estimating crack growth rates, but rather predicting the timing of SCC occurrence, and potentially, the number of cracks that can form. In the Yucca Mountain total system performance assessment (TSPA), crack formation was delayed by low plasticity burnishing of the weld regions canister Alloy 22 outer shell. The burnishing created compressive stresses in the skin of the canister to a depth of a few mm, but tensile stresses still existed at greater depths. SCC would not occur until the compressive zone was removed by general corrosion; in the

Yucca Mountain model for Alloy 22, this took hundreds of thousands of years. The possible number of cracks was limited by stress “shadowing” effects—a SCC crack would relieve local stresses, inhibiting the formation of nearby cracks. Using this approach, possible SCC crack densities can be calculated from the mechanical properties of the metal and the total susceptible area on the canister.

Susceptibility to SCC is not only a function of the metal composition and tensile stresses, but of the microstructure as well. Factors that enhance susceptibility include degree of sensitization and degree of plastic strain (work hardening). SCC commonly occurs near welds not only because of the high residual tensile stresses in the weld heat affected zones, but also because the weld heat input can result in sensitization of the material—diffusion of chrome to the grain boundaries that renders the metal near the grain boundary more susceptible to corrosion. Moreover, as the welds cool and shrink, the nearby metal is subjected to sufficiently high stresses to result in work hardening, which reduces metal ductility and increases susceptibility to SCC.

SCC susceptibility is also controlled by the environment. SCC probability increases with chloride content, although even relatively low chloride concentrations can cause SCC, especially in anoxic settings. This occurs because chloride promotes corrosion and  $H^+$  absorption and reduction at the acidified anode can lead to local hydrogen embrittlement, supporting crack initiation and growth. Moreover, in an anoxic shale repository setting, cathodic reactions such as water or  $H_2S$  reduction will generate hydrogen gas. Because of the low permeability of the backfill and clay host rock, this could accumulate in the region of the waste package, potentially resulting in hydrogen embrittlement of the canister metal and promoting SCC. High hydrogen concentrations are not required for hydrogen embrittlement; data indicate changes in mechanical properties of stainless steels at as low as 40 ppm hydrogen (Graver 1984, Gdowski and Bullen 1988).

#### **7.2.2.1 Copper**

The form of localized copper corrosion considered most likely in granite repository settings is pitting corrosion during the initial oxic period when residual  $O_2$  introduced during the operational period is consumed. Considerable effort, both in terms of modeling and experimental work, has been done to evaluate this in repository settings. In general, there are three phases in the life of a pit: initiation, propagation, and death. Pit initiation is strongly linked to damage of the  $Cu_2O$  layer by precipitation of  $CuCl$  in or under the  $Cu_2O$  layer on the copper surface (Section 7.1.2.1); hence, the pitting potential ( $E_p$ ) is a function of chloride concentration and elevated chloride concentrations, which occur in deep granitic porewaters, promote pitting. However, bicarbonate competes with chloride with respect to  $Cu$  complexation and formation of sorbed surface species, and inhibits pitting. Once a pit is formed,  $O_2$  is required for pit growth, and due to mass transport limitations in  $O_2$  movement through the buffer to the corrosion site and limitations in total  $O_2$ , the pits will rapidly die. A number of experiments have evaluated copper corrosion in contact with oxic, saturated buffer material and have found no evidence for pitting (Kurstien et al. 2004).

Crevice corrosion is not anticipated to affect copper canisters because complexation of  $Cu(I)$  with chloride limits hydrolysis and prevents acidification of the crevice. Moreover, formation of  $Cu(II)$  species, which could hydrolyze, will be inhibited by the restricted access of  $O_2$  to the occluded region (Kurstien et al. 2004).

Stress corrosion cracking is of concern for copper canisters because copper, especially copper containing phosphorous, has been found to be highly susceptible to SCC. Moreover, tensile stresses, either residual manufacturing stresses or stresses due to loading (a combination of hydrostatic pressure and clay swelling pressure), are likely to occur. However, copper waste package SCC is largely a concern in granite-based repositories being considered by the Swedish, Finnish and Canadian programs, due to the presence of ammonia and acetate, two species known to promote SCC, in the groundwater. King et al. (2011) and Kwong (2011) summarize the current understanding of copper SCC and the effects of environmental factors, including ammonia, acetate, and nitrite concentrations. Based on extensive testing by Posiva,

SKB, and the Canadian repository program, SCC was not observed at ammonia, acetate, or nitrite levels that exceeded the naturally occurring levels by orders of magnitude. Sulfite has also been shown to promote SCC if present in high concentrations (Taniguchi and Kawasaki 2008). However, anticipated concentrations at the container surface are low and are limited by diffusion through the buffer material, leading King et al. (2010) to conclude that sulfide induced SCC will not occur under repository conditions. For these reasons, failure of copper waste packages by SCC is not considered credible (Kwong 2011).

As with most metals copper is subject to embrittlement in hydrogen-containing environments (SKB 2019). Hydrogen embrittlement, in addition to degrading the mechanical properties of the metal, will increase susceptibility to SCC. For the Swedish repository, possible hydrogen embrittlement of the canister was eliminated from consideration by mass balance arguments; the hydrogen is generated by anoxic copper corrosion, and as copper does not react with water, the only reaction of interest is reduction of  $H_2S$ . Estimates of  $H_2S$  transport through the bentonite to the copper surface, and subsequent  $H_2$  generation, were too small to result in hydrogen embrittlement of the copper. The mechanical effects of hydrogen adsorption are also enhanced by combination with oxygen in the copper to form water, which is trapped within the copper structure. To mitigate this concern, copper for use in SNF disposal packages is always specified to be oxygen-free.

### **7.2.2.2 Iron-Based Alloys**

Iron and low-carbon steel are susceptible to pitting corrosion under oxic conditions. However, experimental studies show that the pitting factor (the ratio of maximal pit depth to mean corrosion depth) decreases as the mean corrosion depth increases, so in the long term, pitting of these materials can be ignored (Feron et al. 2009). Austenitic stainless steels (304 and 316) are also susceptible to pitting corrosion but do not show this relationship, and the rate of pitting penetration is difficult to predict. Low confidence in the ability to predict pitting penetration rates for stainless steel is a frequently cited-reason for using carbon steel or cast iron waste packages instead. For those materials, general corrosion is much faster than for stainless steel, but pitting can be ignored and canister performance can be much more reliably estimated (Kursten et al. 2004, Féron et al. 2009).

Carbon steels are also susceptible to SCC, especially in an anoxic shale environment. This is because anoxic metal corrosion via water or  $H_2S$  reduction will produce hydrogen, resulting in hydrogen embrittlement of the steel. Hydrogen embrittlement increases susceptibility, resulting in a lower threshold stress intensity factor for crack initiation and faster crack growth rates (Chatterjee and Raman 2011). Austenitic stainless steels are well known to be susceptible to SCC (e.g., Kain 2011) and hydrogen embrittlement increases the stainless steel SCC susceptibility further. Feron et al. (2009) suggest that if hydrogen buildup and hydrogen embrittlement is a concern, use of steels that are not susceptible to embrittlement should be considered. Sulfide ions in solution have also been shown to increase SCC susceptibility for sensitized 304 stainless steel (Lee and Szklarska-Smialowska 1988), and for cold-worked (strained) stainless steels (Asphahani 1981). Although 304L and 316L stainless steel do not easily sensitize, steels will undergo plastic strain near weld zones in response to weld cooling and shrinkage. The degree of work hardening has been estimated to be equivalent to 20% plastic strain, which greatly increases the susceptibility to SCC (Kain 2011).

### **7.2.2.3 GDSA Implementation of Localized Corrosion Processes**

Relevant pit growth rates for stainless steel are difficult measure, as the experimental conditions must duplicate cathode and anode conditions and even possible cathode size. The rate of pit growth and possibly the ultimate size of the pit is a function of the available cathodic current, which in turn is limited by ohmic drop in the ionic solution connecting the two regions. Immersed in a concentrated solution, a large cathodic surface area might be able to support rapid pit growth. For the surface of a waste package embedded in a saturated clay backfill, the available area supporting pit growth will be controlled by the electrical conductivity of the wet, compacted clay; experimental measurements suggest that this material



is an excellent electrical conductor, with conductivities only slightly lower than the pure porewater (Stoulil et al. 2018). It should be possible to estimate the cathode current using a multiphysics code which includes an electrochemical module. However, this only limits the rate of metal oxidation; to determine the rate of pit penetration (downward growth), an assumption has to be made about the geometry of the pit. This would affect the cross-sectional area of the pit, through which advective or diffusive releases could occur. Potential reaction with the backfill must also be considered; Marty et al. (2010) suggest that high pH values in the cathodic regions drove alteration of the bentonite and precipitation of secondary minerals that occluded backfill porosity, resulting in reduced steel corrosion rates. However, this requires additional study; Stoulil et al. (2019) found that the presence of bentonite appeared to enhance steel corrosion, and speculated that it provided a sorption sink for solution  $\text{Fe}^{2+}$ , destabilizing the oxide layer on the steel and permitting more rapid corrosion. Wilson et al. (2015) provides examples of reactive transport modeling of corrosion at a bentonite-steel interface, and found that modeling assumptions played a large role in predicted corrosion rates.

As noted previously, SCC crack growth rates will be very rapid relative to regulatory time scales, so it is not necessary to model crack growth. Rather, once conditions for crack initiation have been met, it can be assumed that through-wall cracks form, if sufficient tensile stresses are present. An analysis of the loading stresses in the repository must be made to see if they are sufficient to support SCC. If not, then weld zones are the only likely locations for SCC. If weld stresses have been mitigated via peening or other treatments that produce surface compressive stresses, then penetration of the surface compressed layer by general corrosion or by pitting must occur before SCC can initiate. Once the compressive layer has been penetrated, then SCC is possible, if the environmental conditions support it. Once an SCC crack has been determined to penetrate the canister wall, structural mechanics calculations can be used to estimate the crack aperture, as it is a function both plastic and elastic deformation of the metal in response to the tensile stress field.

As with pits, the cracks represent small openings, with crack gaps of microns to tens of microns. In the unsaturated zone Yucca Mountain case, SCC cracks only represented pathways for diffusive releases, as capillary pressures prevented flow through the cracks. However, for a shale repository, any canister penetration will allow pore-pressure-driven advective flow into the canisters. Once water enters the canisters, corrosion of internals and possibly radiolysis of water would generate hydrogen gas, which could in turn drive advective flow of gaseous radionuclides and, depending upon the number and location of breaches, possibly dissolved radionuclides, out of the waste packages.

### 7.3 Summary of Copper and Steel Corrosion Behavior

The corrosion behavior of copper and Fe-based alloys have been discussed for potential application of these materials as waste packages or overpacks in a shale repository setting. Copper will undergo rapid but limited corrosion during the initial oxic period via reaction with oxygen trapped in the backfill. Once the repository becomes anoxic, copper corrodes via reaction with sulfides in the backfill porewater, and the rate and extent of corrosion are limited by the rate of  $\text{H}_2\text{S}$  transport to the waste-package surface. For granite-hosted repositories, copper corrosion has been shown to be insignificant over repository time intervals; for a shale-based repository, where the levels of sulfite in the host rock may be much higher, this has not been evaluated. Copper is subject to localized corrosion, and both processes must be evaluated. Screening justifications, if made, would likely involve consideration of the low availability of aggressive species at the metal surface (as in SKB 2019). Other aqueous species, especially chloride, can affect the rate and extent of corrosion, and must be considered.

Carbon steel, cast iron, and stainless steel will rapidly consume the oxygen initially present in the unsaturated backfill, and will then continue to corrode via reaction with water. For cast iron and low-alloy steels, the general, or uniform, corrosion rate slows rapidly to a steady value of approximately 1–10  $\mu\text{m}/\text{yr}$ , based on measured values and archaeological analogs (Féron et al. 2009) (for relatively dilute groundwaters). For stainless steels, the rate is perhaps an order of magnitude lower. Carbon steel and cast

iron are in general not susceptible to localized corrosion under reducing conditions, while stainless steels are highly susceptible to that mode of corrosion. Failure by localized corrosion will not result in large overpack breaches, but will provide entry for brine into the package and exit points for brine release. If extensive, SCC could result in structural weakening or even structural failure of the overpack. Because general corrosion processes are well known, less a function of water chemistry, and easily modeled relative to localized corrosion processes, carbon steel is frequently chosen over stainless steel as a waste package corrosion allowance material (Féron et al. 2009).

Corrosion under anoxic conditions results in hydrogen generation and can lead to hydrogen embrittlement of both copper and Fe-based alloys. Hydrogen embrittlement both increases the risk of SCC and changes the mechanical properties of the metal, potentially resulting in gross structural weakening. For the Swedish granite-based repository, hydrogen embrittlement of the copper canister was screened out based on mass balance arguments—the extent of corrosion was so limited by the availability of H<sub>2</sub>S that significant hydrogen embrittlement could not occur (SKB 2019). A similar analysis might be applicable for copper in a shale repository. However, Fe-based alloys can react with water, and seem likely to embrittle in a shale repository. The potential occurrence and effects of hydrogen embrittlement should be evaluated for a shale repository.



## 8. CHEMICAL CHANGES AT INTERFACIAL AREAS

### 8.1 High-Temperature Waste Canister Overpack-Bentonite Interactions

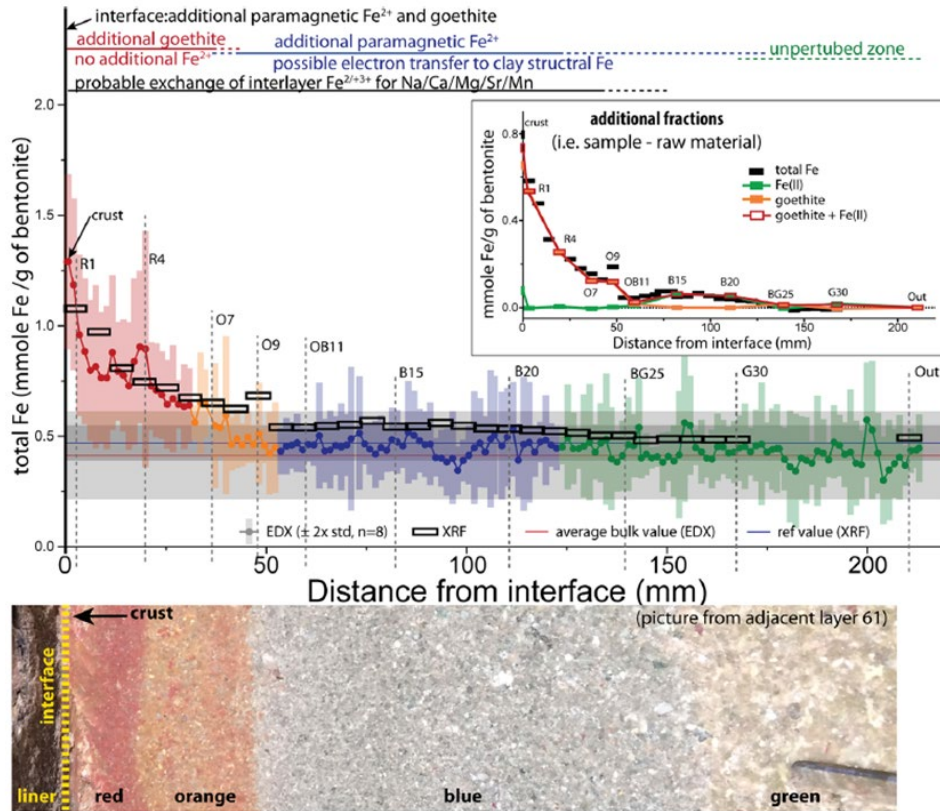
The interface of the waste canister overpack and the EBS represents a chemical boundary at which material interactions may affect bentonite properties as well as the canister surface (e.g., Kaufhold et al. 2015; Hadi et al. 2019). After initial repository closure and when the boundary is experiencing the thermal peak, this boundary will likely be dry. Under dry conditions, bentonite mineralogy will likely be stable and steel corrosion will be minimal. However, the bentonite buffer will gradually become water saturated due to the infiltration of groundwater, leading to canister corrosion, alteration of the bentonite, and reactions between corrosion products and the bentonite. Observations from experimental and modeling studies that include candidate waste canister overpack materials (i.e., stainless steel, carbon steel, and copper) can inform clay-steel interaction in EBS environments relevant to the high-temperature shale case.

#### 8.1.1 Steel-Bentonite Interaction

Interaction of carbon steel and bentonite was examined in the 18-year FEBEX full-scale EBS heater test at the Grimsel Test Site (Martin et al. 2006). Metal corrosion and chemical changes in bentonite chemistry at the buffer-steel interface occurred (Wersin and Kober 2017, Kaufhold et al. 2018, Hadi et al. 2019). Alteration of bentonite in contact with the steel heater surface was examined in detail by Hadi et al. (2019). Bentonite at the heater interface reached temperatures of 30°C–60°C. Corrosion of carbon steel led to a > 140 mm layered zone of iron enrichment extending radially into the bentonite (Figure 8-1). Iron enrichment in the first ~30 mm is interpreted to be hosted in newly formed goethite (FeO(OH)) within the bentonite. The remainder of the Fe-enriched zone is interpreted to be a result of the diffusion and sorption of Fe(II) to clay mineral edge sites (Hadi et al. 2019). This layering is interpreted to be related to initial diffusion of Fe(III) and precipitation during oxidizing conditions, followed by diffusion of Fe(II) when oxygen became depleted. Clay mineral alteration was not observed, likely due to the low temperatures achieved. The results of the FEBEX test demonstrate the potential for steel corrosion and Fe mobility into the bentonite buffer in a relatively short time period.

High-temperature, full-scale experiments are needed to characterize the steel-bentonite interface evolution under conditions relevant to 21-PWR/44-BWR disposal. HotBENT, an experiment conducted by Nagra in the same drift as the FEBEX experiment, is in its initial stages. Peak temperatures will be between 175°C–200°C.

Lab-scale experiments lack the realistic scale and water/rock and clay/steel ratios that are unique to in-situ experiments such as FEBEX but can provide insight into mineral phase stabilities and potential mineral reactions at higher temperatures. Many recent lab-scale experiments have been completed on the interaction of clay minerals/bentonite with steel/Fe-oxide/native iron at temperatures between 25°C and 300°C (Wersin et al. 2007, Mosser-Ruck et al. 2010, Pignatelli et al. 2013, Bourdelle et al. 2014, Pignatelli et al. 2014, Kaufhold et al. 2015, Bourdelle et al. 2017, Cheshire et al. 2018). These studies show that steel corrosion has the potential to have wide ranging effects on the physical and chemical properties of the bentonite buffer in contact with the waste canister overpack, likely dependent on bulk system chemistry. Changes to physical properties include dissolution/recrystallization of montmorillonite, loss of bentonite swelling capacity (due to cementation or recrystallization to nonswelling phases), and development of porosity due to the formation of denser mineral phases (e.g., zeolites).



NOTE: Heat exposure occurred over 18 years during the FEBEX experiment. Red and orange zones are characterized by Fe(II) enrichment, whereas the blue zone is enriched in Fe(III).

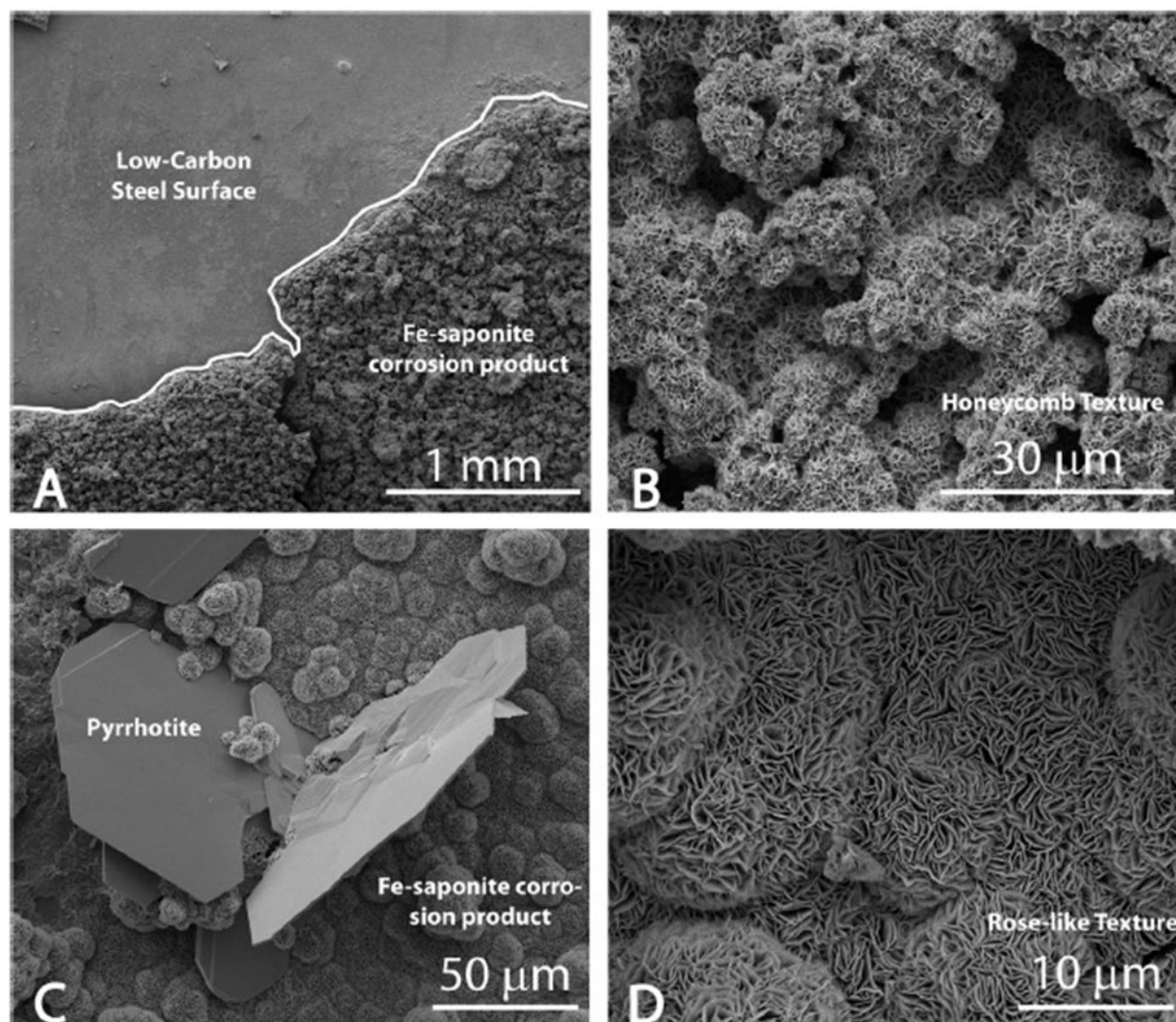
Source: Hadi et al. 2019.

**Figure 8-1. Image of Altered Bentonite and X-ray Fluorescence Results from a Bentonite Block adjacent to the Steel Heater**

In  $>100^{\circ}\text{C}$  experimental systems that utilize reaction solutions with neutral pH values (i.e., porewaters buffered by clay and silicate minerals), iron is transferred from either iron shavings or steel coupons to clay minerals in the bentonite to form different Fe-rich phyllosilicate minerals, such as Fe-saponite, chlorite, berthierine, depending on temperature, bulk system chemistry, and redox conditions (Guillaume et al. 2003, Guillaume et al. 2004, Mosser-Ruck et al. 2010, Cheshire et al. 2018). For example, in  $300^{\circ}\text{C}/6$  week–6 month hydrothermal experiments that include steel coupons embedded in bentonite, stainless steel corrodes to produce a chromite-like ( $\text{FeCr}_2\text{O}_4$ ) passivation layer above unaltered steel, whereas a magnetite-like phase forms on the surface of low carbon steel (Cheshire et al. 2018). Attached to the corroded surface is a  $< 100 \mu\text{m}$  zone of Fe-rich smectite (Fe-saponite) on both steel types (Figure 8-2) (Cheshire et al. 2018). Similar results were observed in Guillaume et al. (2003) in which chlorite, saponite, and silicates were formed in  $300^{\circ}\text{C}/9$ -month experiments that included MX80 bentonite and Fe powder/plates. Experimental studies have also examined the alteration of the bentonite-steel-cement environment in the presence of high pH reaction fluids ( $\text{pH} > 10$ ) at temperatures over  $100^{\circ}\text{C}$  (Charpentiera et al. 2006; Kaufhold et al. 2018). At high pH, steel corrosion is inhibited, leading to less transfer of iron to the bentonite. Observed reaction products in hydrothermal experiments include Fe-rich vermiculite and zeolite minerals (Charpentiera et al. 2006).

Alteration of the bentonite due to reactions with steel corrosion products will likely include the development of porosity, loss of swelling capacity, and formation of secondary mineral phases. Alteration

products, such as zeolites and phyllosilicates, should be included in models of barrier function with respect to radionuclide retention.



Source: Cheshire et al. 2018.

**Figure 8-2. Scanning Electron Microscope Image of the Surface of a Reacted Low Carbon Steel Coupon Showing the Formation of Fe-Saponite and Secondary Pyrrhotite ( $\text{Fe}_{1-x}\text{S}$ )**

### 8.1.2 Clay-Copper Interaction

Copper is an ideal waste canister overpack material in saturated, reducing crystalline environments and is, for example, used as an overpack material in the Swedish disposal concept. Copper is less favored in the shale concept as experiments show that copper is particularly prone to sulfide attack (described in Section 7.1). For example, in hydrothermal experiments that examined the potential of copper interaction with bentonite, corrosion occurred, likely because of pyrite dissolution in bentonite, producing chalcocite ( $\text{Cu}_2\text{S}$ ) growth over the corroded/pitted surface (Caporuscio et al. 2017). Alteration of the bentonite mineralogy due to interaction with copper corrosion byproducts was not observed. Overall, the effect of sulfur-species on copper corrosion must be accounted for in a shale-hosted repository due to the likely



presence of pyrite in the host rock and the presence of sulfide-phases in the buffer, which have the potential to rapidly degrade and migrate towards the waste package surface.

## 8.2 Additional Interactions

The LANL hydrothermal laboratory experiments (Caporuscio et al. 2019, Table 1) investigated the aqueous geochemical evolution in relationship to mineralogical alterations and the formation of secondary minerals under high temperature with a focus on interactions at interfaces:

- Waste package–buffer interface experiments, up to 300°C and 15–16 MPa, involving stainless steel (304, 316, or low carbon), Wyoming bentonite, and a synthetic porewater solution (Stripa sample V2, 69-4 (Frape et al. 2003))
- Buffer–host-rock interface experiments, up to 300°C and 15–16 MPa, involving Wyoming bentonite, Opalinus Clay, and a synthetic Opalinus Clay groundwater
- Buffer–liner material–host rock interface experiments, at 200°C, involving Wyoming bentonite, Opalinus Clay host rock material, Ordinary Portland Cement as the liner material, and a synthetic Opalinus Clay groundwater as the porewater.

Mineral characterization and thermodynamic evaluation suggest the following:

- The changes to smectite structure that occur in 2 months at 200°C in saline condition environment can occur in 6 months at 300°C without the saline environment. This highlights the time- and temperature-dependent structural changes to smectite toward a stable phase as a function of the bulk rock and solution chemistry.
- The bulk chemistry of the overall system may restrict illitization of smectites. Postexperiment mineral characterization and thermodynamic evaluation of phase equilibria suggest that illite (or chlorite) as a nonswelling phase does not form under Si-rich conditions and even if illitization occurs, the condition may not be optimal for it to remain stable. If illite (or chlorite) occurs at high temperatures, it will happen so under only very specific solution chemistry conditions.
- High  $\text{Na}^+$  activity and limited  $\text{K}^+$  supply inhibit/retard bentonite alteration to illite.  $\text{Al}^{3+}$  inhibits illitization and kinetics become very slow with sequestered  $\text{Al}^{3+}$ . Clinoptilolite (a zeolite with a high Si/Al ratio) to analcime (a zeolite with a lower Si/Al ratio) conversion is highly sensitive to reaction conditions. In other words, mineral reactions involving high-Si phase (e.g., zeolites) along with low  $\text{K}^+$  content in the bentonite can play a key role in whether illite would form.
- Low carbon stainless steel–bentonite interactions led to montmorillonite alteration within 1 mm of the metal/alloy surface, thus suggesting that montmorillonite alteration was largely restricted to the steel surface and most of the montmorillonite beyond the steel surface to a large extent remained stable. The interface develops Fe-saponite, a well characterized new mineral phase, especially at 300°C. Pyrite decomposition in the bentonite produces sulfur towards the formation of these sulfide phases. Fe-saponite growth on steel seems to be perpendicular to the surface along with reduced sulfides. This doesn't imply metal surface passivation (even when it looks like it) but it demonstrates what happens to montmorillonite when it degrades to another phase at elevated temperatures. The issue of steel surface passivation is unresolved and needs further investigation.
- The bentonite–Opalinus Clay system showed that precursor illite is needed for the nucleation and further growth of illite in the bentonite portion of the system. The overall high silica saturation appears to inhibit illite formation and favor precipitation of high-silica zeolites such as

analcime/wairakite as a result of the higher amounts of Ca. The abundance of aqueous-phase Ca at 300°C in the bentonite–Opalinus Clay experimental system explained the importance of  $\text{SiO}_{2(\text{aq})}$  activity in determining the zeolite stable assemblage and the absence of illite which is stable at low  $\text{SiO}_{2(\text{aq})}$  activities (Jové Colón et al. 2019).

- The addition of Ordinary Portland Cement to bentonite–Opalinus Clay experimental system affected the smectite mineral structure in the bentonite fraction, resulting in ~10% reduction in expandability of swelling smectite. Combined illite, illite-smectite, and smectite in the bulk system reduced by ~12–19 wt.%. Abundant Ca-rich aluminosilicate hydrate (CASH) mineral formation was observed at 200°C, including analcime, tobermorite, and garronite, which made up ~15–17 wt.% of the reaction products. The implication is that interaction with cement leads to the formation of high-Si phases and partial smectite destruction under alkaline conditions. Although zeolites and CASH minerals may have lower volume percentages than smectite in the bentonite portion, the zeolite radionuclide sorption coefficients are orders of magnitude higher than smectite (Bish et al. 1984). Further research needs to be completed on radionuclide sorption factors of zeolites and CASH minerals, as these minerals may control radionuclide retardation in the EBS system.

The buffer-host rock interaction will be different for different host rocks. The buffer-host rock interaction needs to have better modeling predictability for the migration of radionuclides. The thermodynamic evaluation of this system needs to continue to reconcile experimental observations with equilibria between minerals and the aqueous phase (Jové Colón et al. 2019).

This page intentionally left blank



## 9. SUMMARY AND CONCLUSIONS

Disposal of large, heat-generating waste packages containing the equivalent of 21 PWR assemblies or more is among the disposal concepts under investigation for a future repository for SNF in the United States. Without a long (>200 years) surface storage period, disposal of 21-PWR or larger waste packages (especially if they contain high-burnup fuel) would result in in-drift and near-field temperatures considerably higher than considered in previous generic reference cases that assume either 4-PWR or 12-PWR waste packages (Jové Colón et al. 2014; Mariner et al. 2015; 2017). Sevougian et al. (2019c) identified high-temperature process understanding as a key research and development (R&D) area for the Spent Fuel and Waste Science and Technology (SFWST) Campaign.

A two-day workshop in February 2020 brought together campaign scientists with expertise in geology, geochemistry, geomechanics, engineered barriers, waste forms, and corrosion processes to begin integrated development of a high-temperature reference case for disposal of SNF in a mined repository in a shale host rock. Building on the progress made in the workshop, the study team further explored the concepts and processes needed to form the basis for a high-temperature shale repository reference case. The results are described in this report and summarized below.

**Geologic Setting of Major Shale Deposits (Section 2)**—Two shale endmembers, ductile and brittle, are proposed for future high-temperature shale reference cases. The characteristics of ductile and brittle shales are described and placed in the context of United States sedimentary basins. Whether a shale is ductile or brittle is determined by its original depositional environment and resulting clay content, as well as the maximum depth of burial experienced and resulting degree of induration. The two endmembers differ in mechanical behavior, porewater chemistry, and thermal and hydrologic properties.

**Natural Barrier System (Section 3)**—The ductile shale endmember is characterized by a high clay mineral content, low mechanical strength, low thermal conductivity, and very low permeability within intact blocks of rock (over a scale of several hundred meters). The brittle shale endmember is characterized by a higher proportion of strong grains such as quartz, higher mechanical strength, somewhat higher thermal conductivity, and potentially higher bulk permeability due to the presence of interconnected fractures. The ductile shale endmember has experienced shallower burial depths than the brittle endmember, is less indurated, and has relatively dilute porewater, while the brittle shale endmember has experienced deeper burial depths, is more indurated, and has saline porewater.

**Repository Design and Construction (Section 4)**—Repository depths between 300 and 900 m have been proposed for shale host rock (Shurr 1977); a nominal depth of 500 m is assumed, with the repository situated in a flat-lying stratigraphy and built on a single level.

The repository would be constructed in stages, with access drifts intended to remain open for the lifetime of the repository (approximately 100 years) and disposal drifts intended to remain open for less than about 3 years. Immediate support during or after excavation is necessary in shales to control rock deformation and rockfall hazards. The reference concept assumes a minimal support system consisting of rock bolts, which retain welded wire cloth, covered by a layer of low pH shotcrete (10–30 cm thick). Ground support in temporary openings would be limited to shorter rock bolts and thinner shotcrete, while permanent openings may require multiple applications of shotcrete and steel sets (or other heavy lining) to stabilize against large deformations.

The reference concept assumes axial, in-drift emplacement of waste packages containing 21 PWR assemblies or 44 BWR assemblies. Waste emplacement drifts would be backfilled with crushed rock and/or bentonite buffer to provide shielding during the operational phase and to prevent rock fall.

Large waste packages pose a challenge for thermal management in a shale repository. Repository temperature limits may be based on various temperature constraints designed to ensure material integrity of the fuel cladding, waste package materials, a clay-based buffer, and/or the host rock itself. Waste package and drift spacings are selected to be reasonably large (20 m and 70 m, respectively), and waste

packages are assumed to be loaded and aged (through surface storage) such that the power output at the time of emplacement is less than about 4 kW/waste package. Such a strategy meets potential temperature limits of 250°C at the waste package surface and 100°C at the drift wall or a short distance into the wall rock. The strategy (depending on the engineered thermal properties of the backfill) includes a zone of “sacrificial” backfill surrounding each waste package for which maintenance of favorable mechanical, chemical, and hydrological properties of the backfill/buffer cannot be assumed without site-specific study.

**Disturbed Rock Zone (Section 5)**—The mechanical properties of shale, whether more ductile or brittle, impact the coupled thermal-hydrological-mechanical evolution of the host rock, including the potential for mechanical damage and associated changes in transport properties. In the host rock immediately adjacent to drift walls, both excavation-induced fracturing and thermal spalling are expected. A ductile shale is expected to experience creep (visco-plastic) deformation around excavations and to self-seal fractures on relatively short time scales, while a brittle shale may sustain durable damage. In a high-temperature repository, thermally induced mechanical damage to the host rock may extend beyond the immediate environment of the drift wall if thermal pressurization of porewater is sufficient to cause hydraulic fracturing or activation of pre-existing natural fractures in the host rock. The potential for near-field hydraulic fracturing depends on coupled feedback between permeability, thermal conductivity, and mechanical strength of the host rock.

**Engineered Barrier System (Section 6)**—Two options are proposed for in-drift emplacement of waste packages: (1) waste packages are emplaced on the floor of the drift and (2) waste packages are emplaced on a plinth of compacted bentonite. The first option is operationally simpler, and may be suitable in a self-sealing, low-permeability host rock. The second option presents additional engineering and design challenges, but may be desirable if flow in connected fractures cannot be ruled out.

Several backfill/buffer emplacement concepts are proposed for further study for a high-temperature shale repository. The first concept is for crushed rock backfill to be emplaced in the high-temperature zone around each waste package and compacted bentonite buffer or an admixture of crushed rock and bentonite pellets to be emplaced in the disposal drifts between waste packages. In the second concept, compacted bentonite buffer is emplaced throughout the disposal drifts. For the latter, the high heat load of the waste packages may be managed by (1) enhancing the thermal conductivity of the buffer with additives such as quartz sand, graphite, graphene, or copper wire mesh; or (2) determining for a given set of conditions (including clay mineralogy and porewater composition) that a higher temperature limit is acceptable in the bentonite buffer. Additional research is needed to characterize some of these materials.

The potential reference waste packages are comprised of a stainless steel canister that may serve multiple purposes including transportation, aging, and disposal; canister internals supporting the fuel assemblies and providing criticality control; and a disposal overpack. Carbon steel, stainless steel, and copper are possible overpack materials that have been studied in a variety of repository programs (e.g., Andra 2005; SKB 2010).

The waste form is spent uranium oxide (UO<sub>2</sub>) fuel, a polycrystalline ceramic material stable to high temperatures and likely slow to degrade in the disposal environment (Shoosmith 2007). In spent oxide fuels, the radionuclide inventory is usually considered to consist of two parts: (1) a part that resides in the fuel rod gap and grain-boundary region and (2) a part that is embedded in the fuel matrix and released only upon degradation of the fuel matrix.

Nominal and bounding initial radionuclide inventories and waste package power outputs as functions of time are constructed using assembly and fuel characteristics from the Unified Database.

**Corrosion Behavior of Candidate Waste Package Materials (Section 7)**—Corrosion mechanisms of Fe-based alloys and Cu-based materials are discussed. In the reducing porewater environment of a shale repository, carbon steel would experience general corrosion via reaction with water; copper would experience general corrosion if reduced sulfur species are present; and stainless steel is likely to form a

passive, stable oxide film on the surface that slows general corrosion and leads to localized (less predictable) pitting or crevice corrosion. Corrosion rates and stability of passivation films depend on environmental factors, including concentrations of chemical species, temperature, pH, and radiation flux. Structural damage to waste packages may occur due to extensive general corrosion, stress corrosion cracking, or hydride embrittlement.

**Chemical Changes at Interfacial Areas (Section 8)**—Steel corrosion, cement degradation, and host rock/bentonite interactions have the potential to cause wide-ranging effects on the physical and chemical properties of the bentonite buffer where it contacts other materials (e.g., Caporuscio et al. 2019). Changes to physical properties may include dissolution/recrystallization of montmorillonite, loss of bentonite swelling capacity (due to cementation or recrystallization to nonswelling phases), and development of porosity due to the formation denser mineral phases (e.g., zeolites). Such changes depend on bulk system chemistry and temperature.

**Summary of High-Temperature Effects**—High temperatures in the near field of a shale repository may drive hydrological, mechanical, and chemical changes. Three avenues of future R&D are apparent from the concepts proposed in this report: characterization of materials engineered for thermal management (e.g., buffer materials), development of conceptual models, and investigation of the temperature dependence of coupled processes.

This is the first time that SFWST generic disposal research has made a clear distinction between more ductile and more brittle shales. Each may require a different approach to defense in depth with a different degree of reliance on, for instance, corrosion resistance of the waste package or ability of the buffer/backfill to retard radionuclide transport. Depending on the characteristics of the natural and engineered systems, different processes may play a greater or lesser role, including, for instance, (1) creep deformation, rockfall, or hydrofracturing of the host rock; (2) illitization, porewater chemistry changes, or precipitation of secondary phases in the buffer; and (3) general corrosion, local corrosion, or mechanical damage due to corrosion processes in the overpack.

Conceptual models for some of these processes will include a temperature dependence. This report identifies the potential for (1) development of thermal overpressures and possibility of hydrofracturing in the near field; (2) influence on drift closure processes such as an accelerated rate of creep or thermal spalling; (3) depending on the geochemical environment, enhanced chemical alteration of the bentonite buffer resulting in alteration of swelling capacity or other bentonite properties; (4) faster corrosion rates; and (5) temperature-dependent diffusion, radionuclide solubilities, and sorption. Further evaluation of these and other temperature-dependent coupled processes will enable preliminary material choices and contribute to development of a reference case for a high-temperature repository in shale.

This page intentionally left blank

## 10. REFERENCES

- Abel, J.F. and D.W. Gentry. 1975. *Evaluation of Excavation Experience: Pierre Shale*. ORNL/SUB-75/70347. Oak Ridge, TN: Oak Ridge National Laboratory.
- Adams, B. M., W. J. Bohnhoff, K. R. Dalbey, M. S. Ebeida, J. P. Eddy, M. S. Eldred, R. W. Hooper, P. D. Hough, K. T. Hu, J. D. Jakeman, M. Khalil, K. A. Maupin, J. A. Monschke, E. M. Ridgway, A. A. Rushdi, D. T. Seidl, J. A. Stephens, L. P. Swiler, and J. G. Winokur. 2020. *Dakota, A Multilevel Parallel Object-Oriented Framework for Design Optimization, Parameter Estimation, Uncertainty Quantification, and Sensitivity Analysis: Version 6.12 User's Manual*. SAND2020-5001. Albuquerque, NM: Sandia National Laboratories.
- Andra (Agence nationale pour la gestion des déchets radioactifs [National Radioactive Waste Management Agency]). 2005. *Dossier 2005 Argile. Tome: Architecture and Management of a Geological Disposal System*. Châtenay-Malabry, France: Andra.
- Andra. 2015. *Safety Options Report - Post-Closure Part (DOS-AF)*. CG-TE-D-NTE-AMOA-SR2-0000-15-0062. Châtenay-Malabry, France: Andra.
- Andra. History. In English website. <https://international.andra.fr/about-andra/history>.
- Apotria, T.G., C.J. Kaiser, and B.A. Cain. 1994. Fracturing and stress history of the Devonian Antrim Shale, Michigan Basin. In *Rock Mechanics*, eds. P.P. Nelson and S.E. Lauback, pp. 809–816. Balkema, Rotterdam.
- AREVA Federal Services LLC. 2013. Task Order 12—Standardized Transportation, Aging, and Disposal Canister Feasibility Study. Prepared for the U.S. Department of Energy under contract no. A&AS DE-NE-0000291. RPT-3008097-000.
- Asphahani, A. 1981. Evaluation of highly alloyed stainless materials for CO<sub>2</sub>/H<sub>2</sub>S environments. *Corrosion* 37 (6): 327–335.
- ASTM A887-20. 2020. *Standard Specification for Borated Stainless Steel Plate, Sheet, and Strip for Nuclear Application*. West Conshohocken, PA: ASTM International. [www.astm.org](http://www.astm.org). doi: 10.1520/A0887-20.
- Baeyens, B., T. Thoenen, M.H. Bradbury, and M. Marques Fernandes. 2014. *Sorption Data Bases for Argillaceous Rocks and Bentonite for the Provisional Safety Analyses for SGT-E2*. TR 12-04. Wettingen, Switzerland: National Cooperative for the Disposal of Radioactive Waste (Nagra).
- Banerjee, K., K.R. Robb, G. Radulescu, P.L. Miller, J.M. Scaglione, J.M. Cuta, and H. Liljenfeldt. 2016. “UNF-ST&DARDS: A Unique Tool for Automated Characterization of Spent Nuclear Fuel and Related Systems.” *PATRAM 2016*, Japan Society of Mechanical Engineers and Atomic Energy Society of Japan, Kobe, Japan (September 2016).
- Bauer, J., C. Rowan, A. Barkhurst, J. Digiulio, K. Jones, M. Sabbatino, K. Rose, and P. Wingo. 2018. NATCARB. National Energy Technology Laboratory-Energy Data eXchange; NETL, United States. doi:10.18141/1474110.
- Belonoshko, A.B. and A. Rosengren. 2010. Ab initio study of water interaction with a Cu surface. *Langmuir* 26 (21): 16267–16270.
- Berner, U. 2014a. *Solubility of Radionuclides in a Bentonite Environment for Provisional Safety Analyses for SGT-E2*. Nagra Technical Report 14-06. Wettingen, Switzerland: National Cooperative for the Disposal of Radioactive Waste (Nagra).

- Berner, U. 2014b. *Solubility of Radionuclides in a Concrete Environment for Provisional Safety Analyses for SGT-E2*. Nagra Technical Report 14-07. Wetingen, Switzerland: National Cooperative for the Disposal of Radioactive Waste (Nagra).
- Bernier, F., X.L. Li, W. Bastiaens, L. Ortiz, M. Van Geet, L. Wouters, B. Frieg, P. Blümling, J. Desrues, G. Viaggiani, C. Coll, S. Chanchole, V. De Greef, R. Hamza, L. Malinsky, A. Vervoort, Y. Vanbrabant, B. Debecker, J. Verstraelen, A. Govaerts, M. Wevers, V. Labiouse, S. Escoffier, J.-F. Mathier, L. Gastaldo, and Ch. Bühler. 2007. *Fractures and self-healing within the excavation disturbed zone in clays (SELFRAC)*, SELFRAC Project Final Report. EUR 22585. European Commission.
- Bish, D.L., D.T. Vaniman, R.S. Rundberg, K. Wolfsberg, W.R. Daniels, and E. Broxton. 1984. Natural Sorptive Barriers in Yucca Mountain, Nevada, for Long Term Isolation of High Level Waste. *Radioactive Waste Management* 3:415–432.
- Blink, J., J. Farmer, J. Choi, and C. Saw. 2009. Applications in the nuclear industry for thermal spray amorphous metal and ceramic coatings. *Metallurgical and Materials Transactions* 40A (June):1344–1354.
- Blondes, M.S., K.D. Gans, M.A. Engle, Y.K. Kharaka, M.E. Reidy, V. Saraswathula, J.J. Thordsen, E.L. Rowan, and E.A. Morrissey. 2018. U.S. Geological Survey National Produced Waters Geochemical Database (ver. 2.3, January 2018), U.S. Geological Survey data release. Reston, VA: United States Geological Survey. <https://doi.org/10.5066/F7J964W8>.
- Blümling, P., F. Bernier, P. Lebon, and C.D. Martin. 2007. The excavation damaged zone in clay formations time-dependent behavior and influence on performance assessment. *Phys Chem Earth* 32:588–599.
- Bock, H., B. Dehandschutter, C.D. Martin, M. Mazurek, A. de Haller, F. Skoczylas, and C. Davy. 2010. *Self-sealing of fractures in argillaceous formations in context with the geological disposal of radioactive waste*. OECD/NEA report 6184. Paris, France: OECD Nuclear Energy Agency.
- Börgesson, L., O. Karnland, L.E. Johannesson, and D. Gunnarsson. 2006. Current Status of SKB's Research, Development and Demonstration Programme on Buffer, Backfill and Seals. SKB IC-122. Stockholm, Sweden: Svensk Kärnbränslehantering AB (SKB).
- Börgesson, L. and J. Hernelind. 2006. *Canister displacement in KBS-3V: A theoretical study*. TR-06-04. Stockholm, Sweden: Svensk Kärnbränslehantering AB (SKB).
- Bourdelle, F., L. Truche, I. Pignatelli, R. Mosser-Ruck, C. Lorgeoux, C. Roszypal, and N. Michau. 2014. Iron–clay interactions under hydrothermal conditions: Impact of specific surface area of metallic iron on reaction pathway. *Chemical Geology* 381:194–205. <https://doi.org/10.1016/j.chemgeo.2014.05.013>.
- Bourdelle, F., R. Mosser-Ruck, L. Truche, C. Lorgeoux, I. Pignatelli, and N. Michau. 2017. A new view on iron-claystone interactions under hydrothermal conditions (90° C) by monitoring in situ pH evolution and H<sub>2</sub> generation. *Chemical Geology* 466:600–607. <https://doi.org/10.1016/j.chemgeo.2017.07.009>.
- Bourg, I.C. 2015. Sealing Shales versus Brittle Shales: A Sharp Threshold in the Material Properties and Energy Technology Uses of Fine-Grained Sedimentary Rocks. *Environmental Science & Technology Letters* 2 (10): 255–259.
- Bradbury, M.H., and B. Baeyens. 2011. Predictive sorption modelling of Ni(II), Co(II), Eu(III), Th(IV) and U(VI) on MX-80 bentonite and Opalinus Clay: A “bottom-up” approach. *Applied Clay Science* 52 (1–2): 27–33. doi: 10.1016/j.clay.2011.01.022.
- Bradbury, M.H. and B. Baeyens. 2002. *Porewater chemistry in compacted re-saturated MX-80 bentonite: physico-chemical characterisation and geochemical modelling*. PSI Bericht 02–10; NTB 01–08. Wetingen, Switzerland: National Cooperative for the Disposal of Radioactive Wastes (Nagra).



- Brantley, S.L., M.E. Holleran, L. Jin, and E. Bazilevskaya. 2013. Probing deep weathering in the Shale Hills Critical Zone Observatory, Pennsylvania (USA): the hypothesis of nested chemical reaction fronts in the subsurface. *Earth Surface Processes and Landforms* 38:1280–1298.
- Bredehoeft, J.D., C.E. Neuzil, and P.C.D. Milly. 1983. *Regional Flow in the Dakota Aquifer: A Study of the Role of Confining Layers*. Water-Supply Paper 2237. Alexandria, VA: United States Geological Survey.
- Bryan, C.R., D.G. Enos, N. Brown, L. Brush, A. Miller, and K. Norman. 2011. *Engineered Materials Performance: Gap Analysis and Status of Existing Work*. FCRD-USED-2011-000407. Albuquerque, NM: Sandia National Laboratories.
- BSC (Bechtel-SAIC Co.). 2005. *Cladding Degradation Summary for LA*. ANL-WIS-MD-000021 REV 03. Las Vegas, NV: Bechtel SAIC Company.
- BSC. 2008. *Transport and Emplacement Vehicle Envelope Calculation*. 800-MQC-HE00-00100-000-00C. Las Vegas, NV: Bechtel SAIC Company.
- BSC. 2004. *CSNF Waste Form Degradation: Summary Abstraction*. ANL-EBS-MD-000015 REV 02. Las Vegas, NV: Bechtel SAIC Company.
- Buck, E., J. Jerden, E. Ebert, and R. Wittman. 2013. *Coupling the Mixed Potential and Radiolysis Models for Used Fuel Degradation*. FCRD-UFD-2013-000290; PNNL-22701. Richland, WA: Pacific Northwest National Laboratory.
- Budai, J., A. Martini, L. Walter, and T. Ku. 2002. Fracture-fill calcite as a record of microbial methanogenesis and fluid migration: a case study from the Devonian Antrim Shale. *Michigan Basin Geofluids* 2:163–183.
- Caporuscio, F.A., S. Palaich, M.C. Cheshire, and C.F. Jové Colón. 2017. Corrosion of copper and authigenic sulfide mineral growth in hydrothermal bentonite experiments. *Journal of Nuclear Materials* 485:137–146. doi: 10.1016/j.jnucmat.2016.12.036.
- Caporuscio, F.A., K.B. Sauer, and M.J. Rock. 2019. *Argillite Disposal R&D - LANL FY19*. LA-UR-19-24222. Los Alamos, NM: Los Alamos National Laboratory.
- Chapman, E.C., R.C. Capo, B.W. Stewart, C.S. Kirby, R.W. Hammack, K.T. Schroeder, and H.M. Edenborn. 2012. Geochemical and Strontium Isotope Characterization of Produced Waters from Marcellus Shale Natural Gas Extraction. *Environ Sci Technol* 46:3545–3553.
- Charpentiera, D., K. Devineau, R. Mosser-Ruck, M. Cathelineau, and F. Villiéras. 2006. Bentonite–iron interactions under alkaline condition: An experimental approach. *Applied Clay Science* 32 (1–2): 1–13. <https://doi.org/10.1016/j.clay.2006.01.006>.
- Chatterjee, U. and R.S. Raman. 2011. Stress corrosion cracking (SCC) in low and medium strength carbon steels. In Part III, Chapter 4 of *Stress Corrosion Cracking—Theory and Practice*, eds. V.S. Raja and T. Shoji, 169–198. Woodhead Publishing Series in Metals and Surface Engineering. Woodland Publishing. <https://doi.org/10.1533/9780857093769.3.169>
- Chen, L., G. Duveau, A. Poutrel, Y. Jia, J.F. Shao, and N. Xie. 2014. Numerical study of the interaction between adjacent galleries in a high-level radioactive waste repository. *International Journal of Rock Mechanics and Mining Sciences* 71:405–417. doi: 10.1016/j.ijrmms.2014.07.012.
- Cheshire, M.C., F.A. Caporuscio, C.F. Jové Colón, and K.E. Norskog. 2018. Fe-saponite growth on low-carbon and stainless steel in hydrothermal-bentonite experiments. *Journal of Nuclear Materials* 511:353–366.

- Choi, H.J. and J. Choi. 2008. Double-layered buffer to enhance the thermal performance in a high-level radioactive waste disposal system. *Nuclear Engineering and Design* 238 (10): 2815–2820. doi: 10.1016/j.nucengdes.2008.04.017.
- Clarity, J.B., K. Banerjee, H.K. Liljenfeldt, and W.J. Marshall. 2017. As-Loaded Criticality Margin Assessment of Dual-Purpose Canisters Using UNF-ST&DARDS. *Nuclear Technology* 199 (3): 245–275.
- Clauser, C. and E. Huenges. 1995. Thermal Conductivity of Rocks and Minerals. In *Rock Physics & Phase Relations: A Handbook of Physical Constants*, ed. T.J. Ahrens, 105–126. Washington, D.C.: American Geophysical Union.
- Clayton, D., G.A. Freeze, T. Hadgu, E.L. Hardin, J.Y. Lee, J.L. Prouty, R.D. Rogers, W.M. Nutt, J. Birkholzer, H.H. Liu, L. Zheng, and S. Chu. 2011. Generic Disposal System Modeling - Fiscal Year 2011 Progress Report. FCRD-USED-2011-000184; SAND2011-5828P. Albuquerque, NM: Sandia National Laboratories.
- Crandell, D.R. 1958. Geology of the Pierre Area South Dakota. Geological Survey Professional Paper 307.
- CRWMS M&O (Civilian Radioactive Waste Management System Management and Operating Contractor). 1996. *Thermal Evaluation of the Conceptual 12 PWR Uncanistered Fuel Tube Basket Disposal Canister*. BBAA00000-01717-0200-0004. Las Vegas, NV: Civilian Radioactive Waste Management System Management and Operating Contractor.
- Davies, D. and G. Burstein. 1980. The effects of bicarbonate on the corrosion and passivation of iron. *Corrosion* 36 (8): 416–422.
- de Pablo, J., I. Casas, J. Gimenez, F. Clarens, E. Gonzalez-Robles, D. Serrano-Purroy, J.P. Glatz, D. Wegen, B. Christiansen, A. Martinez-Esparza. 2008. Contribution to Leaching Studies of High-Burnup Spent Nuclear Fuel. Presented at International High-Level Radioactive Waste Management 2008 (IHLRWM 2008), Las Vegas, NV, Sept 7–11.
- DOE (U.S. Department of Energy). 2008. *Yucca Mountain Repository License Application for Construction Authorization*. DOE/RW-0573, Rev. 1. Washington, D.C.: U.S. Department of Energy.
- DOE. 2012. *Used Fuel Disposition Campaign Disposal Research and Development Roadmap*. FCR&D-USED-2011-000065, REV 1. Washington, D.C.: U.S. Department of Energy.
- Dole, L., C. Mattus, M. Fayek, L.M. Anovitz, J.J. Ferrada, D.J. Wesolowski, D. Olander, D.A. Palmer, L.R. Riciputi, L. Delmau, S. Ermichev, V.I. Shapovalov. 2004. *Cost-Effective Cementitious Material Compatible with Yucca Mountain Repository Geochemistry*. ORNL/TM-2004/296. Oak Ridge, TN: Oak Ridge National Laboratory.
- Droste, J.B. and C.J. Vitaliano. 1976. *Geologic Report of the Maquoketa Shale, New Albany Shale, and Borden Group Rocks in the Illinois Basin as Potential Solid Waste Repository Sites*. Y/OWI/SUB--7062/1. Oak Ridge, TN: Oak Ridge National Laboratory.
- Ebrel, D.D., G. Whitney, and H. Khoury. 1978. Hydrothermal reactivity of smectite. *American Mineralogist* 63 (3–4): 401–409.
- EIG EURIDICE. 2020. **2019 Activity Report**, ed. P. De Preter. Doc. 20-101. Mol, Belgium: EIG EURIDICE.
- Ellis, B. 2013. *Hydraulic Fracturing in the State of Michigan - Geology Technical Report*. Graham Sustainability Institute Integrated Assessment Report Series Volume II, Report 3. University of Michigan.
- Engle, M.A., F.R. Reyes, M.S. Varonka, W.H. Orem, L. Ma, A.J. Ianno, T.M. Schell, P. Xu, and K.C. Carroll. 2016. Geochemistry of formation waters from the Wolfcamp and “Cline” shales: Insights

into brine origin, reservoir connectivity, and fluid flow in the Permian Basin, USA. *Chem Geol* 425:76–92.

ENRESA. 2000. *Full-scale engineered barriers experiment for a deep geological repository in crystalline host rock (FEBEX Project)*. European Commission.

EPRI (Electric Power Research Institute) 2019. *High Burnup Dry Storage Research Project Cask Loading and Initial Results*. Report 3002015076. Palo Alto, CA: Electric Power Research Institute.

Fairhurst, C. 2012. *Current Approaches to Surface-Underground Transfer of High-Level Nuclear Waste*. Minneapolis, MN: Itasca Consulting Group.

Fernández, A. M., B. Baeyens, M. Bradbury and P. Rivas. 2004. Analysis of the porewater chemical composition of a Spanish compacted bentonite used in an engineered barrier. *Physics and Chemistry of the Earth, Parts A/B/C* 29 (1): 105–118.

Fernández, A., J. Cuevas, P. Rivas. 2001. Pore water chemistry of the FEBEX bentonite. *Mat. Res. Soc. Symp. Proc.* 663:573–588.

Féron, D., D. Crusset, and J.M. Gras. 2009. Corrosion issues in the French high-level nuclear waste program. *Corrosion* 65 (3): 213–223. doi: 10.5006/1.3319129.

Fluor (Fluor Technology Inc.). 1987. *Site Characterization Plan Conceptual Design Report for a High-Level Nuclear Waste Repository in Salt, Vertical Emplacement Mode (Volume 1)*. DOE/CH/46656-15(1). Prepared for the U.S. Department of Energy, Office of Civilian Radioactive Waste Management, Salt Repository Project Office.

Förster, A., and D.F. Merriam. 1997. Heat flow in the Cretaceous of northwestern Kansas and implications for regional hydrology. *Current Research in Earth Sciences* 240:1–11.

Frape, S.K., A. Blyth, R. Blomqvist, R. McNutt, and M. Gascoyne. 2003. Deep Fluids in the Continents: II. Crystalline Rocks. In *Treatise on Geochemistry*, Volume 5, 541–580. Elsevier. doi: 10.1016/B0-08-043751-6/05086-6.

Freeze, G., M. Voegelé, P. Vaughn, J. Prouty, W.M. Nutt, E. Hardin, and S.D. Sevougian. 2013. *Generic Deep Geologic Disposal Safety Case*. FCRD-UFD-2012-000146 Rev. 1; SAND2013-0974P. Albuquerque, NM: Sandia National Laboratories.

Gale, J.F.W., S.E. Laubach, J.E. Olson, P. Eichhubl, and A. Fall. 2014. Natural fractures in shale: a review and new observations. *AAPG Bulletin* 98 (11): 2165–2216.

Gdowski, G.E., and D.B. Bullen. 1988. *Oxidation and Corrosion*, Volume 2. UCID-21362.

Gilliam, T.M., and I.L. Morgan. 1987. *Shale: Measurement of Thermal Properties*. ORNL/TM-10499. Oak Ridge, TN: Oak Ridge National Laboratory.

Gonzales, S. and K.S. Johnson. 1985. *Shale and other argillaceous strata in the United States*. ORNL Report 84-64794. Oak Ridge, TN: Oak Ridge National Laboratory.

Grauer, R., B. Knecht, P. Kreis, and J. Simpson. 1990. Hydrogen Evolution from Corrosion of Iron and Steel in Intermediate Level Waste Repositories. *MRS Proceedings* 212: 295. doi:10.1557/PROC-212-295.

Graupner, B.J., H. Shao, X.R. Wang, T.S. Nguyen, Z. Li, J. Rutqvist, F. Chen, J. Birkholzer, W. Wang, O. Kolditz, P.Z. Pan, X.T. Feng, C. Lee, K. Maekawa, S. Stothoff, C. Manepally, B. Dasgupta, G. Ofoegbu, R. Fedors, J.D. Barnichon, E. Ballarini, S. Bauer, and B. Garitte. 2018. Comparative modelling of the coupled thermal-hydraulic-mechanical (THM) processes in a heated bentonite pellet column with hydration. *Environmental Earth Sciences* 77 (3). doi: 10.1007/s12665-018-7255-3.

Graver, D.L. 1984. Hydrogen permeation and embrittlement of some nickel alloys. *Corrosion of Nickel-Based Alloys*, 79–85. Metals Park, OH: American Society for Metals.

- Greene, S., J. Medford, and S. Macy. 2013. *Storage and Transport Cask Data for Used Commercial Nuclear Fuel*. Technical Report No. ATI-TR-13047. Oak Ridge, TN: Advanced Technology Insights LLC.
- Grimsel Test Site [Switzerland]. 2020. “High Temperature Effects on Bentonite Buffers (HotBENT) – Introduction.” Grimsel Test Site Underground Research and Development URL. <https://www.grimsel.com/gts-phase-vi/hotbent-high-temperature-effects-on-bentonite-buffers/hotbent-introduction>.
- Gross, M.R. 1995. Fracture partitioning: Failure mode as a function of lithology in the Monterey Formation of coastal California. *Geological Society of America Bulletin* 107 (7): 779–792.
- Guillaume, D., A. Neaman, M. Cathelineau, and R. Mosser. 2003. Experimental synthesis of chlorite from smectite at 300 C in the presence of metallic Fe. *Clay Minerals* 38 (3): 281–302. doi: 10.1180/0009855033830096.
- Guillaume, D., A. Neaman, M. Cathelineau, R. Mosser-Ruck, C. Peiffert, M. Abdelmoula, J. Dubessy, F. Villieras, and N. Michau. 2004. Experimental study of the transformation of smectite at 80 and 300°C in the presence of Fe oxides. *Clay Minerals* 39 (1): 17–34. doi: 10.1180/000985543910117.
- Güven, N. 1990. Longevity of bentonite as buffer material in a nuclear-waste repository. *Engineering Geology* 28 (3–4): 233–247.
- Hadi, J., P. Wersin, V. Serneels, and J.-M. Greneche. 2019. Eighteen years of steel–bentonite interaction in the FEBEX in situ test at the Grimsel Test Site in Switzerland. *Clays and Clay Minerals* 67 (2): 111–131. doi: <https://doi.org/10.1007/s42860-019-00012-5>.
- Hama, K., T. Kunimaru, R. Metcalfe, A.J. Martin. 2007. The Hydrogeochemistry of Argillaceous Rock Formations at the Horonobe URL Site, Japan. *Physics and Chemistry of the Earth* 32:170–180.
- Hammond, G.E., P.C. Lichtner, and R.T. Mills. 2014. Evaluating the Performance of Parallel Subsurface Simulators: An Illustrative Example with PFLOTRAN. *Water Resources Research* 50. doi:10.1002/2012WR013483.
- Hanamuro, T. (ed.) 2016. *Horonobe Underground Research Laboratory project. Investigation program for the 2016 fiscal year*. Horonobe Underground Research Center, Horonobe, Hokkaido (Japan). Tokai, Ibaraki (Japan): Japan Atomic Energy Agency, Sector of Decommissioning and Radioactive Waste Management.
- Hansen, F.D., E.L. Hardin, R.P. Rechard, G.A. Freeze, D.C. Sassani, P.V. Brady, M. Stone, M.J. Martinez, J.F. Holland, T. Dewers, K.N. Gaither, S.R. Sobolik, and R.T. Cygan. 2010. *Shale Disposal of U.S. High-Level Radioactive Waste*. SAND2010-2843. Albuquerque, NM: Sandia National Laboratories.
- Hanson, B., H. Alsaed, C. Stockman, D. Enos, R. Meyer, and K. Sorenson. 2012. *Gap Analysis to Support Extended Storage of Used Nuclear Fuel*. FCRD-USED-2011-000136 Rev. 0; PNNL-20509. Richland, WA: Pacific Northwest National Laboratory.
- Hanson, B.D., and H.A. Alsaed. 2019. *Gap Analysis to Support Extended Storage of Used Nuclear Fuel: Five-Year Delta*. SFWD-SFWST-2017-00005, Rev. 1; PNNL-28711. Richland, WA: Pacific Northwest National Laboratory.
- Hardin et al. 2019. *DPC Criticality Simulation Preliminary Phase: Fuel/Basket Degradation Models*. M3SF-19SN010305071. Albuquerque, NM: Sandia National Laboratories.
- Hardin, E. 2014. *Review of Underground Construction Methods and Opening Stability for Repositories in Clay/Shale Media*. FCRD-UFD-2014-000330 Rev. 0; SAND2014-4745P. U.S. Department of Energy, Office of Used Nuclear Fuel Disposition.

- Hardin, E. and E. Kalinina. 2015. *Cost Estimation Inputs for Spent Nuclear Fuel Geologic Disposal Concepts*. SAND2015-0687. Albuquerque, NM: Sandia National Laboratories.
- Hardin, E. and E. Kalinina. 2016. *Cost Estimation Inputs for Spent Nuclear Fuel Geologic Disposal Concepts (Revision 1)*. SAND2016-0235. Albuquerque, NM: Sandia National Laboratories.
- Hardin, E. et al. 2011. *Generic Repository Design Concepts and Thermal Analysis (FY11)*. FCRD-USED-2011-000143 Rev. 2. Albuquerque, NM: Sandia National Laboratories.
- Hardin, E., T. Hadgu, D. Clayton, R. Howard, H. Greenberg, J. Blink, M. Sharma, M. Sutton, J. Carter, M. Dupont, and P. Rodwell. 2012a. *Repository Reference Disposal Concepts and Thermal Management Analysis*. FCRD-USED-2012-000219 Rev. 2. U.S. Department of Energy, Office of Used Nuclear Fuel Disposition.
- Hardin, E., T. Hadgu, H. Greenberg, and M. Dupont. 2012b. *Parameter Uncertainty for Repository Thermal Analysis*. FCRD-UFD-2012-000097. Used Fuel Disposition Campaign, U.S. Department of Energy.
- Hardin, E.L., D.J. Clayton, M.J. Martinez, G. Neider-Westermann, R.L. Howard, H.R. Greenberg, J.A. Blink, and T.A. Buscheck. 2013. *Collaborative Report on Disposal Concepts*. FCRD-UFD-2013-000170 Rev. 0. Used Fuel Disposition Campaign, U.S. Department of Energy.
- Hardin, E.L., L. Price, E. Kalinina, T. Hadgu, A. Ilgen, C. Bryan, J. Scaglione, K. Banerjee, J. Clarity, R. Jubin, V. Sobes, R. Howard, J. Carter, T. Severynse, and F. Perry. 2015. *Summary of Investigations on Technical Feasibility of Direct Disposal of Dual-Purpose Canisters*. FCRD-UFD-2015-000129 Rev 0. U.S. Department of Energy Office of Used Nuclear Fuel Disposition.
- He, X., T. Ahn, and T. Sippel. 2012. Corrosion of Borated Stainless Steel in Water and Humid Air. Presented at NACE 2012, Salt Lake City Utah, March 11–15, 2012.
- Horseman, S.T., and T.J. McEwen. 1996. Thermal constraints on disposal of heat-emitting waste in argillaceous rocks. *Engineering Geology* 41:5–16.
- Hu, J., and G. Ilas. 2018. *Tutorial: Using ORIGAMI for Detailed Spent Fuel Assembly Analysis in Safeguards Applications*. Paper presented at the SCALE Users' Group Workshop, Oak Ridge National Laboratory.
- Hultquist, G. 1986. Hydrogen evolution in corrosion of copper in pure water. *Corrosion Science* 26 (2): 173–177.
- Hultquist, G., P. Szakálos, M.J. Graham, G.I. Sproule, and G. Wikmark. 2008. Detection of hydrogen in corrosion of copper in pure water. Paper 3884. Presented at 17th International Corrosion Congress 2008: Corrosion Control in the Service of Society.
- Hultquist, G., P. Szakálos, M.J. Graham, A. Belonoshko, G. Sproule, L. Gråsjö, P. Dorogokupets, B. Danilov, T. Aastrup, G. Wikmark, G.-K. Chuah, J.-C. Eriksson, and A. Rosengren. 2009. Water Corrodes Copper. *Catalysis Letters*. 132 (3–4): 311–316. 10.1007/s10562-009-0113-x.
- Hultquist, G., P. Szakálos, M. Graham, A. Belonoshko, and A. Rosengren. 2010. Reply to Lars O. Werme et al.: “Comments on ‘Water Corrodes Copper’”. *Catalysis Letters*. 135 (3–4): 167–168. 10.1007/s10562-010-0310-7.
- Hultquist, G., M.J. Graham, P. Szakálos, G.I. Sproule, A. Rosengren, and L. Gråsjö. 2011. Hydrogen gas production during corrosion of copper by water. *Corrosion Science* 53 (1): 310–319.
- Hultquist, G., M.J. Graham, O. Kodra, S. Moisa, R. Liu, U. Bexell, and J.L. Smialek. 2013. *Corrosion of Copper in Distilled Water without Molecular Oxygen and the Detection of Produced Hydrogen*. Swedish Radiation Safety Authority. <http://urn.kb.se/resolve?urn=urn:nbn:se:du-20256>



- Idiart, A., M. Lavina, B. Cochepin, and A. Pasteau. 2020. Hydro-chemo-mechanical modelling of long-term evolution of bentonite swelling. *Applied Clay Science* 195. doi: 10.1016/j.clay.2020.105717.
- Ilgen, A., C. Bryan, S. Teich-McGoldrick, and E. Hardin. 2014. *DPC Materials and Corrosion Environments*. FCRD-UFD-2014-000597. U.S. Department of Energy, Office of Used Nuclear Fuel Disposition.
- IRSN (Institut de Radioprotection et de Sûreté Nucléaire). 2020. Experimental Facilities and Means—Tournemire experimental station. <https://www.irsn.fr/en/research/scientific-tools/experimental-facilities-means/tournemire/Pages/TOURNEMIRE-experimental-station.aspx>.
- Jacinto, A.C., M.V. Villar, R. Gomez-Espina, and A. Ledesma. 2009. Adaptation of the van Genuchten expression to the effects of temperature and density for compacted bentonites. *Applied Clay Science* 42 (3–4): 575–582. doi: 10.1016/j.clay.2008.04.001.
- JAEA (Japan Atomic Energy Agency). 2005. Japan Atomic Energy Agency Honorobe Underground Research Center. English website. <https://www.jaea.go.jp/english/04/horonobe/index.html>.
- Jerden, J., K. Frey, T. Cruse, and W. Ebert. 2012. *Waste Form Degradation Model Status Report: Electrochemical Model for Used Fuel Matrix Degradation Rate*. FCRD-UFD-2012-000169. Argonne, IL: Argonne National Laboratory.
- Jerden, J., K. Frey, and T. Cruse. 2013. *ANL Mixed Potential Model with Experimental Results: Implementation of Noble Metal Particle Catalysis Module*. FCRD-UFD-2013-000057. Argonne, IL: Argonne National Laboratory.
- Jerden, J., K. Frey, J. Copple, and W. Ebert. 2014. *ANL Mixed Potential Model for Used Fuel Degradation: Application to Argillite and Crystalline Rock Environments*. FCRD-UFD-2014\_000490. Argonne, IL: Argonne National Laboratory.
- Jerden, J., G. Hammond, J.M. Copple, T. Cruse and W. Ebert. 2015. *Fuel Matrix Degradation Model: Integration with Performance Assessment and Canister Corrosion Model Development*. Used Fuel Disposition. FCRD-UFD-2015-000550. Argonne, IL: Argonne National Laboratory.
- Jobmann, M., and G. Buntebarth. 2009. Influence of graphite and quartz addition on the thermo-physical properties of bentonite for sealing heat-generating radioactive waste. *Applied Clay Science* 44 (3–4): 206–210. doi: 10.1016/j.clay.2009.01.016.
- Johansson, L.G. 2008. Comment on “Corrosion of copper by water” *Electrochem. Solid-State Lett.*, 10, C63, (2007). *Electrochemical and Solid State Letters* 11 (4): S1–S1.
- Johnson, L. C. Ferry, C. Poinssot, and P. Lovera. 2005. Spent fuel radionuclide source-term model for assessing spent fuel performance in geological disposal. Part I: Assessment of the instant release fraction. *Journal of Nuclear Materials* 346 (1): 56–65. <https://doi.org/10.1016/j.jnucmat.2005.04.071>
- Joseph, R., J. St. Aubin, B. Craig, C. Olson, L. Vaner Wal, E. Vander Zee, C.D. Trail, R.M. Cumberland, J.J. Jarrell, and E. Kalinina. 2019. The Next Generation System Analysis Model: Capabilities for Simulating a Waste Management System. Paper 19131 presented at the WM2019 Conference, March 3–7, 2019, Phoenix, Arizona.
- Jové Colón, C.F., P.F. Weck, D.C. Sassani, L. Zheng, J. Rutqvist, C.I. Steefel, K. Kim, S. Nakagawa, J. Houseworth, J. Birkholzer, F.A. Caporuscio, M. Cheshire, M.S. Rearick, M.K. McCarney, M. Zavarin, A. Benedicto-Cordoba, A.B. Kersting, M. Sutton, J.L. Jerden, K.E. Frey, J.M. Copple and W.L. Ebert. 2014. *Evaluation of Used Fuel Disposition in Clay-Bearing Rock*. FCRD-UFD-2014-000056, SAND2014-18303 R. Albuquerque, NM: Sandia National Laboratories.



- Jové Colón, C.F., F.A. Caporuscio, K. Sauer, and M. Cheshire. 2019. Engineered Barrier Material Interactions at Elevated Temperatures: Bentonite-Metal Interactions Under Elevated Temperature Conditions. SAND2019-4150C. Albuquerque, NM: Sandia National Laboratories.
- Kahr, G., and M. Müller-Vonmoos. 1982. *Wärmeleitfähigkeit von Bentonit MX80 und von Montigel nach der Heizdrahtmethode*. NTB 82-06, Nagra, Hardstrasse 73, CH-5430 Wettingen, Schweiz.
- Kain, V. 2011. Stress corrosion cracking (SCC) in stainless steels. In Part III, Chapter 5 of *Stress Corrosion Cracking—Theory and Practice*, eds. V.S. Raja and T. Shoji, 199–244. Woodhead Publishing Series in Metals and Surface Engineering. Woodland Publishing.  
<https://doi.org/10.1533/9780857093769.3.199>.
- Kaufhold, S., A.W. Hassel, D. Sanders, and R. Dohrmann. 2015. Corrosion of high-level radioactive waste iron-canisters in contact with bentonite. *Journal of Hazardous Materials* 285: 464–473.  
<https://doi.org/10.1016/j.jhazmat.2014.10.056>.
- Kaufhold, S., R. Dohrmann, K. Ufer, and F. Kober. 2018. Interactions of bentonite with metal and concrete from the FEBEX experiment: mineralogical and geochemical investigations of selected sampling sites. *Clay Minerals* 53 (4): 745–763. <https://doi.org/10.1180/clm.2018.54>.
- Kharaka, Y., K. Gans, E. Rowan, E., J. Thordsen, C. Conaway, M. Blondes, and M. Engle. 2019. Chemical Composition of Formation Water in Shale and Tight Reservoirs: A Basin-Scale Perspective. In *Shale: Subsurface Science and Engineering*, pp. 27–43, eds. T. Dewers, J. Heath, and M. Sánchez. Geophysical Monograph Series. American Geophysical Union (AGU).
- Kim, K. 1978. *Mechanical Characteristics of Antrim Shale: Interim Report, April 1977- January 1978*. FE-2346-24. Dow Chemical Co. and U.S. Department of Energy, Office of Fossil Energy.
- King, F., C. Lilja, K. Pedersen, P. Pitkänen, and M. Vähänen. (2010). *An update of the state-of-the-art report on the corrosion of copper under expected conditions in a deep geologic repository*. Technical Report TR-10-67. Stockholm, Sweden: Svensk Kärnbränslehantering AB.
- King, F., M. Kolar, M. Vhnen, and C. Lilja. (2011). Modelling long term corrosion behaviour of copper canisters in KBS-3 repository. *Corrosion Engineering Science and Technology* 46 (2): 217–222. doi: 10.1179/18211Y.0000000004.
- Korzhavvi, P.A., and B. Johansson. 2010. *Thermodynamic properties of copper compounds with oxygen and hydrogen from first principles*. Stockholm, Sweden: Svensk Kärnbränslehantering AB.
- Kreis, P. 1991. *Hydrogen evolution from corrosion of iron and steel in low/intermediate level waste repositories*. Wettingen, Switzerland: National Cooperative for the Disposal of Radioactive Wastes (Nagra).
- Krumhansl, J.L. 1979a. *Preliminary Results Report: Conasauga Near-Surface Heater Experiment*. SAND79-D745. Albuquerque, NM: Sandia National Laboratories.
- Krumhansl, J.L. 1979b. *Final Report: Conasauga Near-Surface Heater Experiment*. SAND79-1855. Albuquerque NM: Sandia National Laboratories.
- Kursten, B., E. Smailos, I. Askarate, L. Werme, N.R. Smart, and G. Santarini. 2004. COBECOMA: State-of-the-art document on the CORrosion BEhaviour of COntainer MATerials. European Commission 5th Euratom Framework Programme, 1998-2002, European Commission.
- Kwong, G.M. 2011. *Status of corrosion studies for copper fuel containers under low salinity conditions*. Toronto, Canada: Nuclear Waste Management Organization.
- LaForce, T., K.W. Chang, F.V. Perry, T.S. Lowry, E. Basurto, R. Jayne, D. Brooks, S. Jordan, E. Stein, R. Leone, and M. Nole. 2020. *GDSA Repository Systems Analysis Investigations in FY2020*. Albuquerque, NM: Sandia National Laboratories.

- Lappin, A.R., R.K. Thomas, and D.F. McVey. 1981. *Eleana Near-Surface Heater Experiment Final Report*. SAND80-2137, UC-70. Albuquerque, NM: Sandia National Laboratories.
- Laubach, S.E., J.E. Olson, and M.R. Gross. 2009. Mechanical and fracture stratigraphy. *AAPG Bulletin* 93 (11): 1413–1426.
- Lee, A. and R. Heystee. 2014. *Used Fuel Deep Geological Repository Shaft versus Ramp Trade-off Study*. NWMO TR-2014-22. Toronto, Canada: Nuclear Waste Management Organization.
- Lee, J. and Z. Szklarska-Smialowska. 1988. Stress corrosion cracking of sensitized AISI 304 stainless steel in aqueous chloride solutions containing sulfur species at 50 through 200 C. *Corrosion* 44 (8): 560–565.
- Lee, J.O., H. Choi, and J.Y. Lee. 2016. Thermal conductivity of compacted bentonite as a buffer material for a high-level radioactive waste repository. *Annals of Nuclear Energy* 94:848–855. doi: 10.1016/j.anucene.2016.04.053.
- Lenhard, R., R. Fedors, C. Manepally, R. Pabalan, G. Ofoegbu, K. Chiang, J. Bradbury, and C. Markley. 2011. *Buffer and Backfill Workshop Report*. San Antonio, TX: Center for Nuclear Waste Regulatory Analyses.
- Li, V.C. 2019. High-Performance and Multifunctional Cement-Based Composite Material. *Engineering* 5:25–260.
- Lichtner, P., G. Hammond, C. Lu, S. Karra, G. Bisht, B. Andre, R.T. Mills, J. Kumar, and J.M. Frederick. 2019. *PFLOTRAN User Manual*.
- Lindquist, K. 2009. *Handbook of Neutron Absorber Materials for Spent Nuclear Fuel Transportation and Storage Applications: 2009 Edition*. Palo Alto, CA: Electric Power Research Institute.
- Lister, T.E., R.E. Mizia, and S.M. Birk. 2005. *Electrochemical testing of Ni-Cr-Mo-Gd alloys*. EXT- 05-00713. Idaho Falls, ID: Idaho National Laboratory.
- Lister, T.E., R.E. Mizia, A.W. Erickson, and B.S. Matteson. 2008. General and localized corrosion of borated stainless steel. *Corrosion: NACE*.
- Liu, H.H., J. Houseworth, J. Rutqvist, L. Zheng, D. Asahina, L. Li, V. Vilarrasa, F. Chen, S. Nakagawa, S. Finsterle, C. Doughty, T. Kneafsey, and J. Birkholzer. 2013. *Report on THMC Modeling of the Near Field Evolution of a Generic Clay Repository: Model Validation and Demonstration*. FCRD-UFD-2013-000244. Berkeley, CA: Lawrence Berkeley National Laboratory.
- Lomenick, T.F., S. Gonzales, K.S. Johnson, and D.W. Byerly. 1983. *Regional Geological Assessment of the Devonian-Mississippian Shale Sequence of the Appalachian, Illinois, and Michigan Basins Relative to Potential Storage/Disposal of Radioactive Wastes*. ORNL-5703. Oak Ridge, TN: Oak Ridge National Laboratory.
- Macdonald, D.D. 1992. The point defect model for the passive state. *Journal of the Electrochemical Society* 139 (12): 3434.
- Mariner, P.E., E.R. Stein, J.M. Frederick, S.D. Sevougian, and G.E. Hammond. 2017. *Advances in Geologic Disposal System Modeling and Shale Reference Cases*. SFWD-SFWST-2017-000044; SAND2017-10304 R. Albuquerque, NM: Sandia National Laboratories.
- Mariner, P.E., W.P. Gardner, G.E. Hammond, S.D. Sevougian, and E.R. Stein. 2015. *Application of Generic Disposal System Models*. FCRD-UFD-2015-000126; SAND2015-10037R. Albuquerque, NM: Sandia National Laboratories.
- Mariner, P.E., L.A. Connolly, L.J. Cunningham, B.J. Debusschere, D.C. Dobson, J.M. Frederick, G.E. Hammond, S.H. Jordan, T.C. LaForce, M.A. Nole, H.D. Park, F.V. Perry, R.D. Rogers, D.T. Seidl, S.D.

- Sevougian, E.R. Stein, P.N. Swift, L.P. Swiler, J. Vo, and M.G. Wallace. 2019. *Progress in Deep Geologic Disposal Safety Assessment in the U.S. since 2010*. SAND2019-12001 R; M2SF-19SN010304041. Albuquerque, NM: Sandia National Laboratories.
- Mariner, P.E., E.R. Stein, J.M. Frederick, S.D. Sevougian, G.E. Hammond, and D.G. Fascitelli. 2016. *Advances in Geologic Disposal System Modeling and Application to Crystalline Rock*. FCRD-UFD-2016-000440; SAND2016-96107R. Albuquerque, NM: Sandia National Laboratories.
- Martin C.D., P.K. Kaiser, and D.R. McCreath. 1999. Hoek–Brown parameters for predicting the depth of brittle failure around tunnels. *Can. Geotech. J.* 36:136–151.
- Martin, P., J.M. Barcala, and F. Huertas. 2006. Large-scale and long-term coupled thermo-hydro-mechanic experiments with bentonite: the FEBEX mock-up test. *Journal of Iberian Geology* 32 (2): 259–282.
- Marty, N.C., B. Fritz, A. Clément, and N. Michau. 2010. Modelling the long term alteration of the engineered bentonite barrier in an underground radioactive waste repository. *Applied Clay Science* 47 (1–2): 82–90.
- Mastalerz, M, A. Schimmelmann, A. Drobniak, and Y. Chen. 2013. Porosity of Devonian and Mississippian New Albany Shale across a maturation gradient: Insights from organic petrology, gas adsorption, and mercury intrusion. *AAPG Bulletin* 97:1621–1643.
- McDuff, R.E., and R.A. Ellis. 1979. Determining Diffusion-Coefficients in Marine-Sediments - Laboratory Study of the Validity of Resistivity Techniques. *American Journal of Science* 279 (6): 666–675. doi: 10.2475/ajs.279.6.666.
- Miller, A.W., and Y.F. Wang. 2012. Radionuclide Interaction with Clays in Dilute and Heavily Compacted Systems: A Critical Review. *Environmental Science & Technology* 46 (4): 1981–1994. doi: 10.1021/es203025q.
- Mizia, R.E., T.E. Lister, P.J. Pinhero, and T.L. Trowbridge. 2005. *Localized corrosion of a neutron absorbing Ni-Cr-Mo-Gd Alloys*. Con-02578. Idaho Falls, ID: Idaho National Engineering and Environmental Laboratory (INEEL).
- Mosser-Ruck, R., M. Cathelineau, D. Guillaume, D. Charpentier, D. Rousset, O. Barres, and N. Michau. 2010. Effects of temperature, pH, and iron/clay and liquid/clay ratios on experimental conversion of dioctahedral smectite to berthierine, chlorite, vermiculite, or saponite. *Clays and Clay Minerals* 58 (2): 280–291.
- Müller, H.R., B. Garitte, T. Vogt, S. Köhler, T. Sakaki, H. Weber, T. Spillmann, M. Hertrich, J.K. Becker, N. Giroud, V. Cloet, N. Diomidis, and T. Vietor. 2017. Implementation of the full-scale emplacement (FE) experiment at the Mont Terri rock laboratory. *Swiss Journal of Geosciences* 110 (1): 287–306. doi: 10.1007/s00015-016-0251-2.
- Nagra (Swiss National Cooperative for the Disposal of Radioactive Wastes). 2002. *Project Opalinus clay safety report*. Technical Report TR 02-05. Wettingen, Switzerland: National Cooperative for the Disposal of Radioactive Wastes (Nagra).
- Nagra. 2003. *Canister options for the disposal of spent fuel*. Nagra Technical Report NTB 02-11, 2003. Wettingen, Switzerland: National Cooperative for the Disposal of Radioactive Wastes (Nagra).
- Nagra. 2009. *A review of materials and corrosion issues regarding canisters for disposal of spent fuel and high-level waste in Opalinus Clay*. Nagra Technical Report NTB 09-02, 2009. Wettingen, Switzerland: National Cooperative for the Disposal of Radioactive Wastes (Nagra).
- Nagra. 2019. *Implementation of the Full-scale Emplacement Experiment at Mont Terri: Design, Construction and Preliminary Results*. Technical Report TR 15-02. May 2019. Wettingen, Switzerland:

- National Cooperative for the Disposal of Radioactive Wastes (Nagra). <https://www.nagra.ch/en/cat/publikationen/technicalreports-ntbs/ntbs-2001-2013/downloadcentre.htm>.
- NEA (Nuclear Energy Agency). 2012. *Cementitious Materials in Safety Cases for Radioactive Waste: Role, Evolution and Interactions—A workshop organized by the OECD/NEA Integration Group in the Safety Case and hosted by ONDRAF/NIRAS*. NEA/RWM/R(2012)3/REV March 2012. Organisation for Economic Co-operation and Development (OECD).
- NEA. 2014. Clay Club. <https://www.oecd-nea.org/rwm/clayclub/>.
- Neretnieks, I., L. Liu, and L. Moreno. 2009. *Mechanisms and models for bentonite erosion*. Stockholm, Sweden: Svensk Kärnbränslehantering AB (SKB).
- Neuzil, C.E. 1993. Low fluid pressure within the Pierre Shale: A transient response to erosion. *Water Resources Research* 29 (7): 2007–2020.
- Neuzil, C.E. 2019. Permeability of Clays and Shales. *Annual Rev. Earth Planet. Sciences* 47:247–73.
- Neuzil, C.E. 2000. Osmotic generation of ‘anomalous’ fluid pressures in geologic environments. *Nature* 403:182–184.
- Nichols, Jr., T.C., and D.S. Collins. 1986. *In Situ and Laboratory Geotechnical Tests in the Pierre Shale Near Hayes, South Dakota*. Open-File Report 86-152. United States Geological Survey.
- Nichols, Jr., T.C. 1992. *Rebound in the Pierre Shale of South Dakota and Colorado: Field and laboratory evidence of physical conditions related to processes of shale rebound*. Open-File Report 92-440. United States Geological Survey.
- Nichols, T.C., S.C. Donley, M. Jones-Cecil, and H.S. Swolfs. 1994. Faults and structure in the Pierre Shale, central South Dakota. *Geologic Society of America Special Paper* 287, 211–235.
- Noger, M.C., and J.A. Drahovzal. 2005. *Lithostratigraphy of Precambrian and Paleozoic Rocks along Structural Cross Section KY-1, Crittenden County to Lincoln County, Kentucky*. Kentucky Geological Survey, Report of Investigations 13, Series XII.
- Nopola, J.R. 2013. Preliminary Evaluation of the Pierre Shale as a Nuclear Waste Repository. MS thesis, South Dakota School of Mines and Technology.
- Nopola, J.R., and L.A. Roberts. 2013. Viscoplastic Behavior of Fine-Grained Geological Units and its Applicability to Compressed Gas Caverns. In *47th U.S. Rock Mechanics/Geomechanics Symposium, 23-26 June, San Francisco, California*. ARMA-2013-561. American Rock Mechanics Association.
- Nopola, J.R., and L.A. Roberts. 2016. Time-dependent deformation of Pierre Shale as determined by long-duration creep tests. In *50th U.S. Rock Mechanics/Geomechanics Symposium, 26-29 June, Houston, Texas*. ARMA-2016-508. American Rock Mechanics Association.
- NRC (U.S. Nuclear Regulatory Commission) 2014. *Generic Environmental Impact Statement for the Continued Storage of Spent Nuclear Fuel - Final Report*. NUREG-2157. Washington, DC: U.S. Nuclear Regulatory Commission. <https://www.nrc.gov/reading-rm/doc-collections/nuregs/staff/sr2157/>.
- Nuttal, B.C., 2013. *Middle and Late Devonian New Albany Shale in the Kentucky Geological Survey Marvin Blan No. 1 Well, Hancock County, Kentucky*. Kentucky Geological Survey, Report of Investigations 17, Series XII.
- NWMO (Nuclear Waste Management Organization). 2012. *Used Fuel Repository Conceptual Design and Postclosure Safety Assessment in Crystalline Rock*. NWMO TR-2012-16. Toronto, Ontario: Nuclear Waste Management Organization.



- NWTRB (Nuclear Waste Technical Review Board). 2016. Table 1 – Canister Attributes. Presented at the NWTRB Summer 2016 Board Meeting on August 24, 2016. <https://www.nwtrb.gov/docs/default-source/meetings/2016/august/table1.pdf?sfvrsn=10>.
- Nygård, R., M. Gutierrez, R.K. Bratli, K. Høeg. 2006. Brittle–Ductile Transition, Shear Failure and Leakage in Shales and Mudrocks. *Marine and Petroleum Geology*. 23:201–212.
- OECD (Organisation for Economic Co-Operation and Development). 2004. *Post-Closure Safety Case for Geological Repositories Nature and Purpose*. Nuclear Energy Agency No. 3679; ISBN 92-64-02075-6. Paris, France: Organisation for Economic Co-Operation and Development, Nuclear Energy Agency.
- Oelkers, E.H. 2001. General kinetic description of multioxide silicate mineral and glass dissolution. *Geochimica et Cosmochimica Acta* 65 (21): 3703–3719.
- ONDRAF/NIRAS (Belgian Agency for Radioactive Waste and Enriched Fissile Materials) 2001. *SAFIR 2: Safety Assessment and Feasibility Interim Report 2*. NIROND 2001-06 E. Brussels, Belgium: Belgian Agency for Radioactive Waste and Enriched Fissile Materials.
- ORNL (Oak Ridge National Laboratory). 2015a. *Performance Specification for Standardized Transportation, Aging, and Disposal Canister Systems*. FCRD-NFST-2014-000579, Rev. 2; ORNL/SPR-2015/251. Oak Ridge, TN: Oak Ridge National Laboratory.
- ORNL 2015b. *Rationale for the Performance Specification for Standardized Transportation, Aging, and Disposal Canister Systems*. FCRD-NFST-2015-000106, Rev. 1. Oak Ridge, TN: Oak Ridge National Laboratory.
- Pardoen, B. 2015. Hydro-mechanical analysis of the fracturing induced by the excavation of nuclear waste repository galleries using shear banding. PhD dissertation, University of Liège, Faculty of Applied Sciences, France.
- Parris, T.M., D.J. Webb, K.G. Takacs, and N. Fedorchuk, 2010. Geochemical Characterization of Formation Waters in Kentucky and Implication for Geologic Carbon Storage. Chapter 3 in *Evaluation of Geologic Sequestration Potential and Enhanced Oil Recovery in Kentucky*, ed. T.M. Parris, S.F. Greb, and B.C. Nuttall. KGS Report of Investigations 17414.
- Pena, P.A.P. 2015. The Effect of Rock Properties on Fracture Conductivity in the Marcellus Shale. MS Thesis, Texas A&M University.
- Perry, F.V. and R.E. Kelley. 2017. *Regional Geologic Evaluations for Disposal of HLW and SNF: The Pierre Shale of the Northern Great Plains*. SFWD-SFWST-2017-000119; LA-UR-17-27829. Los Alamos, NM: Los Alamos National Laboratory.
- Perry, F.V., R.E. Kelley, P.F. Dobson and J.E. Houseworth. 2014. *Regional Geology: A GIS Database for Alternative Host Rocks and Potential Siting Guidelines*. LA-UR-14-20368, FCRD-UFD-2014-000068. Los Alamos, NM: Los Alamos National Laboratory.
- Pignatelli, I., E. Mugnaioli, J. Hybler, R. Mosser-Ruck, M. Cathelineau, and N. Michau. 2013. A multi-technique characterization of cronstedtite synthesized by iron-clay interaction in a step-by-step cooling procedure. *Clays and Clay Minerals* 61 (4): 277–289. doi: 10.1346/CCMN.2013.0610408.
- Pignatelli, I., F. Bourdelle, D. Bartier, R. Mosser-Ruck, L. Truche, E. Mugnaioli, and N. Michau. 2014. Iron–clay interactions: Detailed study of the mineralogical transformation of claystone with emphasis on the formation of iron-rich T–O phyllosilicates in a step-by-step cooling experiment from 90° C to 40° C. *Chemical Geology* 387:1–11. <https://doi.org/10.1016/j.chemgeo.2014.08.010>.
- Rebak, R.B. 2007. Environmental Degradation of Materials for Nuclear Waste Repositories Engineered Barriers. Presented at 3rd International Environmental Degradation of Engineered Materials (EDEM 2007), May 2007, Gdansk, Poland. UCRL-PROC-227056.

- Rebak, R.B. and R.M. McCright. 2006. Corrosion of containment materials for radioactive waste isolation. In *Metals Handbook 13C*. Houston, TX: ASM International.
- Rice, T.L. 1987. *Estimates of Maximum Past Overburden for the Pierre Shale, Hayes Area, South Dakota*. Science and Mathematics Faculty Publications. [http://digitalcommons.cedarville.edu/science\\_and\\_mathematics\\_publications/306](http://digitalcommons.cedarville.edu/science_and_mathematics_publications/306) Rice 1987.
- Richards, J.A., J.M. Budai, L.M. Walter, and L.M. Abriola. 1994. Fracture analysis of the Upper Devonian Antrim Shale, Michigan Basin (abs.). *American Association of Petroleum Geologists Bulletin* 78 (8): 1333.
- Robertson, E.C. 1988. Thermal Properties of Rocks. Open-File Report 88-441. United States Geological Survey.
- Rondinella, V.V., D.S. Purroy, J.-P. Hiernaut, D.H. Wegen, D. Papaioannou, and M. Barker. 2008. Grain Boundary Inventory and Instant Release Fractions for SBR MOX. Presented at International High-Level Radioactive Waste Management 2008 (IHLRWM 2008), Las Vegas, NV, Sept 7–11.
- Rutqvist, J. 2020. Thermal Management Associated with Geologic Disposal of Large Spent Nuclear Fuel Canisters in Tunnels with Thermally Engineered Backfill. *Tunnelling and Underground Space Technology* 102:103454. doi: 10.1016/j.tust.2020.103454.
- Rutzvist, J., Y. Guglielmi, H. Xu, Y. Tian, P. Zarzycki, H. Deng, P. Li, M. Hu, P. Nico, S. Borglin, P. Fox, R. Sasaki, and J. Birkholzer. 2020. *Investigation of Coupled Processes in Argillite Rock: FY20 Progress*. LBNL-2001324. Berkeley, CA: Lawrence Berkeley National Laboratory.
- Ryder, R.T. 1996. *Fracture patterns and their origin in the Upper Devonian Antrim Shale gas reservoir of the Michigan basin: A review*. Open-File Report 96-23. United States Geologic Survey.
- Sassani, D.C., C.F. Jové Colón, P. Weck, J.L. Jerden, K.E. Frey, T. Cruse, W.L. Ebert, E.C. Buck, R.S. Wittman, F.N. Skomurski, K.J. Cantrell, B.K. McNamara, and Z. Soderquist. 2012. *Integration of EBS Models with Generic Disposal System Models*. FCRD-UFD-2012-000277, SAND2012-7762P. Albuquerque, NM: Sandia National Laboratories.
- Sassani, D., J. Jang, P. Mariner, L. Price, R. Rechard, M. Rigali, R. Rogers, E. Stein, W. Walkow, and P. Weck. 2016. *The On-line Waste Library (OWL): Usage and Inventory Status Report*. FCRD-UFD-2016-000080. Albuquerque, NM: Sandia National Laboratories.
- Sass, J.H., and S.P. Galanis, Jr. 1983. *Temperatures, Thermal Conductivity, and Heat Flow from a Well in Pierre Shale near Hayes, South Dakota*. Open-File Report 83-25. United States Geological Survey.
- Sauer, K., M. Rock, F. Caporuscio, and E. Hardin. 2020. Hydrothermal reactivity of neutron absorber composites. *Journal of Nuclear Materials* 531:152033.
- Savage, D. 2014. *An Assessment of the Impact of the Long Term Evolution of Engineered Structures on the Safety-Relevant Functions of the Bentonite Buffer in a HLW Repository*. Technical Report TR 13-02. Wettingen, Switzerland: National Cooperative for the Disposal of Radioactive Waste (Nagra).
- Schneider, R., E.H. Roseboom, Jr., J.B. Robertson, and P.R. Stevens. 1979. *U.S. Geological Survey Research in Radioactive Waste Disposal-Fiscal Year 1979*. Geological Survey Circular 847. Alexandria, VA: United States Geological Survey.
- Schultz, L.G., H.A. Tourtelot, J.R. Gill, and J.G. Boergnen. 1980. Composition and Properties of the Pierre Shale and Equivalent Rocks, Northern Great Planes Region. Geological Survey Professional Paper, 1064-B.
- Sevougian, S.D., P.E. Mariner, L.A. Connolly, R.J. MacKinnon, R.D. Roger, D.C. Dobson, and J.L. Prouty. 2019c. *DOE SFWST Campaign R&D Roadmap Update*. M2SF-19SN010304042; SAND2019-5179R. Albuquerque, NM: Sandia National Laboratories.



Sevougian, S.D., E.R. Stein, T. LaForce, F.V. Perry, M. Nole, and K.W. Chang. 2019b. *GDSA Repository Systems Analysis FY19 Update*. M3SF-19SN010304052; SAND2019-11942R. Albuquerque, NM: Sandia National Laboratories.

Sevougian, S.D., E.R. Stein, T. LaForce, F.V. Perry, T.S. Lowry, L.J. Cunningham, M. Nole, C.B. Haukwa, K.W. Chang, and P.E. Mariner. 2019a. *GDSA Repository Systems Analysis Progress Report*. M2SF-19SN010304051; SAND2019-5189R. Albuquerque, NM: Sandia National Laboratories.

She, H.Y., and B.E. Sleep. 1998. The effect of temperature on capillary pressure-saturation relationships for air-water and perchloroethylene-water systems. *Water Resources Research* 34 (10): 2587–2597. doi: 10.1029/98wr01199.

Shoesmith, D.W. 2006. Assessing the corrosion performance of high-level nuclear waste containers. *Corrosion* 62 (8): 703–722. <https://doi.org/10.5006/1.3278296>.

Shoesmith, D.W. 2007. *Used Fuel and Uranium Dioxide Dissolution Studies – A Review*. NWMO TR-2007-03. Toronto, Canada: Nuclear Waste Management Organization.

Shurr, G.W. 1977. *The Pierre Shale, Northern Great Plains: A Potential Isolation Medium for Radioactive Waste*. Open File Report 77-776. United States Geological Survey.

Siegmann, E.R. 2000. Clad Degradation - Summary and Abstraction. ANL-WISMD-000007 REV 00 ICN 01. Las Vegas, NV: Civilian Radioactive Waste Management System Management and Operating Contractor (CRWMS M&O).

Siegmann, E.R., and R.P. Rechard. 2001. *Cladding Degradation Component in Waste Form Degradation Model in TSPA-SR*. Las Vegas, NV: Civilian Radioactive Waste Management System Management and Operating Contractor (CRWMS M&O). doi: 10.2172/860279.

Siegmann, E.R., J.K. McCoy, R. Howard. 2000. Cladding Evaluation in the Yucca Mountain Repository Performance Assessment. *Mat. Res. Soc. Symp. Proc.* 608:3–9.

Simpson, H.E., J.E. Weir, Jr., and L.A. Woodward. 1981. *Inventory of Clay-Rich Bedrock and Metamorphic Derivatives in Eastern Nevada Excluding the Nevada Test Site*. Open-file Report 79-760. Denver, CO: United States Geological Survey.

Simpson, J.P., and R. Schenk. 1987. Hydrogen evolution from corrosion of pure copper. *Corrosion Science* 27 (12): 1365–1370.

Simpson, J.P., R. Schenk, and B. Knecht. 1985. Corrosion rate of unalloyed steels and cast irons in reducing granitic groundwaters and chloride solutions. *MRS Online Proceedings Library Archive* 50. doi: <https://doi.org/10.1557/PROC-50-429>.

SKB (Svensk Kärnbränslehantering AB [Swedish Nuclear Fuel and Waste Management Co.]). 2006. *Long-term safety for KBS-3 repositories at Forsmark and Laxemar—A first evaluation*. Technical Report TR-06-09. Stockholm, Sweden: Swedish Nuclear Fuel and Waste Management Co.

SKB 2010. *Design, production and initial state of the canister*. SKB TR-10-14. Stockholm, Sweden: Swedish Nuclear Fuel and Waste Management Co.

SKB. 2011. *Long-term safety for the final repository for spent nuclear fuel at Forsmark*. Technical Report TR-11-01. Stockholm, Sweden: Swedish Nuclear Fuel and Waste Management Co.

SKB. 2019. *Supplemental Information on canister integrity issues*. Stockholm, Sweden: Swedish Nuclear Fuel and Waste Management Co.

Smart, N.R., D.J. Blackwood, G.P. Marsh, et al. 2004. The anaerobic corrosion of carbon and stainless steels in simulated cementitious repository environments: A summary review of NIREX Research. AEA Technology report AEAT/ERRA-0313. Harwell, England: AEA Technology.

- Smart, N.R., P.A.H. Fennell, R. Peat, K. Spahiu, and L. Werme. 2006. Electrochemical measurements during the anaerobic corrosion of steel. pp. 477–487 in *Scientific Basis for Nuclear Waste Management XXIV*. Warrendale, PA: Materials Research Society.
- Smith, D.D. 1978. *Thermophysical properties of Conasauga Shale*. Oak Ridge Y-12 Plant, Y-2161. Oak Ridge, TN: U.S. Department of Energy.
- SNL (Sandia National Laboratories). 2004. *Aqueous Corrosion Rates for Waste Package Materials*. ANL-DSD-MD-000001 REV 01. Las Vegas, NV: Sandia National Laboratories.
- SNL. 2007a. *EBS Radionuclide Transport Abstraction*. ANL-WIS-PA-000001 REV 03. Las Vegas, NV: Sandia National Laboratories.
- SNL 2007b. *Total System Performance Assessment Data Input Package for Requirements Analysis for Transportation Aging and Disposal Canister and Related Waste Package Physical Attributes Basis for Performance Assessment*. TDR-TDIP-ES-000006 REV 00. Las Vegas, NV: Sandia National Laboratories.
- SNL. 2008a. *Postclosure analysis of the range of design thermal loadings*. ANL-NBS-HS-000057 REV 00. Las Vegas, NV: Sandia National Laboratories.
- SNL. 2008b. *Total System Performance Assessment Model/Analysis for the License Application, Volume 1*. Las Vegas, NV: Sandia National Laboratories.
- SNL. 2019. *A Salt Repository Concept for CSNF in 21-PWR Size Canisters*. SFWD-IWM-2017-000246 Rev. 2. Albuquerque, NM: Sandia National Laboratories.
- Soler, J.M. 2001. The effect of coupled transport phenomena in the Opalinus Clay and implications for radionuclide transport. *Journal of Contaminant Hydrology* 53 (1–2): 63–84. doi: 10.1016/s0169-7722(01)00140-1.
- Stewart, B.W., E.C. Chapman, R.C. Capo, J.D. Johnson, J.R. Graney, C.S. Kirby, and K.T. Schroeder. 2015. Origin of brines, salts and carbonate from shales of the Marcellus Formation: Evidence from geochemical and Sr isotope study of sequentially extracted fluids. *Appl Geochem* 60:78–88.
- Stoulil, J., M. Kouřil, L. Pavlova, D. Dobrev, J. Gondolli. 2018. 1D simulation of canister galvanic corrosion in saturated compacted bentonite. *Materials and Corrosion* 69 (9): 1163–1169. doi: 10.1002/maco.201710014.
- Stoulil, J., L. Pavlova, and M. Kouřil. 2019. Localised corrosion of stainless steels 316L and 2205 in synthetic bentonite pore water and bentonite slurry. *Acta Metallurgica Slovaca* 25 (1): 24–32.
- Swedish National Council for Nuclear Waste (Kärnavfallsrådet). 2009. *Mechanisms of copper corrosion in aqueous environments*. Stockholm, Sweden: Swedish Government Inquiries.
- Szakálos, P., G. Hultquist, and G. Wikmark. 2007. Corrosion of copper by water. *Electrochemical and Solid State Letters* 10 (11): C63–C67. doi: 10.1149/1.2772085.
- Szakálos, P., G. Hultquist, and G. Wikmark. 2008. Response to the comment on “Corrosion of copper by water” in *Electrochemical Solid State Letters* (2007) 10:C63. *Electrochemical and Solid State Letters* 11 (4): S2–S2.
- Szklarska-Smialowska, Z. 1999. Pitting corrosion of aluminum. *Corrosion Science* 41 (9): 1743–1767.
- Tang, A.M., Y.J. Cui, and T.T. Le. 2008. A study on the thermal conductivity of compacted bentonites. *Applied Clay Science* 41 (3–4): 181–189. doi: 10.1016/j.clay.2007.11.001.
- Taniguchi, N. and M. Kawasaki. 2008. Influence of sulfide concentration on the corrosion behavior of pure copper in synthetic seawater. *Journal of Nuclear Materials* 379 (1–3): 154–161.

- Teague, M., S. Saltzstein, B. Hanson, K. Sorenson, and G. Freeze. 2019. *Gap Analysis to Guide DOE R&D in Supporting Extended Storage and Transportation of Spent Nuclear Fuel: An FY2019 Assessment*. SAND2019-15479 R. Albuquerque, NM: Sandia National Laboratories.
- Telander, M.R., and R.E. Westerman. 1993. *Hydrogen generation by metal corrosion in simulated Waste Isolation Pilot Plant environments—Progress report for the period November 1989 through December 1992*. SAND-92-7347. Albuquerque, NM, Sandia National Laboratories. doi: 10.2172/10189324.
- Telander, M.R., and R.E. Westerman. 1997. *Hydrogen generation by metal corrosion in simulated Waste Isolation Pilot Plant environments*. SAND96-2538. Albuquerque, NM: Sandia National Laboratories. doi: 10.2172/461274.
- Thomas, Jr., J. and R.R. Frost. 1980. Adsorption/Desorption Studies of Gases through Shales. Chapter XIV, pp. 143–183 in *Geologic and Geochemical Studies of the New Albany Shale Group (Devonian-Mississippian) in Illinois, Final Report: Urbana, Illinois*. eds. R.E. Bergstrom, N.F. Shimp, and R.M. Cluff. Open File Series 1980-2. DOE/METC/12142-26. Urbana, IL: Illinois State Geological Survey.
- Thyne, G. and P. Brady. 2016. Evaluation of formation water chemistry and scale prediction: Bakken Shale. *Appl Geochem* 75:107–113.
- Tinnacher, R.M., M. Holmboe, C. Tournassat, I.C. Bourg, and J.A. Davis. 2016. Ion adsorption and diffusion in smectite: Molecular, pore, and continuum scale views. *Geochimica et Cosmochimica Acta* 177:130–149. doi: 10.1016/j.gca.2015.12.010.
- Tournassat, C., R.M. Tinnacher, S. Grangeon, and J.A. Davis. 2018. Modeling uranium(VI) adsorption onto montmorillonite under varying carbonate concentrations: A surface complexation model accounting for the spillover effect on surface potential. *Geochimica et Cosmochimica Acta* 220:291–308. doi: 10.1016/j.gca.2017.09.049.
- Tournassat, C., A. Vinsot, E.C. Gaucher, and S. Altmann. 2015. Chemical Conditions in Clay-Rocks. In Chapter 3 of *Developments in Clay Science*, Volume 6, 71–100. Elsevier.
- Trevani, L.N., E. Calvo, and H.R. Corti. 2000. Diffusion coefficients of iodide in high temperature aqueous solutions. *Electrochemistry Communications* 2 (5): 312–316. doi: 10.1016/s1388-2481(00)00023-0.
- Tsang, C.F., F. Bernier, and C. Davies. 2005. Geohydromechanical processes in the excavation damaged zone in crystalline rock, rock salt, and indurated and plastic clays—in the context of radioactive waste disposal. *Int Rock Mech Min Sci* 42:109–125.
- Turrero, M., A. Fernández, J. Peña, M. Sánchez, P. Wersin, P. Bossart, M. Sánchez, A. Melón, A. Garralón, and A. Yllera. 2006. Pore water chemistry of a Paleogene continental mudrock in Spain and a Jurassic marine mudrock in Switzerland: Sampling methods and geochemical interpretation. *Journal of Iberian Geology* 32:233–258.
- Van Loon, L.R. 2014. *Effective Diffusion Coefficients and Porosity Values for Argillaceous Rocks and Bentonite: Measured and Estimated Values for the Provisional Safety Analyses for SGT-E2*. Technical Report TR 12-03. Wetingen, Switzerland: National Cooperative for the Disposal of Radioactive Waste (Nagra).
- Volckaert, G., F. Bernier, X. Sillen, M. van Geet, J.C. Mayor, I. Göbel, P. Blümling, B. Frieg, and K. Su. 2005. Similarities and Differences in the Behaviour of Plastic and Indurated Clays. In *Proceedings Euradwaste'04. Radioactive waste management community policy and research initiatives*, EUR-21027, 281–291.

- Vomvoris, S., A. Claudel, I. Blechschmidt, and H.R. Müller. 2013. The Swiss Radioactive Waste Management Program - Brief History, Status, and Outlook. *Journal of Nuclear Fuel Cycle and Waste Technology* 1 (1). Korean Radioactive Waste Society.
- von Damm, K.L. 1987. *Geochemistry of shale groundwaters: survey of available data and postulated mineralogic controls on composition*. Publication No. 2941. Oak Ridge, TN: Environmental Sciences Division, Oak Ridge National Laboratory.
- Vosteen, H.D., and R. Schellschmidt. 2003. Influence of temperature on thermal conductivity, thermal capacity and thermal diffusivity for different types of rock. *Physics and Chemistry of the Earth* 28 (9–11): 499–509. doi: 10.1016/s1474-7065(03)00069-x.
- Wakeley, L.D. 1990. Grouts and Concretes for the Waste Isolation Pilot Project (WIPP). *Mat. Res. Soc. Symp. Proc.* 176.
- Wang, M., Y.F. Chen, S. Zhou, R. Hu, and C.B. Zhou. 2015. A homogenization-based model for the effective thermal conductivity of bentonite-sand-based buffer material. *International Communications in Heat and Mass Transfer* 68: 43–49. doi: 10.1016/j.icheatmasstransfer.2015.08.007.
- Weast, R.C., and M.J. Astle, eds. 1981. *CRC Handbook of Chemistry and Physics*. 62nd edition. Boca Raton, Florida: CRC Press.
- Weber, J.R., S. Keller, S. Mrugalla, J. Wolf, D. Buhmann, J. Mönig, W. Bollingerfehr, J. Krone, and A. Lommerzheim. 2011. Safety strategy and assessment for a HLW repository in Germany. In *Proceedings of the International High-level Radioactive Waste Management Conference, American Nuclear Society Albuquerque, NM, April 2011*.
- Werme, L.O., and P.A. Korzhavyi. 2010. Comment on Hultquist et al. “Water Corrodes Copper” *Catal. Lett.* 132 (2009) 311. *Catalysis Letters* 135 (3–4): 165–166.
- Werme, L., N.R. Smart, and D.J. Blackwood. 2002. Anaerobic corrosion of carbon steel and cast iron in artificial groundwaters: Part 2—Gas Generation. *Corrosion* 58 (8): 627–637.
- Wersin, P. and F. Kober. 2017. *FEBEX-DP: Metal Corrosion and Iron-Bentonite Interaction Studies*. Nagra Arbeitsbericht, NAB 16–16. Wettingen, Switzerland: Nagra.
- Wersin, P., M. Birgersson, S. Olsson, O. Karnland, and M. Snellman. 2007. *Impact of Corrosion-Derived Iron on the Bentonite Buffer within the KBS-3H Disposal Concept – the Olkiluoto Site as Case Study*. POSIVA 2007-11. Eurajoki, Finland: Swedish Nuclear Fuel and Waste Management Co.
- Wierschke, J.B. 2015. Evaluation of Aluminum-Boron Carbide Neutron Absorbing Materials for interim Storage of Used Nuclear Fuel. Ph.D dissertation, University of Michigan.
- Wilson, J.C., S. Benbow, H. Sasamoto, D. Savage, and C. Watson. 2015. Thermodynamic and fully-coupled reactive transport models of a steel–bentonite interface. *Applied Geochemistry* 61:10–28. <https://doi.org/10.1016/j.apgeochem.2015.05.005>.
- Wolery, T.J., and R.L. Jarek. 2003. *EQ3/6, Version 8.0: Software User's Manual*. Albuquerque, NM: Sandia National Laboratories.
- Xiong, Y., and Y. Wang. 2019. Saponites and New Generation Engineered Buffer Materials for Harsh Environments. In *Proceedings of International High-Level Radioactive Waste Management 2019 (IHLRWM 2019), Knoxville, TN, April 14–18*, 186–188.
- Xu, Y.S., D.A. Sun, Z.T. Zeng, and H.B. Lv. 2019. Temperature dependence of apparent thermal conductivity of compacted bentonites as buffer material for high-level radioactive waste repository. *Applied Clay Science* 174:10–14. doi: 10.1016/j.clay.2019.03.017.

Yang, T., R. Pusch, S. Knutsson, X.-D. Liu. 2014. The assessment of clay buffers for isolating highly radioactive waste. *WIT Transactions on Ecology and The Environment* 180:403–413.

YMP (Yucca Mountain Project) 2003. *Disposal Criticality Analysis Methodology Topical Report*. YMP/TR-004Q, Rev. 02. Las Vegas, NV: Yucca Mountain Site Characterization Office.

Zhang, C-L., and T. Rothfuchs. 2008. Damage and sealing of clay rocks detected by measurements of gas permeability. *Physics and Chemistry of the Earth* 33:S363–S373.

Zheng, L.E., J. Rutqvist, H.H. Liu, J.T. Birkholzer, and E. Sonnenthal. 2014. Model evaluation of geochemically induced swelling/shrinkage in argillaceous formations for nuclear waste disposal. *Applied Clay Science* 97–98:24–32. doi: 10.1016/j.clay.2014.05.019.

Zheng, L.E., J. Rutqvist, J.T. Birkholzer, and H.H. Liu. 2015. On the impact of temperatures up to 200 degrees C in clay repositories with bentonite engineer barrier systems: A study with coupled thermal, hydrological, chemical, and mechanical modeling. *Engineering Geology* 197:278–295. doi: 10.1016/j.enggeo.2015.08.026.

Zheng, L.G., H. Xu, J. Rutqvist, M. Reagan, J. Birkholzer, M.V. Villar, and A.M. Fernández. 2020. The hydration of bentonite buffer material revealed by modeling analysis of a long-term in situ test. *Applied Clay Science* 185. doi: 10.1016/j.clay.2019.105360.

Zheng, L., J. Rutqvist, H. Xu, and J.T. Birkholzer. 2017. Coupled THMC models for bentonite in an argillite repository for nuclear waste: Illitization and its effect on swelling stress under high temperature. *Engineering Geology* 230:118–129. doi: 10.1016/j.enggeo.2017.10.002.

Zhou, X., Zeng, Z., and H. Liu. 2010. Laboratory Testing on Pierre Shale for CO<sub>2</sub> Sequestration under Clayey Caprock. Presented at the 44<sup>th</sup> US Rock Mechanics Symposium, Salt Lake City, UT June 27–30, 2010.

Zhou, Y., R. Rajapakse, and J. Graham. 1999. Coupled fields in a deformable unsaturated medium. *International Journal of Solids and Structures* 36 (31–32): 4841–4868. doi: 10.1016/s0020-7683(98)00268-6.

This page intentionally left blank